Hematopoietic Niches Promote Initiation of Malaria Transmission and Evasion of Chemotherapy

Rebecca Sarah Lee

BSc (Hons), MRes

May, 2017

Submitted in fulfilment of the requirements for the Degree of Doctor of Philosophy

Institute of Infection, Immunity & Inflammation

College of Medicine, Veterinary Medicine & Life Sciences

Wellcome Trust Centre for Molecular Parasitology

University of Glasgow

Abstract

The transmission of the malaria parasite (*Plasmodium spp*) is effected by a small proportion of the population that commit to sexual development forming either male or female gametocytes. Currently front-line anti-malarials are developed to treat the asexual life stage parasitising mature erythrocytes. While circulating mature erythrocytes form a relatively homogenous population, it has been recently established that *Plasmodium spp* can colonise progenitor cells in the erythroid lineage. I hypothesised that these tissue-resident erythroid precursors may form a niche for preferential development of gametocytes, and therefore developed a quantitative approach to enumerate *Plasmodium*-infected erythropoietic intermediate cells in haematopoietic tissues. We demonstrate that within erythropoietic tissues, early reticulocytes preferentially drive commitment to gametocytogenesis, with the splenic niche contributing the quantifiable majority of gametocytes. Furthermore, this same erythropoetic niche offers the parasite protection against antimalarial drug treatment and, as such, may serve as origins of recrudescent infection and continuing transmission. My data therefore demonstrate that host cell phenotype and location play an active role in determining the developmental fate of malaria parasites and furthermore suggests a mechanism for the persistence of malaria parasites.

Author's Declaration

I declare that the results presented in this thesis are my own work, expect where stated otherwise, and that this work has not been submitted for a degree at any institution.

Rebecca Sarah Lee

Acknowledgments

Firstly, I am extremely grateful to Prof. Andy Waters and Prof. Jim Brewer for providing me with the opportunity to undertake my PhD in their labs and for their continuous supervision, support and advice over the last few years.

I wish to thank the MRC for providing the funding for this work.

I want to thank my assessors Dr Tom Barr, Dr Lisa Randford-Cartwright and Prof. Rick Maizels for their useful feedback. In a similar fashion, I would also like to thank Prof. Paul Gardside and Prof. Matt Marti for taking the time to discuss my data and suggest experiments.

This work would not have been possible without all the help, guidance and training I received from the members of the Waters and GBM labs. In particular I wish to thank Katie, Nisha, Anu and Anne for their endless patience in teaching me the ropes. I also want to thank Marianna de Niz and Robyn for assisting with the epically long drug dosing experiments and Brett for reading over drafts of this thesis.

I would like to thank the JRF staff, in particular Collin, and the flow facility manager, Diane, for all the technical support over the last few years.

Jagtar, thank you for your advice and support through difficult times.

Thank you to the occupants of the student room, in particular Shaf, Jonny, Alan, Shaima, Josh, Claire, Marija and Joanne. Without yous we all would have finished sooner, published faster and still fit into our old clothes. Your technical, emotional and gastronomic support has been invaluable and kept me sane over the last few years.

A big shout out to Rosh for never failing as a provider of vegan cake, bubbly and chat (both English and French).

To my parents and James, thank you for your unwavering encouragement and support throughout everything I have done. I am, and will always be, eternally grateful.

Lastly, thank you to my partner and best friend, Vijay. I could not have completed my PhD without you. This thesis is therefore dedicated to you (and Millie, of course).

Table of Contents

Table of Figures

Table of Tables

Abbreviations

° C	Degrees Celsius
dl	decilitre
µl	Microlitre
ml	Milliliter
l	Litre
µg	Microgram
mg	Milligram
g	Gram
kg	Kilogram
nM	Nano mole
µM	Micromole
mM	Micromole
M	Mole
µm	Micrometer
mm	Millimeter
cm	Centimeter
cm^2	Centimeter squared
hrs	Hours
mins	Minutes
bp	Base pairs
Kb	Kilobase
Mb	Megabase
%	Percentage
v/v	Volume/ Volume
w/v	Weight/Volume
rpm	Revolutions per minute
g	Relative centrifugal force
IC_{50}	Half maximal inhibitory concentration
kDa	Kilodalton
V	volts

3’ UTR	Three prime untranslated region
5’ UTR	Five prime untranslated region
5-FC	5-Fluorocytosine
AMA1	Apical membrane antigen 1
ANOVA	Analysis of variance
ARTs	Artemisinins
ART	Artemisinin
ATCs	Artemisinin combination therapies
ATP	Adenosine triphosphate
BFU-E	Burst forming unit-erythroid
BM	Bone marrow
BMP4	Bone morphogenetic protein 4
BrUTP	5-bromouridine 5’-triphospate
BSA	Bovine Serum Albumin
BSG	Basigin
CFU-E	Colony forming unit-erythroid
cKO	Conditional knock out
CLAG3	Cytoadherence-linked asexual gene 3
ChIP	Chromatin immunoprecipiation
CIDR	Cysteine rich inter-domain regions
cys	Cysteine
CR1	Complement receptor 1
CQ	Chloroquine
DBL	Duffy binding like domain
DHFR/TS	Dihydrofolate reductase-thymidylate synthase
DNA	Deoxynucleic acid
dNTP	Deoxynucleotide Triphosphate
DMSO	Dimethyl sulphoxide
EB	Erythroblasts
EBA	Erythrocyte binding antigen
EBD	Erythrocyte binding domain
EBL	Erythrocyte binding ligand
ECM	Experimental cerebral malaria
EDTA	Ethylene diamine tetraacetic acid

EGF	Epidermal growth factor
EPO	Erythropoietin
ER	Early reticulocytes
EV	Extracellular vesicles
FACS	Fluorescence activated cell sorting
FS-A	Forward scatter area
GC	Glucocorticoid receptor
gDNA	Genomic DNA
GFP	Green fluorescent protein
GPI	Glycosylphosphatidylinositol
GPA	Glycophorin A
hdfr	Human dihydrofolate reductase
Hifs	Hypoxia-inducible factors
HMS	Hyper-reactive malarial splenomegaly
hpi	Hours post invasion
HP1	Heterochromatin protein 1
HSC	Hematopoietic stem cell
ICAM	Intercellular adhesion molecule
IFN-gamma	Interferon
IgG	Immunoglobulin G
IMC	Inner membrane complex
IP	Intraperitoneal
IV	Intravascular
KAHRP	Knob-associated histidine-rich protein
KO	Knock out
LDH	Lactate dydrogenase
MFI	Mean fluorescence intensity
$MgCl_2$	Magnesium Chloride
MHC class I	Major histocompatibility complex
MSC	Mesenchymal stem cell
MSP	Merozoite surface protein
MTRAP	Merozoite thrombospindin-related anonymous protein
MyoA	Myosin A
NaCl	Sodium chloride
N-terminal	Amino terminal

OXPHOS	Oxidative phosphorylation
PADH	Post Artesunates delayed hemolysis
PALS	Periarterial lymphatic sheaths
PBS	Phosphate Buffered Saline
PCR	Polymerase chain reaction
PEXEL	*Plasmodium* export element
PfCRT	*P. falciparum* chloroquin resistance transporter
PfEMP1	*P. falciparum* erythrocyte membrane protein 1
PfEVs	Extracellular vesicles secreted from *P. falciparum*
PfRH	*P. falciparum* reticulocyte-binding protein homologues
PHZ	Phenylhydrazine-hydrochloride
pi	Post infection
PKG	Protein Kinase G
PLC	Phospholipase C pathway
PRY	Pyrimethamine
PTEX	*Plasmodium* translocon of exported proteins
PvDBP	*P. vivax* duffy binding protein
PvRBP	*P. vivax* reticulocyte binding protein
qPCR	Quantitative PCR
RESA	Ring-infected erythrocyte surface antigen
RFP	Red fluorescent protein
RFU	Relative fluorescent unit
Rif	Repetitive interspersed family
RON	Rhoptry neck protein
RNA	Ribonucleic acid
rPBS	Rich PBS
SCF	Stem cell factor
SD	Standard deviation
SEM	Standard error of the mean
SNP	Single nucleotide polymorphism
SMAC	Schizont membrane associated cytoaherence protein
SP	Sulphadoxine-pyrimethamine
SPN	Subpellicular network
SS-A	Side scatter area
stevor	Subtelomeric variant open reading frame

TAREs	Telomere-associated repeat elements
TBE	Tri-Borate containing EDTA
TCA cycle	Tricarboxylic acid cycle
TNF-alpha	Tumor necrosis factor
VCAM	Vascular cell adhesion protein
yfcu	Uridyl phosphoribosyl transferase

1 Introduction

1.1 Introduction Outline

This introduction will address the structure and function of the *Plasmodium* parasite's sexual and asexual forms in the context of both immature erythroid cell infection and the perpetuation of disease. Moreover, the case for the development of a murine model of tissue resident erythroid infection and its subsequent combination with a quantitative analytical approach will be made.

The first two sections (sections 1.2 & 1.3) will provide a comprehensive overview of the background literature needed in order to contextualise the third section (section 1.4).

1.2 Malaria and *Plasmodium spp*

The key points in this section are:

- Features defining a parasite's cellular tropism.
- Features defining a host cell's susceptibility to *Plasmodium*.
- Environmental and parasite cues facilitate gametocyte commitment.
- Immature gametocytes develop out of circulation.
- The gametocyte ultra-structure and motility.
- Drug resistance and recrudescence highlight the need to fully understand the temporal and dynamics of infection.
- The use of a murine model organism to advance the study of multiple aspects of *Plasmodium* biology and malaria pathology.

The conclusions to these points are reviewed in the summary: section 1.2.37.

1.2.2 Malaria

Malaria is a mosquito-borne infectious disease that The World Health Organization (The WHO) describes as an acute febrile illness ranging in severity from mild chills and headaches through to respiratory disease and cerebral malarial (The WHO, 2017). It is endemic within a global band of tropical and sub-tropical countries (Figure 1.1). Consequently, the international strategies for control and elimination of the disease transcend geographical boundaries. Nonetheless the political, social and economic stability of endemic countries influence the current rate of local progress. There has been a 37% decrease in reported global disease incidences between the years 2000 and 2015. Despite this, 3.2 billion people remain at risk, with 214 million incidences and 400,000 deaths reported in 2015 alone. The sheer scale of eradication challenges are directly and indirectly highlighted by the recently adopted WHO-led 15 year strategy that estimates the need for a $8.7 billion annual spend by 2030 (WHO, 2015).

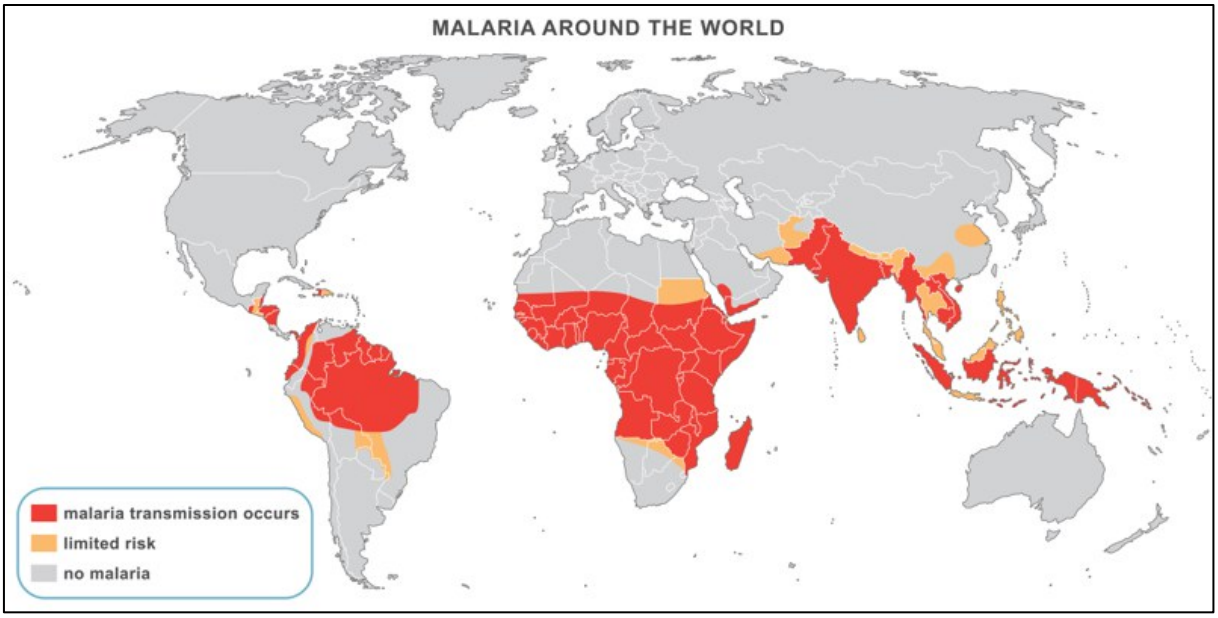

Figure 1.1 Global distribution of malaria (WHO, 2015).

1.2.3 Plasmodium spp

The causative agent of malaria is the unicellular, eukaryotic *Apicomplexa* parasite, *Plasmodium*. There are five human infective species of *Plasmodium* that cause malaria: *P. falciparum, P. vivax, P. ovale, P. malariae,* and *P. knowlesi*. The species that cause the greatest mortality and morbidity are *P. falciparum* and *P. vivax,* respectively (Figure 1.2). As such, current research in the field, from basic through to clinical, has focused on the prevention and cure of disease caused by these two particular species.

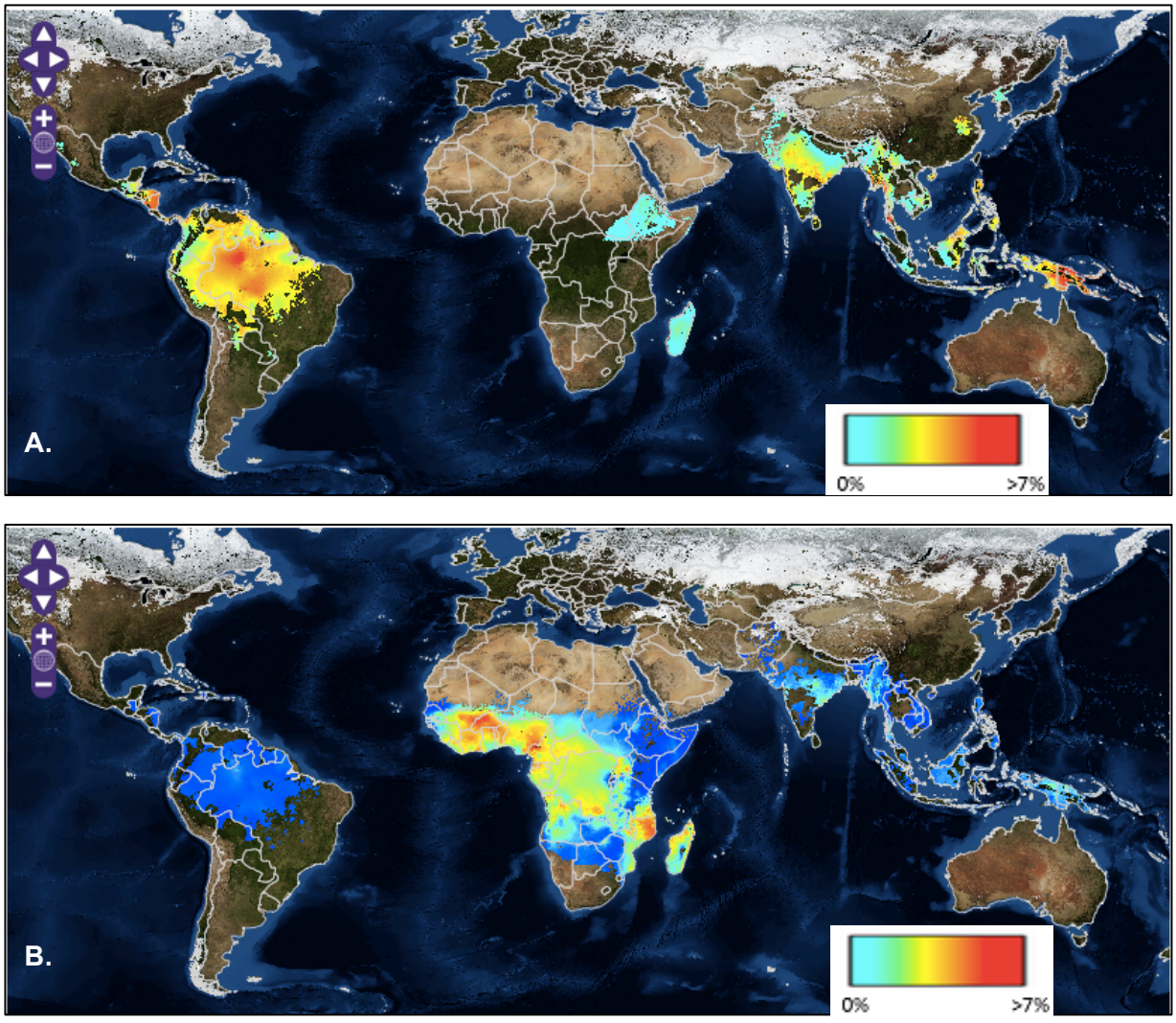

Figure 1.2 Global distribution of A. *P. vivax* and B. *P. falciparum* (MAP, 2015)**.** Key displays the estimated percentage of the population (country) infected at any given time during 2010.

1.2.4 *Plasmodium* Life Cycle Overview

All *Plasmodium* parasites have a life cycle split between a vertebrate host and a female *Anopheles* mosquito (the vector). Host to vector transmission events are flanked by the survival and proliferation of *Plasmodium spp* within two different host environments. Reflecting this, the parasite undergoes a sequential transition between morphologies (Figure 1.3), with specialised invasive forms facilitating the parasite's establishment of infection within the host. There are three invasive forms of *Plasmodium:* the sporozoite (Figure 1.3 A), the merozoite (Figure 1.3 B & Ci) and the ookinete (Figure 1.3 F3).

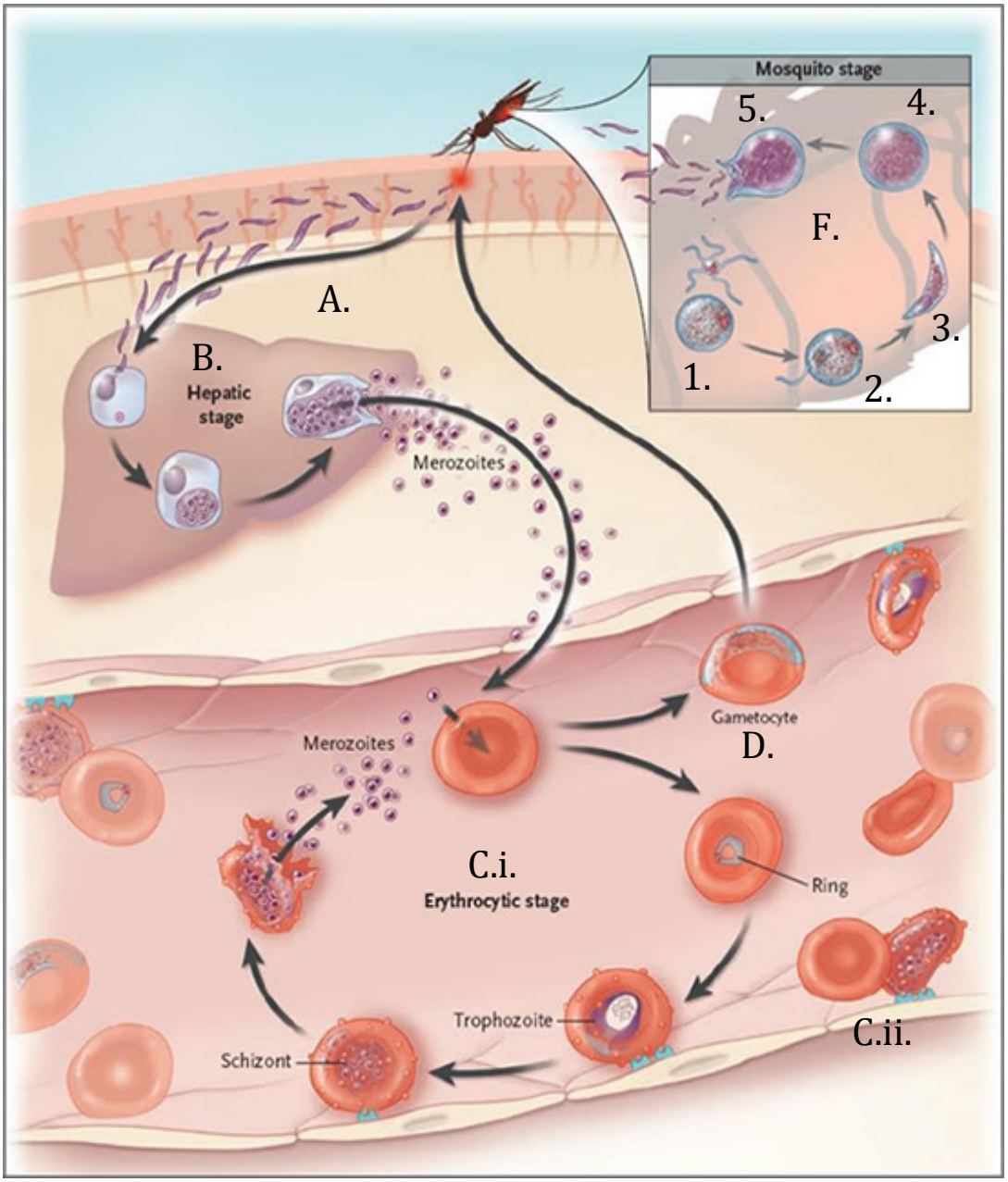

Figure 1.3 Life cycle of *Plasmodium* (Rosenthal, 2008)**. A.** The host is infected with sporozoites during a blood meal. **B.** The sporozoites rapidly translocate to the liver and undergo multiple rounds of asexual reproduction within hepatocytes. **C.i.** The released merozoites invade circulating erythroid cells and undergo asexual reproduction. **C.ii.** Erythrocytes containing mature asexual forms of certain *Plasmodium spp* cytoadhere to the endothelium lining of blood vessels and uninfected erythrocytes. **D.** A number of parasites commit themselves to a parallel developmental pathway that generates sexual cells called gametocytes. **F.** The gametocytes are taken up in the blood meal; activate (1) and fertilize (2) in the insect's midgut forming a zygote that matures into an ookinete (3). This stage translocates the midgut wall and develops into oocyst that contains sporozoites (4), and ruptures (5) releasing sporozoites that migrate to the insect's salivary glands.

1.2.5 *Plasmodium spp* and Evolutionary Distance

Gathering *in vivo* data for human parasites is ethically restricted, therefore making the investigation of parasite dynamics during infection difficult. As such, murine infective species have been used as model organisms to supplement the study of the *Plasmodium* life cycle within the host. There are four species of murine infective *Plasmodium: P. chabaudi, P. vinckei, P. berghei and P. yoelii* (Wykes and Good, 2009). The relevance of animal models to key features of human malaria will be reviewed in Section 1.2.36. Nonetheless, it is important at this point to address the phylogenetic groupings (Figure 1.4) within the *Plasmodium* genus in order to provide clear context to the contrasts between species biology.

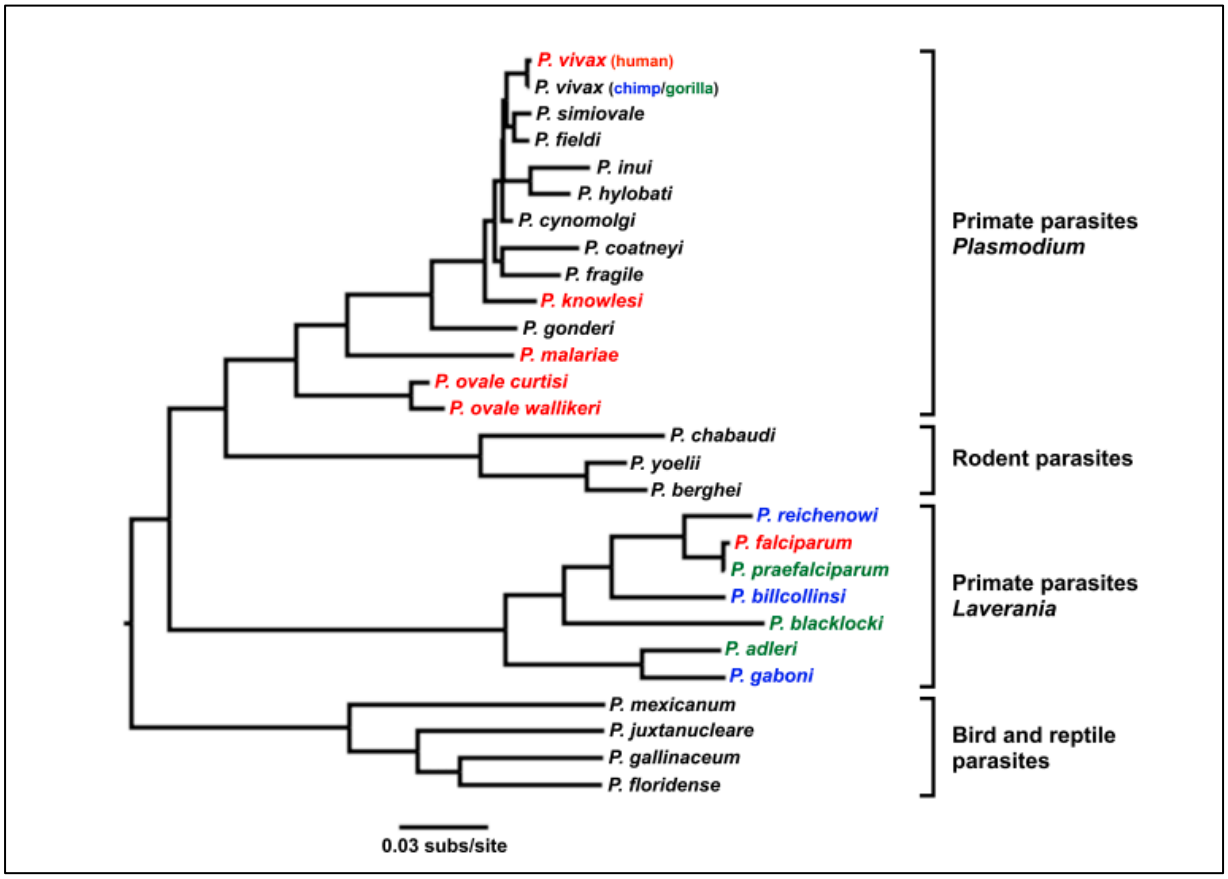

Figure 1.4 Evolutionary relationships between *Plasmodium spp* (Loy et al., 2016)**.** Human (red), chimpanzee (blue) and gorilla (green) infective species. The scale bar indicates 0.03 substitutions per site. Phylogeny was estimated by maximum likelihood analysis on 2.4kb mitochondrial genome.

Following the sequencing and annotation of DNA from ape-infective *Plasmodium* species it became clear that *P. falciparum* arose via a zoonotic infection from African gorillas around 10,000 years ago, rather than the previous theory of cross infection from chimpanzees (Loy et al., 2016). The evolutionarily closest relative of *P. falciparum* is a gorilla-infective *Plasmodium*, *P. praefalciparum*. Both species are grouped within the *Laverania* clade of the *Plasmodium* phylogenetic tree, which was generated based on the nucleotide sequences of the mitochondrial genome. This clade is distinct from the other human and murine infective *Plasmodium spp* which cluster within the subgenus of *Plasmodium* (Duval et al., 2010).

The four rodent infective *Plasmodium* species were isolated between 1948 and 1974 from Africa (Perkins et al., 2007). The WHO registry of standard malaria parasites contains 70 field isolates of rodent malaria parasites and these isolates are classified into subspecies (Ramiro et al., 2012). Recent work into comparing the polymorphisms at 11 nuclear gene loci suggested that the subspecies are independently evolving and should in fact be consisted distinct species, therefore potentially drastically expanding the number of rodent malaria parasites (Ramiro et al., 2012). A phylogenetic study using the apicoplast genome noted an evolutionary closeness between the rodent malaria clade and human infective *P. ovale*, leading the authors to hypothesise a host switch event between rodents and humans reflective of the gorilla to human event giving rise to *P. falciparum* (Arisue et al., 2012). This clade arrangement is not reflected in Figure 1.4, which was generated by Loy *et al* (2016), but it is supported by recent work using a manually curated genome for *P. ovale* (Rutledge et al., 2017). The manual annotation protocol allowed for the novel analysis and comparison of differently distributed pseudogenes between *Plasmodium* genomes (Rutledge et al., 2017). It also allowed the authors to highlight that the disparities observed within the phylogenetic groupings of *Plasmodium* is due in part to the low quality reference genomes available for the less studied species (Rutledge et al., 2017).

1.2.6 The Merozoite

Due to the early establishment of continuous *in vitro* culturing conditions for *P. falciparum* (Trager and Jensen, 1976) and the continuing relative lack of protocols for robustly propagating *P. vivax,* much merozoite structural biology has conducted using the *Laverania Plasmodium* species (Mons, 1990; Trager and Jensen, 1976). Despite the species divergence there is speculation that the overarching features of their biology is shared (Hanssen et al., 2013).

The merozoites of *Plasmodium spp* have a highly polarised morphology that is defined by the apical complex (Figure 1.5). Recently, high definition electron tomography has confirmed historical observations that the apical complex of *P. falciparum* consists of an arrangement of three dense proteinaceous rings. These anchor the microtubule filaments that run longitudinally under the plasma membrane (Hanssen et al., 2013; Langreth et al., 1978). The plasma membrane encapsulates the vital eukaryotic organelles required for physiology and metabolic function. The cell also contains the *Apicomplexa*-specific metabolic organelle, the apicoplast, alongside the characteristic apical structures: the rhoptries, micronemes and dense granules (Hanssen et al., 2013).

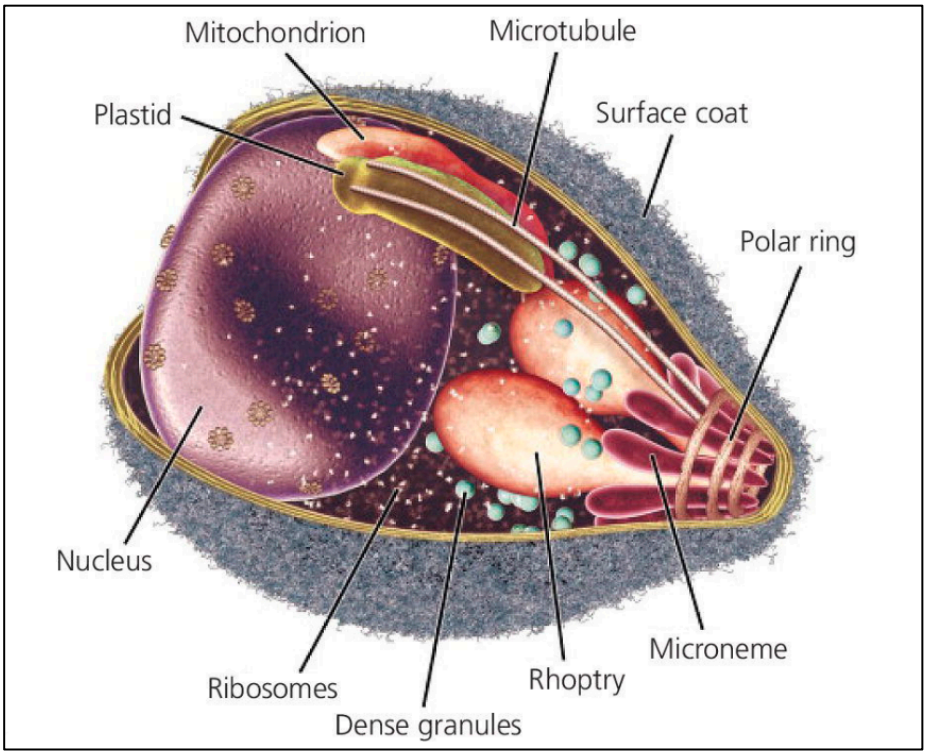

Figure 1.5 Merozoite structure (Gaur et al., 2016)

The cytoskeleton of the merozoite is composed of three elements: the microtubules, actin microfilaments and intermediate filaments known as the subpellicular network (SPN) (Etienne-Manneville, 2004). The SPN supports the cytoplasmic side of the double membrane layer named the inner membrane complex (IMC) (Tremp et al., 2014). The IMC structure is further supported by the microtubules, a polarised network facilitating protein distribution throughout the cell. The actin filaments of most eukaryotic cells exert protrusive and contractile forces to facilitate cellular motility, this does not occur in *Plasmodium* as the parasite does not modify its shape in order to gain motility (Etienne-Manneville, 2004; Ménard, 2001). Nonetheless, the motility that *Apicomplexa* parasites do display, gliding (sporozoites) and cell invasion (all zoites), is sensitive to blocking the polymerisation of actin with drugs such as cytochalasin B (Miller et al., 1979; Russell and Sinden, 1981). *Plasmodium* contains two variants of actin: actin I and actin II, with the filaments of the actin 1 forming a scaffold for the myosin class of mechanochemical enzymes (ATPases). Myosin A (MyoA) is the motor of a structure collectively known as the glideosome (Figure 1.6), in which MyoA pulls on the actin 1 filament generating force through the hydrolysis of ATP (Ménard, 2001; Kumpula and Kursula, 2015; Etienne-Manneville, 2004). This complex was initially believe to interact with an aldolase tetramer (Starnes et al., 2009; Jewett and Sibley, 2003), which was proposed to act as a bridging protein connecting the actin filaments to the C- terminal tails of extracellular parasite ligands (Starnes et al., 2009; Jewett and Sibley, 2003). Directed point mutations in the aldolase putative binding site disrupted the interaction between the enzyme and the adesin protein as judged by *in vitro* pull down assays (Buscaglia et al., 2004; Starnes et al., 2009). Moreover, conditional aldolase knockout (cKO) parasites had a attenuated growth phenotype (Starnes et al., 2009). Nonetheless, a later study that cultured aldolase cKO parasites in glucose rich media attributed the attenuated growth phenotype to decreased enzymatic activity of aldolase rather than the dysfunction of the glideosome, as such the authors concluded that aldolase is dispensable in parasite motility (Shen and Sibley, 2014).

The parasite surface adhesions bind to their respective receptors and are translocated to the posterior pole of the parasite; thus binding to a fixed ligand

would lead to a forward motion, be it gliding forward or penetration into a host cell (Hanssen et al., 2013; Koch and Baum, 2015).

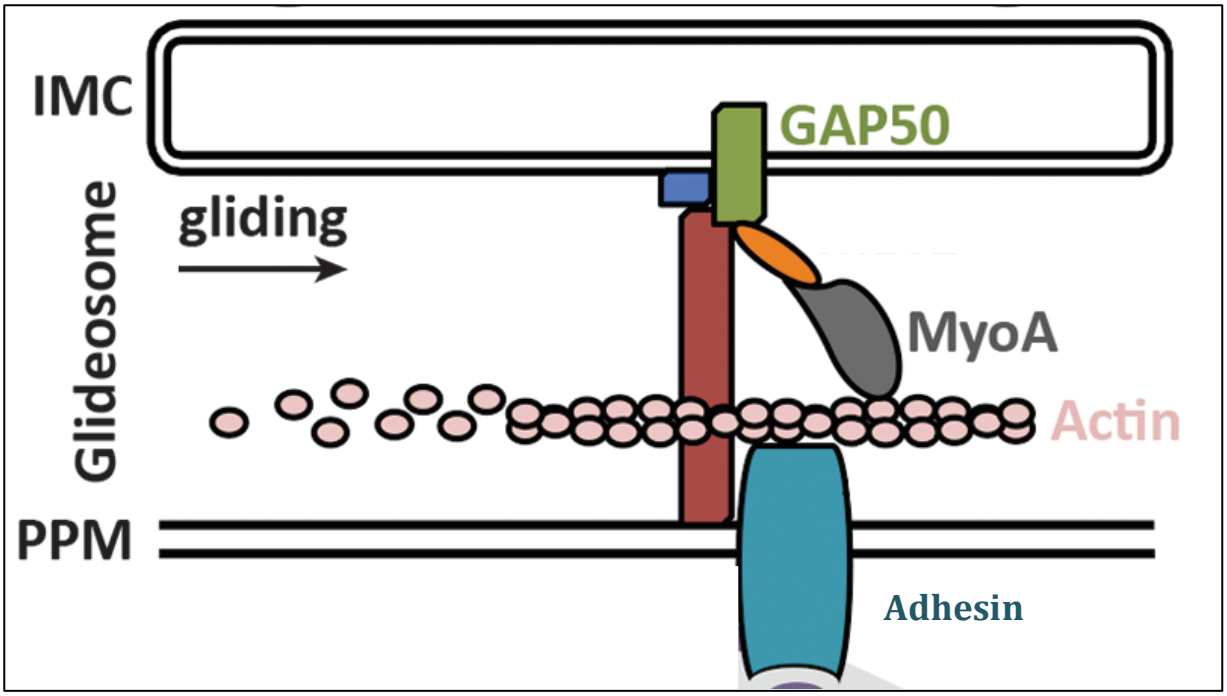

Figure 1.6 The location of the IMC and glideosome within the merozoite and sporozoite (Bargieri et al., 2014). Associated with the IMC are the proteins associated with the glideosome complex. The direction of gliding is indicated. PPM; parasite plasma membrane.

1.2.7 Host Cell Preference: The Invasion of Erythrocytes or Reticulocytes

The preferential and restricted invasion of particular erythrocyte age classes in the host peripheral blood is characteristic of some *Plasmodium spp*. *P. falciparum* is capable of invading all erythroid cells in the peripheral blood, whereas *P. vivax* and *P. berghei* demonstrate preferential invasion of younger red blood cells (reticulocytes).

The reticulocyte population within the peripheral blood is a small heterogeneous subset of enucleated erythroid cells containing vestigial reticular network ribosomal RNA that is lost during maturation into erythrocytes (Motoi Ishidate, 1990). The restrictive tropism *P. vivax* has for this erythroid subset was described almost 80

years ago (Hegner, 1938). However, *P. vivax* exhibits high genetic diversity between geographical isolates. Moreover, cellular tropism differs greatly between *P. vivax* isolates from ethically different patients, for example patients in Thailand and India (Lim et al., 2016). This suggests that the parasite invasion preference is influenced by both the parasite and the host genetic background.

1.2.8 Merozoite Invasion

The ability of a free merozoite to invade a host cell is a prerequisite for the parasite intra erythrocyte life cycle. Thus, in order to understand the parameters that restrict *Plasmodium* to a particular erythroid age class it is essential to discuss the requirements for merozoite invasion. This section will therefore be a discussion concerning ligand receptor interactions that facilitate erythroid cell invasion in the peripheral blood, with note of interactions that restrict the parasites to reticulocyte invasion.

The merozoite is the only extracellular stage of the erythrocytic asexual life cycle, having been released from the host cell via parasite-mediated egress. It is molecularly primed for re-invasion from this point due to the exocytosis of the micronemes. The release of these proteins has been linked to merozoite exposure to the low potassium ion concentration in the blood, an event that is speculated to trigger the successive activation of protein kinase G (PKG) and the phospholipase C (PLC) pathway, resulting in the release of calcium from internal parasite store (Taylor et al., 2010; Singh et al., 2010; Farrell et al., 2012; Brochet and Billker, 2016). However, the contribution of environmental potassium concentrations to this model has recently been re-evaluated as evidence exists suggesting that merozoites can also invade in high ion concentrations (Badalà et al., 2008).

Merozoite invasion of host cells, first described in the monkey-infective parasite *P. knowlesi* using light microscopy and rudimentary time lapse imaging, is broken down into four distinct phases: initial attachment, apical re-orientation, formation of the tight/-moving junction and sealing of the parasitophorous vacuole (PV) (Figure 1.7) (Hanssen et al., 2013; Dvorak et al., 1975). This process of invasion

takes approximately 1 minute from the point of egress and broadly, many of the key events and checkpoints are be similar throughout the *Plasmodium* genius (Yahata et al., 2012; Gilson and Crabb, 2009).

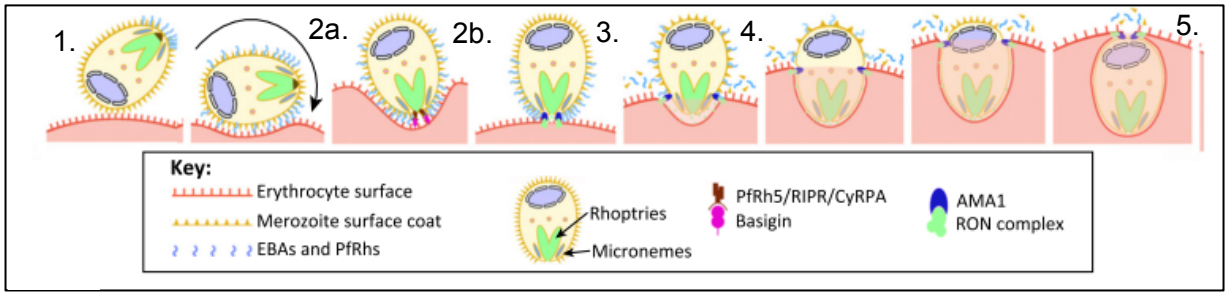

Figure 1.7 Merozoite invasion is rapid and involves many ligands (adapted from Weiss et al., 2016). 1. Initial low affinity attachment. 2a and b. High affinity binding and reorientation. 3. Formation of the tight junction. 4. The moving junction. 5. Sealing of the PV.

1.2.9 Low Affinity Initial Attachment

Early electron microscopy studies observed that the merozoite fibrillar coat consists of surface proteins (Ladda et al., 1969). Many of these are glycosylphosphatidylinositol (GPI) anchored proteins, but a small proportion are integral membrane and peripherally associated surface proteins (Figure 1.8 & Table 1.1). *P. falciparum* merozoite surface protein 1 (MSP-1) was the first of these proteins to be characterised (Perkins and Rocco, 1988) and orthologs have been subsequently identified in *P. vivax* and *P. berghei* (del Portillo et al., 1991; Babon et al., 2007; Jennings et al., 1998). MSP-1 is expressed during late schizogony as an ~190 kDa precursor protein. It is initially cleaved into four fragments, through a sequence of proteolytic events mediated by the subtilisin- like protease SUB1, which remain bound in a non-covalent complex to the parasite surface. Presumably this processing event conveys a functional change to the protein that is now displayed on the surface of the free merozoite and binds Band 3 on the host erythrocyte (Goel et al., 2003). At the point of merozoite invasion the MSP-1_{42} fragment is cleaved by SUB2 into two additional fragments, the smaller of which

(MSP-1_{19}) is retained on the parasite surface (Seong-kyun et al., 2016; Holder et al., 1985; Babon et al., 2007; Holder, 2009).

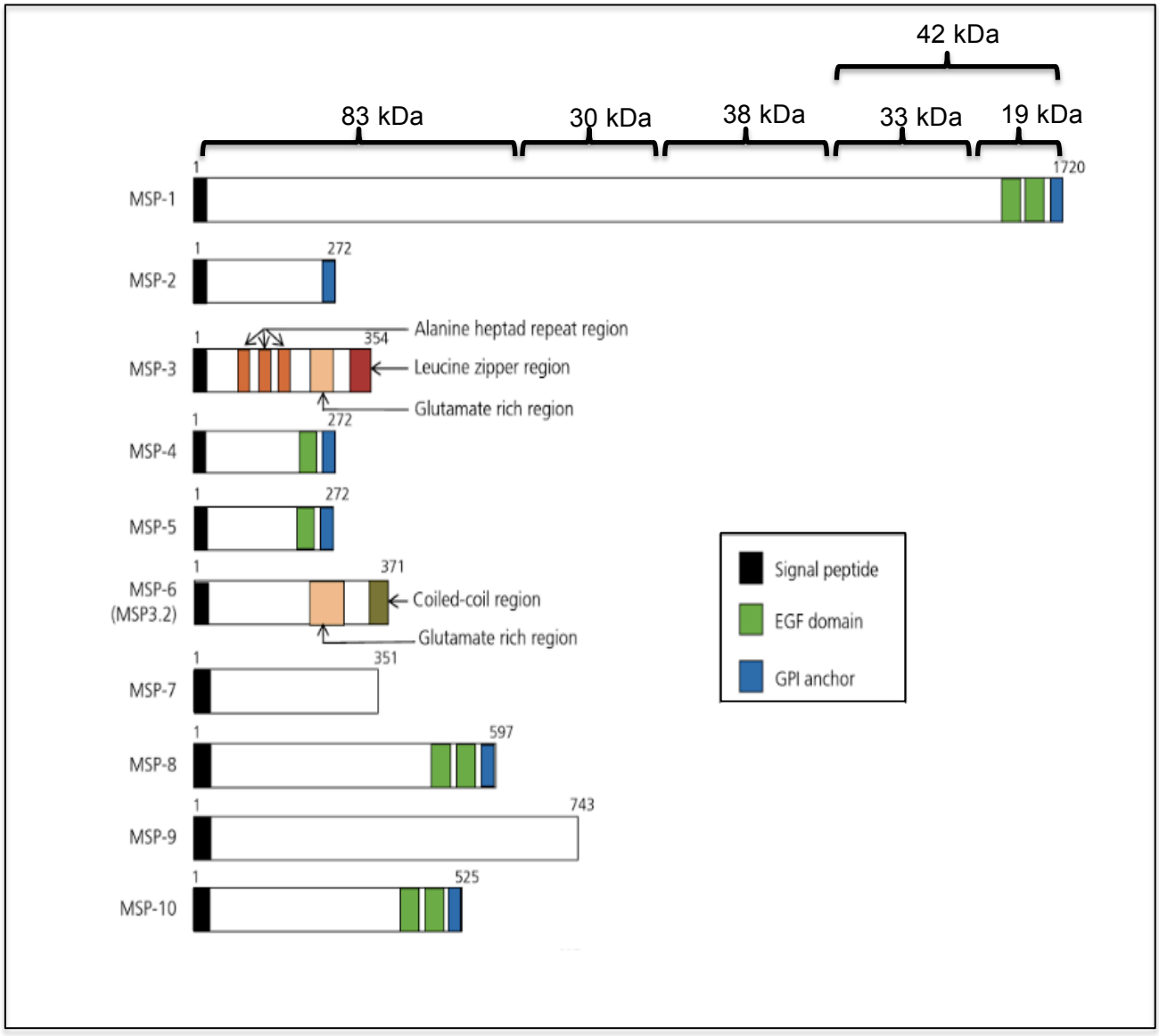

Figure 1.8 Structural domains of merozoite surface proteins (MSP, adapted from Gaur et al., 2016). MSP-1 is the largest of the MSPs and is proteolytically processed. The first four fragments are 83kDa (MSP-1_{83}: derived from the N-terminus of the full MSP-1 molecule), 38kDa, 30kDa (MSP-138 and MSP-1_{30}: central regions) and 42kDa. The latter fragment is then cleaved into 33kDa and 19kDa (MSP-1_{33} and MSP-1_{19}: C-terminus). MSP-1_{19} contains two EGF-like domains all except one (MSP-1_{19}) is shed during entry into the host cell. A **signal peptide** is a short sequence at the N-terminus that directs the protein towards the secretory pathway. An epidermal growth factor domain (**EGF**) is a secondary amino acid structure and includes 6 cysteine residues that form 3 disulfide bonds. The main structure is a two-stranded beta-sheet followed by a loop. Tandem repeats typically fold to form a single solenoid domain. A glycosylphosphatidylinositol (**GPI**) domain at the C-terminus acts to anchor proteins to the cell surface (Gaur et al., 2016).

P. falciparum gene	RBC binding in *P. falciparum*	Protein function and characteristics in *P. falciparum*	Homolog in *P. vivax*	Homolog in *P. berghei*
msp-1 (Perkins and Rocco, 1988)	Yes. Receptor is Band 3. (Goel et al., 2003).	MSP-1/6/7 binds MSPDBL-1/2 (Carlton et al., 2008). As a complex binds to host glycophorin A (Baldwin et al., 2015).	Contains GPI anchor. Two EGF domains (del Portillo et al., 1991; Babon et al., 2007). Novel MSP1P paralog (Cheng et al., 2013).	Contains GPI anchor. Two EGF domains (Jennings et al., 1998)
msp-2 (Clark et al., 1989)	Unknown*	Essential, cannot be KO. (Cowman et al., 2015; Sanders et al., 2006).	Homolog not present at corresponding loci (Black et al., 2002).	Homolog not present at corresponding loci (Kedzierski et al., 2000)
msp-3 (McColl et al., 1994; Oeuvray et al., 1994)	Unknown*	Mutigene family; 8 paralogs, including MSPDBL-1 & 2, H101 & 3. Non-essential (study didn't state which paralog targeted) (Mills et al., 2002).	multi-gene family. Two paralogs;. Lacks GPI anchor, alanine-rich heptads, leucine-zipper, DBL domain (Galinski et al., 2001; Jiang et al., 2013).	Putative ortholog (Rice et al., 2014).
msp-4 (Marshall et al., 1997)	Unknown*	Non-essential (Sanders et al., 2006).	Surface membrane GPI anchored. Single EGF domain (Black et al., 2002).	A single protein homology to both MSP-4 and MSP-5 (Kedzierski et al., 2000).

P. falciparum gene	RBC binding in *P. falciparum*	Protein function and characteristics in *P. falciparum*	Homolog in *P. vivax*	Homolog in *P. berghei*
msp-5 (Marshall et al., 1998)	Unknown*	Non-essential (Sanders et al., 2006).	Associated with the micronemes. Single EGF domain (Black et al., 2002).	A single protein homology to both MSP-4 and MSP-5 (Kedzierski et al., 2000)
msp-6 (Singh et al., 2009)	Unknown*	Member of MSP-3 family. Non-covalently binds with MSP-1 and MSP-7. (Carlton et al., 2008). KO studies not published.	No homolog (Carlton et al., 2008)	Unknown*. Work on MSP-7 KO did not investigate relationship (Tewari et al., 2005).
msp-7 (Stafford et al., 1996)	Unknown. Binding observed to non-RBC ligand P-Selection (Perrin et al., 2015)	Forms a complex with MSP-1 and MSP-6 Multi-gene family. Includes MSRP genes (Kadekoppala et al., 2010)	Multi-gene family. No reported EGF domains (Castillo et al., 2017)	KO: invasion attenuated. Impaired invasion of erythrocytes but not reticulocytes (Tewari et al., 2005).
msp-8 (RMP-1) (Black et al., 2001)	Unknown*	Not present on the merozoite surface. Expressed during ring stage. Non-essential. (Black et al., 2001).	Surface membrane GPI anchored. Smaller protein then in *P. falciparum* (Fearon et al., 2015).	Surface membrane GPI anchored. KO: Non-essential. Highly conserved EGF domains between *P. falciparum and P. vivax* (de Koning-Ward et al., 2008; Fearon et al., 2015).

P. falciparum gene	RBC binding in *P. falciparum*	Protein function and characteristics in *P. falciparum*	Homolog in *P. vivax*	Homolog in *P. berghei*
msp-10 (Black et al., 2003)	Unknown*	Esential (Sanders et al., 2006).	Surface membrane GPI anchored. Smaller protein then in *P. falciparum.* Two EGF domains (Fearon et al., 2015).	Surface membrane GPI anchored. KO: Non-essential Relatively highly conserved EGF domains between *P. falciparum and P. vivax* (Fearon *et al.*, 2015).
pf38 (Sanders et al., 2005)	Unknown*	GPI-anchored. 6-cys domain (Feller et al., 2013).	Located on merozoite surface (Mongui et al., 2008).	Non-essential (Van Dijk et al., 2010).
pf92 (Sanders et al., 2007)	Unknown*	6-cys domain. Essential (Sanders et al., 2006).	Highly conversed N-terminal cysteine residues (Seong-kyun et al., 2016)	Unknown*
pf41 (Sanders et al., 2005)	Unknown*	Two tandem 6-cys domains (Parker et al., 2015)	Two s45/48 domains. 6-cys domain (Angel et al., 2008)	Syntenic with *P. falciparum* (Thompson et al., 2001a).
Stevor (Blythe et al., 2008)	Glycophorin C (Niang et al., 2014)	Multi variant gene family	Unknown*	Unknown*

Table 1.1 Characteristic features of parasite ligands that facilitate initial low affinity binding. Asterisk (*) denotes where literature could not be found.

The refractory nature of *pfmsp1* to genetic disruption highlights its essential role in host cell invasion (Sanders et al., 2006). Thus it is unsurprising that despite being under selection pressures from the host antibody response, the genetic sequence of *pfmsp-1* contains regions of highly conversed sequence, in particular the region containing MSP-1_{19} (Takala and Plowe, 2009). Predictably, many invasion inhibiting antibodies bind to MSP-1_{19}, with the abundance of anti- MSP-1_{19} antibodies correlating strongly with *P. falciparum* malaria resistance in West African countries (Branch et al., 1998). Consequently, this fragment has become a vaccine target (Ockenhouse et al., 2006).

Additional surface proteins localising to the merozoite surface have been identified in *P. falciparum,* including a number of MSPs, some of which also undergo proteolytic-processing and form complexes with MSP-1 (MSP-6&7, MSP-9)(Baldwin et al., 2015). Many of these identified proteins have homologs in both *P. vivax* and *P. berghei*. Nonetheless there are structural differences between corresponding MSPs homologs indicative of functional differences (Table 1.1). This could be a mechanism for the divergent tropisms between the parasite species, with the *P. vivax* and *P. berghei* MSP homologs binding reticulocytes preferentially. Moreover, the corresponding host receptor for the vast number of surface proteins has not been identified. As such, the role initial binding plays in restricting the parasite to a particular host cell lineage and maturation point are under-investigated.

1.2.10 High Affinity Binding

After initial low affinity attachment, the merozoite must re-orientate to bring its apical end in contact with the host cell plasma membrane. Live cell imaging of merozoites treated with a drug inhibiting the actin-myosin (glideosome) motor showed that the motor is not required for apical reorientation (Weiss et al., 2015). However, the GPI-anchored merozoite surface coat proteins are only attached to the outer leaflet of the parasite plasma membrane. Reorientation requires ligands that can span the whole plasma membrane and can associate with the parasite cytoskeleton (Weiss et al., 2016).

High affinity binding between the apical end of *P. falciparum* merozoites and the host cell is mediated by proteins from two families: the erythrocyte-binding antigens (EBA) [also known as erythrocyte-binding ligands: EBL] and the reticulocyte-binding protein homologues (PfRH family). The availability of the complete *P. falciparum* genome has indicated that EBA family consists of the functional proteins: EBA-175, EBA-181 (as known as JESEBEL), EBA-140 (BAEBL) and EBA-1 (Figure 1.9). The PfRH family consists of the functional proteins: PfRH1, PfRH2a, PfRH2b, PfRH4 and PfRH5 (Figure 1.10). Singh *et al* (2010) observed that the binding of an EBA (EBA-175) protein to its corresponding host receptor restores the cytosolic calcium levels to basal levels, triggering the release of PfRH proteins from the rhoptry neck (Weiss et al., 2016). Nonetheless, there is evidence that the release of the rhoptry neck proteins occur in a more staggered and sequence manner. Antibodies against PfRH1 block the surface localisation of EBA-175 and subsequent invasion, thus indicating that at least one PfRH protein is released prior to EBA-175 binding (Gao et al., 2013).

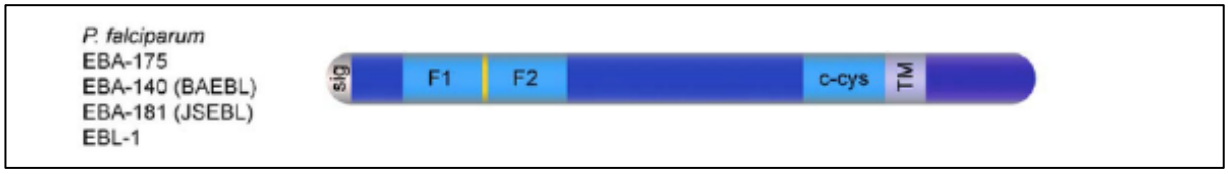

Figure 1.9 Secondary domains of EBA proteins (Howell et al., 2006). F1 and F2 are the two Duffy binding like (DBL) domains. This domain derives its name from its homology to the domains of the *P. vivax* ligand that binds the Duffy antigen receptor. TM is the trans membrane domain; c-cys is the C terminal cysteine rich domain; sig is the signal sequence.

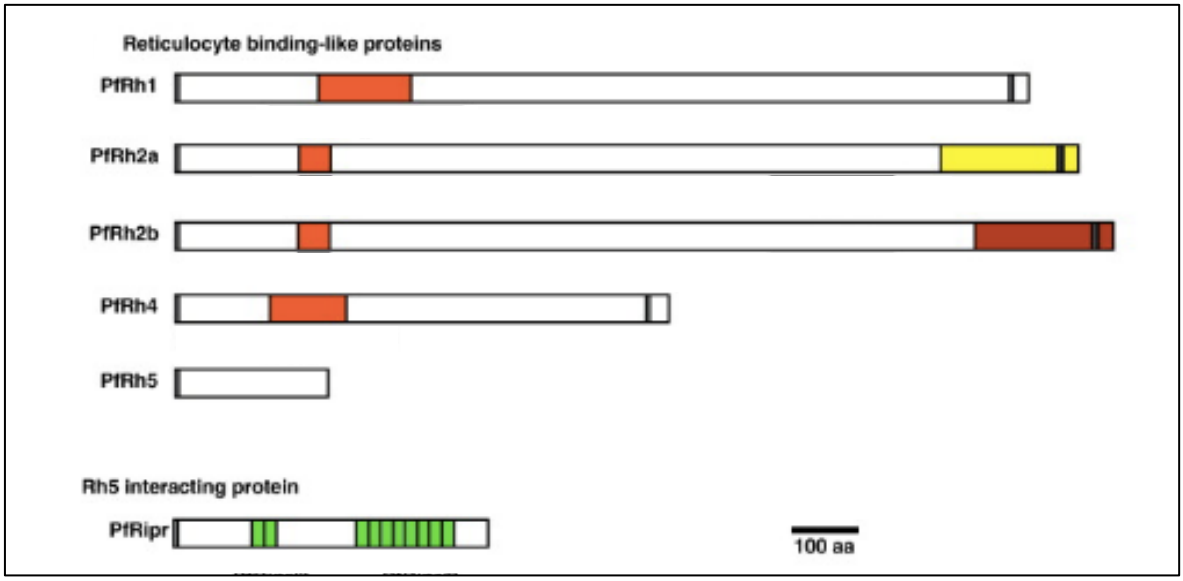

Figure 1.10 Secondary domains of PfRH proteins (Gaur et al., 2016). **Orange** are the erythrocyte binding domains (EBD). This domain contains a high alpha helical content reflective of DBL domains. Not marked here are the nucleotide binding region that is in close proximity to the EBD (Grüber et al., 2011). The C-terminus is on the right hand side; the N-terminus is on the left. The former contains a trans-membrane domain and the latter a signal peptide. Pfrh5 does not have a transmembrane domain, instead it is held at the merozoite surface by PfRipr. **Yellow and red** are the sequence difference between PfRH2a/b. **Green** are EGF domains (Weiss et al., 2016).

The irreversible, stable binding mediated by the EBA and PfRh proteins indicates that the attachment of these adhesins to their erythrocyte receptors commits the merozoite to invasion (**Figure 1.**11). Evidence has also been presented that indicates apical adhesin binding is somewhat of a 'starting pistol' for erythrocyte invasion and the sequential downstream events take place without any further checkpoints ensuring co-ordination or successful execution (Riglar et al., 2011, 2015). Secretion of rhoptry bulb proteins has been observed during the inhibition of moving junction formation leading to the organelles contents being erroneously discharged onto the erythrocyte surface (Treeck et al., 2009).

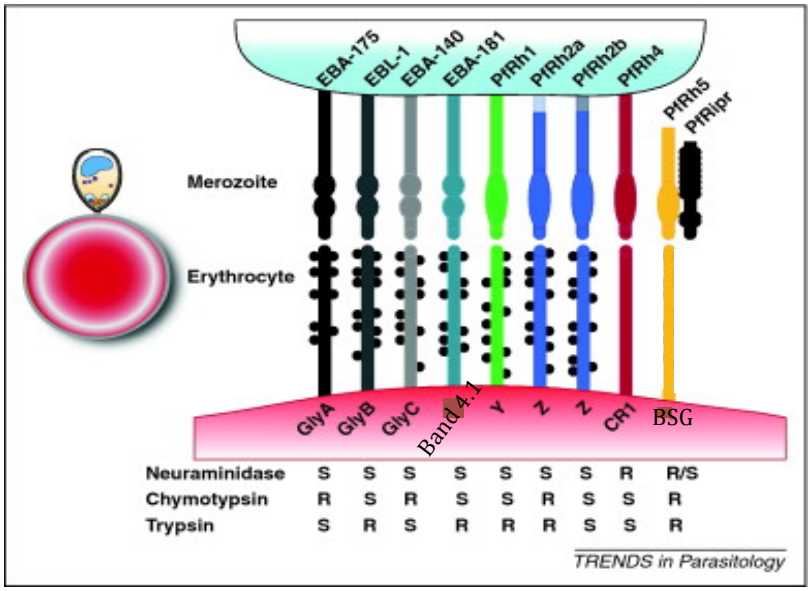

Figure 1.11 Ligand receptor binding (Tham et al., 2012)**.** Resistance (R) or sensitivity (S) of a ligand-receptor interaction to enzyme treatment (neuraminidase; chymotrypsin; trypsin) is indicated in the bottom part of the diagram. EBA-175 and EBA-140 bind to Glycophorins A and C respectively in what is considered a sialic acid-dependent manner due to the sialic acid residues attached to the O-linked oligosaccharides. Likewise, EBA-181 (receptor band 4.1), EBA-1 (binding Glycophorin B), PfRH2a/b (binding Receptor Z), and PfRH1 (unknown receptor Y) all bind to the erythrocyte in a sialic acid-dependent manner. PfRH4 (binding CR1) and PfRH5 (binding BSG; Basigin) both bind to the host cell in a manner considered to be

1.2.11 Transcriptional Regulation

Transcriptomics and proteomics investigations have observed differential patterns of expression for the functional members of the *eba* and *pfrh* gene families between laboratory strains originally isolated from different global locations (Gaur and Chitnis, 2011). The first evidence for variegated expression in *P. falciparum* was obtained from two studies which identified that *pfrh2a* and *pfrh2b* were transcriptionally silent in certain long term clonal culture adapted parasite lines, but not in others despite all strains containing both genes intact within their genome (Taylor et al., 2002). The cohort of ligands expressed together defines what is called the parasite's 'invasion pathway'.

The invasion pathways have been characterised based on the chemical properties of the host receptors required to achieve invasion (Figure 1.11). The 'invasion pathway' of a particular parasite can be phenotyped as either sialic acid dependent or independent through the use of erythrocytes which are

depleted of certain classes of host receptors. Classically this has been achieved through treatment of the host cells with particular enzymes. The three most common treatments use the enzymes neuraminidase (removes sialic acid from glycophorins), trypsin (cleaves glycophorin A and glycophorin C) and chymotrypsin (cleave glycophorin B). Such experiments classify a parasites invasion pathway broadly as either sensitive (cannot invade) or resistant (can invade). Sensitivity to neuraminidase characterises a parasite strain's invasion pathway as sialic acid-dependent, whereas, resistance to this treatment indicates a sialic acid-independent invasion pathway. (Cortés, 2008; Tham et al., 2012).

The variant expression patterns of *eba* and *pfrh* have hallmarks of epigenetic regulation, a bistable and consequently reversible mechanism that governs phenotypes without genomic editing. The *P. falciparum* genome is 22.9 Mb in size and organised across 14 chromosomes (Gardner et al., 2013) with a high proportion maintained as euchromatin (open/ accessible chromatin). However, regions of heterochromatin (inaccessible chromatin) have been reported to stretch from telomeres to subtelomeric domains, which, incidentally are the location of the *eba* and *pfrh* genes (Weber and Henikoff, 2014; Duffy et al., 2014; Gardner et al., 2002). The heterochromatin maintains clusters of silenced genes through an increased presence of histone-packed nucleosomes governed by associated post-translation modifications and histone tail binding proteins such as canonical heterochromatin protein 1 (HP1) (Weber and Henikoff, 2014; Duffy et al., 2014; Flueck et al., 2009). Various histone tail modifications have been identified in the parasite, with 88 of them being unique to *Plasmodium* (Saraf et al., 2016). Various epigenetic modulators catalysing the removal or addition of histone tail marks also have been identified in *Plasmodium* (Volz et al., 2010). *Plasmodium* contains only a single HP1 protein that localises primarily to the trimethylation lysine 9 of histone 3 (H3k9me3) mark and in turn recruits methyltransferases that modify adjacent nucleosomes, thus self-perpetuating heterochromatin spread (Lomberk et al., 2006).

Alongside the four canonical histones (H1-4) *Plasmodium* also expresses four variants: PfCenH3, PfH3.3, PfH2A.z and PfH2B.z (Duffy et al., 2014). These variants presumably have evolved to provide unique transcription regulation that

facilitates the transient and temporal expression of all stage specific open reading frames throughout the parasite life cycle. Supporting this, the PfH2A.z and PfH2B.z variants are enriched at the 5' UTRs of genes expressed during the blood stage development (Bártfai et al., 2010; Hoeijmakers et al., 2013). The covalent modification of histone protein tails is a stable mechanism of heritable epigenetic transcriptional regulation. The histone tails undergo a number of posttranslational modifications that interact with DNA cytosine (me^5C) methylation, which, by broad definition, regulate the bistable compact structure of chromatin, thus controlling the physical accessibility of DNA to transcriptional regulators (Jin et al., 2011). A chromatin immunoprecipitation (ChIP) study on a parasite line that expresses *pfrh4* during merozoite invasion showed that the transcriptional regulation of this gene is sequentially controlled by the removal of the silencing H3k9me3 mark and the addition of the activating acetylation during schizont maturation (H3K9ac) (Jiang et al., 2010). The low GC content of the *Plasmodium* genome was an impediment to early investigations into the parasite me^5C content. Nonetheless, a recent study coupling the bisulfite conversion of unmethylated cytosines with high throughput sequencing generated a genome wide map of *P. falciparum* me^5C (Ponts et al., 2013).

As discussed, the malaria parasite nucleus is a heterogeneous organelle containing multiple active and silent chromatin domains. Studies of the incorporation of 5-bromo-uridine 5'-triphospate (BrUTP) in mammalian cells showed that transcription occurs at discrete foci throughout the nucleus (Iborra et al., 1996). The same is true for *Plasmodium*. Active genes are preferentially localised to transcriptionally permissive regions containing the histone tail-modifying enzymes and DNA methylases, whereas silent genes group outwith this region in perinuclear repressive subtelomeric clusters (Coleman et al., 2012). The telomeric sequences tether chromosomes to the perinuclear region in these clusters through interactions between telomere-associated repeat elements (TAREs) and additional uncharacterised proteins (Duffy et al., 2016). Coleman *et al* (2012) showed that *pfrh4* clusters within the repressive perinuclear regions within clonal parasites that do not express it. Activation of *pfrh4* could be forced in these parasites by the expression of an adjacent transgene, thus forcing recruitment of this chromosomal region to an active site. For a silenced gene to be activated it could either leave the subtelomeric cluster and move to

the active site as a solitary chromosome (Mok et al., 2008), or form an active site *in situ* (Marty et al., 2006), evidence exits to supporting both theories (Figure 1.12).

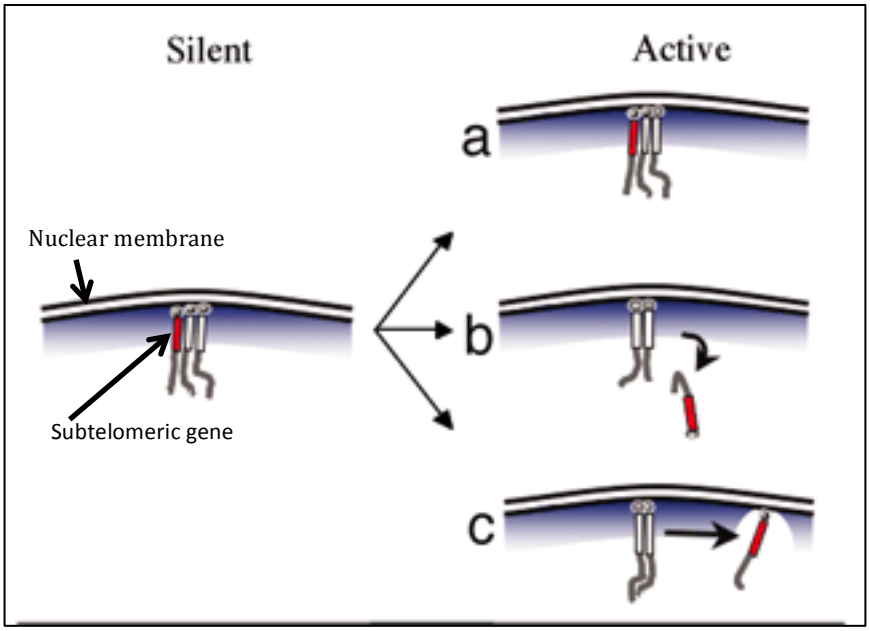

Figure 1.12 Subtelomeric multi gene family silencing and activation (Ralph et al., 2005)**.** Inactive genes cluster within subtelomeric clusters (left hand side; silent) associated with the nuclear membrane. Circles associated with the nuclear membrane represent telomere ends. Rectangles represent subtelomeric genes; lines protruding from rectangles represent the rest of the chromosome. Red rectangle represents subtelomeric gene about to be/ being transcribed. Several mechanisms of activation have been proposed. A. *in situ* recruitment of machinery for activation (red) telomeric gene. B and C activation of (red) gene after moving from the cluster. This can either be away from the nuclear membrane periphery (B) or remaining at the nuclear periphery but disassociating from the cluster (C).

1.2.12 Functional Redundancy

Genetic disruption studies have shown the variantly expressed invasion ligands are largely functionally redundant, with the loss of any given ligand being compensated by transcription and utilisation of an alternative ligand-receptor interaction (Duraisingh et al., 2003; Gunalan et al., 2011). It has been observed that high *pfrh1* expression negatively correlated with the expression of *pfrh2a/b* implying overlapping function in invasion and consequently, functional

redundancy within the PfRh family (Duraisingh et al., 2003; Nery et al., 2006). Moreover, overlapping function does not exclusively reside within a gene family; there is evidence to indicate functional compensation between *eba* and *pfrh* genes (Stubbs et al., 2005). Stubbs et al (2005) observed an increased expression pattern for PfRH4 when *eba-175* was genetically disrupted. Interestingly, PfRH5 is not only structurally distinct from the other proteins in its family, it is also ubiquitously expressed and functionally essential among all laboratory strains (Weiss et al., 2016).

Interestingly, simultaneous genetic disruption of the three genes *eba-175*, *pfrh4* and *pfrh2b* produces a nonviable parasite line in any laboratory parasite strain tested. The refractory nature of the triple knockout is highly indicative of a minimal requirement in ligand-receptor complement for invasion (Tham et al., 2012). Moreover, antibodies reactive with specific EBA and PfRH proteins inhibit invasion, thus indicating that each specific ligand in any given cohort of temporally expressed ligands is essential for invasion (Table 1.2).

Ligand	Genetic disruption
EBL-175 (Lee et al., 1990)	KO. Non essential (Lopaticki et al., 2011)
EBL-1 (Peterson and Wellems, 2000)	Not expressed in some clonal lines (Lopaticki et al., 2011)
EBA-140 (Thompson et al., 2001b)	KO. Non essential (Lopaticki et al., 2011)
EBA-181 (Gilberger et al., 2003)	KO. Non essential (Lopaticki et al., 2011)
PfRH 1 (Rayner et al., 2001)	KO. Non essential (Gao et al., 2008)
PfRH 2a (Rayner et al., 2000)	KO. Non essential (Duraisingh et al., 2003)
PfRH 2b (Rayner et al., 2000)	KO. Non essential (Duraisingh et al., 2003)
PfRH 4 (Kaneko et al., 2002)	KO. Non essential (Reiling et al., 2012)
PfRH 5 (Kaneko et al., 2002)	Cannot be disrupted (Baum et al., 2008)

Table 1.2 Genetic disruption of EBA and PfRH proteins

1.2.13 *P. vivax* Alternative Invasion Pathways

Whilst the literature is conspicuously silent in terms of studies on *P. berghei* merozoite invasion ligands, a protein (PBANKA_1332700) was identified in a proteomic and transcriptomic study containing a Duffy binding domain (Hall et al., 2005). In contrast, *P. vivax* has been highly characterised as containing the Duffy binding protein (DBP) paralogs and the reticulocyte-binding proteins (RBPs) (Menard et al., 2013; de Sousa et al., 2014). The formation of irreversible merozoite attachment is mediated by PvDBP, a microneme protein that is related to *P. falciparum* EBA protein family, binding to the Duffy blood group antigen (Figure 1.13). As such, Duffy binding was believed to be essential for *P. vivax* invasion. This was supported by the discovery of a second Duffy-dependent ligand, antigenically distinct from PvDBP, the erythrocyte binding protein (EBP2) that binds exclusively to reticulocytes (Ntumngia et al., 2016). Moreover, studies in the monkey-infective parasite *P. knowlesi,* showed that genetic disruption of the PvDBP homolog prevented merozoite invasion (Singh et al., 2005). This species is evolutionarily related to *P. vivax* and relies exclusively on the Duffy receptor for invasion of human erythrocytes *in vitro*. However, *P. knowlesi* can invade rhesus monkey erythrocytes in a Duffy-independent manner (Paul et al., 2016). Recent work has identified that the PvRBP family contains 11 paralogs, two of which (PvRBP1a and PvRBP2a) can also bind independently of the Duffy antigen (Figure 1.14) (Li and Han, 2012; Galinski et al., 1992; Han et al., 2016). Moreover, the qPCR analysis of different *P. vivax* Thailand isolates demonstrated a high variation in PvRBP expression (Hietanen et al., 2016). Taken together this suggests that additional *Plasmodium* species can achieve invasion via an alternative pathway reflective of the multiple invasion pathways exhibited by *P. falciparum*

Figure 1.13 Secondary domains of DBP proteins (Howell et al., 2006). DBL is the Duffy binding like domains. TM is the trans membrane domain; c-cys is the C terminal cysteine rich domain; sig is the signal sequence. Note the difference between *P. falciparum* EBA and this DBP: this protein contains only one DBL domain.

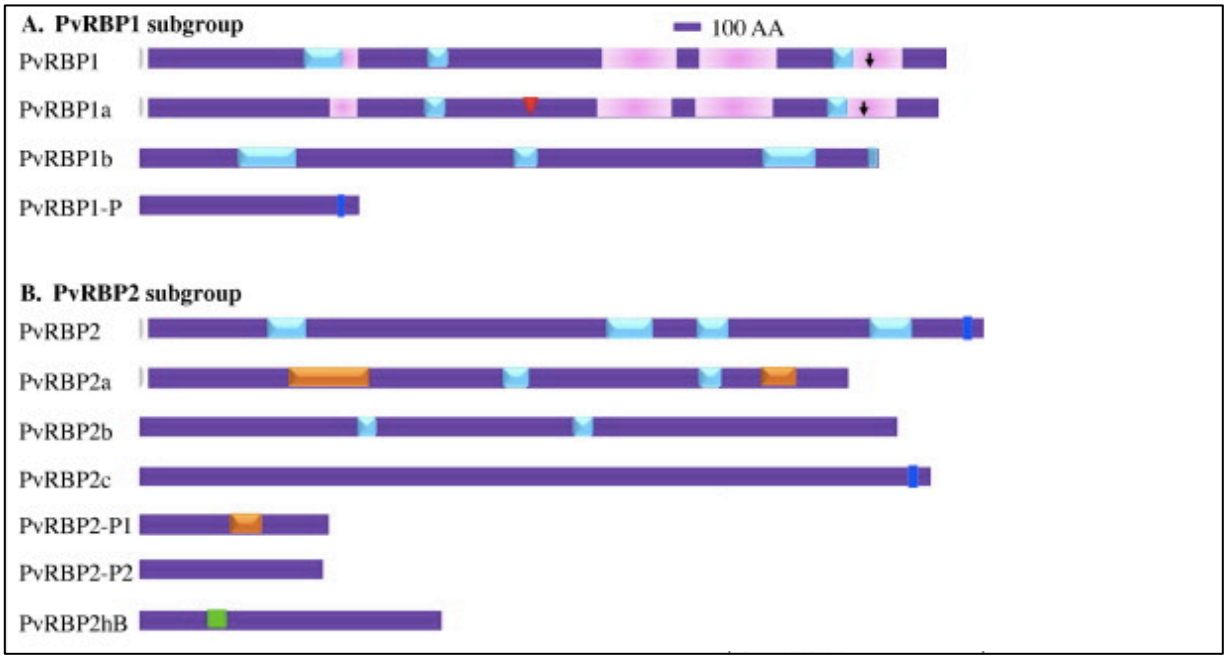

Figure 1.14 Secondary domains of the PvRBP proteins (Li and Han, 2012). White region; signal peptide. Dark blue region; trans membrane domain. Light blue region; internal repeat region. Pink domain; reticulocyte binding domains. Green region: ribosomal protein S1-like RNA-binding domain.

1.2.14 Confining *P. vivax* to Reticulocytes

Although *P. vivax* lacks an obvious homolog to the essential and ubiquitous PfRH5 ligand, analysis of the PvRBP2a crystal structure showed structural conservation with that of the PfRH5 scaffold (Gruszczyk et al., 2016). Although the invasion pathway of PvRBP2a was characterised as different to the host receptor of PfRH5, the authors noted that PvRBP2a could bind equally to erythrocytes and reticulocytes (Gruszczyk et al., 2016). The erythrocyte-binding domain of PvRBP1a has been identified as a homologous region to PfRH4, suggesting that they may share a common host receptor, the complement receptor 1 (CR1) (Han et al., 2016). CR1 is present on both erythrocytes and reticulocytes (Gruszczyk et al., 2016), nonetheless, Han *et al* (2016) observed a significantly higher binding activity of PvRBP1a to reticulocytes compared with erythrocytes. However, Han *et al* (2016) based their assessments on the expression of only the putative functional domain of PvRBP1a, whereas a contemporary study that attributed significant erythrocyte binding to PvRBP1a used the whole protein (Franca et al., 2016). The Duffy binding protein PvDBP, has been identified as

having a significant reticulocyte binding preference (Han et al., 2016). This may be reflective of the decrease in Duffy abundance during reticulocyte to erythrocyte maturation (Liu et al., 2010). Taken together, it can be suggested that the *P. vivax* expressed cohort of invasion ligands defines parasite cellular tropism. However, it could also be suggested that the phenotype of the host cell supplies a selection pressure in terms of the cohort of invasion ligands the parasite expresses.

1.2.15 Host Genotype Influencing the Tropism of *P. vivax*

Efforts to identify host determinants for *Plasmodium* invasion have been hindered by the absence of a nucleus in peripheral blood erythrocytes and reticulocytes. This precludes direct genetic manipulation of these maturation stages. Nonetheless, aberrant erythrocyte receptor phenotypes and additional polymorphisms that confer resistance to malaria have been identified through epidemiological studies (Network, 2015). For example, the West African centric polymorphisms in the Duffy blood group antigen overlaps with the geographical low prevalence of *P. vivax* (Gething et al., 2012). The monogenic Duffy antigen (FY) exhibits two main co-dominant alleles known as Fya and Fyb, the result of a single point mutation swapping glycine to asparagine within the protein. These alleles combine as four erythrocyte phenotypes; Fya+b+, Fya-b+, Fya+b-, Fya-b-. The latter phenotype is the result of disruption within the Fy promoter region thus preventing transcription (Howes et al., 2011). Recent mapping of the global distribution of the mutated promoter revealed a 90% fixation of this allele within sub-Saharan Africa, with a 98-100% frequency of the homozygous Duffy negative phenotype (Figure 1.15) (Howes et al., 2011).

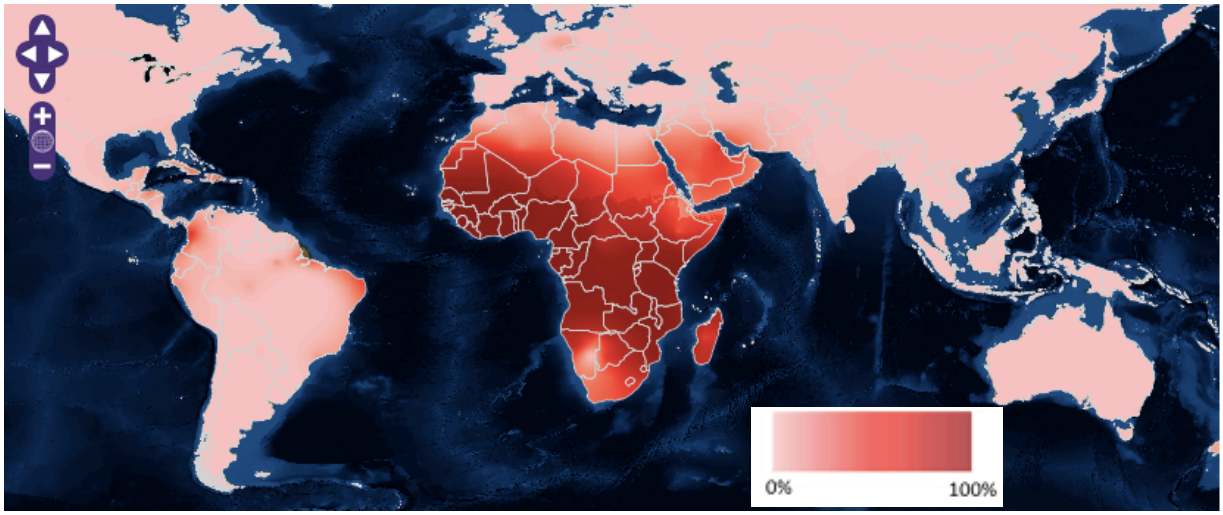

Figure 1.15 Global distribution of homozygous Duffy negative phenotype (MAP, 2015). Key displays the estimated percentage of the population (country) effected at any given time during 2010.

Unsurprisingly, due to the previous discussion concerning alternative invasion pathways, Duffy negative individuals have been observed to be infected with *P. vivax* in Africa. What is surprising though, is that genetic screens have attributed this parasite invasion phenotype to copy number variations in the PvDBP (Gunalan et al., 2016; Pearson et al., 2016; Hostetler et al., 2016), paralogs that were later shown to bind in only a Duffy-dependent manner (Gunalan et al., 2016). The absence of transcriptional studies on these isolates is probably the reason that their Duffy negative invasion phenotype has not been discussed in the context of the variant expression of the PvRBP family (Gunalan et al., 2016; Pearson et al., 2016; Hostetler et al., 2016). Exasperatingly the reports also lack a description of whether these parasites are invading reticulocytes or erythrocytes.

Nevertheless, studies investigating the reticulocyte preference of *P. vivax* isolates from India noted high erythrocyte invasion (Lim et al., 2016). The most frequent Fy allele in this region is Fya (Howes et al., 2011). The homozygous expression of Fya has been observed to decrease *P. vivax* binding by 50% compared to Fyb (King et al., 2011). Thus it is tempting to conclude that the host FY phenotype is exerting a selection pressure on the parasite to invade using a PvRBP pathway, which culminates in parasitisation of erythrocytes.

1.2.16 Host Genotype and *P. falciparum* Invasion

Naturally occurring host receptor polymorphisms, such as Basigin Ok(a-) variants and glycoprotein null cells, have also been used to determine the specificity of ligand binding and how essential particular interactions are to invasion by *P. falciparum* (Bei and Duraisingh, 2012). However, unlike the FY phenotypes, such polymorphisms are rare and are as such unlikely to be under balancing selection by regional *Plasmodium* infection rates. A recent large scale knockdown study genetically manipulated the nucleated erythrocyte precursor cells of human blood *in vitro* and identified the glycophorin proteins as non-essential for *P. falciparum* invasion (Egan et al., 2015). As such, there would be no selective advantage for the glycophorin null cell phenotypes in malaria endemic regions. During this large scale knockdown, Egan *et al* (2015) also identified a host receptor that had not previously been implicated in *P. falciparum* invasion. The screen observed that multiple laboratory strains and field isolations could not infect $CD55^{-/-}$ cells, nonetheless, the corresponding parasite ligand is yet to be identified (Egan et al., 2015).

Intriguingly, it has been shown in *P. falciparum* that the EBA and PfRH proteins mediating attachment of merozoites to an erythrocyte induce the local phosphorylation of the host cell cytoskeleton (Zuccala et al., 2016). In circulation, the host erythrocyte is subjected to large shearing forces, and as such, the cell has unrestricted deformability in order to prevent structural damage. The biochemical dimerisation and disassembly of spectrin, a protein that lies under the plasma membrane, facilitates cellular distortion (An et al., 2002). Antibodies targeting the EBA-175 receptor GPA have been shown to decrease the erythroid cells deformability due to increased cross-linking between the cytoskeleton and the receptor cytoplasmic tail (Chais et al., 2011; Koch and Baum, 2015). In stark contrast, PfRH4 binding to the CR1 receptor triggers phosphorylation of spectrin decreasing membrane stability (Glodek et al., 2010). Although it remains unclear how changes to the spectrin cytoskeleton that increase rigidity would facilitate invasion, it is clear that surface ligand-receptor interactions trigger internal processes in the host cell altering its biophysical architecture (Koch and Baum, 2015).

1.2.17 Moving Tight Junction

Once apical re-orientation is complete (Figure 1.16), the rhoptry neck (RON) protein complex is discharged and implanted into the erythrocyte so that apical membrane antigen 1 (AMA1) can lock with it and form a tight junction. The tight junction is a ring of direct association between the invading parasite and host membrane. There is evidence that the trigger for RON secretion is PfRh5 binding in *P. falciparum*. Antibodies against this parasite ligand block invasion at a point after apical reorientation (Weiss et al., 2015).

Although it is possible that the RON complex proteins associate with a host cell receptor to provide anchorage, this has not been shown experimentally. However, there is indirect evidence that AMA1 forms an association with the host's Kx protein (Kato et al., 2005). Kato *et al* (2005) showed that recombinantly expressed AMA1 could bind wild type erythrocytes but not Kx $^{-/-}$ cells. This interaction may define the localisation of the tight junction on the erythrocyte surface (Satchwell, 2016). Nonetheless, there is strong but controversial evidence that the AMA1 interaction with the RON complex is not essential for tight junction formation and that this complex, when formed, is not involved in transduction of the force generated by the glideosome (Bargieri et al., 2013). In contrast, the microneme-secreted merozoite thrombospondin-related anonymous protein (MTRAP), a transmembrane protein, has been identified as an essential bridge between the actin-myosin motor and the extracellular surface. The *mtrap* gene is conserved and syntenic among *Plasmodium* species (Baum et al., 2006). Its essential contribution to merozoite invasion was illustrated by unsuccessful attempts to genetically disrupt it (Baum et al., 2006). The host receptor for MTRAP is believed to be Semaphorin 7a (Bartholdson et al., 2012)

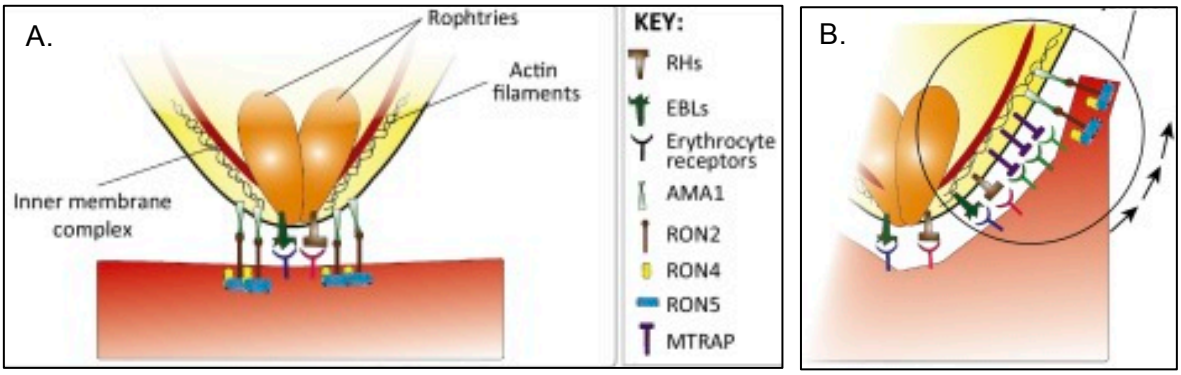

Figure 1.16 Formation of the tight and moving junction (Ahouidi et al., 2016). A. Merozoite re-orientation is associated with ligand-receptor binding. B. The secretion of MTRAP, a protein associated to the glideosome, and its binding to its host receptor allows the parasite to move into the host cell.

1.2.18 The Parasitophorous Vacuole

The invasion event places the parasite within a parasitophorous vacuole (PV), the membrane of which (PVM) is derived from the host plasma membrane. (Dluzewski et al., 1992). The PVM forms a significant barrier to the uptake of nutrients or the export of parasite-derived proteins, although one parasite protein EXP2, is thought to be involved in both processes. This protein was initially characterised as localising to the PVM and being expressed throughout the entire intra-erythrocytic lifecycle (Fischer et al., 1998). Genetic disruption experiments in the *Apicomplexa* parasite, *Toxoplasma gondii,* targeting the EXP2 ortholog, GRA17, showed that the PV of GRA17 null parasite was impermeable to fluorescent solutes that can diffuse into the PV of wild type parasite (Gold et al., 2016). This suggested a role for EXP2 in forming a pore in the PVM (Figure 1.17). In contrast to nutrient uptake, export of parasite derived proteins is mediated by a protein complex called the *Plasmodium* translocon of exported proteins (PTEX)(Sherling and van Ooij, 2016). Recent work has shown that improperly folded exported proteins jam EXP2 suggesting that this protein is the central translocation channel for exported proteins (Mesen-Ramirez et al., 2016). Interestingly, data exists suggesting that the localisation of the PTEX to the PVM varies according to host cell. The PTEX and EXP2 of *P. falciparum* and *P. berghei* parasitised reticulocytes were partially located outside of the PVM in vesicles (Meibalan et al., 2015). Although these structures have been linked to

the relatively heightened nutrient contents of the reticulocyte compared to erythrocytes, a functional role in parasite metabolism has yet to be assigned to them.

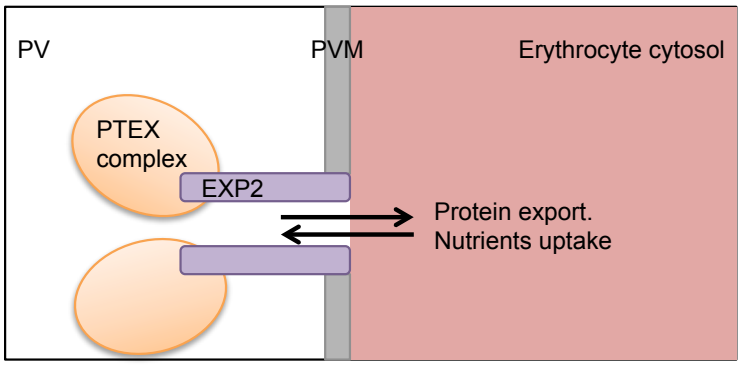

Figure 1.17 The EXP2 pore in the PVM. Simplified schematic of the proposed mechanism of PTEX mediated protein export and nutrient uptake. After being desposited into the PV, proteins destined for export cross the PVM via the EXP2 channel in association with the PTEX complex (Sherling and van Ooij, 2016).

1.2.19 Intracellular Life Cycle

The asexual life cycle of both *P. falciparum* and *P. vivax* is completed in 48 hours (hrs) from the point of invasion to the point of egress, whereas, murine infective *P. berghei* has a life cycle duration of 22-24 hrs. Initially, within the erythrocyte, the parasite takes on a flattened ring morphology, before morphing into an engorged, rounded trophozoite after which the multiply-nucleated schizont breaches the host cell releasing invasive merozoites (Bannister et al., 2000).

During development, the parasite exports 8% of its predicted proteome (400 proteins) to the host cell, 25% of which are essential to parasite survival (de Koning-Ward et al., 2016). Proteins such as the ring-infected erythrocyte surface antigen (RESA) become associated with the host's cytoskeleton and others, such as the *P. falciparum* erythrocyte membrane protein 1 (PfEMP1) protein family, are inserted into the host cell plasma membrane (Da Silva et al., 1994; Kriek et al., 2003). These proteins are tracked through the PTEX via the inclusion of the pentameric *Plasmodium* export element (PEXEL) (Mesen-Ramirez et al., 2016). Nonetheless, a number of exported proteins, such as the PfEMP1, are PEXEL

negative and instead contain an internal transmembrane segment or N-terminal signal sequence that functions as an endoplasmic reticulum target and license for export (de Koning-Ward et al., 2016). A prominent feature of parasite protein export is the creation of an exomembrane, a system strongly characterised by the Maurer's clefts. These structures are closed cisternal compartments that are formed by the parasite within the host cytosol soon after invasion. Maurer's clefts are believed to act as a depot and chaperone for parasite proteins that are exported to the host membrane (Lanzer et al., 2006; de Koning-Ward et al., 2016). The structure is also associated with resident proteins, such as the PfEMP1 trafficking protein 1 (PTP1). During *P. falciparum* asexual development, the host erythrocyte membrane also becomes distorted with knob-like protrusions (Rug et al., 2014). These structures are created by the exported knob-associated histidine-rich protein (KAHRP) forming links with the erythrocyte cytoskeleton (Watermeyer et al., 2016). Host membrane remodeling decreases the deformability of the erythrocyte. Additional structural modifications have also been implicated in decreased deformability. Atomic force microscopy observed that the host's erythrocyte spectrin-actin cytoskeleton expands as the asexual parasite matures (Shi et al., 2013; Millholland et al., 2011). The parasite also seems to mine the host actin from the erythrocyte cytoskeleton junction points, redistributing it between the Maurer's cleft and the knob structures (Zhang et al., 2015). Moreover, *Plasmodium* conveys novel channel activity to the infected cell through formation of new permeation pathways that increase membrane conductance and induce uptake of small molecules, such as sugars and amino acids, used by the parasite for rapidly generating biomass (Decherf et al., 2004). Currently, the only characterised component of this pathway is cytoadherence-linked asexual gene 3 (CLAG3) (de Koning-Ward et al., 2016).

Interestingly, *P. falciparum* can establish infection within erythrocytes with mutations that reduce the host cells basal deformability (Boctor and Dorion, 2008; Muley et al., 2011; Makani et al., 2017). A comparison of *P. falciparum in vitro* growth within erythrocyte with the sickle cell or the wild type phenotype concluded that proliferation is dependent on oxygen availability rather than host cell rigidity (Orjih, 2005). It should be noted that the sickle cell mutation prevents the parasite actin remodeling of the host cell, thus preventing *P.*

falciparum displaying its adhesion proteins (Cyrklaff et al., 2010). Taken together, it would seem that the parasite growth and intra-erythrocyte survival is not dependent on initial erythroid cell deformability.

The parasite genome encodes for a complete *de novo* heme biosynthesis pathway (Sigala et al., 2015). However, genetic knock-out studies have shown the pathway is redundant during blood-stage infection, suggesting that the parasite can adequately scavenge host heme (Ke et al., 2014). From later ring stages, the parasite endocytoses large quantities of the host cell cytosol in order to digest the erythrocyte haemoglobin in an acidic compartment called the digestive vacuole. Excess heme, which is toxic to the parasite, is biomineralised into non-toxic hemozoin (Figure 1.18). Nonetheless, the fact that the pathway is essential for all other parasite life stages (Ke et al., 2014) highlights three things: firstly, the pathway is truly functional; secondly, heme is essential to metabolism at all stages; and thirdly, as the parasite can synthesise heme *de novo,* developing within a cell expressing hemoglobin is not a prerequisite to survival. This is interesting in the context of recent work that suggested that asexual blood stage *Plasmodium* could replicate within dendritic cells (Wykes and Horne-Debets, 2012).

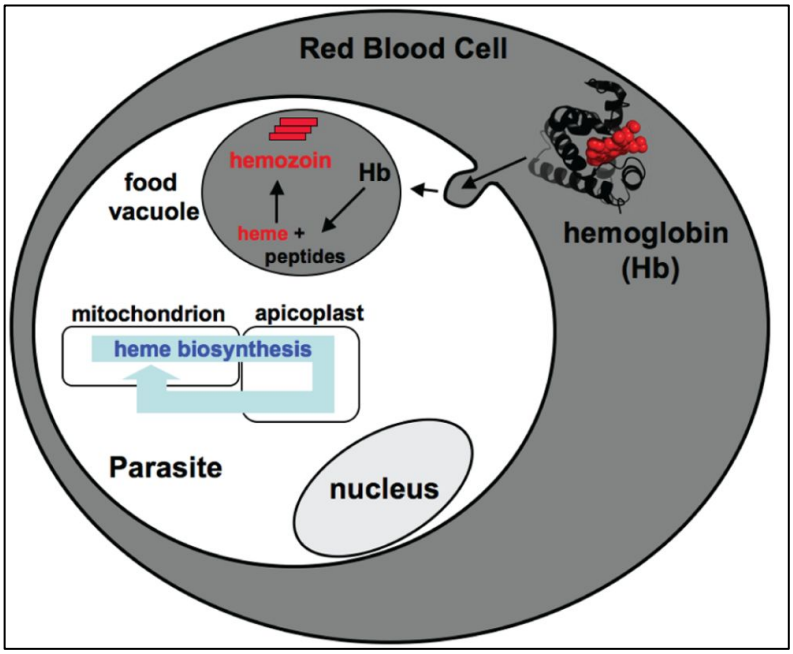

Figure 1.18 Heme metabolism (Sigala et al., 2012). Intra-erythrocyte parasite (white) generates heme by either degradation of host hemoglobin in the food vacuole (digestive vacuole), or by *de novo* biosynthesis co-ordinated between the mitochondria, apicoplast and cytosol. The mitochondria and the apicoplast are both symbiogenic organelles, with the apicoplast defining the phylum of *Apicomplexa*.

1.2.20 Sequestration of *Plasmodium*

Maturing trophozoites are the point in the parasite life cycle that the pathogenesis of *P. vivax* and *P. falciparum* malaria was classically believed to diverge. From this stage onwards *P. falciparum* is absent from peripheral blood (Carvalho et al., 2010). This is attributed to the ability of the parasite to sequester in the small blood vessels of organs. This is a cellular characteristic shared with *P. berghei* schizonts, although in this species the parasite-expressed proteins mediating cytoadherance remain undefined (Franke-Fayard et al., 2010, 2005). Recently, the low prevalence of circulating *P. vivax* schizonts lead researchers to postulate that this species also sequesters (Lim et al., 2016).

By the 1980's the proteins from the *P. falciparum* erythrocyte membrane protein 1 (PfEMP1) family were described to mediate the sequestering of the parasite by binding to multiple host receptors (Berendt et al., 1989; Udeinya et al., 1983). These parasite ligands are encoded by the diverse *var* multigene family that are mutually exclusively expressed (Baruch et al., 1995; Smith et al., 1995). There is some evidence that more than one *var* gene can be expressed at one time in a single cell (Joergensen et al., 2010). The same *var* gene(s) is transcribed from the immature trophozoite over many generations, but the parasite can switch to expression of a different *var* gene(s) therefore altering binding specificity and causing clonal antigenic variation (Duffy et al., 2016).

1.2.21 Epigenetic Expression of *var* Genes

The expression of *var* genes, like the invasion ligands, is regulated by epigenetic mechanisms. Silencing is associated with the enrichment of H3K9me3 and subteleomeric clustering at peri-nuclear locations, whilst enrichment in H3K9ac at 5'UTR is associated with transcriptional activation (Duffy et al., 2016). Moreover, the active *var* gene is transiently repressed in the mature trophozoite, an event associated with enrichment in H3K4me2 at the 5'UTR. This histone modification has been linked to epigenetic memory as the transiently repressed *var* gene is activated in the subsequent life cycle (Lopez-rubio et al., 2007; Duffy et al., 2016).

1.2.22 Diversity in the Genetic Sequence and Primary Structure

The *var* genes (approx. 60 prologs within the *P. falciparum* 3D7 genome) are divided into groups based on chromosomal location, upstream promoter sequence and transcriptional direction (Rovira-Vallbona et al., 2011). Group A, Group B and chimeric Group B/A var genes are located at subtelomeric regions of all chromosomes, but are transcribed in opposite directions (Claessens et al., 2014). Group C and chimeric Group B/C genes are found typically at internal regions on chromosomes 4, 7, 8 and 12 (Claessens et al., 2014). There is a single member of Group E *vars* called *var2csa* (Rovira-Vallbona et al., 2011).

The *var* genes contain two exons. Exon 1 encodes the extracellular part of the protein, whilst exon 2 encodes the trans membrane and intra-cellular segment. Exon 1, in contrast to Exon 2, is very genetically diverse leading to high inter and intra clonal variability between PfEMP1 protein primary structures (Rovira-Vallbona et al., 2011). Claessens *et al* (2014) was the first to show, using genetic crosses and whole genome sequencing of the cloned parental and prodigy lines, that *var* genes within groups B and C undergo ectopic recombination at a higher rate than any other region in the *P. falciparum* genome. The authors also observed that the greatest rates of recombination occurred during asexual mitosis. As such, they proposed a model whereby *var* gene diversity is generated during the asexual life cycle, while later meiosis events generate a new, although similar, repertoire of *var* genes derived from both parents (Claessens et al., 2014). Recombining var genes have low levels of sequence homology, thus the process is unlikely to be controlled by homologous recombination. Instead, subtelomeric clustering has been proposed as a mechanism of co-localising *var* genes from different regions in order to facilitate ectopic recombination (Claessens et al., 2014).

1.2.23 Conserved Secondary Domain Cassettes

The first exon of the *var* genes encodes a secondary structure containing a N-terminal segment followed by a succession of DBL and cysteine rich inter-domain regions (CIDR) domains (Claessens et al., 2014). The DBL and CIDR domains are subdivided into six and four major classes, receptively (Figure 1.19) (Smith et al., 2000). The architecture of these domains is preserved during the ectopic

recombination between subtelomeric *var* genes that fuels inter and intra clonal diversity (Claessens et al., 2014).

The different domain cassettes bind to different host receptors within a limited pool of specificity (Figure 1.19). All parasites seem to have the same fundamental repertoire of host receptor specificities (Mkumbaye et al., 2017). The group E VAR2CSA protein binds to placental chondroitin sulfate on chondroitin sulfate proteoglycans in the placenta syncytium. There is a clear link between this sequestration pattern and placental malaria in pregnant women (Pereira et al., 2016). As such, a number of studies have sought to correlate additional parasite sequestration patterns with disease outcome in paediatric malaria (Janes et al., 2011). While observations indicate that severe malaria pathology is associated with a limited number of antigen variants, this still remains relatively less established compared with pregnancy related malaria. (Janes et al., 2011; Nielsen et al., 2002). This may reflect acquisition of immunity to severe malaria following infection by a limited range of antigen variants associated with severe disease (Gupta et al., 1999). Moreover, sero-epidemological and var transcriptional studies have suggested that group A variants are more represented in isolates taken from African patients with severe malaria (Janes et al., 2011).

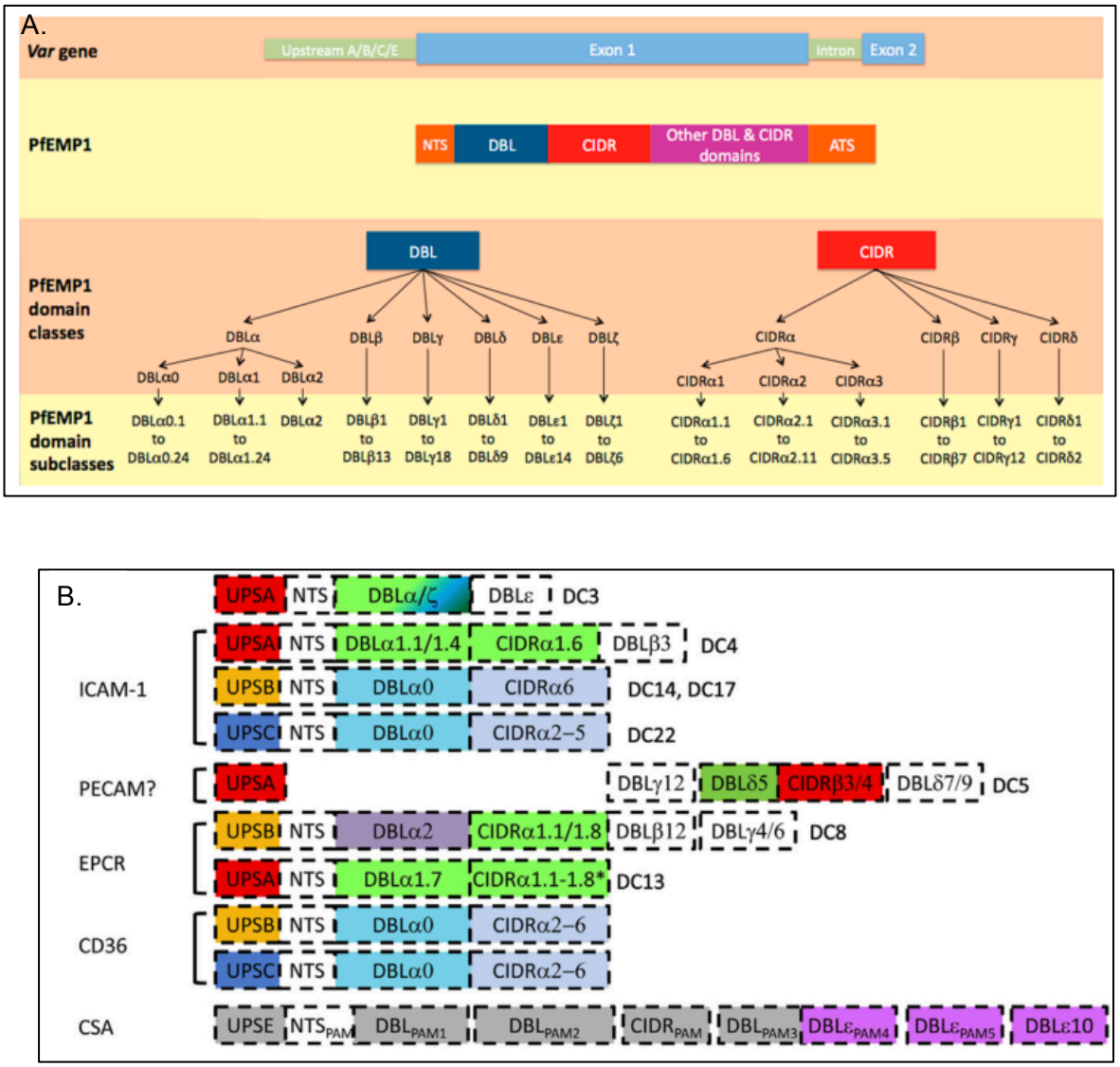

Figure 1.19 PfEMP1 structure and *var* gene groupings (Claessens et al., 2014; Hviid and Jensen, 2015)**. A.** schematic of *var* gene, exon 1 translated as PfEMP1 with different domain classes and further groupings. **B.** Tandem domain arrangements in the different var gene groups and the adhesion phenotypes.

To date most *P. falciparum* sequestration studies have focused on PfEMP1, however the gene families of repetitive interspersed family (*rif*) and the subtelomeric variant open reading frame (*stevor*) proteins also play a role. The *rif* genes encode the second largest variant surface antigen protein family in the *P. falciparum* genome (Goel et al., 2015). These proteins are expressed on the surface of asexual infected erythrocytes and mediate PfEMP1 independent rosetting, thus contributing to microvascular obstruction (Goel et al., 2015). The rif proteins (RIFIN), like PFEMP1 and STEVOR proteins are localised to Maurer's

clefts (Wang and Hviid, 2015; Goel et al., 2015). Recent work has shown that STEVOR proteins can directly mediate binding to glycophorin C, thus mediating rosetting (Niang et al., 2014).

The adverse consequences of parasite sequestration, which has been well-characterised in *P. falciparum*, remains controversial for *P. vivax*. Rosetting (Marín-Menéndez et al., 2013; Chotivanich et al., 2012), placental mono infections (Mayor et al., 2012) and lack of schizonts within peripheral blood have all been reported during *P. vivax* infections (Lim et al., 2016). Genomic analysis of *P. vivax* has identified a subtelomeric, multigene family called *vir*, which encodes immunovariant proteins (del Portillo et al., 2001) that have been implicated in parasite adherence to spleen and lung tissue (Carvalho et al., 2010; del Portillo et al., 2001). Two endothelium expressed receptors, CD36 and ICAM-1, implicated in *P. falciparum* binding have been shown to interact, although to a lesser extent, with *P. vivax* infected erythrocytes (Carvalho et al., 2010; Bernabeu et al., 2012). However, it is important to note that *vir* genes, unlike *var* genes, do not undergo clonal variant expression (Fernandez-Becerra et al., 2005).

P. berghei also has the ability to sequester, however, unlike *P. falciparum*, whole body bioluminescence imaging of schizont sequestration in $CD36^{-/-}$ mice indicated that this host receptor is the only one utilised by the parasite. (Franke-Fayard et al., 2005; El-Assaad et al., 2013). Nevertheless, it could be postulated that the sequestration patterns of *P. berghei* are reflective of group B and C PfEMP1 structures that are characterised as binding to CD36 (Figure 1.19). Through genetic disruption, a small single gene protein, schizont membrane associated cytoadherence protein (SMAC) has been implicated in *P. berghei* binding to CD36 (Fonager et al., 2012). Nonetheless SMAC null in *P. berghei* retain the ability to sequester, although to a greatly reduced extent compared to the wild type phenotype, suggesting additional redundant proteins can mediate CD36 binding (Fonager et al., 2012).

The intra-erythrocytic life cycle results in the release of multiple invasive merozoites. Interestingly, the localisation of GFP-tagged GAP50 has implied that the parasite glideosome is unassembled during ring to mid-trophozoite stage

parasites. It is not until late schizogony that the protein localises into distinct foci at the periphery of the parasite, probably to ensure its later distribution around the periphery of and act as a architectural scaffold for the daughter merozoites (Yeoman et al., 2011).

1.2.24 Commitment to Gametocytogenesis

In parallel to the asexual cycle, a flexible number of parasites commit themselves to a developmental pathway that generates (pre-) sexual cells called gametocytes (Smalley et al., 1981b). These cells are the only transmission competent form within the host and as such, must be taken up within the blood meal of the vector to continue the *Plasmodium* life cycle. Gametocytes are cell cycle arrested, thus do not multiply by mitotic division.

The continuous culture of *P. falciparum* has implied that asexual development is the default pathway. Nonetheless, the decision to undergo gametocytogenesis is still largely, from a spectator's point of view, a stochastic one. Identifying the physiological mechanism that influences parasite metamorphosis has proven challenging in the absence of an extreme environmental change.

1.2.25 Gametocytogenesis: Metabolism and Host Environment

Structurally, the metabolic organelles undergo divergent development during gametocytogenesis. The mitochondrion enlarges throughout gametocyte maturation, whereas, in contrast the apicoplast remains relatively small and closely associated with the nucleus (Sinden, 2015). As with asexual blood stages, the *de novo* heme biosynthesis pathway is redundant in maturing gametocytes, suggesting they also scavenge host heme (Ke et al., 2014). Nonetheless, a recent metabolomic study of *in vitro P. falciparum* gametocytes observed oxidative metabolism differs significantly from asexual parasites (Lamour et al., 2014). Intriguingly, there are differences between the glucose consumption pathways used by sexual and asexual parasites to generate energy, and inferences can be drawn from this in regards to gametocyte commitment in 'nutrient deprived' environments. During asexual proliferation the parasite relies heavily on relatively rapid aerobic fermentation glycolysis and glutaminolysis (with a low flux TCA cycle) to convert scavenged glucose and glutamine into biomass and

energy (Salcedo-Sora et al., 2014). Traditionally fermentative glycolysis was considered a feature exclusive to anaerobic metabolism, nonetheless it has become widely described under aerobic conditions in rapidly proliferating cancer cells (Warburg, 1959). Under these conditions the asexual parasite scavenges purine precursors, amino acids and fatty acids from the host (Salcedo-Sora et al., 2014). Interestingly, during gametocytogenesis (non-proliferating development) energy production shifts towards the less rapid oxidation of glucose in the mitochondria via the canonical tricarboxylic acid cycle (TCA) (Figure 1.20). Significantly, the *in vitro* methodologies used to enhance the gametocytogenesis of *P. falciparum* are all centered around nutrient deprivation (Salcedo-Sora et al., 2014). Moreover, transcriptional analysis of *P. falciparum* gametocytes observed an up-regulation of the type II fatty acid synthesis pathway compared with asexual development (Young et al., 2005). This suggests that gametocyte-specific metabolic pathways are a reaction to development within a nutrient deficient environment in which *Plasmodium* cannot readily scavenge abundant metabolites, such as the hypoglycemia observed in severe malaria and patients with hyperparasitaemia (Binh et al., 1997).

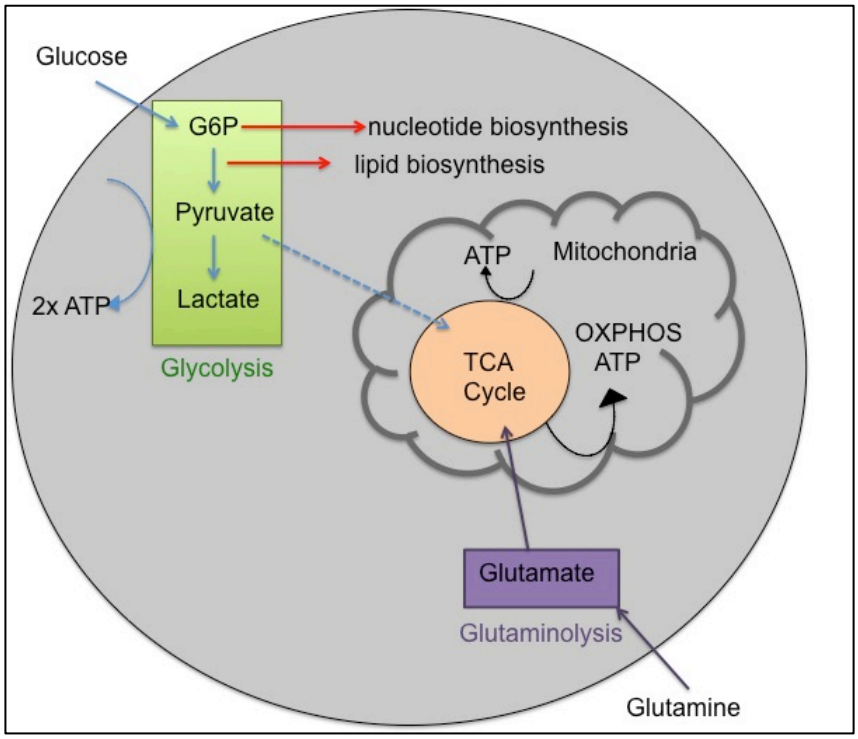

Figure 1.20 Schematic of major energy- producing metabolic pathways. Glucose and Glutamine contribute to energy production. After transport into the parasite, glucose gives rise to glucose-6-phosphate (G6P). Under anaerobic or aerobic fermentation, glucose is rapidly metabolised to lactate and other byproducts in the cytoplasm. A high flux glycolysis maintains metabolic intermediates that support nucleotide and lipid biosynthesis. Anaerobic glycolysis generates a net energy production of 2 ATP molecules per glucose. Pyruvate can be metabolised in the mitochondrion, replenishing the tricarboxylic acid (TCA) cycle. Nutrients in the TCA undergo oxidative phosphorylation (OXPHOS) at the mitochondria membrane to generate ATP (Oburoglu et al., 2016).

The conversion of the human infective eukaryotic parasite *Trypanosoma brucei* to its quiescent transmission competent form has been described as being triggered by parasite derived cell to cell signaling mediated in order control parasite density (Seed and Wenck, 2003). There has been an observed positive correlation between hyperparasitaemia and *P. falciparum* gametocyte carriage in patients (Nacher et al., 2002). Moreover there is *in vitro* evidence that *Plasmodium* gametocyte conversion is influenced by secreted parasite factors, however the authors did not comment on a correlation between parasite density and secretion (Mantel et al., 2013; Regev-Rudzki et al., 2013). Additionally high gametocyte carriage has also been observed within asymptomatic *P. falciparum*

and *P. vivax* infected patients, thus suggesting there is not a link between parasite density and gametocyte formation (Degefa et al., 2016).

Recently, two studies have observed extracellular vesicles (EVs) secreted from *P. falciparum* (PfEVs) (Mantel et al., 2013; Regev-Rudzki et al., 2013). Eukaryotic EVs are used by cells to shuttle functional cargo, such as mRNA and proteins, between each other. Both Mantel *et al* (2013) and Regev-Ridzki *et al* (2013) independently described the parasite-infected erythrocyte derived PfEVs as being formed from the Maurer's cleft and containing the Maurer's cleft resident protein PTP2. Moreover, Mantel *et al* (2013) demonstrated that the PfEVs carry host derived microRNA and functional Argonaute 2 complexes (RNA interference protein). Phagocytosis of infected erythrocyte derived PfEVs induces inflammatory responses from macrophages (Mantel et al., 2013). The PfEVs can also be internalised by infected erythrocytes in culture and a positive correlation was observed between PfEVs uptake and gametocyte formation, although the signaling pathways they manipulate and the trigger for their release have yet to be identified (Mantel et al., 2013; Regev-Rudzki et al., 2013). It should be noted that EV have only been investigated and observed in *P. falciparum* cultures and due to the architectural involvement of the Maurer's cleft, it could be postulated that EV could be restricted to species that display such structures.

1.2.26 Gametocytogenesis: AP2G

The parasite symbiogenic genomes, located in the apicoplast and the mitochondria, only encode a combined total of 33 proteins, all of which are involved in metabolic-related activities (Gardner et al., 2002; Hikosaka et al., 2011). The nuclear karyotype of *Plasmodium* contains 14 chromosomes, all of which are autosomal (Gardner et al., 2002). Therefore, gametogenesis-related transcriptional changes must be both distributed throughout the nuclear genome and regulated on an epigenetic and post-transcriptional level.

A transcription factor, AP2-G, has recently been identified in both *P. falciparum* and *P. berghei* as the master regulator of gametocyte-specific transcription (Sinha et al., 2014; Kafsack et al., 2014). AP2-G, which is believed to facilitate its own positive feedback regulation, is also enriched at its locus for the

epigenetic silencing factor HP1(Rovira-Graells et al., 2012; Josling and Llinás, 2015). The depletion of HP1 in *P. falciparum* leads to the derepression of *ap2-g* and a subsequent increase in gametocyte conversion (Brancucci et al., 2014), thus implying that the epigenetic regulation of *ap2-g* contributes to sexual commitment. Posttranscriptional regulation also plays a role, although functionally undefined, in gametocyte commitment. The deletion of one of two *P. falciparum* RNA-binding proteins, PfPuf1, results in a decrease in gametocyte production (Josling and Llinás, 2015).

The onset of AP2-G expression has yet to be defined in the literature, however commitment to gametocytogenesis is widely believed to take place at the 'ring stage' of the preceding erythrocyte cycle, thus producing schizonts containing exclusively sexually committed merozoites that are restricted to one gender (Bruce et al., 1990; Salcedo-Sora et al., 2014). However, there is conflicting evidence that suggests that the invading merozoite remains plastic in terms of its commitment to gametocytogenesis (Mons et al., 1985). Nevertheless, it is likely that commitment takes places whilst the parasite genome is in a state amenable to high gene expression. The ring stages of *P. falciparum* have been observed to contain relatively less compact centromeric histone cores than later stages, a chromatin conformation generally linked to transcriptional regulation (Hoeijmakers et al., 2012). However, parallel studies by other authors have observed the highest level of nucleosome depletion, and thus gene expression, in the trophozoite stage (Bunnik et al., 2014; Ponts et al., 2010). Ultimately, it is likely that a combination of parasite signaling and metabolic cues influence upstream events of AP2-G, thus driving gametocyte commitment.

1.2.27 Female and Male Gametocytes

Superimposed onto sexual development, the haploid parasite becomes either a female or a male gametocyte. Within the vector mid-gut, the quiescent mature gametocytes activate to form gametes and rapidly emerge from the erythrocyte. For the male, this process comes after 3 rounds of DNA replication and axoneme assembly, resulting in the release of <8 motile gametes, a process called exflagellation. The single female gamete is fertilised by a single male gamete forming a zygote.

The sex ratio of *Plasmodium*, like gametocyte conversion rates, is plastic and as such can be considered an adaptive phenotype. Considering gender allocation within the evolutionary principles that govern most eukaryotes, there are two complementary forces influencing the sex ratio of *Plasmodium*. Firstly, ensuring successful fertilisation, particularly within a clonal low gametocyte density infection, the sex ratio generally skews towards a positive female bias, thereby promoting random mating. Secondly, there is evidence that a long-term genetically diverse infection applies a selection pressure to deviate from random mating and thus promote genetic inbreeding (Talman et al., 2004; Nee et al., 2002).

Unsurprisingly, proteomic studies have highlighted a dramatic divergence between the genders and also asexual stages of *Plasmodium* (Khan et al., 2005; Lasonder et al., 2002). Following male activation, DNA replication and axoneme assembly are initiated through calcium dependent kinase activity (Khan et al., 2005). Gene-deletion studies in *P. berghei* have shown that exflagellation is reliant on numerous protein kinases and protein phosphatases, whose functions seem to be unnecessary or redundant in the asexual stage (Guttery et al., 2015). Moreover, the disruption of the cell division cycle 20 (CDC20) protein generates parasites with a functional asexual cycle and subsequent multiple fission, however, the male gametes fail to undergo mitotic separation after DNA replication (Guttery et al., 2012). On the completion of male DNA replication, the basal bodies of the axonemes egress to form flagella (Guttery et al., 2015). From this point fertility is dependent on fusion with the female gamete, a process mediated by the 6-cys proteins P48/45, P230 and P47 and the plant-sterility gene hap2/gcs1 (Van Dijk et al., 2001; Liu et al., 2008; Laurentino et al., 2011). Disruption of P48/45 or P230 in *P. berghei* produces male gametes that cannot attach to female gamete through a multi protein interaction believed to involve P47 (Van Dijk et al., 2010). Observations made using a *P. falciparum* P230 mutant indicated this protein might also have a role in the interaction between the male gamete and erythrocytes (Eksi et al., 2006). Nonetheless this function of P230 may not be conversed across *Plasmodium* species, as it was not observed in *P. berghei* (Van Dijk et al., 2010). Male gametes lacking hap2/gcs1 do attach to females but do not fuse (Liu et al., 2008).

Initial post-fertilisation development in metazoans relies on mRNAs supplied by the oocyst in translationally quiescent cytoplasmic processing bodies (P bodies) and stored in particles known as P granules. The translation of these pools of mRNA is triggered by fertilisation and occurs prior to the transition to transcription of the zygotic genome (Stitzel and Seydoux, 2008). Within *Plasmodium,* translationally quiescent mRNA are found within the cytoplasm of female gametocytes associated with the DEAD-box RNA helicase DOZI and the Sm-like factor CITH, which together define a protozoan maternal P granule (Mair et al., 2010, 2006). Gene deletions of either DOZI or CITH in *P. berghei* results in zygotes that do not develop into ookinetes (Mair et al., 2010). Through liquid chromatography-mass spectrometry Mair *et al* (2010) identified 16 proteins associated with DOZI and CITH with roles in rapid recruitment of ribosomes, post translation repression and glycolysis. Notably the authors observed an absence of proteins involved in RNA degradation, thus emphasising that the *Plasmoidum* P granules are a site of mRNA storage. Moreover, a recent study has demonstrated that the stored mRNA is only involved in parasite growth up to the post-fertilisation development of the zygote. Using alpha-amanitin to inhibit *de novo* transcription in *in vitro* ookinete cultures the authors observed a lack of maturing ookinetes (Guerreiro et al., 2014).

1.2.28 Immature Gametocytes of *P. falciparum* are not in Circulation

The developing gametocytes of *P. falciparum* display different characteristics compared with *P. vivax* and the murine *Plasmodium spp* (Figure 1.21). The development of *P. falciparum* is highly protracted relative to both its asexual cycle and the maturation of other *Plasmodium spp* gametocytes (Table 1.3). Uniquely, the morphological transitions *P. falciparum* undergoes across the 10-12 day development period can be divided into five discrete stages (stages I-V). Although it should be noted that initially after invasion the gametocyte takes on a ring like morphology (<30 hrs post-invasion) and cannot be distinguished morphologically from asexual parasites until >30 hrs post-invasion. The immature stages (stages I-IV) are undetectable in samples taken from peripheral blood, although recent transcriptional profiling of *ex vivo* samples indicated that gametocytes circulate within peripheral blood up to 20hrs post-invasion (Pelle et

al., 2015). As such, features of *P. falciparum* gametocyte development must both necessitate and facilitate the parasites transient removal from circulation.

Species	Subgenus	Asexual cycle duration	Gametocyte maturation
P. falciparum	*Laverania*	48 hrs	10- 12 days
P. vivax	*Plasmodium*	48 hrs	48 hrs
P. berghei	*Plasmodium*	22-24 hrs	30-48 hrs

Table 1.3 Asexual and gametocyte maturation time frames

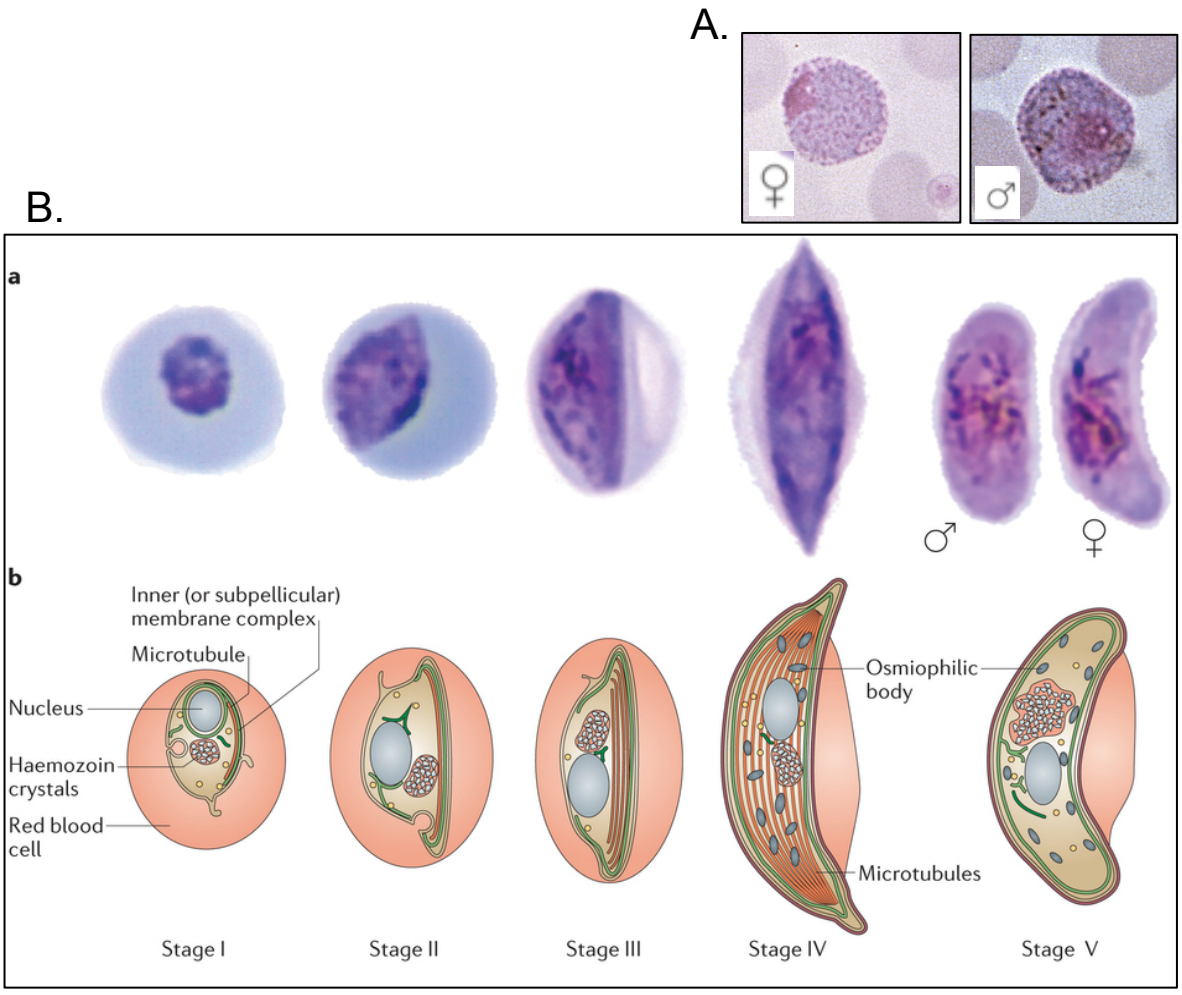

Figure 1.21 Gametocyte morphology (Josling and Llinás, 2015). A. Rounded morphology of *P. vivax* mature gametocytes on a Giemsa stained blood smear and viewed under light microscopy. B. The five stages of *P. falciparum* gametocyte morphology; a. Giemsa stained and viewed under light microscope, b. schematic of microtubules and IMC.

As discussed above, the major *P. falciparum* ligand defining the infected erythrocyte's cytoadherence phenotype is PfEMP1. Interestingly, an early proteomic overview detected *var* gene expression in stage IV gametocytes (Florens et al., 2002). Nonetheless, this finding was starkly contradicted by a later proteomic study that noted an absence of proteins involved in PFEMP1 processing and export (Silvestrini et al., 2010). This is in agreement with the consistent observation that the *var* gene family is down-regulated at the onset of gametocyte development (Duffy and Tham, 2007; Sharp et al., 2006; Tibúrcio et al., 2013). However, antibodies in the plasma of malaria patients have indicated the existence and immune recognition of gametocyte specific antigens (Dinko et al., 2012; Saeed et al., 2008). The parasite switch to sex exclusive ligands correlates with the reports that gametocytes bind to host receptors displayed on bone marrow derived endothelial cells that have not previously been implicated in *Plasmodium* asexual cytoadhesion (Rogers et al., 2000). Nonetheless, the early reports of gametocyte cytoadherence lacked biological relevance in terms of binding frequency and strength (Rogers et al., 2000; Day et al., 1998). As such, a later assay concluded that immature gametocytes of both a reference clone and a field isolate lacked a biologically relevant binding affinity to bone marrow endothelium (Silvestrini et al., 2012). Consequently, these results, coupled with the observations that stage I-IV gametocytes lack adhesive knob like structures (Crabb et al., 1997; Sinden, 1982), point to immature gametocytes being unable to undergo ligand-receptor mediated cytoadhesion.

The need of asexual parasites to sequester is a reaction to the decrease in the cells deformability and, as such, its inability to circulate through splenic sinusoids (Glenister et al., 2002; Tibúrcio et al., 2015b). 3D imaging experiments have determined that, despite the extensive morphological change *P. falciparum* gametocytes undergo, there is no significant increase in surface area or volume of the host cell (Aingaran et al., 2012). Nonetheless, measuring the shear modulus of infected erythrocytes has revealed a systematic decrease in host cell membrane deformability in immature gametocytes compared to stage V mature gametocytes (Aingaran et al., 2012). Computer modeling has indicated that the physical parameters of immature gametocytes would prevent passage through splenic slits (Aingaran et al., 2012). This data was consistent

with results from ektacytometry and microsphiltration studies showing that immature *P. falciparum* gametocytes are less deformable than stage V gametocytes (Dearnley et al., 2012; Tibúrcio et al., 2012).

Surface remodeling of infected erythrocytes through the export of parasite derived proteins, such as the variant STEVOR ligands, and the mechanical re-structuring of the intracellular parasite have been implicated in the decreased deformability of mature asexual *P. falciparum* (Glenister et al., 2002; Nunes et al., 2007). STEVOR proteins are also highly expressed and associated with the erythrocyte membrane in stages III-IV gametocytes but not in stage V. It has been shown, through the overexpression of STEVORs in stage V gametocytes, that these proteins have a direct link with the cells decreased deformability (McRobert et al., 2004; Tibúrcio et al., 2012). This combined with the disassembly of the microtubule subpellicular network are likely the reason for the sharp drop off in rigidity in stage V gametocytes (Dearnley et al., 2012; Tibúrcio et al., 2015a). It can therefore be speculated that the systematic increase in gametocyte deformability, may play a role in retaining immature sexual cells within specific anatomical foci.

Currently, the removal of immature gametocytes from circulation has not been observed in species within the *Plasmodium* subgenera. This is predominately due to gametocytes being indistinguishable from asexual parasites prior to full maturation. A recent microarray comparison between the transcriptome of a *P. berghei ap2-g* null line with wild type was performed to identify early-transcribed genes downstream of PbAP2-G. The dynamics of 18 promoters with PbAP2-G binding motifs identified from this screen were investigated. From this pool, the promoter of PBANKA_101870 was identified as being transcribed pan sexually and relatively early in gametocyte maturation (Sinha et al., 2014).

1.2.29 The Gametocyte Glideosome

Plasmodium gametocytes contain a ‘subpellicular membrane complex’, which has been shown to be analogous to the IMC of the motile zoite stages. It is speculated that this membrane structure serves a purely structural role as the gametocyte (stages I-IV) elongates by establishing a cytoskeleton of

microtubules beneath the IMC. Intriguingly even though the gametocyte has no reported motile ability, the integral proteins of the glideosome, such as Gap-50 and actin, are expressed and localise correctly in the gametocyte (Poulin et al., 2013; Hliscs et al., 2015; Dearnley et al., 2012). Thus, this stage possesses the parasite machinery that enables both gliding and cell invasion.

1.2.30 Malaria: Treatment Failure

The treatment of malaria is an arms race; efforts to control the disease have been hampered by the widespread and rapid emergence of parasite resistance to, and treatment failure of front-line anti-malarial drugs (Table 1.4). For example, in 1993 Malawi had to replace its front line use of chloroquine (CQ) to treat *P. falciparum* malaria with the combination therapy sulphadoxine-pyrimethamine (SP) due to high levels of treatment failure caused by drug resistance. By 2007, SP resistance had emerged and treatment efficiency had fallen in Malawi from 100% to 61-73% (Nkhoma et al., 2007). The WHO defines drug resistance as "the ability of a parasite strain to survive or multiply despite the administration…. of drug given in doses equal to or higher than…recommended" (WHO, 2010). The drive towards drug resistance occurs in two phases. Firstly, a spontaneous genetic event occurs producing a drug resistant parasite. Secondly, under drug selection pressure the mutation is selected for and spreads throughout the population.

Chemical Family	Drugs
4-Aminoquinolines	Chloroquine. Amodiaquine, piperaquine
Amino-alcohols	Quinine, quinidine, mefloquine, halofantrine, lumefantrine
Dulfonamides and sulfones	Sulfadoxine, sulfalene, dapsone
Biguanides	Proguanil, chlorproguanil
Diaminopyrimidine	Pyrimethamine
8-Aminoquinoline	Primaquine
Sesquiterpene lactones	Artemisinin, arteether, artemether, artesunate, dihydroartemisinin
Naphthoquinene	Atovaquone
Antibiotics	doxycyline, tetracycline

Table 1.4 Anti malarials (WHO, 2010)**.** Generic name and chemical family of approved anti malarials.

1.2.31 Mutation for CQ Resistance

The intrinsic mutation rate of *Plasmodium* is assumed to be very low, ~ 10^{-9} (the probability that a unit of DNA mutates with time), and it is only mutations within a drug target or drug transporter that will convey resistance (Su et al., 1999; Hastings, 2011). Interestingly, epidemiological studies have suggested that the resistance of *P. falciparum* to CQ is not the result of a single genetic mutation event, but rather resistance emerged independently within a number of geographical foci (WHO, 2010). CQ, in its uncharged form, diffuses across membranes and in drug sensitive parasites it accumulates in the acidic digestive vacuole, where the now protonated drug is trapped. The drug is believed to combine with the toxic byproduct of heme digestion, thereby interfering with the parasite endogenous detoxification processes. CQ resistant parasites carry synonymous mutations within a digestive vacuole transporter protein, *P. falciparum* chloroquine resistance transporter (PfCRT) that facilitates drug export; three mutually exclusive changes in the amino acid sequence have been identified in the field (Chinappi et al., 2010). The *pfmdr1* gene also encodes a transporter associated with chloroquine resistance in *P. falciparum* (Pisciotta et al., 2017). However, the mechanism of chloroquine resistance in *P. vivax* and *P. berghei* is not understood. Mutations in *pvmdr1* have been reported to play a

role in chloroquine resistance, although there is evidence that the global pattern of mutation doesn't directly correlate with chloroquin resistance (Pisciotta et al., 2017; Melo et al., 2014).

1.2.32 Mutation for ART Resistance

The prominent use of CQ was replaced by alternative synthetic antimalarials, which in turn fueled treatment specific failure. The global use of ARTs began in the 1990s. Artemisinin (ART) and its derivatives (ARTs) contain a 1,2,4- trioxane core containing an endoperoxide ring (Table 1.4) and become widely used as front line antimalarials in the 1990s (Lin, 2011). The mechanism(s) of action of ARTs is/are still unclear but are likely to involve activation of the pro-drug within the body by cleavage of its endoperoxide ring, resulting in the release of free radicals (Klonis et al., 2013a). Interestingly, parasite sensitivity to ARTs positively correlates with its progression through the asexual cycle. In a tightly synchronised *in vitro* culture, ring parasites were less sensitive to the drug than later stages (Klonis et al., 2013b). This suggests that ART activation, and therefore potency, is driven by the accumulation of end products of the parasite's own metabolism. Indeed, *in vitro* and *in vivo* studies have both suggested that the end products of hemoglobin digestion, heme and ferrous iron, are the activators of ART (Klonis et al., 2013a). Recent biochemical and cellular evidence has linked ART sensitivity to decreased phosphatidylinositol-3-phosphate (PI3P) abundance, an endoplasmic reticulum export protein, as a result of the direct inhibition of *P. falciparum* phosphatidylinositol-3-kinase (PfP13K) in early ring stages (Mbengue et al., 2015).

Although ART monotherapy has been reported to clear initial blood stage infection rapidly (Nguyen Duy Sy et al., 1993) currently, WHO advocates Artemisinin Combination Therapies (ACTs) as the front line treatment against all species of malaria parasite (WHO, 2015) (Table 1.5). The rationale for ACT (**Table 1.5**) is simple; firstly, ARTs are rapidly cleared from the body, therefore are co-dosed with a prolonged-acting drug. Secondly, if the drugs each have a target encoded by a different gene the likelihood of parasites containing a spontaneous resistance to treatment is halved. As a result, the use of ACT was designed to delay the spread of resistance for the highly potent ART and stems the spread of resistance against the older secondary drug.

ART resistance was first described in Cambodia in 2008 and as of 2014 it was well established within South East Asia with ACT failure also becoming widely reported in the region (Anderson et al., 2014). Resistance to other antimalarial drugs, such as CQ, is described in terms of recrudescence of infection; however, due to the fast clearance of parasites, ART resistance is described in terms of a protected parasite clearance time. Crudely this is measured as the proportion of patients exhibiting stage blood infections at day 3 after treatment (Baumgärtner et al., 2017). There is strong evidence that the ART resistance phenotype has a genetic linkage to single nucleotide polymorphisms (SNP) in a region of *P. falciparum* chromosome 13 encoding the propeller region of a kelch protein, *kelch13* (Anderson et al., 2014; Takala-harrison et al., 2015). Nonetheless, genome-wide association studies have indicated that the genetic basis for ART resistance is complex (Fairlamb et al., 2016). Nonsynonymous mutations on chromosomes 10, 13 and 14, which lie in or near genes involved in post-replication DNA repair, are at high frequency in ART resistant *P. falciparum* populations (Takala-harrison et al., 2013; Cheeseman et al., 2012). As such, it has been postulated that these genetic markers are indicative of genomes in which ART resistant conferring kelch 13 mutations can occur (Fairlamb et al., 2016).

Despite the recent evidence that ART targets and inhibits PfP13K, polymorphisms in the gene are not detectible in all resistant strains, however, decreased ubiquitination of PfP13K was consistently observed in ART resistant *P. falciparum* (Mbengue et al., 2015). Mbengue *et al* (2015) observed that ART resistant associated mutations in kelch 13 reduced the binding of PfPI3K to the its propeller domain, this in turn reduced PfP13K ubiquitination increasing its stability and leading to an increase in downstream PI3P levels. The authors suggested that increased PI3P levels may be involved in a downstream cascade influencing transcriptional and DNA repair pathways (Mbengue et al., 2015). The 20 or so kelch 13 mutations are associated with ring-stage parasites entering a quiescent state during exposure to ART (Baumgärtner et al., 2017).

ARTs	Combination drug
Artesunate	Amodiaquine
Artesunate	Mefloquine
Dihydroartemisinin	Piperaquine
Artemether	Lumefantrine
Artesunate	SP

Table 1.5 ACT combinations

1.2.33 Selection Pressure for Resistance: Ineffective Treatment

In the simplest terms, two aspects of a drug define its function: pharmacodynamics and pharmacokinetics. The former is the mechanism of drug action. The latter, on the other hand, is a description of what the drug does in the body. This includes the mechanisms of drug absorption, bioavailability, metabolism and excretion. Pharmacokinetics also takes into account the drug's distribution within tissue, which is dependent on blood perfusion, tissue mass, regional pH and the partition characteristic between the blood and tissue (such as cell membrane permeability).

Classically, the treatment outcome of malaria is believed to be determined by the concentration of active drug in the blood stream (White, 2013). As such, drug pharmacokinetics need to be taken into account when administering antimalarials to ensure the dose translates directly to the optimal drug concentration in the blood. If this is not taken into consideration, there is a risk that the patient will receive a dose that equates to sub optimal concentrations in the blood.

It is well established that resistance can be selected for *in vivo* when the parasite is exposed to sub-optimal concentrations of antimalarials. This ties into the epidemiological observations that low transmission areas are the epicenter of emerging drug resistance. The level of an individual's acquired immunity to malaria is a function of the regional intensity of transmission, within high transmission areas partially immune individuals can experience asymptomatic malaria infection, thus these individuals do not seek therapeutic treatment (WHO, 2010). Moreover, many of the front-line drugs currently used were

initially prescribed at sub-optimal levels. For example, the optimal dose for SP in children was extrapolated only from pharmacokinetic studies carried out in adults and as such led to treatment failure in children (Barnes et al., 2006). In parallel, there is a wide distribution and self-prescription of counterfeit and poor-quality antimalarial drugs within endemic regions (Nayyar et al., 2012). The spread of resistance is dependent on the transmission of the mutant from the initial host to the susceptible population. This is therefore contingent on the mutant generating a recrudescent infection in the initial host, producing gametocytes and infecting a vector.

1.2.34 Recrudescence of ART Sensitive Parasites

Interestingly, treatment failure for ART monotherapy administered at reported curative concentration was due to infection recrudescence after complete clearance from the peripheral blood (Cheng et al., 2012; Looareesuwan et al., 1997; Ittarat et al., 2003). As such, these reported recrudescent events have distinct infection dynamics compared with treatment failure due to ART resistance. Moreover, multiple reports have stated that the parasites contributing to the recrudescing infection post ART treatment are not resistant to ART *in vitro* and re-administration of ART to patients is effective in clearing the recrudesced infection (Cheng et al., 2012; Looareesuwan et al., 1997; Ittarat et al., 2003). Recrudescence after ART treatment, like ART resistance, has been linked to drug induced dormancy of ring stage parasites (Cheng et al., 2012). Evidence has been generated from both *in vitro* cultures and *in vivo* infected using ART sensitive parasite lines of a number of *Plasmodium* species that ART treatment results in a populations of morphologically distinct dormant ring stage parasites (LaCrue et al., 2011; Teuscher et al., 2010). Teuscher et al. 2010 observed that approx. 2 % of an *in vitro* culture of drug sensitive *P. falciparum* entered dormancy under various concentrations of ART (200, 500 and 20 ng/mL). Within 5-9 days post treatment 50% of the dormant parasites had recovered and re-entered the growth cycle. Nonetheless, it remains to be seen whether dormancy observed in ART resistant and ART sensitive parasites are governed by genetic and mechanistic similarities.

1.2.35 Post Artesunates Delayed Hemolysis

Post artesunates delayed hemolysis (PADH), marked by high lactate dehydrogenase (LDH) and low haptoglobin plasma levels well after the complete clearance of parasites, has been reported in both adults and children after both parenteral and oral administration of chemotherapy. As such, it would seem that PADH is not the result of the incorrect extrapolation of dosing concentrations from pharmacokinetic studies carried out on adults, as was the case for the sub-optimal dosing of SP (Barnes et al., 2006). Host genetic markers for the prediction of immune-mediated or drug induced hemolysis, such as glucose-6-phosphate dehydrogenase deficiency or the 'direct antiglobulin test' have yet to be conclusively identified. Moreover, there remains inconsistency within field reports as to whether hemolysis is occurring in a predominately intravascular manner via complement fixation or by extravascular removal of erythrocytes by splenic phagocytes. Recent work favoring the extravascular hemolytic explanation for PADH has linked ART induced expulsion of dead parasites from circulating erythroid cells ('pitting') and the subsequent later, but premature, clearance of these pitted cells by the spleen (Jaureguiberry et al., 2014).

1.2.36 *P. berghei*: a Model Organism

As mentioned previously, there are ethical barriers to studying the spatial and temporal dynamics of human infective *Plasmodium in vivo*. To overcome this barrier, researchers have used murine *Plasmodium* infections of laboratory rodents as a model for malaria.

Although *P. chabaudi* provides insight into chronic infection and self-resolving infection (therefore host immunity), the availability of efficient genetic technologies for *P. yoelii* and particularly *P. berghei* have made these two species the predominant models for gene function (Janse et al., 2011). The genomes of human and murine infective *Plasmodium* are highly conserved with approximately 80% of the open reading frames being orthologous (Janse et al., 2011).

The work in this thesis is focused on the blood stage infection of *Plasmodium*. *P. berghei* can mimic a number of severe human malaria pathologies in several strains of mice, such as cerebral complication, pregnancy-associated pathology and acute lung injury (Franke-Fayard et al., 2010). However, the extent to which these pathologies, especially experimental cerebral malaria (ECM), are representative of human disease is hotly contested in the literature (Craig et al., 2012). Nonetheless, the use of *P. berghei* to investigate host immunopathology has fueled the genetic manipulation of the species; there are now numerous clonal lines expressing either fluorescent or bioluminescent markers (Janse et al., 2006; Franke-Fayard et al., 2005). The use of these transgenic *P. berghei* lines facilitates the imaging of parasites within host tissue either *in vivo* or *ex vivo* (Franke-Fayard et al., 2005; Claser et al., 2014). Moreover, the use of rodents allows for the host genetic background to be controlled.

The long-standing investment in technologies and methodologies has made *P. berghei* an obvious choice for visualising and analysing host-parasite interactions. Nonetheless, the divergences between human and murine infective *Plasmodium* must be taken into account when translating laboratory findings to a clinical setting. It is thus important that there is cross talk between experimental and field studies, therefore enabling the use of the developmental murine models to temporally and spatially study host-parasite phenotypes that human field samples have shown light on.

1.2.37 Summary

The key points in this section were:

- The expression of host receptors defines a host cell's susceptibility to *Plasmodium* (section 1.2.15 page 27).
- Immature gametocytes develop out of circulation (section 1.2.28; page 47).
- The gametocyte has a fully assembled glideosome (section 1.2.29; page 50).
- The temporal and spatial dynamics of infection influences drug pharmacology (section 1.2.33; page 55).
- *P. berghei* is a valuable model organism (section 1.2.36; page 57).

1.3 Structure and Function of the Bone Marrow and Spleen

The key points in this section are:

- Where stress and homeostatic erythropoiesis occurs in mice and humans.
- Whether erythroid progenitors have the ligands and cytoskeleton allowing for *Plasmodium* invasion.
- Whether there is a metabolic advantage to invading erythroblasts.
- The effect malaria has on erythropoiesis.

The conclusions to these points are reviewed in the summary: section 1.3.14.

1.3.1 Bone Marrow Structure and Function: Mice and Human

In both mice and humans, the bone marrow is the viscous tissue found within the cavities of the axial and long bones. It is the major source of hematopoietic stem cells (HSCs), the multipotent, self-renewing progenitors that give rise to all cellular elements in the blood (both myeloid and lymphoid) and immune system, thus making it a primary immunological organ (Figure 1.22). Adult bone marrow also contains mesenchymal stem cells (MSCs), the progenitors of the cellular components of tissues (Travlos, 2006; Gurkan and Akkus, 2008). Structurally, the marrow supports the proliferation of its stem cells in a highly organised stroma, which is composed of reticular cells that form a spongy scaffold.

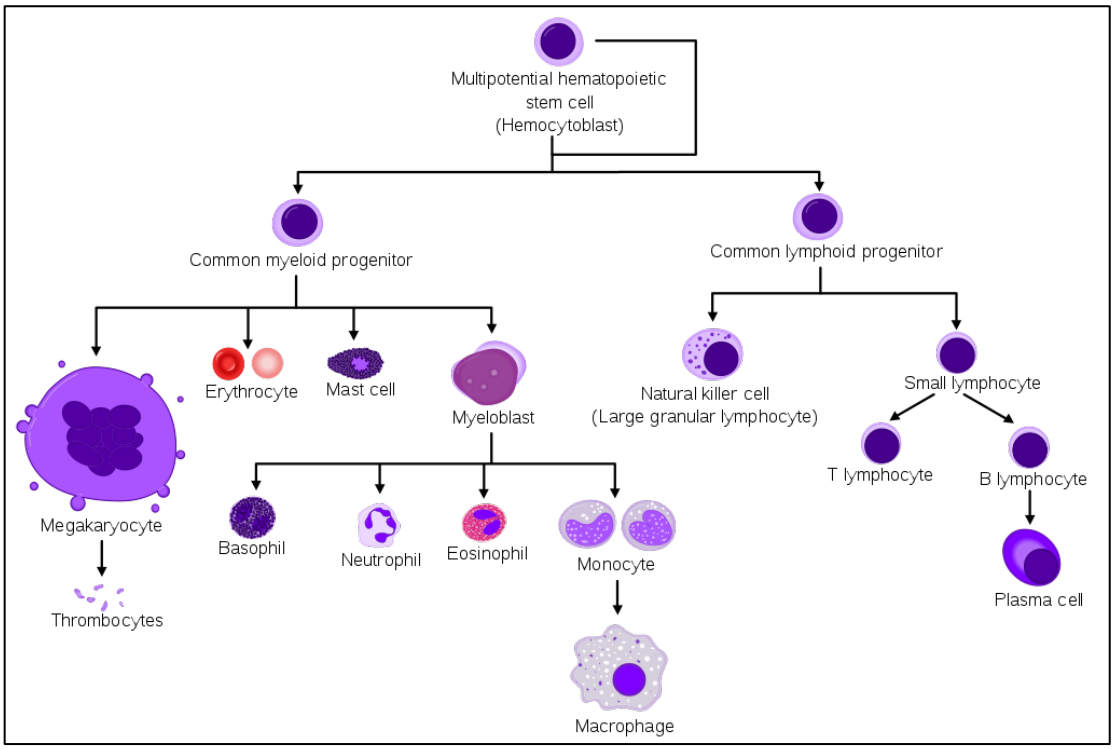

Figure 1.22 HSC differentiation pathways (Haggstrom, 2009). Schematic showing development of myeloid and lymphoid lineages from Hematopoetic Stem Cell precursors.

The diaphysis portion (Figure 1.23) of adult long bones consists largely of mesenchymal cells and adipose tissue (yellow marrow). At birth, the entire skeleton is filled with active hematopoietic tissue (red marrow), from this point onwards red marrow is steadily converted into yellow marrow. Conversion is finite, with an end point in early adulthood. At this point red marrow is restricted to the axial skeleton and the epiphysis/metaphysis of the humeral and femoral bones (Małkiewicz and Dziedzic, 2012). Nonetheless, a recent deep imaging study of murine adult long bones observed the highest frequency of HSCs were located in the diaphysis compared to the metaphysis and epiphysis (Acar et al., 2015).

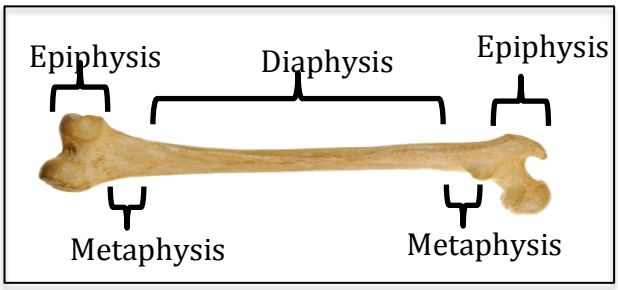

Figure 1.23 Structure of the long bones (Nrpt.co.uk, 2017)

Blood is delivered to the bone marrow by the nutrient artery, which splits into ascending and descending branches that run along the longitudinal axis of the tissue. These branches then spilt into small radial arterioles and capillaries that extend towards the cortical bone. Near the bone, the vessels become venous sinusoids that drain via the central sinus and the collecting venules back into the centre vein and away from the marrow through the nutrient vein. This structure makes the bone marrow a highly vascularised tissue (Figure 1.24). The bone marrow does not have draining lymphatic vessels (Travlos, 2006; Gurkan and Akkus, 2008).

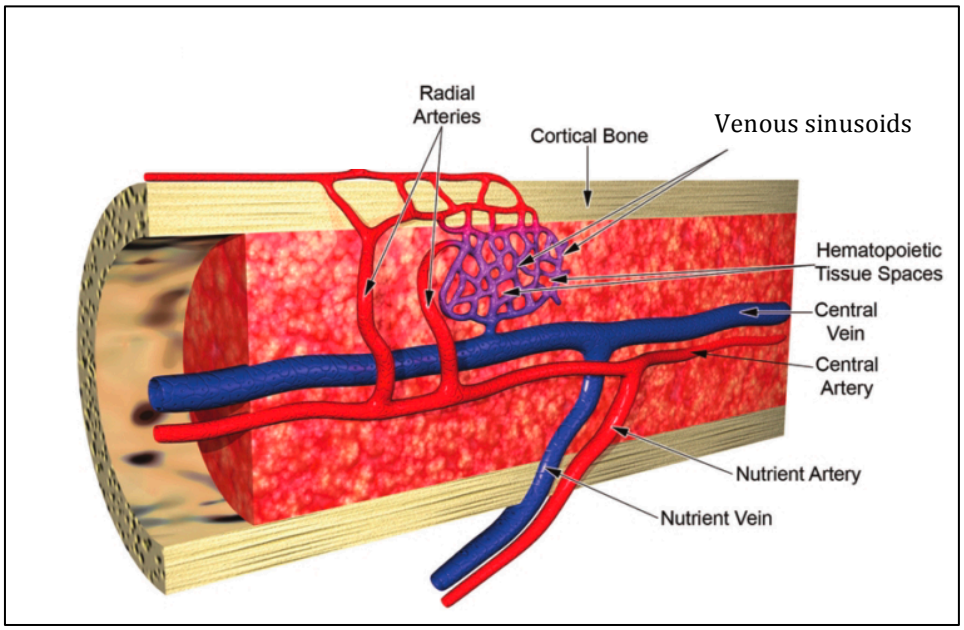

Figure 1.24 Bone marrow is a highly vascularised tissue (adapted from Travlos, 2006)

Sinusoidal walls, which consist of a single layer of endothelial cells, are fenestrated, not supported by a complete basement membrane and are in direct contact with parenchymal (extra vascular) cells. This lack of regular vessel wall structures allows for a high level of permeability (Kopp et al., 2005; Itkin et al., 2016), allowing the mature cells arising from the HSCs to migrate out of the tissue into the blood stream.

The maturation and commitment of lineage-negative HSCs to the wide variety of blood cell lineages is called Hematopoiesis. The maturation of the discrete cell lineages is a compartmentalised process within the hematopoietic tissue. Osteoblasts and other mesenchymal stromal cells construct a supportive niche for quiescent HSC within the deep peri-sinusoidal regions (Acar et al., 2015; Kaplan et al., 2007). The bone marrow sinusoidal endothelium creates a second scaffold structure, forming the vascular HSC niche where differentiation occurs (Kaplan et al., 2007).

1.3.2 Cellular Transmigration into Tissue

The process of extravasation through the endothelium into a tissue is termed diapedesis (Schmidt et al., 2011). The vascular endothelium has an active role in diapedesis through its reorganisation of its cytoskeleton and membrane. Currently, there are two identified routes of diapedesis for leukocytes

migration: between endothelial cells (paracellular) or through individual endothelial cells (transcellular), both of which occur during inflammation and immune responses (Schmidt et al., 2011). The leukocytes choice of the transcellular pathway is regulated by the relative stiffness of endothelial cell and the tightness of the endothelial cell junction, with high endothelial rigidity promoting this pathway (Martinelli et al., 2014; Schaefer et al., 2014). Within the bone marrow endothelial cells exhibit prominently different functions in different vascular beds, with arterial and sinusoidal endothelial cells displaying different anatomical, hemodynamic, molecular and metabolic signatures (Itkin et al., 2016). Evidence exists showing that the permeable fenestrated sinusoids are the preferential site of leukocyte trafficking (Itkin et al., 2016), thus suggesting that paracellular migration is the predominant route to access the bone marrow tissue.

Both migratory pathways are highly regulated through sequential ligand-receptor interactions between the migrating cell and the endothelium, including, for example, binding of selectins, integrins and intercellular adhesion molecules (ICAM) (Filippi, 2016). Alongside promoting cellular adhesion, these binding interactions also instigate bidirectional signaling between the leukocyte to the endothelial cells that establish leukocyte polarity, crawling, and loosening of the endothelial cell junctions (Filippi, 2016).

Under inflammatory conditions, endothelial cells express vascular cell adhesion protein endothelial (E)- and platelet (P)- selectin. These receptors capture leukocytes through binding to an array of sialylated carbohydrate ligands and P-selectin glycoprotein ligand 1 (Muller, 2013). The subsequent leukocyte rolling is controlled by adhesion between class dependent leukocyte integrins (lymphocyte function-associated antigen 1; CD11a/CD18), Mac-1 (macrophage-1 antigen; CD11b/CD18) and Very late antigen -4 (VLA-4) which bind to their corresponding endothelial ligands ICAM-1 and VCAM -1, respectively (Nourshargh and Alon, 2014). The leukocyte binding to ICAM-1 and VCAM-1 triggers internal endothelial signalling leading to the formation of ICAM-1 and VCAM-1 clusters supported by actin thus enhancing leukocyte binding (Vestweber, 2015). Moreover, the binding of leukocytes to these ligands triggers additional internal endothelial signals, such as transient $Ca2^{+}$ signals that stimulates the active opening of the endothelial cell junction through actinomyosin filament mediated

contraction and the production of reactive oxygen species that triggers the dissociation of endothelial cell junction cadherin proteins (Vestweber, 2015). Consequently, the process of diapedesis is restricted to cells that have the capability to undergo these complex and sequential interactions.

A novel mechanism of extravasation of intravascular non-leukocyte cells has been reported and termed angiopellosis (Allen et al., 2017). Allen *et al* (2017) used intravital microscopy to visualise the dynamics of injected cardiac stem cells in transgenic zebrafish embryos. The authors reported that angiopellosis differs both morphologically and temporally from diapedesis. The former process took significantly longer to occur, the stem cells retained their shape opposed to undergoing deformable morphological changes and the endothelial cells actively remodeled to form pockets in order to accommodate the transmigrating cell. Moreover, through inhibiting a characterised cell endothelial receptor (CD11a; a member of the β_2 integrin complex lymphocyte function-associated antigen 1) used during leukocyte diapedesis the authors showed that the cardiac stem cells were utilising unique and likely β_2 integrin independent ligand-receptor interactions to achieve angiopellosis (Allen et al., 2017). This therefore opens the possibility for other mechanisms of transmigration to exist for cells that have the ability to adhere to endothelial receptors, such as ICAM, but have no characterised integrin expression, such as *Plasmodium*-infected erythrocytes.

1.3.3 Spleen Structure and Function

The human and mouse spleen consists of distinct micro-anatomical zones: the white pulp and the red pulp. Although there are a great number of similarities between the spleens of the two species, there are also some structural differences. Both of which will be highlighted in this section.

Electron microscopy has shown that the white pulp is composed of lymphocytes, phagocytes and blood vessels arranged in a reticular framework (Saito et al., 1988). The white pulp makes the spleen a secondary immunological organ and in both species it can be sub-categorised into three compartments: the periarteriolar lymphoid sheath (PALS), the follicles and the marginal zone (Cesta, 2006a). T-cells dominate the PALS that surround the arterioles that enter the parenchymal tissue of the spleen. The follicles are continuous with the PALS

but are areas of B cell prevalence. Both the PALS and the follicles are surrounded by the marginal zone. The correct organisation and maintenance of these structures is controlled by specific chemokines (Mebius and Kraal, 2005). In rodents the marginal sinus, which forms a border between the PALS/follicles and the marginal zone, mediates lymphocyte re-circulation via endothelial transmigration (Ferrer et al., 2014). A relatively recent immunohistological study showed that this structure is not present in human spleen, however, a species-specific lymphoid-rich perifollicular zone was detected on the outer region of the marginal zone (Steiniger et al., 1997). The structural differences between human and mouse marginal zones indicates that there is divergence in patterns of lymphocyte recirculation, however the significance of this in terms of splenic immunological function remains undetermined (Steiniger et al., 2001).

The red pulp is composed of a 3D meshwork of reticular fibres, myofibroblastic reticular cells and associated macrophages, all arranged into ‘splenic cords’. The reticular fibres are composed of collagenous and elastic fibres, basal laminae and unmyelinated adrenergic nerve fibres (Cesta, 2006b). Species-specific differences in the red pulp remain poorly studied (Ferrer et al., 2014). The environment within the cords is believed to be acidotic and hypoxic (Cesta, 2006b; Malley, 2007).

The blood flow through the human microvasculature of the spleen is highly complex and somewhat controversial (Steiniger, 2015; Maxie, 2015; Ferrer et al., 2014; Steiniger et al., 2011). Historically this may be due to the misinterpretations of structures observed in post mortem corrosion casts and the over interpretation of non-human species-specific structures. Nonetheless, it is widely expected that a proportion of blood enters and filters through an ‘open circulatory system’, where it enters spaces not lined by endothelium or barrier-forming cells (Steiniger et al., 2011).

In the human spleen, blood (lymphocytes, erythroid cells and all other components) enters the spleen via the splenic artery, which then divides into the trabecular arteries within the splenic parenchyma. These blood vessels branch further into smaller arterioles, terminating at the perifollicular zone or in the red pulp. The blood from these arterioles either flows directly into adjacent venous sinuses via vascular conduits (closed circulation) or enters the

reticular meshwork of the red pulp (open circulation), where blood borne pathogens are cleared by the associated macrophages. The blood from the red pulp must re-enter closed circulation (Steiniger, 2015; Ferrer et al., 2014; Balogh, 2011; Cesta, 2006b). Transmission electron microscopy has shown that this is done by the erythrocytes transmigration through the sinusoidal walls of the venous sinuses within the red pulp (Figure 1.25) (Drenckhahn and Wagner, 1986). Thus, erythrocytes re-entering closed circulation are subjected to a 'physical fitness test', with cells displaying atypical geometry and deformability being excluded (Pivkin et al., 2016). This has led to the human spleen being classified as sinusoidal.

Mice, like many domestic animals, have a spleen that is non-sinusoidal or 'reticular'. In this structure there is no closed circulation, arterioles empty entirely into the red pulp (Figure 1.25). Nonetheless, the blood does not re-enter the circulation via the walls of venous sinuses, instead it drains into open-ended venules (Maxie, 2015). As such, re-entry into the vasculature does not require the erythrocytes to display the deformability range of healthy erythrocytes. Nonetheless, comparisons between the deformabilities of erythrocytes within the peripheral blood and erythrocytes retained within the spleen indicates that the mouse spleen has a method to exclude atypical cells from circulation (Huang et al., 2014).

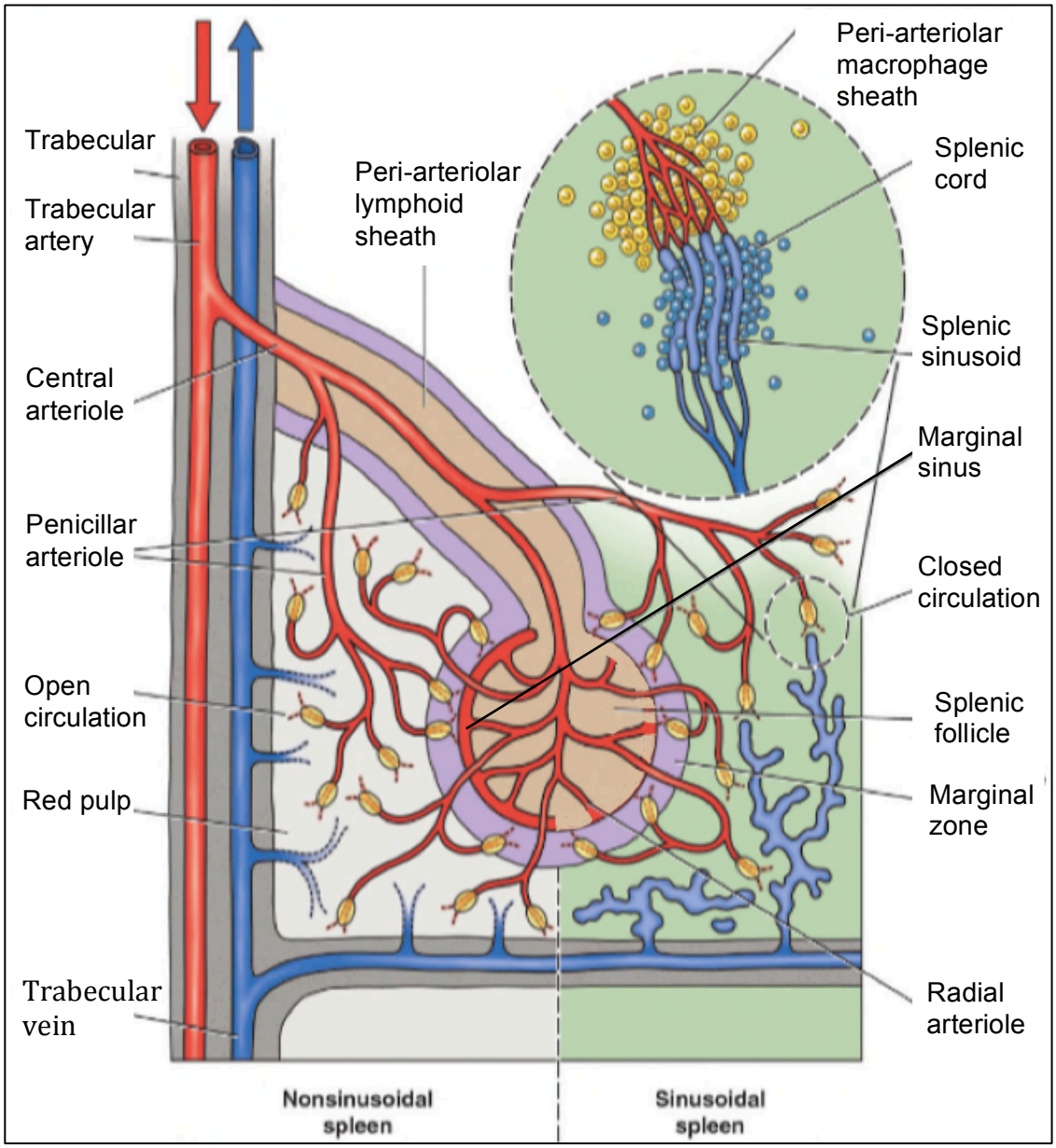

Figure 1.25 Blood flow in non-sinusoidal and sinusoidal spleens (Maxie, 2015)**.** Humans (sinusoidal) lack a marginal sinus, blood from the radial arteriole empties into the marginal zone and red pulp. Some arterioles are continuous with splenic sinusoids, creating the closed circulation where the (~90%) blood never leaves endothelial-lined vessels. The rest of the blood drains through the splenic cords entering the sinusoids through the endothelial slits. In mice, all blood is emptied into the red pulp or marginal sinus and drains through the red pulp into open-ended venous vessels.

1.3.4 Primary and Definitive Erythropoiesis

It was observed as early as 1875 that the erythroid cells within the postnatal mammalian bloodstream lack a nucleus (Gulliver, 1875). This is in stark contrast to the bloodstream of mammalian embryos that contain two temporally overlapping erythroid populations, the first containing large nucleated cells and the second consisting of smaller enucleated cells (Palis, 2014). As such, the first wave of early fetal erythropoietic development is termed 'primary' erythropoiesis in order to distinguish it from 'definitive' erythropoiesis that generates enucleated cells from later fetal development onwards. HSCs arise in the fetal yolk sac and migrate to the fetal liver where they undergo expansion before reaching the bone marrow where postnatal definitive erythropoiesis occurs (Nandakumar et al., 2016).

1.3.5 Maturation of Definitive Erythroid Cells

HSCs lack lineage specific cell markers, but within mice they express stem cell antigen 1 (Sca1) and the stem cell growth factor, c-Kit. For both mice and humans it is believed that under homeostatic conditions stem cells give rise to two non-identical daughter cells: one stem cell (for self-renewal) and one differentiating cell (Wilson and Trumpp, 2006). The earliest stage in cellular development where cells become restricted to the erythroid lineage is called the 'blast forming unit-erythroid' (BFU-E). These cells respond to erythropoiesis stimulating factors and give rise to the rapidly proliferating 'colony forming unit-erythroid (CFU-E) (Barminko et al., 2016). Several studies have observed circadian oscillations in the colony-forming ability in the human and murine bone marrow, raising the possibility that homeostatic HSC proliferation and differentiation may follow circadian variations (Mendez-Ferrer et al., 2009; Abrahamsen et al., 1997; Bourin et al., 2009). Five subsequent discrete developmental stages separate CFU-E from terminally differentiated erythrocytes: pro-erythroblast, basophilic erythroblast, polychromatic erythroblast, orthochromatic erythroblast and reticulocyte (Figure 1. 26).

The differentiation and proliferation of CFU-E are also regulated by erythropoiesis stimulating factors. The cell's transition to pro-erythroblast is accompanied by the loss of c-Kit but the gain of the ubiquitous erythroid

marker, Ter119, a protein associated with glycophorin A (Barminko et al., 2016). The pro-erythroblasts proliferate and sequentially differentiate through the subsequent erythroid stages (Figure 1.26). Within both mice and humans, the pro-erythroblast undergoes 4 mitotic divisions, giving rise to a basophilic, polychromatic, orthochromatic ratio of 1:2:4:8 (Liu et al., 2013). Erythroblast development is accompanied a progressive decrease in cellular size, as well as condensation of the nucleus and an accumulation of cytoplasmic hemoglobin (Barminko et al., 2016). The former developmental characteristic has been linked to a successive shortening of the G1 phase (cell growth) between each division, thus also temporally shortening the cell cycle of each erythroblast stage (Dolznig et al., 1995). However, this observation was made in an avian model of erythropoiesis in which nuclear condensation is not associated with maturation, therefore it unlikely to be relevant to mammals. Moreover, *in vitro* culture systems with murine erythroblasts have reported progressive differentiation of subsequent stages at approximately twelve-hour intervals (Chen et al., 2009; Koury et al., 1984).

At the orthochromatic stage, the erythroid cell has exited the cell cycle and the highly condensed nucleus and additional organelles are extruded, forming a reticulocyte. It has been hypothesised that enucleation occurs in order to prevent the dedifferentiation of erythrocytes during their exposure to external regulatory factors such as cytokines (Raess et al., 1985). Moreover, there is a direct link between enucleation and increases in cellular deformability; therefore erythroid cells may lose their nucleus in order to facilitate passage through narrow vessels such as capillaries (Gaehtgens et al., 1981; Barminko et al., 2016).

The reticulocyte stage can be further sub-divided into four sub-categories (Heilmeyer stages I- IV) based on the gradual reduction in supravital staining patterns. Stages I-II are confined to the bone marrow, whereas stages III-IV are observable within circulation where they mature into terminally differentiated erythrocytes (Malleret et al., 2015). The bone marrow restricted reticulocytes are endocytic and motile (Griffiths et al., 2012). The stage III cell egresses from the bone marrow parenchyma by diapedesis to the sinusoidal capillary lumen (Sage and Carman, 2012). Under homeostatic conditions it takes 2 – 3 days for

stage I reticulocytes to sequentially mature into erythrocytes (Raess et al., 1985). In this work erythroblasts and stage I-II reticulocytes will be referred to as tissue resident erythroid cells.

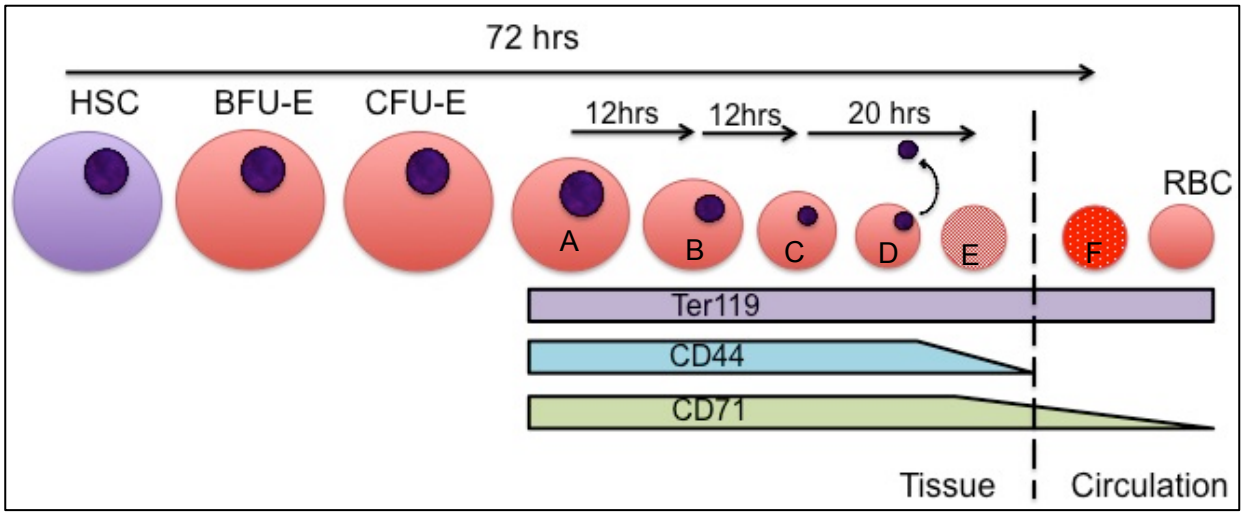

Figure 1.26 Schematic of erythroid cells and precursors. CFU-E transform into A. pro-erythroblast, which then successively differentiate into B. basophilic erythroblast, C. polychromatic erythroblast and D. orthochromatic erythroblast. The orthochromatic stage enucleates to become an enucleated reticulocyte. The differentiation times in mice are marked above the cells (Chen et al., 2009; Filmanowicz and Gurney, 1961). E. Stage I-II reticulocytes mature within the tissue. F. Stage III-IV reticulocytes are within the circulation. The final differentiation stage is erythrocytes (RBC). From pro-erythroblasts the erythroid lineage expresses Ter119. This stage also expresses CD44 and CD71. The former is down-regulated systemically in relation to diapedesis.

Flow cytometric approaches have recently been developed to identify the distinct stages of erythroid cells based on defined cellular characteristics. In the mouse, the transferrin receptor, CD71, is expressed highly in erythroid precursors and down-regulated during maturation (Lok and Ponka, 2000). This marker can be combined with Ter119 in order to identify $CD71^{+}$ $Ter119^{+}$ erythroblasts and $CD71^{-}$ $Ter119^{+}$ erythrocytes (Socolovsky et al., 2001; Liu et al., 2006). Recently, Chen et al (2009) have shown that the expression of the cell surface glycoprotein, CD44, is more systemically decreased during maturation than CD71, therefore allowing for a higher level of discrimination between the erythroblast stages. Using a combination of Ter119, CD44 and cell size, it is

possible to resolve all 6 stages from pro-erythroblast through to terminally differentiated erythrocytes (Table 1.6) (Chen et al., 2009; Liu et al., 2013).

Cellular marker	Protein	Cell lineage
Ter119	Associated with glycophorin A	Erythroid lineage
CD44	Glycoprotein involved in cell-cell interactions and diapedesis	Leukocytes and erythroid cells
CD45	Protein tyrosine phosphatase	Pan leukocyte and early erythroblasts
CD11b	Subunit of integrin CR3	Myeloid and NK cells

Table 1.6 Cellular markers used to resolve erythroid cells.

It is interesting to note that Chen *et al* (2009) also measured the protein abundance of three of the host receptors for *Plasmodium* invasion during erythroid maturation. Glycophorin A, the Duffy antigen and Band 3 are only detectible, at relatively low levels, from the basophilic erythroblast stage with abundance increasing through maturation (Chen et al., 2009). It is also interesting to note that immature erythroid progentiors are positive for beta 2 integrin, as judged by immunoadherence to a anti-cd18 coated plates (Papayannopoulou and Brice, 1992). This adhesion molecule is lost from the surface of erythroid cells as they mature to become $CD18^-$ cells (Papayannopoulou and Brice, 1992).

1.3.6 Erythroblast Islands

Within *in vitro* cultures, erythroblasts differentiate in the absence of other cell lineages. However, *in vivo,* erythropoiesis occurs within specialised multi-lineage niches termed erythroblast islands. They comprise of a central 'nurse' macrophage, which engulfs the expelled erythroid nuclei, and erythroid cells at various stages of development (Chasis and Mohandas, 2009). Depletion studies in mice have shown that the central macrophages directly promote the retention

and maturation of the physically associated erythroid cells within hematopoietic tissue (Chow et al., 2011, 2013). The strength of the cellular adhesion between the central macrophage recedes prior to enucleation, thus allowing the subsequent reticulocyte to egress from the bone marrow (Toobiak et al., 2012).

1.3.7 Regulation of Steady State Definitive Erythropoiesis

In mice and humans the hematopoietic tissue is located within the postnatal bone marrow. Adult mouse splenic red pulp has also been recognised as a site of erythropoiesis (Sadahira et al., 1990). Under steady state conditions, erythrocyte production is regulated at the rapidly proliferating CFU-E population by the peptide hormone erythropoietin (EPO), which is synthesised primarily in the kidney by peritubular fibroblasts, and Stem cell factor (SCF) (Barminko et al., 2016). The *epo* locus contains an enhancer region that is regulated by hypoxia inducible transcription factors (Hifs) (Barminko et al., 2016). This permits transcriptional regulation in response to local oxygen levels in peripheral blood, which is an indirect measure of hematocrit. As such, hypoxic conditions in the blood leads to elevated levels of EPO in serum. Once hematocrit and consequently hemoglobin levels are restored, *epo* transcription returns to steady state levels (Barminko et al., 2016).

Under steady state conditions, 10-20% and 40-60% of the CFU-Es undergo apoptosis in the murine bone marrow and spleen, respectively (Liu et al., 2006). CFU-E apoptosis also occurs in the human bone marrow under the same conditions (Muta and Krantz, 1993; Kelley et al., 1994). Increased EPO levels in both species stimulate CFU-E survival by increasing expression of cellular pro-survival factors, such as BCL-X_L, and down-regulation of pro-apoptotic factors (Koulnis et al., 2011, 2012). Moreover, the apoptotic signaling proteins, Fas and Fas-ligand, expressed by erythroblasts are down-regulated in the presence of EPO. It is interesting to note that splenic erythroblasts express a significantly higher Fas and Fas-ligand during basal state compared to their bone marrow counterparts (Liu et al., 2006). This homeostatic system compensates for minor fluctuations in hemoglobin levels without exhausting the slow dividing, earliest form of erythroid progenitor, the BFU-Es (Barminko et al., 2016).

1.3.8 Definitive Erythropoiesis under Stress

CFU-Es populations undergo 4 divisions before becoming terminally mature. As such, elevated EPO levels stimulated by minor hematocrit fluctuations can only regulate a limited increase in erythrocyte numbers. Therefore this mechanism cannot counteract erythrocyte deficiency under extreme conditions of hypoxic stress. As such, in these circumstances erythropoiesis is regulated at the BFU-E population level (Barminko et al., 2016).

In both humans and mice, glucocorticoid (GC) nuclear hormone receptor signaling regulates stress erythropoiesis (Varricchio et al., 2012). GC signaling induces expression of a BFU-E *hif* (Hif-1 alpha) transcriptional regulator that promotes expansion of the BFU-E population (Flygare et al., 2011). Hif-1 alpha activation in turn synergises with GC signaling, thus suggesting that hypoxia (EPO) and stress signaling cooperate to restore erythrocyte numbers (Barminko et al., 2016). Interestingly, mice deficient in the GC receptor have an impaired phenotype that only manifests itself in the spleen under stress. The murine bone marrow does not exhibit GC receptor dependent regulation (Bauer et al., 1999; Reichardt et al., 1998). This therefore implicates the murine spleen as the predominant site of stress erythropoiesis.

Both BMP4 and SCF also play significant roles in stress erythropoiesis (Barminko et al., 2016). The former signals through the Smad5 receptor of Sonic hedgehog primed BFU-Es in the murine spleen in order to regulate the erythroid response to anemia (Perry et al., 2009). Mice deficient in Smad5, although viable, fail to produce a compensatory erythroid response to anemia (Lenox et al., 2017; Barminko et al., 2016). The SCF and its signaling pathway work in synergy with the GC receptor; in the absence of SCF signaling the GC receptor cannot mediate prolonged BFU-E expansion (Lindern et al., 2017). Therefore, EPO, SCF, and BMP4 signaling synergise to increase proliferation.

1.3.9 Extra Medulla and Stress Erythropoiesis in Humans

The *in vivo* analysis and location of stress erythropoiesis in humans is difficult. Direct experiments examining the regulation of stress erythropoiesis are not possible and the analysis of erythropoiesis in patients with severe anemia is

complicated by the effects of pathology (Paulson et al., 2011). Nonetheless, extramedullary (outwith the bone marrow) erythropoiesis has been reported to occur when the bone marrow is compromised, such as in myeloproliferative disorders, lymphomas and leukaemias (Freedman and Saunders, 1981). Extramedullary erythropoiesis has also observed in the spleen and liver in patients without bone marrow dysfunction (Palitzsch et al., 1987; Deiwick, 1992).

Stutte *et al* (1986) speculated that murine and human splenic extramedullary erythropoiesis is fundamentally different. They proposed that murine splenic erythropoiesis involved endogenous splenic progenitors, whereas in humans they suspected that bone marrow endogenous erythroid cells migrated to the spleen (Stutte et al., 1986; Freedman and Saunders, 1981). However, this was directly contradicted by recent transplant experiments that observed the mobilisation of bone marrow HSCs to the murine spleen. This indirectly suggests that the establishment and replenishment of the murine splenic erythroid progenitor cells is dependent on bone marrow derived progenitors (Paulson et al., 2011; Perry et al., 2009). Interestingly, human bone marrow derived HSCs can also be mobilised (Broxmeyer et al., 2005) and their migratory pattern is controlled by the same chemokine as in mice, stromal cell derived factor 1 (SDF-1/ CXCL12) (Aiuti et al., 1997). This was confirmed by engraftment experiments where human HSCs homed to the spleen of irradiated mice in a SDF-1 dependent manner (Lapidot and Kollet, 2002). Interestingly, it should also be noted the stromal cells of the splenic red pulp in both species produce SDF-1 (Ellyard et al., 2005; Hargreaves et al., 2001).

The investigation of mechanisms that regulate erythropoiesis in humans relies on *in vitro* culture systems and the non-invasive study of patients with various forms of anemia. The disease studies discussed above show that mechanistically, splenic erythropoiesis in humans is possible. Moreover, the Palizsch *et al* (1987) histological study of spleens harvested from deceased cirrhotic liver patients also reported splenic erythroblast islands within their ‘healthy’ control spleen samples, therefore providing evidence that the human spleen can be functionally permissive to erythropoiesis. However, it remains to be directly

investigated whether erythroid cells in the human spleen are regulated in a stress erythropoiesis manner similar to the mouse spleen.

1.3.10 The Cytoskeleton of Erythroblasts

As discussed previously, terminally differentiated erythrocytes have a cytoskeleton assembly that facilitates high cellular deformability. Protein expression profiling performed on highly synchronous erythroblast populations observed an increase in expression of all cytoskeletal proteins, except for actin, during maturation (Chen et al., 2009). The immunoblots of the skeletal proteins indicate that the earliest stage that all proteins are present at their maximum abundance is the polychromatic erythroblast. Therefore, it is likely that the complete assembly of a functional spectrin-based cytoskeletal network can only occur from this stage onwards (Chen et al., 2009).

This is interesting in the context of *Plasmodium* invasion. As discussed previously it is believed that the parasite takes advantage of the deformable properties of erythrocyte cytoskeleton in order to gain entry to the cell (Zuccala et al., 2016).

1.3.11 The Metabolism of Erythroblasts

Intravital imaging of the murine bone marrow indicated there is a steep oxygen tension gradient across the tissue that forms relatively oxygen rich regions around the vasculature and hypoxic zones within the deep perisinusoidal regions (Spencer et al., 2014; Acar et al., 2015). Both regions are niches for HSCs. Hypoxic conditions disrupt the oxidative phosphorylation pathway leading to oxygen independent glycolysis (Solaini et al., 2010). Prolonged hypoxia leads to the stimulation of HIF transcription factors. It has been determined that HSCs undergo HIF dependent differentiation in the bone marrow (Oburoglu et al., 2016; Mantel et al., 2010), thus establishing parenchymal lineage committed populations within the vascular niche. This niche is relatively less hypoxic, thus allowing restoration of oxidative phosphorylation (Oburoglu et al., 2016; Kaplan et al., 2007).

There has yet to be a metabolomics profile generated for the maturation stages of the erythroid lineage prior to diapedesis. As such, clear metabolic differences between the stages have yet to be identified. A recent comparison of reticulocytes (stage III &IV) with terminally mature erythrocytes observed that the former were more metabolically complex and rich in carbon metabolites (Srivastava et al., 2015). Mature erythrocytes do not contain mitochondria, thus the principal method of energy generation is via glycolysis. Within the reticulocyte the mitochondria is degraded, but Srivastava *et al* (2015) observed that this erythroid stage has a functional TCA cycle. Taking into account that erythroblasts undergo oxidative phosphorylation, it is likely they are more metabolically rich than reticulocytes.

The metabolic environment of the erythroid cell is interesting when considered in the context of *Plasmodium*. As discussed previously parasite asexual proliferation is dependent on the availability of host-derived nutrients. Srivastava *et al* (2015) directly linked the nutrient rich environment of the reticulocyte to *P. berghei* tolerance of genetic disruption of parasite metabolic pathways. The metabolically active host cell made the parasite's corresponding pathways redundant. Interestingly, when *P. falciparum* is cultured in mature erythrocytes, viability is lost when the parasite's metabolic pathways are disrupted.

1.3.12 Erythropoiesis during Malaria

Anemia is a common complication in patients presenting with malaria. The WHO defines anemia as hemoglobin levels <13.0 g/dL at sea level in adult men (WHO, 2011). During the disease, the parasite lyses its host erythrocyte in order to gain entry to a new cell and the spleen removes both infected and uninfected erythrocytes from circulation (Safeukui et al., 2015). Nonetheless, the pathology of malaria-associated anemia is complex. As discussed above, a fluctuation in circulating hemoglobin levels would stimulate an increase in erythropoiesis. Malaria anemia is characterised by low reticulocytosis, and as such, it has been suggested that erythropoiesis is suppressed during infection (Pathak and Ghosh, 2016). It has been observed in both human samples and murine models that malaria decreases the numbers of BFU-E and CFU-E in the bone marrow (Maggio-Price et al., 1985; Wickramasinghe and Abdalla, 2000). This is not likely due to a

deficiency in the mechanism of homeostatic regulation, the evidence regarding the status of EPO production during malaria remains conflicted (Chang and Stevenson, 2004). Instead inadequate erythropoiesis is likely mediated by the inflammation within the erythropoietic tissue (Haldar and Mohandas, 2009). Malaria infection induces the release of high levels of inflammatory IFN-gamma and TNF-alpha over a short period (Wickramasinghe and Abdalla, 2000). While there have not been direct studies on erythroblast maturation in malaria infection, an *in vivo* study into *Leishmania donovani* induced anemia concluded that inflammatory cytokines mediated apoptosis of erythroblasts (Lafuse et al., 2013). It is also interesting to note that pro-inflammatory cytokines can also induce the expression of hepcidin from hepatocytes, leading to a decrease in serum iron. As erythropoiesis dominates iron metabolism, there is a direct link between low circulating iron concentration and diserythropoiesis (Cavill, 2002). Therefore, the host's immune response to infection probably makes a significant contribution to anemia.

1.3.13 Organ Remodeling during Malaria

Alongside diserythropoiesis, malaria causes architectural remodeling of the spleen and endothelial cell activation. Hyper-reactive malarial splenomegaly (HMS) is a leading cause of increased spleen weight in malaria endemic areas. It is caused by a aberrant immune response resulting from chronic antigenic stimulation and is distinct from splenomegaly that results directly from malaria parasitaemia (Leoni et al., 2015). The latter pathophysiology is associated with the expansion of the red and white pulp, with the white pulp becoming markedly disorganised (Buffet et al., 2011).

It is interesting to note that infected erythrocytes released extracellular vesicles have been reported to activate endothelial cells, up regulating the expression of ICAM-1 and CD36, thus exacerbating inflammation at the blood-brian barrier (Nantakomol et al., 2011; Campos et al., 2010; Combes et al., 2005).

1.3.14 Summary

The key points in this section were:

- Erythroblasts are extravascular in the bone marrow but in open circulation in the spleen (sections 1.3.1 & 1.3.3; pages 59 & 63)
- Extra medulla erythropoiesis occurs under stress in mice and has been observed in humans (section 1.3.9; pages 72).
- Dyserythropoiesis during malaria contributes to anemia (section 1.3.12; pages 75).
- Defined host invasion ligands are only expressed from the basophilic erythroblast stage (section 1.3.5; page 67).
- Erythroid cytoskeletal proteins are only fully assembled from the polychromatic stage (section 1.3.10; page 74).

1.4 *Plasmodium* within the Erythropoietic Organs of the Host

The key points in this section are:

- All stages of *Plasmodium* are present within the human bone marrow.
- *Plasmodium* can invade erythroblasts.
- There are two predominant models of *in vivo* extravascular infection.

The conclusions to these points are reviewed in the summary: section 1.4.7

1.4.1 Evidence for *Plasmodium* in Human Bone Marrow

Bone marrow aspirates from malaria patients infected with *P. falciparum* (Aguilar et al., 2014a; Abdulsalam et al., 2010; Smalley et al., 1981a; Aguilar et al., 2014b), *P. vivax* (Pothapregada and Kamalakannan, 2014; Imirzalioglu et al., 2006; Yoeli et al., 1948; Tiab et al., 2000; Ru et al., 2009) or *P. malariae* (Imirzalioglu et al., 2006) have consistently contained detectible numbers of parasites. Taking into account the high density of tissue vasculature these observations are not surprising (section 1.3.1). However, many samples were obtained from patients presenting malaria-associated symptoms but with undetectable blood parasitaemia (Aguilar et al., 2014a; Abdulsalam et al., 2010; Aguilar et al., 2014b; Imirzalioglu et al., 2006; Ru et al., 2009). Aspirating and smearing bone marrow samples disturbs the endogenous tissue architecture, consequently studies using these techniques could not determine the location of parasites in relation to the vascular lumen or extravascular tissue. Nonetheless, these observations were the initial indication that the bone marrow is a site of parasite accumulation.

Despite the observable presence of all stages of parasites, Smalley *et al*. (1981) were the first to note the enrichment of *P. falciparum* immature gametocytes within bone marrow aspirates compared with the peripheral blood. This was supported by a recent single patient study in which the authors performed histological analysis of bone marrow samples and reported high numbers of immature *P. falciparum* gametocytes compared with mature gametocytes (Farfour et al., 2012). Significantly, due to the study's use of intact bone marrow sections, Farfour *et al*. (2012) were the first to report the presence of *Plasmodium* within the extravascular spaces of the bone marrow. The

observation that *P. falciparum* immature gametocytes localised within extravascular spaces offers an explanation for their conspicuous absence from peripheral blood (section 1.2.28). Nonetheless, the bone marrow was the only organ biopsied in this patient, and as such, the dynamics of extravascular infection throughout the host's anatomy were not fully addressed in such studies.

The first multi-organ, wide scale histology screen carried out on patient autopsy samples presented evidence that immature gametocytes of *P. falciparum* are over represented within the extra vascular spaces of the bone marrow compared with all other sampled organs (Joice et al., 2014). However, it should also be noted that the authors indirectly stated that ~55% of all parasites detected within extravascular bone marrow were asexual (Joice et al., 2014). Thus, despite immature gametocytes enrichment being the exciting observation, the evidence also interestingly indicates that the erythropoietic tissue may be an uninvestigated niche for both sexual and asexual development of *Plasmodium*.

1.4.2 Invasion of Erythroblasts by Asexual Parasites

The extravascular spaces of the bone marrow contain micro-environmental compartments in which immature erythroid cells proliferate and differentiate (section 1.3.5). Histological *ex vivo* studies of *Plasmodium*-infected bone marrow have not conclusively identified the maturation stage of the extravascular cells containing asexual parasites (Joice et al., 2014; Farfour et al., 2012). However, there is *in vitro* evidence that asexual *P. falciparum* (Peatey et al., 2013; Tamez et al., 2009, 2011; Joice et al., 2014) and *P. vivax* (Panichakul et al., 2007) can invade erythroblasts. This is supported by both an *ex vivo* flow cytometry-based study that reported schizont-like parasites of the murine parasite *P. yoelii* within nucleated Ter119^{+} cells (Imai et al., 2013) and an electron microscopy study that observed *P. vivax* in erythroblasts from bone marrow smears (Ru et al., 2009).

1.4.3 The Two Models of Extravascular Gametocytaemia

The studies discussed in section 1.4.1 (gametocytes within the extravascular spaces of the bone marrow) and those discussed in section 1.4.2 (erythroblast

susceptibility to asexual *Plasmodium*) are complimentary. Drawn together this evidence could support a hypothesis that merozoites establish an extravascular asexual micro-cycle that promotes the parallel development of gametocytes within immature tissue resident erythroid cells (erythroblasts and stage I-II reticulocytes) (Nilsson et al., 2015). However, confusion has arisen from the Joice *et al*. (2014) histological study where the majority of extravascular gametocytes were observed within cells that lacked markers associated with immature erythroid cells, therefore the authors considered these enucleated erythroid cells as 'mature' erythrocytes. As such, a second model has been proposed to address how *Plasmodium* establishes its extravascular gametocytaemia. This model hypothesises that immature gametocyte-infected erythrocytes actively 'home' to the extravascular spaces, transmigrating out of circulation into tissue (Figure 1.27) (Nilsson et al., 2015).

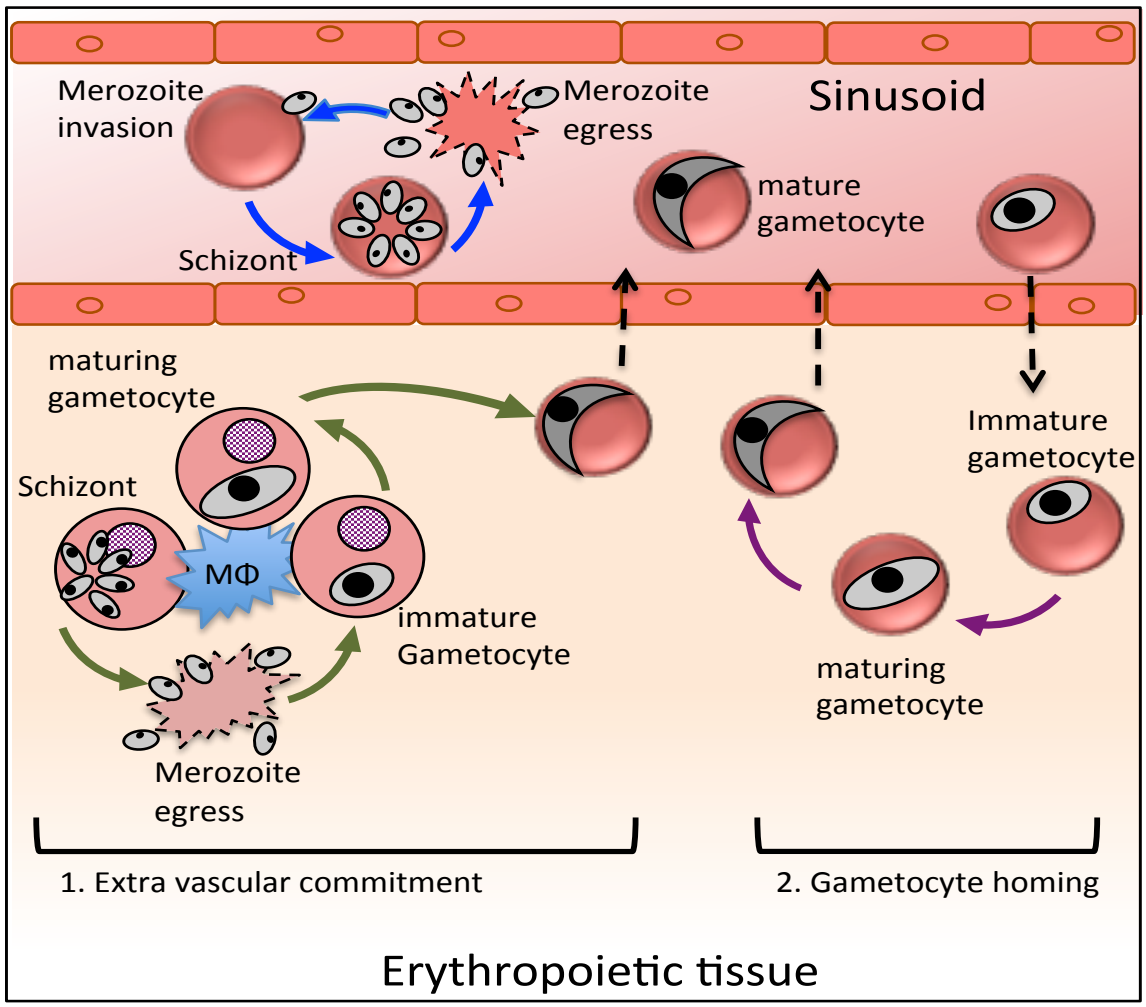

Figure 1. 27 Establishing extravascular gametocytaemia. Two models predominate within the literature to explain the presence of gametocytes within erythropoietic tissue. **1.** Merozoites enter the tissue through an unknown route or mechanism. These merozoites invade immature erythroid cells and form either asexual or sexual parasites. The asexual parasites can go on to seed further gametocyte infection within the tissue. Immature gametocytes mature within the tissue in parallel with their host cell. Mature gametocytes emerge into circulation in enucleated erythroid cells. **2.** Ring stage gametocyte-infected erythrocytes actively home to the erythropoietic tissue through an unknown mechanism. These cells translocate out of circulation into the tissue through an unknown mechanism and gametocyte maturation and decreases in cellular deformability occur here. Terminal gametocyte maturation results in an increase in deformability, which co-insides with the cell detection in peripheral blood.

1.4.4 Gametocyte homing

It is widely accepted that circulating maturing reticulocytes and terminally differentiated erythrocytes are non-motile. However, *in vitro* cultures of *P. falciparum* schizonts with human brain endothelium cell monolayers observed

formation of structures that resembled podosomes, which are involved in leukocyte transmigration (section 1.3.2) (Jambou et al., 2010). It is interesting to note that although erythrocytes do not express cd18 (section 1.3.5), infected erythrocytes display parasite derived ligands that can bind to endothelial cell receptor ICAM-1 and PECAM (section 1.2.23), both of which mediate steps in leukocytes transendothelial migration (section 1.3.2) and both of which are up regulated by endothelial cells during malaria infection (section 1.3.13). Nonetheless, it can be argued that the Jambou *et al* (2010) study was not biologically relevant as the monolayers were derived from an immortalised cell line and the parasitaemia was enriched to 90%. More recently, *in vivo* work from a humanised mouse model indirectly observed the migration of infected erythrocytes into the bone marrow parenchyma (Duffier et al., 2016). Yet, this work relied solely on histological detection of hemozoin within the parenchyma, and as such, conclusions cannot be made about the parasite life stage or viability. A contemporary intravital imaging study directly observed *P. berghei* gametocyte-infected erythrocytes translocating across bone marrow endothelium (De Niz, submitted; Marti Lab, Glasgow, 2016). Though, it should be noted that the authors relied on a constitutive fluorescent proxy and asexual parasite drug depletion in order to infer life cycle stage. Yet, this is the first direct evidence that gametocyte-infected erythrocytes may have the ability to actively and selectively migrate into tissue *in vivo*. Although gametocyte infected erythrocytes do not display parasite derived adhesion ligands (section 1.2.28), it could be hypothesised that the parasite itself conveys motility to the infected cell and this can be tentatively linked to the fully assembled glideosome present within gametocytes during development.

The gametocyte cytoskeleton has also been implicated in extravascular retention. Immature erythroid cells are retained within the erythropoietic tissue through their direct association with ‘nurse’ macrophages (section 1.3.6). Joice *et al* (2014) observed that the majority of extravascular gametocyte-infected ‘mature’ erythroid cells were associated with erythroblastic islands. However, there is no direct evidence that stage III-IV reticulocytes or terminally differentiated erythrocytes can sustain a physical attachment to macrophages. This can largely be attributed to the fact that the adhesion ligands expressed on erythroblasts that are responsible for their attachment are absent from

circulating erythroid cells (Joneckis et al., 1993; Zennadi et al., 2012). It has therefore been suggested that the relatively decreased deformability of immature gametocytes promotes their retention within the extravascular erythropoietic tissue. Furthermore, the increase in deformability of maturing gametocytes mirrors their appearance in the peripheral blood, thus suggesting that the changes in gametocyte physicality is linked to translocation into circulation (Nilsson et al., 2015; Aingaran et al., 2012; Dearnley et al., 2012; Tibúrcio et al., 2012, 2015b).

1.4.5 Model 1 and Model 2 May Coexist

Sexual commitment has been observed to be enhanced when *P. falciparum* is cultured in early erythroid cells compared to terminally differentiated erythrocytes (Peatey et al., 2013; Joice et al., 2014). It has also been observed that erythroblasts are permissive to gametocyte development *in vitro* and infected erythroblasts in culture are able to develop to the point of enucleation (Peatey et al., 2013; Joice et al., 2014). Therefore, *in vitro* evidence suggests that gametocyte infection of erythroblasts is not a dead end and it can therefore be argued that the two models for establishing extravascular gametocytaemia are not mutually exclusive.

1.4.6 Immunological Implications of Erythroblast Infection

Erythroblasts express a high levels of MHC class I molecules and as such there are immunological implications of *Plasmodium* parasitising these cells (Imai et al., 2013). Consequently, there must be a trade off between developing within immature erythroid cells and the potential for killing via $CD8^+$ cytotoxic T cells and subsequent clearance by phagocytic cells (Imai et al., 2015, 2013). However, the literature has not yet directly addressed ability of *Plasmodium* to establish a micro-environmental life cycle within immature erythroid cells, nor the implications this niche could have on malaria.

1.4.7 The Need for a Murine Model of Immature Erythroid Infection

Farfour *et al*. (2012) and Joice *et al*. (2014) were the first to comprehensively show *Plasmodium* has the ability to access the bone marrow extravascular niche. Nonetheless the use of human samples brings a number of limitations. Systematic analysis of the dynamics of infection cannot be performed. Ethically,

administration of chemotherapy cannot be withheld, therefore such studies cannot directly untangle the role chemotherapy plays in either the enrichment of immature gametocytes within the bone marrow or the overall dynamics of extravascular infection. Moreover, the use of frozen or formalin-fixed human samples restricted the authors to histological methodologies and precluded the use of flow cytometry. Only the latter can discretely identify the maturation stages of parasite-infected erythroblasts or early reticulocytes (stage I- II) using cellular markers (Joice et al., 2014; Farfour et al., 2012).

Imai *et al*. (2013, 2015) and Ru *et al* (2009) presented *ex vivo* evidence that *Plasmodium* can invade nucleated non-circulating erythroid cells, however, the authors did not investigate the maturation stage of the parasitised erythroid cell stage, nor the enrichment of parasite life stages.

Here we propose the development of a murine model of tissue resident erythroid infection. This will circumvent and control for the ethical requirement for use of chemotherapeutics. Moreover, this will also open the door to temporal studies that are impossible in humans. Another advantage of using a murine model is that, unlike field samples, the harvested tissue can be analysed rapidly, therefore making the use of flow cytometry a feasible option. The hematology literature has developed robust flow cytometry-based strategies to distinguish the maturing stages of immature erythroblasts in the murine bone marrow and spleen in order to study erythropoiesis (Chen et al., 2009; Liu et al., 2013, 2006). These strategies, with limited modification, could be applied to the investigation of the maturation stages of *Plasmodium* infected immature erythroblasts.

Calculating the parasitaemia of the different erythroid cell stages will reveal the parasite invasion preference, which in itself is interesting. However, as maturation along the erythroid lineage is accompanied by multiple rounds of cell division the cell numbers of different stages of immature erythroid cells are not equal (Liu et al., 2013). This is exacerbated during malaria by *Plasmodium*-induced anemia (Chang et al., 2004; Villeval et al., 1990). As such, the quantifiable feature of flow cytometry will also allow us to identify the immature erythroid cell stage that contains the highest parasite burden, information that may prove biologically relevant to future chemotherapy trials.

Recently, the development of humanised mice models has allowed for the ethical manipulation of human *Plasmodium* infection *in vivo* (Duffier et al., 2016; Moreno et al., 2006; Sabater et al., 2005). Nonetheless, there is a trade off with the use of such models. Murine host immunodeficiency is a prerequisite for human erythrocyte maintenance (Duffier et al., 2016; Moreno et al., 2006; Sabater et al., 2005). The NSG mouse strain used in such studies has a plethora of mutations that manifest as deficiencies in both the innate and adaptive immune systems (C.River, 2017). Considering that host erythropoietic tissue(s) are located within immunological organs, the depletion of the host immune system may have significant effects on erythropoiesis that cannot be experimentally controlled. Moreover, transferring infected human erythrocytes into a murine host precludes the investigation of immature erythroid cells infection. Human-infective *Plasmodium* cannot infect any stage of murine erythroid cells. Therefore in a humanised mouse model, merozoites will not be able to invade murine immature erythroid cells and establish a non-circulating infection. Taking this into account we have chosen to use a murine infective *Plasmodium* species, specifically *P. berghei*, to establish our model.

1.4.8 Summary

- There are two models of extravascular infection (section 1.4.3; page 79).
- The literature has not yet directly addressed *Plasmodium's* ability to establish a micro-environmental life cycle within immature erythroid cells, nor the implications this niche could have on malaria recrudescence (section 1.4.7; page 82).

1.5. Conclusions

Histological studies have observed *Plasmodium* within extravascular spaces of the bone marrow. Although there is evidence that *Plasmodium* can invade immature erythroid cells *in vitro* and *in vivo*, the temporal and spatial dynamics of extravascular infection has not been investigated. Due to the ethical and methodology restrictions imposed on the analyses of human field samples, we propose the development of a *P. berghei* model of immature erythroid infection.

1.6 Aim and Hypothesis

The hypotheses of this work are:

- *P. berghei* invades immature erythroid cells *in vivo*.
- A significant proportion of *P. berghei* parasites within immature erythroid cells undergo gametocytogenesis.
- The immature erythroid cells offer a protective niche during drug administration; thus retaining a pool of parasites that could seed a recrudescent infection.

In order to test the hypotheses, the overarching aim of this project is to establish a murine model of tissue resident erythroid infection. This will be compartmentalised into two questions (Figure 1.28):

1. Does *P. berghei* parasitise tissue resident cells and is there enrichment for a particular life stage?
2. Is erythropoietic tissue infection a source of recrudescence?

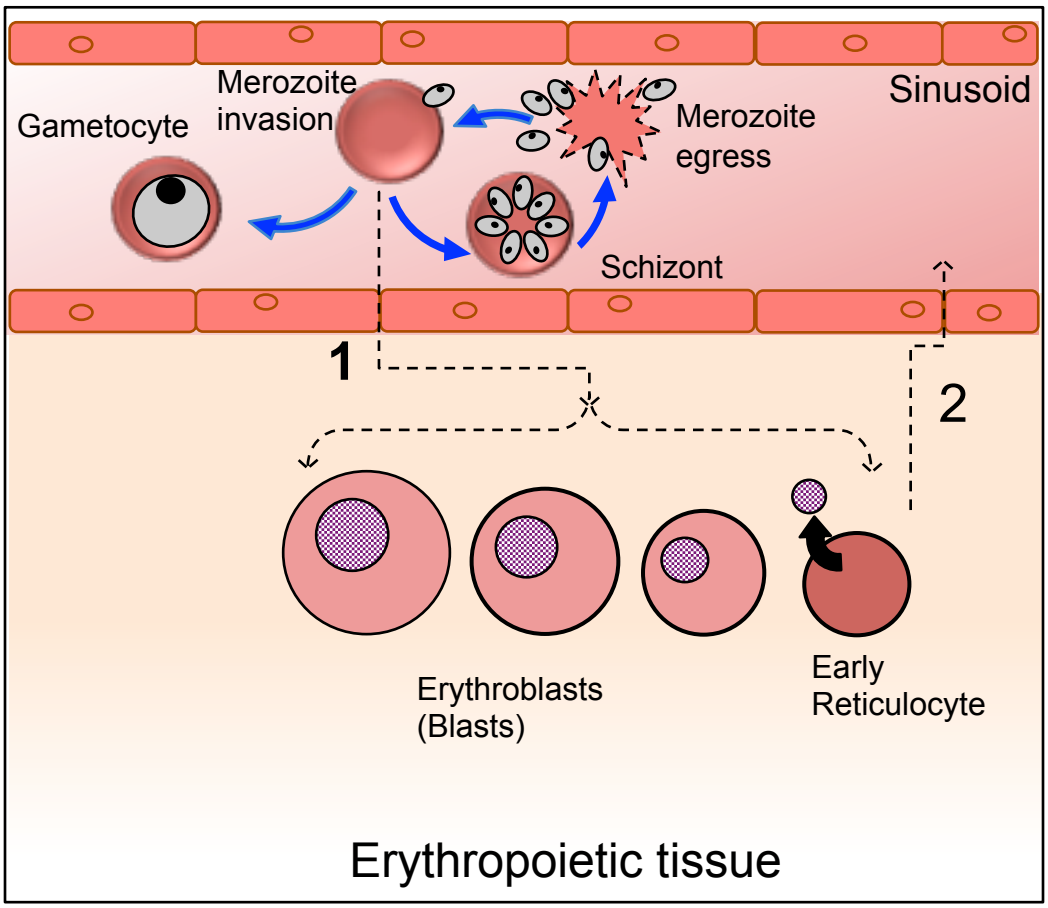

Figure 1.28. **Project aim.** Diagram depicting: the intra vascular (sinusoid) life cycle (blue arrows) of *P. berghei*; the immature erythroid cells (erythroblasts and early reticulocytes) within the erythropoietic tissue. It should be noted that this diagram is more representative of the endothelial lined bone marrow vessels rather than the open circulation of the splenic red pulp, nonetheless, the two questions being asked remain applicable for both tissues. The first question (**1**) asks whether a *P. berghei* merozoite can invade and replicate within erythroblasts and early reticulocytes. Dotted line and arrows associated with question 1 represent the migration of a parasite into the tissue and the parasite's invasion of one of the age classes of erythroid cells. The second question (**2**) asks whether a pool of infected immature erythroid cells remain after drug treatment (complete clearance of peripheral blood infection) and whether this pool could establish a recrudescent infection. The dotted lines and arrows associated with question 2 represent the migration of infected early reticulocytes into the peripheral circulation.

2. Materials and Methods

2.1 Mice

All animal experiments were performed within the strict parameters defined by the Home Office and UK Animals (Scientific Procedures) Act 1986 and approved by the University of Glasgow Ethics Committee.

Female BALB/c (Harlan) and NIH (Harlan) mice were age and weight matched.

6-8 week old female outbred Theiler's Original (TO) mice weighting 25-30 g were procured from Harlan Laboratories (Shardlow, England, UK) and used to maintain parasite stocks.

2.2 *P.berghei* Parasite lines

The characterised *P. berghei*- ANKA PbGFPko230p-SMCON (507 clone1) (Janse *et al.*, 2006) was used to infect mice and as the parental line to *P. berghei* –ANKA $PbGFP_{CON}/RFP_{GAM}$ line. The parasites were asynchronous in order to reflect the dynamics of a natural *P. berghei* infection. This was to reflect the presidence in the literature for observing parasite dynamics across seven days (Franke-Fayard *et al.*, 2005, 2010)

2.3 Statistics

Graphs, means, SEM and SD were calculated from 3 experimental repeats in triplicate unless stated otherwise using Prism 6 (graphPad Software). Error bars are generated from SD unless stated otherwise. Normality was tested. p values were calculated using paired Student *t* test (comparisons of organs and erythroid compartments within a group), unpaired Student *t* test (comparisons between groups), one-way ANOVA in Prism 6 (graphPad Software). p values were calculated for non normal data using mann-whitney U test (graphPad Software). Significant difference between groups or samples were indicated with asterisks, denoting as follows: * $p < 0.05$, ** $p < 0.01$, *** $p < 0.001$, **** $p < 0.0001$.

2.4 Methodologies Used for Identifying Erythroid Cells by Flow Cytometry.

2.4.1 Establishing infection

Infection of laboratory animals with *P. berghei ANKA* was performed intra-peritoneal (IP) using cryopreserved parasites. Cryopreserved parasites were thawed at room temperature for 30 mins and 0.2-0.5 ml of the cryovial contents taken up into a 1 ml syringe. Using a 26G, 0.45x12 mm needle (14-12117, 2019-20, Henke sass wolf) the infected blood was injected IP into the right hand side (avoiding the spleen) of a securely scuffed uninfected animal. Parasitaemia was monitored daily by visual inspection of Giemsa stained thin blood smears.

2.4.2 Seven-day infection

Infection was established by the mechanical passage of tail blood obtained from a previously infected animal (Section 2.4.1). Vasodilation of uninfected mice was induced at 37 °c for 15-20 mins. Mice were appropriately restrained and infected intravenously (IV) with 10^4 parasites diluted in 1 x PBS (Gibco). Parasitaemia was monitored daily either by visual inspection of Giemsa stained thin blood smears or by flow cytometry

2.4.3 Giemsa staining of thin blood smears

Tail blood was used to make thin blood smears on standard microscope slides. The blood was air-dried, fixed for 30 seconds in 100 % methanol and stained in 12 % (v/v) Giemsa for 15 mins. The slides were washed in water, dried and examined under a standard light microscope using a 100 x objective and immersion oil. 10 fields were examined and parasitaemia was expressed as a percentage of infected erythroid cells in the total population of erythroid cells.

2.4.4 Whole body perfusion

Once mice had been anesthetised (Isoflurane), a 5 cm incision was made through the integument and abdominal wall just below the rip cage. Incisions were made through the diaphragm and long the rib cage to expose the pleural cavity. 1.5 ml of blood was exsanguinated via cardiac puncture of the left atrium. Mice were then culled by schedule 1 neck dislocation (The Humane Killing of Animals under Schedule 1 to the Animals Act 1986). 10 ml of 1 x PBS (Gibco) was perfused through the animal using a 10 ml syringe (BD Plastipak) and a 26G, 0.45x12 mm needle (14-12117, 2019-20, Henke sass wolf) inserted into the right atrium. Successful body perfusion was judged by the absence of blood when performing tail vein puncture.

2.4.5 Tissue harvesting

Mice were culled by schedule 1 neck dislocation. Death was confirmed by cardio-respiratory failure and unresponsiveness to pain stimuli. 2-5 µl of peripheral blood was collected in 1 ml of 1 x PBS (Gibco). The spleen was removed, weighted and placed in 1 ml of 1 x PBS (Gibco) and transported on ice. The femur was dislocated from the pelvis and the skin and muscle removed fully from the femur and tibia before the bones were added to 1 ml 1 x PBS (Gibco) and transported on ice. The epiphysis of the femur and tibia were removed using a single edge razor blade (Swann Morton). The bone marrow was perfused from the diaphysis and epiphysis using a 5 ml syringe (BD Plastipak) and 26G, 0.45x12 mm needle (14-12117, 2019-20, Henke sass wolf) containing 3 ml 4 °C 1 x PBS (Gibco). The bone marrow and the spleen were gently dissociated into a 50 ml falcon tube (Greiner) on ice using a 40 µm cell strainer (Greiner), the plunger of a 5 ml syringe (BD Plastipak) and 4 °C 1 x PBS (Gibco). The blood, bone marrow and spleen cells were centrifuged at 400 g for 10 mins at 4 °C and the supernatant discarded. The bone marrow cells were suspended in 1 ml 4 °C 1 x PBS (Gibco) and the spleen in 10 ml. 10 µl of the single cell suspension was suspended 1:1 in 0.04 % trypan blue (Sigma). Viable cells (non stained) were counted using a haemocytometer (Nano Entek) and the total number of cells calculated for each sample. Approx. 3 $x10^7$ cells (total viable cells) of each sample were added per well to a 96 well plate (Costar). The plate was centrifuged at 400 g for 5 mins and the supernatant discarded.

2.4.6 Erythrocyte lysis

Cells were centrifuged at 450 g for 8 mins and then the pellet suspended in 14 ml 1 x erythrocyte lysis buffer (Roche) and incubated at 4 °C for 20 mins. The sample was wash for twice for 5 mins at 400 g in 1 x PBS. This process removed enucleated erythroid cells (early reticulocytes, reticulocytes and erythrocytes).

2.4.7 DyeCycle Ruby optimisation

The appropriate working concentration and staining temperature for DyeCycle Ruby (thermofisher) staining was determined through serial dilution. Blood, spleen and bone marrow tissue was collected from mice infected with 507 clone1 and uninfected controls. Samples of blood and tissue were stained at different DyeCycle Ruby (thermofisher) concentrations and temperatures (Table 2.1). Samples were then stained with the erytrhoid cell flow panel.

Concentration	Temperature
1:100	37°C
1:1000	37°C
1:2000	37°C
1:2000	4°C

Table 2.1 Concentration and Temperature used for DNA stain optimisation

2.4.8 Antibody titration

To determine the appropriate working concentration of each antibody uninfected tissue was prepared and stained with a serial dilution and the data analysed (Table 2.2).

Anti- mouse	Clone	Fluorophore	Company	Dilution
CD44	IM7	PE	BD Biosciences	1 :200
CD71	R17	APC	eBioscience	1 :200
CD71	R17	e450	eBioscience	1 :200
CD45	30-F11	PECY5.5	BD Biosciences	1 :200
CD11b	M1/70	Alexa Fluor 700	eBioscience	1 :200
CD11b	M1/70	eFluor 450	eBioscience	1 :200
CD44	IM7	PECP CY5.5	eBioscience	1 :200
CD45	30-F11	eFluor 450	eBioscience	1 :200
Ter119	Ter119	PECY7	eBioscience	1 :200
Ter119	Ter119	APC	eBioscience	1 :2000 (imageStream)
Sca-1	D7	PE	eBioscience	1 :200
c-kit	2BB	FITc	eBioscience	1 :200
c-Kit	2BB	APC	eBioscience	1 :200
Isotype	Rat IgG2b K Iostype control	PE	eBioscience	1 :200
Isotype	Rat IgG2b K Iostype control	PECP CY5.5	eBioscience	1 :200

Table 2.2 Antibody working concentrations

2.4.9 Flow cytometry

Cell pellets (3 x 10^7 cells) were suspended in 50 µl mouse Fc block targeting CD16/CD32 (grown in house from 2.4G2 cell line) and incubated at 4 °C for 30 mins. The cells were then stained with fluorescently labeled antibodies diluted appropriately in 50 µl mouse Fc block and Vybrant DyeCycle Ruby stain (thermofisher) at a 1 in 2000 concentration before incubating in the dark at 4 °C for 30 mins. The cells were washed twice at 400 g for 3 mins with 4 °C 1 x PBS (Gibco), then stained with fixable viability dye eFluor 506 (ebioscience) at a 1 in 1000 concentration in 4 °C 1 x PBS (Gibco). The cells were incubated at 4 °C for 30 mins in the dark. The cells were washed once at 400 g for 3 mins with 1 x PBS

(Gibco) and suspended in FACS buffer (0.5 M EDTA in 1 x PBS). The cell suspensions were filtered over Nitex mesh (0.2 µm mesh) into FACS tubes (Falcon). Cells were analysed on MACSquant (Miltenyi Biotec) on the low flow rate setting. Quantitative cell numbers were derived from running 10 µl of each fully stained sample on the low flow rate setting. Data were analysed with FlowJo software (Treestar inc.).

2.4.10 Statistical considerations for Flow Cytometry

Identifying infected erythroblasts meant observing populations < 1 % of the sample population. In order accurately report the parasitaemia of the erythroblast stages and to satisfy the issue of poisson statisitcs (the counting of randomly distributed objects in a volume) the whole bone marrow sample was acquired. For the spleen the aim was to satisfy a calculation of the coefficient of variation at 10 – 15 %. A previously published calculation was carried out: $r= (100/CV)^2$; where r is the number of events of a target population to be acquired (Hedley and Keeney, 2013).

2.4.11 Intravascular staining of erythroid cells

Intravascular staining for the discrimination of bone marrow vascular and extra vascular erythroid cells was adapted from a previously described protocol (Anderson *et al.*, 2014). Briefly, mouse reactive fluorescent conjugated antibody was prepared in sterile 1 x PBS (Gibco) and kept on ice. The antibody was injected IV into an uninfected mouse. The mouse was culled by neck dislocation after injection. The femur, tibia and spleen were immediately removed and the bone marrow perfused out with Fc block (grown in house from 24G2 cell line) and all tissue dissociated separately over a 40 µm cell strainer (Greiner). The tissues were immediately washed three times at 400 g for 1 mins with 1 x PBS. The cells where then processed and stained *ex vivo* for flow cytometery (2.4.9).

2.4.12 Image stream

Single cell suspensions of spleen samples from 507 clone1 infected mice were erythrocyte lysed (2.4.6). GFP^+ cells were sorted on a S3 sorter (BioRad) into FACS tubes (Falcon) containing 100 μl 4 °C 1 x PBS (Gibco). The cells were centrifuged at 400 g for 10 mins and the supernatant removed. The cells were blocked in 50 μl mouse Fc block (grown in house from 24G2 cell line) and incubated at 4 °C for 30 mins. Cells were then stained for APC conjugated anti-Ter119 (ebioscience) at 4 °C for 30 mins, then stained for DNA (0.25 μM DyeCycle Violet) at 37 for 30 mins. The sample was run on a ImageStream (amnis) flow cytometer. Images were analysed on the Ideas software (amnis) selecting for $Ter119^+$ cells.

2.4.13 Cell sorting

Erythroid cells were sorted on a FACSARIA III (BD Biosciences), and using a 70 μm nozzle, into FACS tubes (Falcon) containing 1 ml 4 °C 1x PBS (Gibco).

2.4.14 Imaging sorted cells

The sorted cells were centrifuged at 400 g for 10 mins and the cell pellet smeared onto a standard microscope slide. The slides were stained in 12% (v/v) Giemsa or May-Grünwald (0.25 % (w/v) in methanol) (Sigma Aldrich) for 5 mins, washed in 1 % PBS (Gibco) or water. The slides were examined under a standard light microscope using a 100 x objective and immersion oil.

2.4.15 Infection of mice with sorted cells

Uninfected BALB/c mice were infected IV with 100 cell sorted GFP^+ erythroid cells. Parasitaemia was monitored daily.

2.5 Methodologies Used for Generating a *P. berghei* Parasite Line

2.5.1 PCR reaction

Protocol for PCR amplification of *P. berghei* genome fragments and *rfp* (Table 2.3 and 2.4) using a master mix as follows:

Step	Temperature (°C)	Time
Denaturation	95	10 mins
	95	30 s
Annealing	Tm ° C	30 s
Extension	68	1 min/ kb
	To go step 2	X 30
Extension	68	10 mins
Hold	10	∞

Table 2.3 PCR parameters

Reagents	Volume (µl)	Final concentration
10 x PCR buffer	2.5	1x
25mM dNTPs	0.5	0.5 nM
10pmol sense primer	1	1 µM
10pmol anti-sense primer	1	1 µM
50mM $MgCl_2$	1	2 mM
Plat Taq polymerase	0.2	1 Unit
DNA template	1	(50-100 ng)
ddh_20	To 50 µl	

Table 2.4 Master mix reagents

2.5.2 PCR amplification of *rfp*

DNA constructs for used in the genetic modification of *P. berghei* were prepared using standard molecular biology techniques. The *rfp* gene was amplified using a standard PCR reaction (section 2.5.1) from plasmid pG0161 (unpublished). The pair of sense and anti-sense oligonucleotides had the restriction sites for XhoI and XmaI incorporated at the 5' end respectfully. Primers designed using CLC workbench 5.0 and ordered from Eurofins MWG operons (Ebersberg, Germany) (Table 2.5).

Gene	Sense 5'-3'	Antisense 5'-3'
rfp	attctcgagATGAGTAGATCT TCTAAGAACGTC	attcccgggTTACAAGAACAAGTGG TGTCTAC

Table 2.5 Primes for *rfp* amplification. Lower case sequence indicated restriction enzyme site.

2.5.3 Construct assembly

The PCR products were purified using the Qiaquick PCR purification kit (Qiagen) following manufacturer's instructions and the nucleic acid concentration measured using a nanodrop spectrotometer. During the molecular cloning workflow, the purified PCR product and the target plasmid were digested with the same appropriate enzyme(s). XmaI (New England Biolabs) and XhoI (New England Biolabs) were used to facilitate ligation into plasmid pG306 to create pG403 (Figure 2.1). The restriction digestions were carried out in accordance with the manufacturer's instructions. The digested PCR product was purified using the Qiaquick PCR (Qiagen) kit. The digested plasmid was run on a 0.8 % (w/v) agarose gel using 5 x loading dye (Thermo) and 1 kb+ DNA ladder (Thermo). The vector backbone was excised and purified using the Qiaquick gel purification (Qiagen) kit, following the manufactures instructions. The nucleic acid concentrations of the purified PCR product and vector were measured using a nanodrop spectrotometer. A vector and insert ligation reaction was set up in a molar ratio of 1:3 using the Rapid DNA ligation kit (Roche Diagnostics), following

the manufactures instructions. The ligated plasmid was transformed into competent *E. coli* cells by gently mixing 5 µl of the ligation reaction with 60 µl of cells and incubating on ice for 30 mins. The mixture was then heat-shocked at 42 °C for 30 seconds and incubated on ice for 5 mins. The bacteria was then added to 250 µl LB broth (10 g/l tryptone, 5 g/l yeast extract, 5 g/l NaCl) and incubated at 37 °C for 45 mins, before being streaked out on a LB agar (1.5 % (w/v) agar in LB medium) (Amp^+ 100 mg/ ml) plate and incubated for 37 °C overnight.

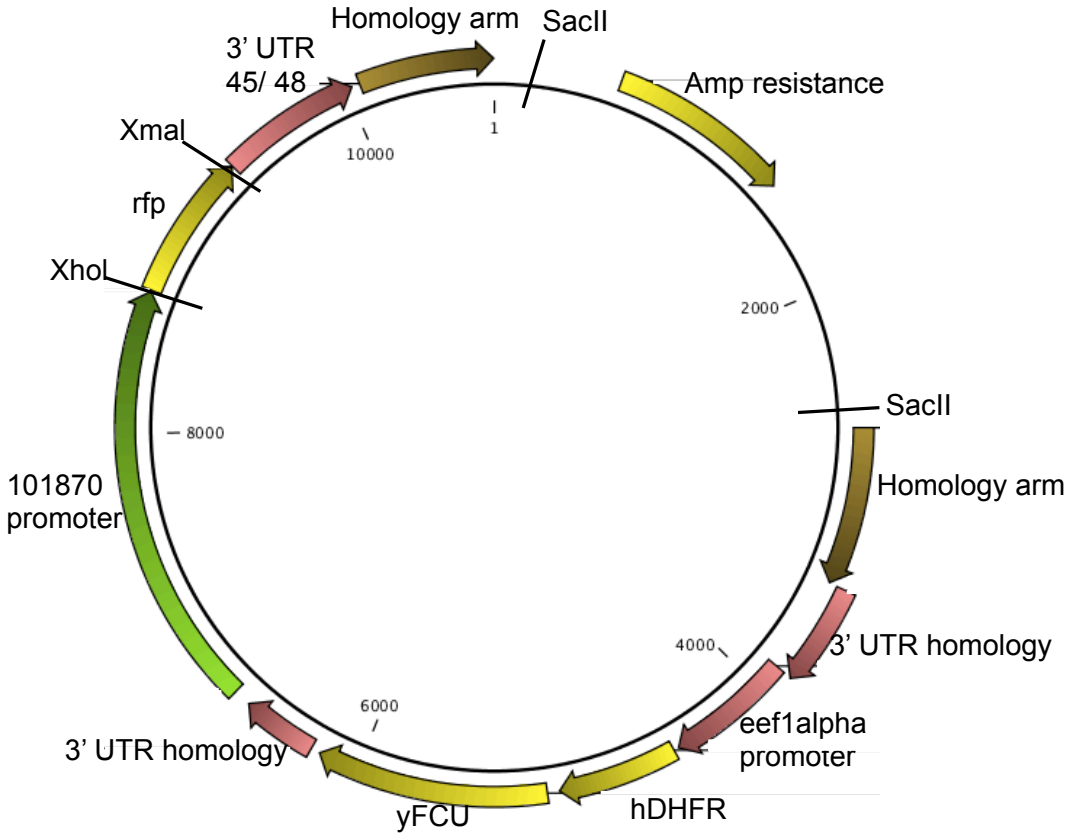

Figure 2.1 Schematic of plasmid pG403. Restriction enzyme sites labeled.

2.5.4 Construct confirmation

Individual bacterial colonies were isolated and incubated in 3 ml LB broth (Amp+) at 37 °C overnight. 1 ml of each culture was added to a cryovial along with 200 µl of 100 % glycerol to make glycerol stocks which where then stored at -80 °C. The plasmid was extracted from the overnight culture using the Qiaquick

miniprep kit (Qiagen), following the manufactures instructions. The extracted plasmids were digested with the appropriate restriction enzymes to excise the open reading frame and 10 µl of the reaction was analysis on a 0.8 % (w/v) agarose gel using 5 x loading dye (Thermo) and 1 kb+ DNA ladder (Thermo). This was done as a diagnostic step to confirm the open reading frame and plasmid had ligated. The sequence of the open reading frame in each plasmid was validated by DNA sequencing (MWG eurofins) using appropriate primers.

2.5.5 Preparation of construct for transfection

The glycerol stock of the bacterial colony containing the confirmed plasmid was used to inoculate 25 ml LB broth (Amp+) and the plasmid extracted using the Qiagen midiprep kit (Qiagen). Plasmids were linearised with SacII (New England Biolabs) digestion in preparation for transfection and double homologous recombination integration within the parasite genome (Figure 2.1).

2.5.6 Phenylhydrazine induced stress erythropoiesis

To increase the percentage of circulating reticulocytes stress erythropoiesis was induced through hemolysis. 0.1 ml phenylhydrazine-Hcl (Sigma) (PHZ) (12.5 mg/ ml) was administered IP using a 26G, 0.45x12 mm needle (14-12117, 2019-20 and 1 ml syringe (BD Plastipak) to an uninfected animal. PHZ was administered two days prior to any subsequent infection.

2.5.7 Short-term culture of asexual stages

Three days post infection 1-1.5 ml of blood was exsanguinated via cardiac puncture under anesthetic (Isoflurane), with 50 µl heparin (200 units/ ml). Death was confirmed by the permanent cessation of the circulation by the severing of the major blood vessels close to the heart. The infected blood was added to 150 ml complete culture medium (RPMI1640, Sodium Bicarb, Hepes, HT suppl. FBS) split across two 75 cm^2 non-vented flasks (falcon). The cultures were gassed (5 % CO_2, 5 % O_2, 90 % N_2) for 30 seconds and incubated at 37 °C, 40 rpm over night. Thin blood smears were made the following day, Giemsa stained, parasitaemia calculated and maturation state of parasites examined (2.4.3).

2.5.8 Purification of schizonts

The 75 cm^2 asexual cultures were combined and centrifuged at 450 g for 10 mins to pellet the erythrocytes. All but 15 ml of the supernatant was removed. The pellet was suspended in the remaining 15 ml supernatant and 55 % (v/v) Nycodenz (Lucron bioproduct) solution was introduced slowly under the culture suspension to create two distinct layers. The Nycodenz culture was centrifuged for 20 mins at 450 g with no break. The thin brown interface between the medium and the nycodenz was gently removed. This layer contained schizonts that were then pelleted by centrifugation for 8 mins at 450 g.

2.5.9 Transfection

Transfection of $PbGFP_{con}$ parasites with linearised constructs, positive and negative selection and cloning of the $PbGFP_{CON}/RFP_{GAM}$ were performed as previously described (Chris J Janse, 2006; Janse *et al.*, 2006; Orr, Philip and Waters, 2012). Briefly, 100 µl nucleofector solution and 5-10 µg linearasised DNA were added to Nycodenz purified schizonts and electroporated using an Amaxa Nucleofector device set to program U-33. The parasites where injected IV into an uninfected animal.

2.5.10 Positive selection of transfected parasites

Pyrimethamine (70 µg/ ml) (Sigma) was administered in the drinking water of the animals one day post infection and continued for 5 days. The correctly integrated construct conveys pyrimethamine resistance from the gene *hdhfr*.

2.5.11 Cryopreserving

When an infected mouse exhibiting 1-2 % parasitaemia 1-1.5 ml of blood was exsanguinated via cardiac puncture under anesthetic (isoflorane) with 50 µl heparin (200 units/ ml). Death was confirmed by the permanent cessation of the circulation by the severing of the major blood vessels close to the heart. 0.4 ml of infected blood was added to an appropriately labeled cryovial and mixed with 0.4 ml 30 % (v/v) glycerol solution (Hparin, glycerol, 1 x PBS). Tubes were incubated at 4 °C for 5 mins then incubated at -80 °C for 1 week before being transferred to liquid nitrogen.

2.5.12 Extraction of parasite genomic DNA

Peripheral blood was erythrocyte lysed (section 2.4.6). The lysis solution was centrifuged at 1700 rpm for 8 mins. The parasite pellet was suspended in 350 µl TNE buffer (10mM Tris (pH 8.0) and 5 mM EDTA (pH 8.0), 100 mM NaCl were subsequently added. The solution was incubate at 37 °C for 10 mins, 200 µg Proteinase K (Sigma) added and then incubated again at 37 °C for 1 hr. 1.5 ml Buffered Phenol (Sigma) was added to the solution, the ependorf tube inverted several times and centrifuged at 4 °C for 5 mins at 14000 rpm. The aqueous upper phase was gently removed and transferred to a new ependorf tube and 1.5 ml buffered phenol: chloroform: isoamylalcohol (25:24:1) (Sigma) was added. The tube was inverted several times and centrifuged at 4 °C for 5 mins at 14000 rpm. Again, the aqueous upper phase was transferred to a new ependorf tube and 1.5 ml chloroform: isoamylalcohol (24:1) (Sigma) was added. The tube was inverted several times and centrifuged at 4 °C for 5 mins at 14000 rpm. The aqueous upper phase was transferred to a new ependorf tube and 0.1 volume of 3 M Sodium acetate, pH 5.2, and 2 volumes of 100 % ethanol were added. The tube was inverted several times and incubated at -20 °C overnight in order to precipitated the DNA. The tube was then centrifuged for 20 mins at 14000 rpm at 4 °C and the DNA pellet washed with 500 µl 70 % (v/v) ethanol. The tube was then centrifuged for 10 mins at 14000 rpm at 4 °C. The supernatant was removed and the DNA pellet was air-aired and suspended in 50 µl double distilled water.

2.5.13 PCR confirmation of construct integration

A PCR reaction was carried out on the extracted parasite gDNA to confirm the correct and full integration of the introduced construct (Table 2.6). The PCR product was visualised on a 0.8 % (w/v) agarose gel using 5 x loading dye (Thermo) and 1 kb+ DNA ladder (Thermo)

Pair name	Primer ID	Sequence
3' integration	GU1682	CATAAACGGTTTATTTAAAGTCATTTTTGG
	GU706	CGACTAGTCCCGGGCTTAACATTCACATATATTAATAATTTTAAT
5' integration	GU1681	TAGTTAGCTTAAATTGTCCAACTGG
	GU1132	GGTATTCTGGCAGAAG

Table 2.6 Sequence of primers used for integration

2.5.14 Cloning By limiting dilution

In order to obtain a clonal parasite line from a single parent a limiting dilution of the desired genotype was carried out. Briefly, a previously PHZ treated donor mouse (2.5.6) was infected IP using a stabolite of the desired genotype. 5 µl of tail blood was harvested from the donor mouse when peripheral blood parasitaemia reached 0.5 %. The tail blood was added to 1 ml 1 x PBS and the erythrocyte concentration determined using a haemocytometer. The parasite suspension was then diluted to 0.8 parasites/ 150 µl 1 x PBS. 10 mice were then inoculated IV with 150 µl of the parasite suspension. Parasitaemias were monitored from day 10 post infection and the infected blood exsanguinated exsanguinated via cardiac puncture under anesthetic (Isoflurane), with 50 µl heparin (200 units/ ml) when peripheral blood parasitaemia reached 1-5 %. Death was confirmed by the permanent cessation of the circulation by the severing of the major blood vessels close to the heart. Clonal populations were checked by PCR and cryopreserved.

2.5.15 Negative selection

5- Fluorocytosine (5-FC)(1.5 mg/ ml) (Sigma) was administered in the drinking water of the animals one day post infection with a clonal parasite line and continued for 5 days. The selection pressure of this drug promotes the spontaneous excision (homologous recombination between 3' UTR homology regions) of the drug selection cassette from the parasites genome due to *yfcu* encoding 5-FC sensitivity. When an infected mouse exhibited 1-2 % parasitaemia, 1-1.5 ml of blood was exsanguinated via cardiac puncture (Isoflurane) with 50 µl heparin (200 units/ ml). The gDNA extracted (2.5.12) and PCR used to check for the loss of the drug selection cassette from the genome (2.5.1). Samples were cryopreserved (Table 2.7).

Primer ID	Sequence
GU1682	CATAAACGGTTTATTTAAAGTCATTTTTGG
GU1681	TAGTTAGCTTAAATTGTCCAACTGG

Table 2.7 Sequence of primers used for identifying the excision of the drug selection cassette.

2.6 Methodologies Used for Characterising a *P. berghei* Parasite Line

2.6.1 *In vitro* reinvasion assay

A erythrocyte invasion assay was performed as described previously (Philip and Waters, 2015). Briefly, Nycodenz purified schizonts (2.5.8) were stained with anti Ter119 at a 6:100 concentration at room temperature for 3 mins before being washed with 1 x PBS (Gibco). Merozoites were released by rupturing schizonts by serially passing through a 5 µm (Acrodisc) and a 1.6 µm (Puradisc, Whatman) and adding to uninfected unstained blood (10 % haematocrit). Cells were incubated at 37 °C and 800 rpm for 10 mins before being added to schizont media. Samples were taken at various time points and analyzed by flow cytometry.

2.6.2 Magnetic column removal of mature gametocytes

Nycodenz enriched schizonts (2.5.8) where injected IV into uninfected mice. 15 mins post injection blood was exsanguinated via cardiac puncture under anesthetic (Isoflurane), with 50 µl heparin (200 units/ ml). Blood was passed over a magnetic column (Macs) at 37 °C to remove mature gametocytes and residual schizonts. The flow through blood containing uninfected erythrocytes and ring stage parasite was collected and cultured (2.5.7).

2.6.3 Gametocyte enrichment with Sulphadimizine

Animals were phenylhydrazine treated (2.5.6) prior to infected IP with $PbGFP_{CON}/RFP_{GAM.}$ Sulphadiazine (30 mg/ ml) was administered to the drinking water of the animals when blood parasitaemia reached >5 %. 48 hrs post drug administration peripheral blood was exsanguinated via cardiac puncture under anesthetic (Isoflurane).

2.6.4 Gametocyte cell sorting

Gametocytes from the sulphadimizine treated peripheral blood (2.6.3) were sorted on a S3 sorter (BioRad), into FACS tubes (Falcon) containing 1 ml 4 °C 1 x PBS (Gibco). Gametocytes were activated by incubating the cells at room temperature (approx. 25 °C). Cells were imaged as descripted in section 2.4.14.

2.7 Methodologies used for the Drug Protection Study.

2.7.1 Drug dosing

Peters' 4 day suppression test was carried out as previously described (Vega-Rodríguez *et al.*, 2015). A 10 mg/ ml stock solution was prepared for CQ diphosphate salt (Sigma-Aldrich) in 1 x PBS (Gibco) and subsequently diluted in 1 x PBS (Gibco). A 10 mg/ ml stock solution was prepared for Pyrimethamine (PRY) (Sigma-Aldrich) in 100 % dimethyl sulfoxide (DMSO) and subsequently diluted in 1 x PBS (Gibco). A 10 mg/ ml and 100 mg/ ml stock solutions of Artemisinin (ART) were prepared in 100 % dimethyl sulfoxide (DMSO). The 100 % DMSO ART stock solution was diluted in sterile water and 45 % cyclodextrin (Sigma) (final concentration of 10 %)(Sigma-Aldrich) so that the final concentration of DMSO was 3 %. BALB/c mice were infected IV with 10^6 $PbGFP_{CON}/RFP_{GAM}$ parasites (Section 2.4.1 and 2.4.2) before being treated with either CQ (IP), PRY (IP) or ART (subcutaneous) 1 hr post infection and every 24 hrs for three additional doses. Mice in control groups received vehicle control (1 x PBS or 3 % DMSO and 10 % cycle dextrin in sterile water). Parasitaemia was monitored daily by flow cytometry. On day 4-post infection parasitaemia was measured for all mice in the group. Bone marrow and spleen were harvested from 3-4 mice per group and flow cytometry analysis performed (Section 2.4.5 and 2.4.9) The parasitaemia of the remaining mice was monitored daily by flow cytometry.

3. Establishing a Quantitative Approach to Investigating *P. berghei* Infection of Tissue Resident Erythroid Cells

3.1. Introduction

The mammalian bone marrow and the murine spleen are characterised sites of erythropoiesis, a dynamic process that gives rise to erythrocytes via sequential maturation and differentiation of nucleated erythroblasts and enucleated reticulocytes. Histological analyses of intact autopsy samples have observed *Plasmodium* within the extravascular spaces of the bone marrow (Farfour *et al.*, 2012; Joice *et al.*, 2014). A direct link can be drawn between this observation and evidence that *Plasmodium* can invade erythroblasts (Ru *et al.*, 2009; Tamez *et al.*, 2009; Imai *et al.*, 2013; Peatey *et al.*, 2013; Joice *et al.*, 2014). While a number of *Plasmodium* species such as *P. berghei* and *P. vivax* isolates have a characterised tropism for circulating reticulocytes (stage III-IV), their tropism for stage I-II reticulocytes found in erythropoietic tissues (Malleret *et al.*, 2015) is unclear. Therefore, the *in vivo* preference of *Plasmodium* within the different stages of maturing tissue resident erythroid cells is worthy of investigation.

The pathology of *in vivo* infection adds an additional level of complexity to studying the infection of tissue resident erythroid cells. Malaria triggers anaemia and splenic remodelling, both are a consequence of the dynamic interplay between the parasite and the host immune system (Haldar and Mohandas, 2009; Buffet *et al.*, 2011). Superimposed on this, the two erythropoietic tissues in the mouse (the bone marrow and the spleen) are accessible via different routes. The bone marrow parenchyma is reached via the active transmigration of cells out of the sinusoidal lumen, whereas arterial blood empties into the red pulp of the murine spleen as part of the open circulation (Travlos, 2006; Maxie, 2015). Furthermore, the maturation of erythroid cells within the murine bone marrow and the spleen are regulated under distinct conditions of homeostasis and stress respectively (Reichardt *et al.*, 1998; Bauer *et al.*, 1999). As such, alongside parasite preference, this chapter will identify the tissue specific erythroid stage that presents the highest tissue resident parasite burden within an infection.

Here a flow cytometric approach for identifying erythroid cells will be optimised for use with a *P. berghei* line constitutively expressing GFP (Janse *et al.*, 2006; Liu *et al.*, 2013). As such, the aims of this chapter are to:

- Identify *P. berghei* susceptible erythroid cells.
- Identify the tissue-specific erythroid stage with the highest parasitaemia.
- Establish that tissue resident erythroid cells are also permissive to *P. berghei* development.
- Identify erythroid cell stages that present the highest parasite burden *in vivo* in tissue resident infections.

3.2. Results

3.2.1. CD71 is an Unreliable Marker for Detecting Different Stages of Erythroid Cells

Immunofluorescence identification of the surface proteins CD71 and Ter119 is currently the only protocol used to distinguish between different stages of circulating erythroid cells during *Plasmodium* infection (Martín-jaular *et al.*, 2013; Lelliott *et al.*, 2014; Lelliott, Mcmorran and Foote, 2015). As such, the detection of tissue resident erythroid cells was initially optimised based on this combination of surface markers. Spleen, bone marrow and peripheral blood were harvested from uninfected, non-perfused mice to allow direct comparison with the established haematology literature (Figure 3.1A). Using flow cytometry analysis of relative CD71 expression (Figure 3.1B) (Liu *et al.*, 2006), viable erythroid cells ($CD45^{-/low}$, $Ter119^{+}$) cells identified in both organs were separated into erythrocytes (EryA; $CD71^{-}$ small cells), reticulocytes (EryB; $CD71^{+}$ small cells) and erythroblasts (EryC; $CD71^{+}$ large cells) (Figure 3.1C). Cells were detectable within the EryB gate of peripheral blood, thus making it impossible to distinguish between circulating and tissue resident reticulocytes (Figure 3.1B). This observation is corroborated by previous flow and immunoblot analysis (Chen *et al.*, 2009; Martín-jaular *et al.*, 2013). As such, the combination of these markers could not discretely resolve tissue resident and peripheral blood erythroid cells. Moreover, when this gating strategy was applied to samples harvested from *P. berghei* infected mice there was an obvious disparity (Figure 3.1A & D). A significant decrease in CD71 abundance was observed, as determined by mean fluorescence intensity (MFI), in the EryB and EryC populations derived from infected spleen samples compared with uninfected samples (Figure 3.1E). To examine whether decreased CD71 expression was restricted to infected cells a *P. berghei* line that constitutively expresses GFP throughout its life-cycle (PbGFPko230p-SMCON: 507 clone1) was used (Janse *et al.*, 2006). A difference in CD71 MFI between parasitised (GFP^{+}) and non-parasitised (GFP^{-}) EryB or EryC populations in the *P. berghei* infected spleen was not observed (Figure 3.1F). This suggests that *P. berghei* infection results in the loss of CD71 from the maturing erythroid cell surface at a population level. More

importantly, this observation makes CD71 an unreliable marker for defining erythroid populations during *Plasmodium* infection.

A.

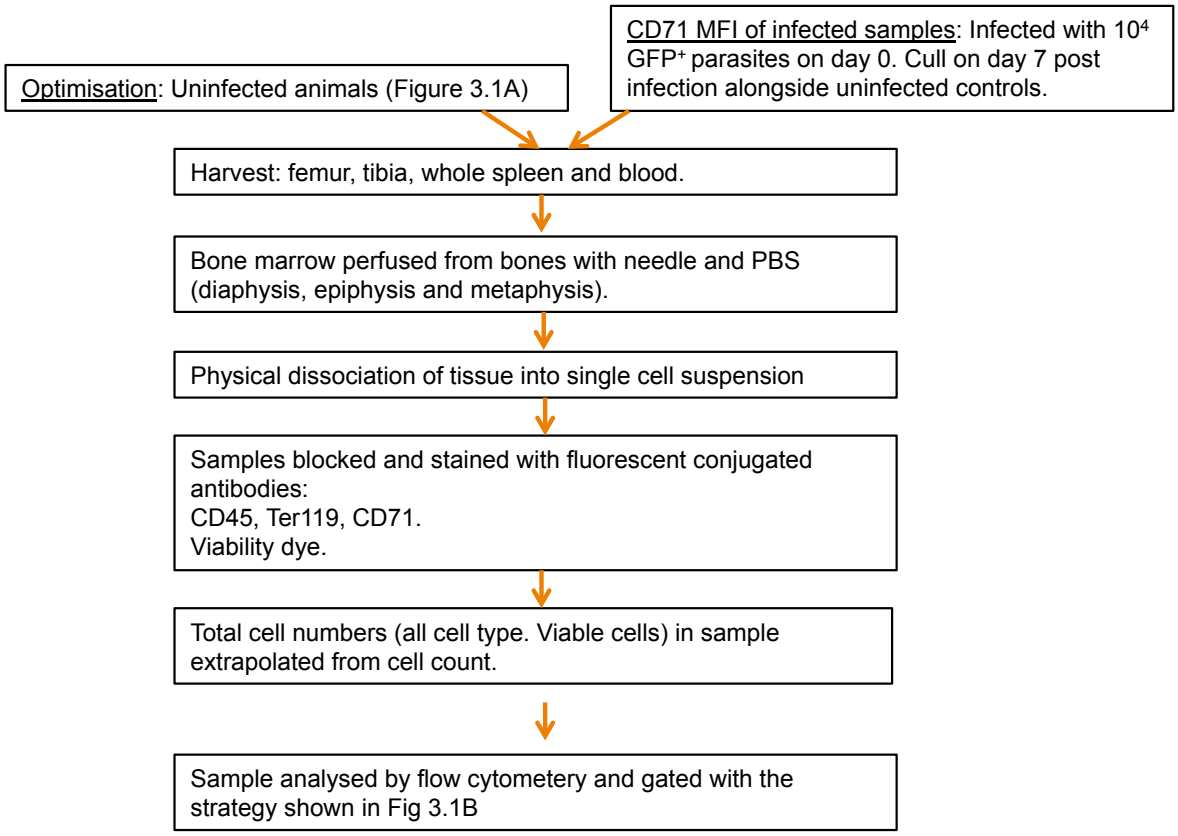

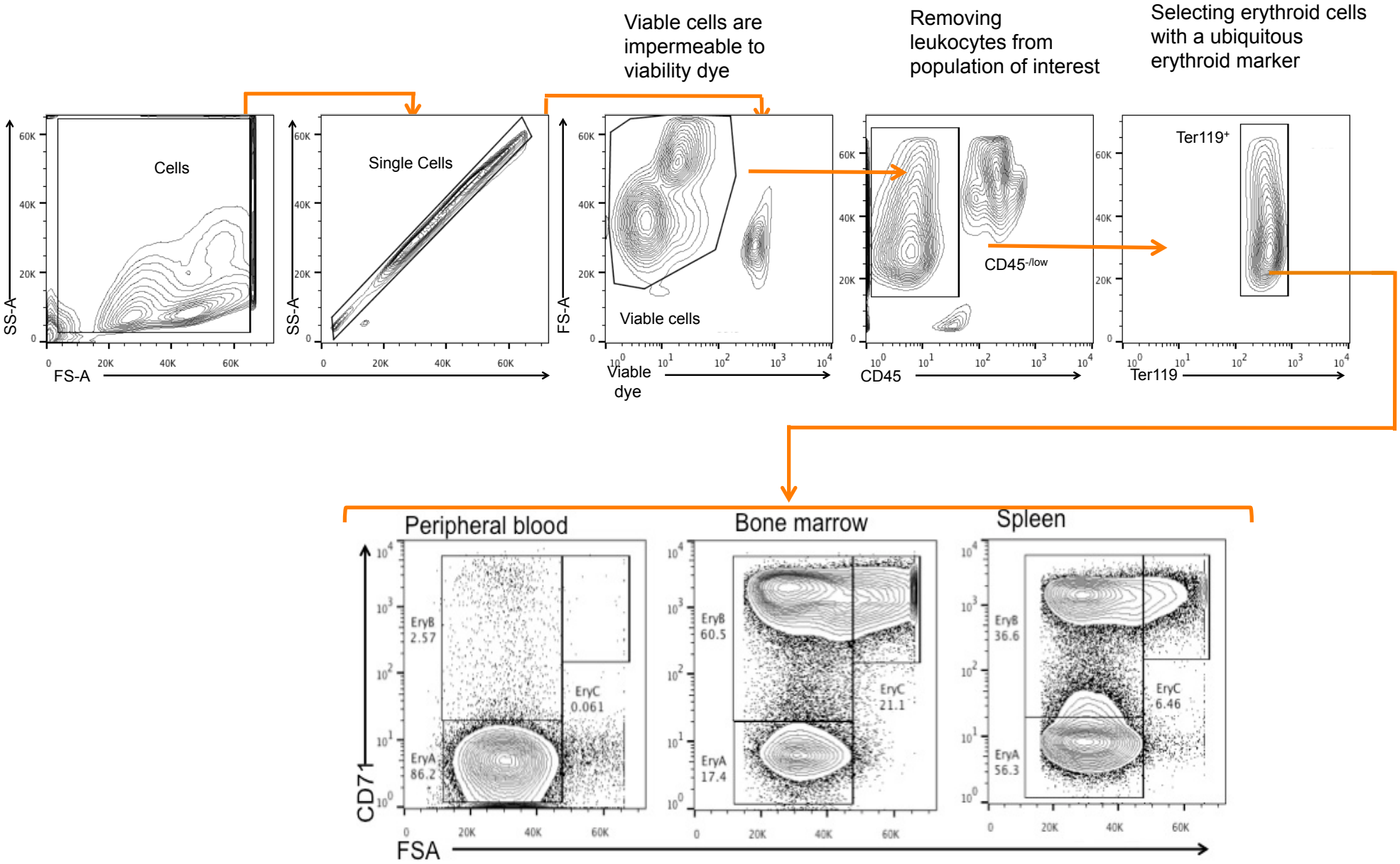
Viable cells are impermeable to viability dye
Removing leukocytes from population of interest
Selecting erythroid cells with a ubiquitous erythroid marker
Cells
Single Cells
Viable cells
CD45-/low
Ter119+
SS-A
FS-A
Viable dye
CD45
Ter119
Peripheral blood
Bone marrow
Spleen
CD71
FSA
EryB 2.57
EryC 0.061
EryA 86.2
EryB 60.5
EryC 21.1
EryA 17.4
EryB 36.6
EryC 6.46
EryA 56.3

C.

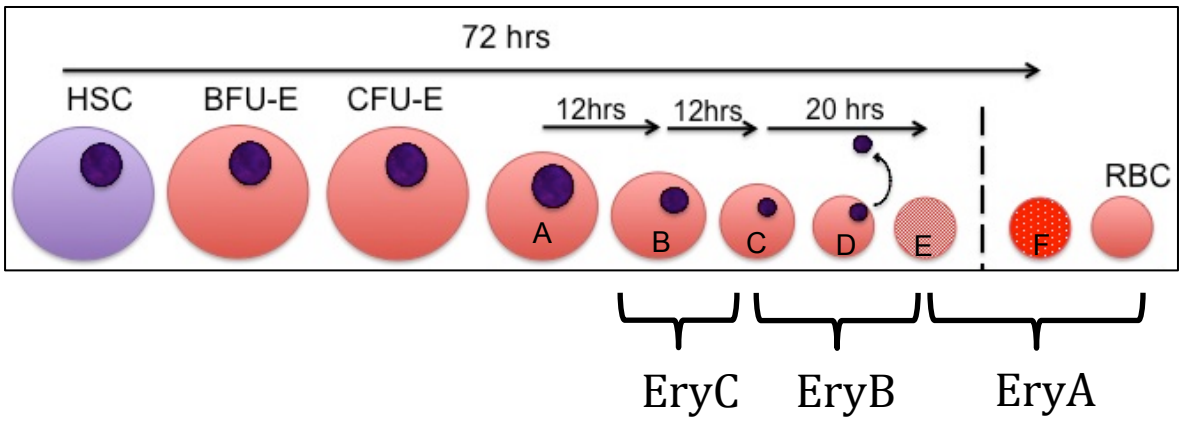
72 hrs
HSC
BFU-E
CFU-E
12hrs
12hrs
20 hrs
RBC
A
B
C
D
E
F
EryC
EryB
EryA

D.

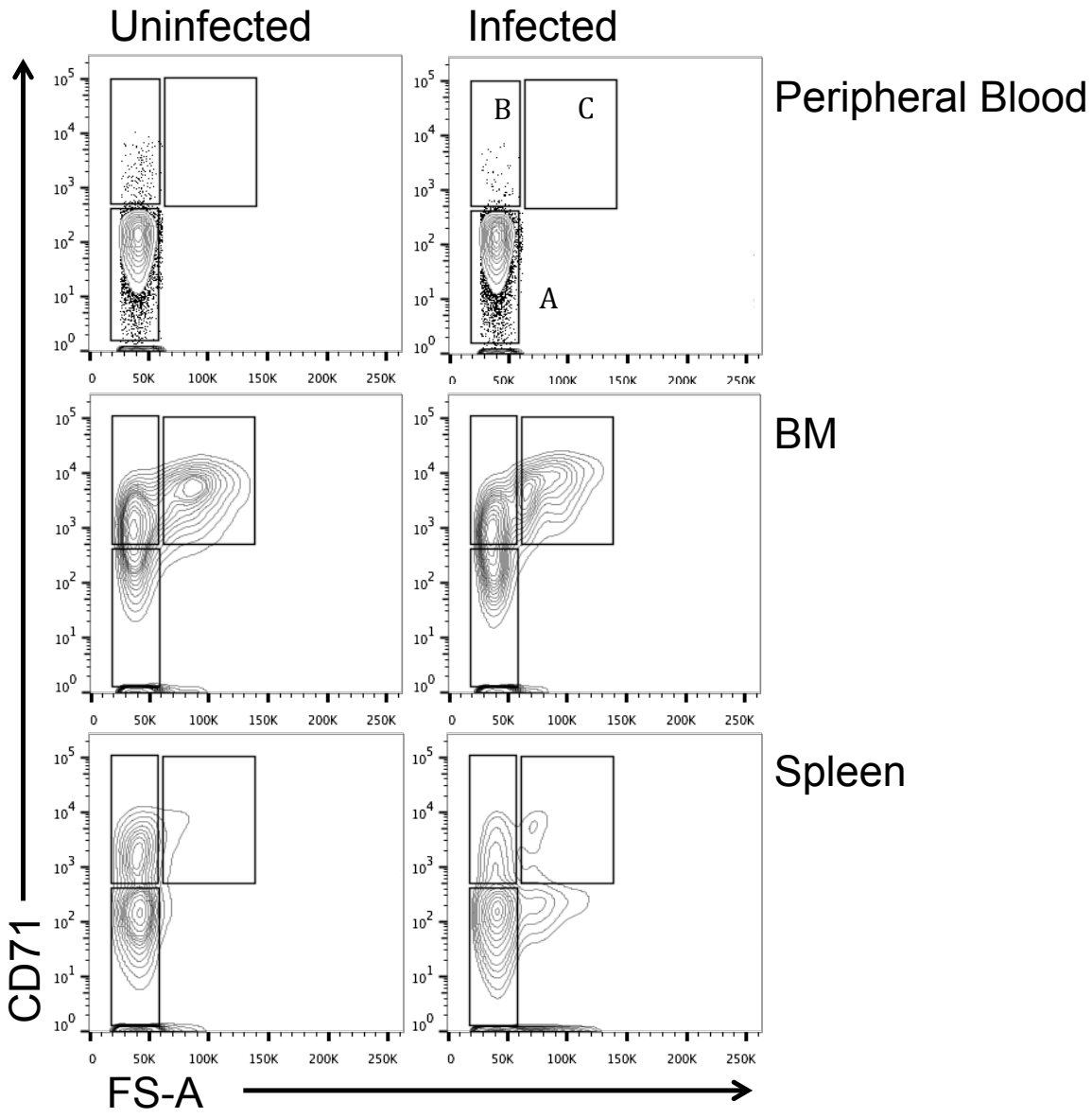
Uninfected
Infected
Peripheral Blood
BM
Spleen
B
C
A
CD71
FS-A

E.

	Peripheral blood		Bone marrow		Spleen	
	gate A	gate B	gate B	gate C	gate B	gate C
uninfected	75 ± 4	3500 ± 1618	1648 ± 79	3694 ± 494	2194 ± 255	4508 ± 614
infected	82 ± 3	1423 ± 212	1549 ± 30	4160 ± 541	1767 ± 43	2495 ± 187
	p = 0.06	p = 0.09	p = 0.2	p = 0.3	* p = 0.04	** p = 0.005

F.

	Spleen	
	ER	EB
GFP-	1561 ± 444	2079 ± 603
GFP+	1902 ± 131	2626 ± 214
	p = 0.1	p = 0.6

Figure 3.1 CD71 is an unreliable marker for resolving different erythroid populations during *P. berghei* infection. A. Flow diagram of methodology used to generate data with the CD71 vs Ter119 gating strategy **B**, Representative FACS plots of uninfected bone marrow. Representative plots for spleen and peripheral blood can be found in the Appendix 8.1.1 The orange arrows indicate the sequential hierarchy of the gating strategy. Cells were gated successively as singlets and then as viable cells based on their impermeability to a viability dye. Leukocytes were removed from the viable population by excluding cells expressing the pan leukocyte marker CD45. The gate was set as $CD45^{-/low}$ due to the most immature stages of erythroblasts expressing a low level of CD45 (Gordon *et al.*, 2008). Next erythroid cells were selected from the $CD45^{-/low}$ population based on their expressed of the ubiquitous erythroid marker Ter119. Erythroid cells were separated into three populations based on their size (FS-A) and their expression of the transferrin receptor CD71 (a erythroid specific marker down regulated during maturation). Previous studies had determined that erythrocytes and mature reticulocytes fall into the EryA gate, maturing reticulocytes and late erythroblasts fall into the EryB gate and early erythroblasts into the EryC gate (Liu *et al.*, 2006). The plots show that the reticulocytes within the peripheral blood and the tissue expressed similar levels of CD71. **C.** Schematic indicating which developmental stages of erythroid cells that fall into the gates EryC, EryB and EryA. CFU-E transform into A. pro-erythroblast, which then successively differentiate into B. basophilic erythroblast, C. polychromatic erythroblast and D. orthochromatic erythroblast. The orthochromatic stage enucleates to become an enucleated reticulocyte. The differentiation times in mice are marked above the cells (Chen et al., 2009; Filmanowicz and Gurney, 1961). E. Stage I-II reticulocytes mature within the tissue. F. Stage III-IV reticulocytes are within the circulation. The final differentiation stage is erythrocytes (RBC). The vertical dotted line indicates the separation between circulating and tissue resident stages. **D.** Representative Flow cytometry plots of viable, $CD45^{-}$, $Ter119^{+}$ cells gated against CD71 and FS-A. Left hand column contains plots from uninfected animals; right hand column contains plots from infected animals. The tissue from which the cells derive is labeled down the right hand side. BM: bone marrow **E**, Mean expression levels of CD71 as demonstrated by MFI (± SD) within the $CD45^{-/low}$, $Ter119^{+}$ circulating cell population (EryA) from the peripheral blood. The table also shows the mean MFI of CD71 (± SD) of EryB and EryC extracted from organs of uninfected and *P. berghei* infected mice. The p values, calculated from a t test, describe the difference between the CD71 MFI of the corresponding populations in the uninfected and infected mice (n=3). **F**, Mean expression levels of CD71, shown by MFI (± SD) of parasitised cells (GFP^{+}) compared with non parasitised cells (GFP^{-}) in the EryB and EryC gates taken from the spleens of *P. berghei* infected animals (n = 3). NS= not significant.

3.2.2. Identifying Erythroid Cell Maturation Stages: Optimising the Methodology with CD44

3.2.2.1 CD44 vs Ter119

Flow based approaches in the haematology literature have recently defined that a combination of CD44 detection and cell size (FS-A) can separate Ter119^{+} cells into discrete stages of erythroid maturation (Chen *et al.*, 2009; Liu *et al.*, 2013). Using this combination of immunofluorescence markers, optimisation was again initiated with uninfected non-perfused samples (Figure 3.2A). Viable, CD45$^{-/low}$, CD11b^{-}, Ter119^{+} were identified in the peripheral blood samples using flow cytometry (Figure 3.2B). The isotype control for CD44 staining indicated that this cell marker is not completely lost from erythroid cells in peripheral blood (Figure 3.2C). This is in agreement with both immunoblotting and flow analysis from previous studies (Bony *et al.*, 1999; Chen *et al.*, 2009).

A.

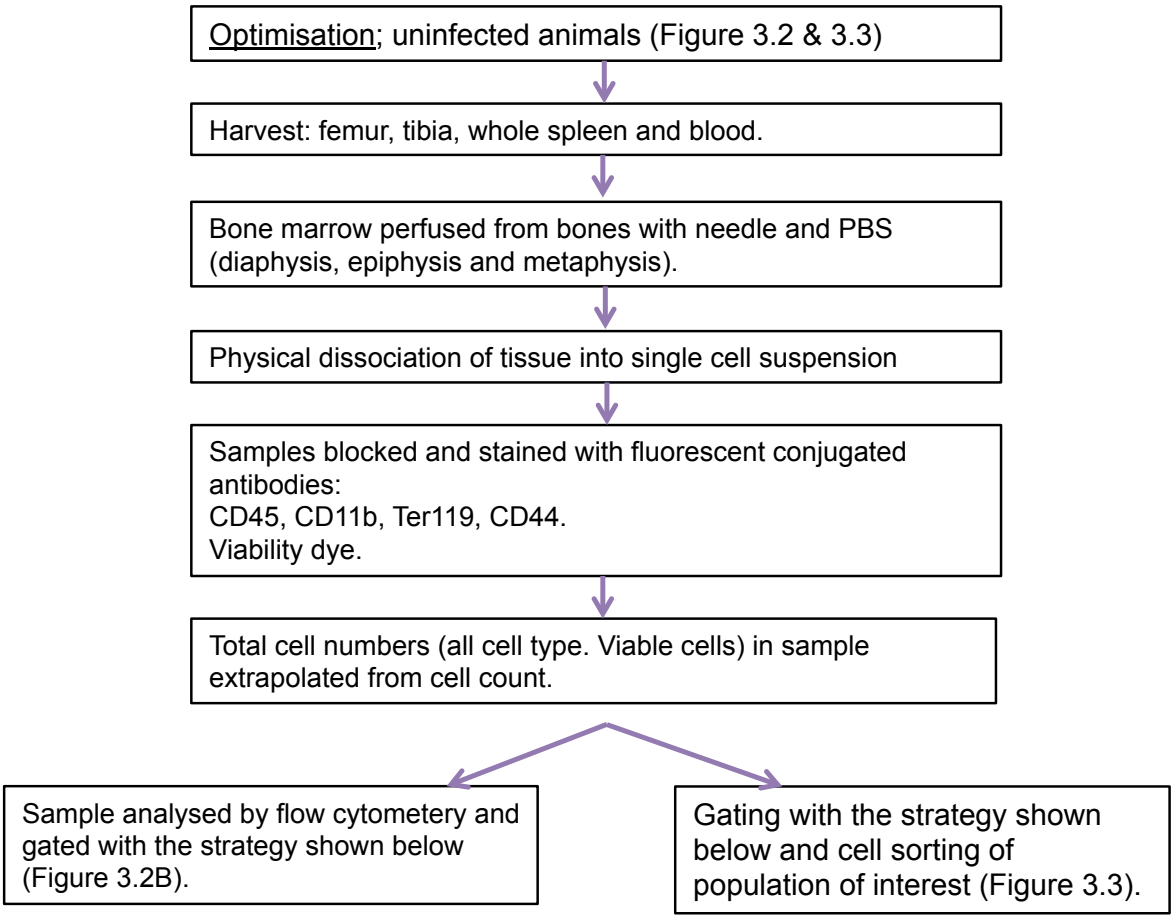

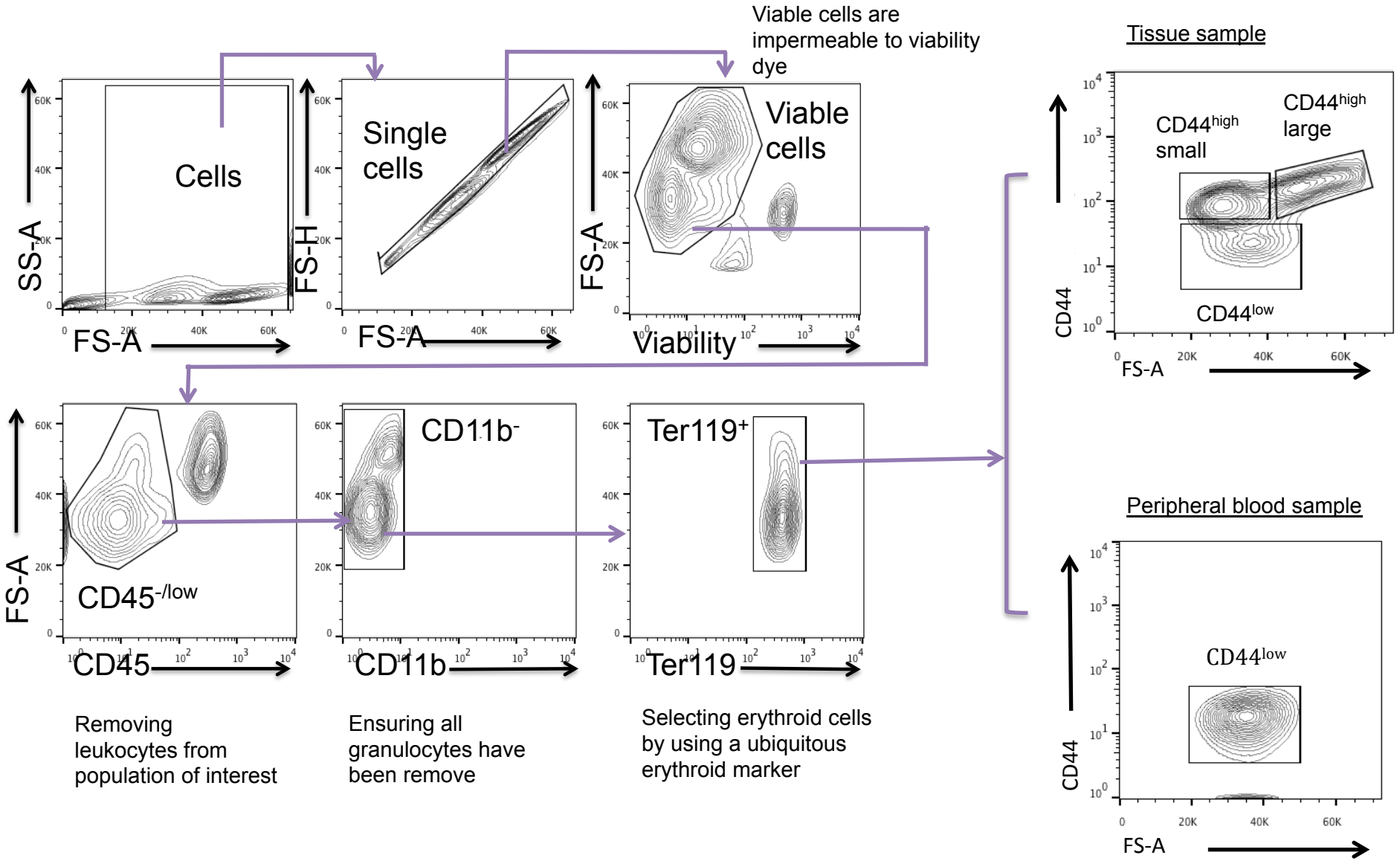
Viable cells are impermeable to viability dye
Cells
SS-A
FS-A
Single cells
FS-H
FS-A
Viable cells
FS-A
Viability
CD45-/low
FS-A
CD45
CD11b-
CD11b
Ter119+
Ter119
Removing leukocytes from population of interest
Ensuring all granulocytes have been remove
Selecting erythroid cells by using a ubiquitous erythroid marker
Tissue sample
CD44high small
CD44high large
CD44low
CD44
FS-A
Peripheral blood sample
CD44low
CD44
FS-A

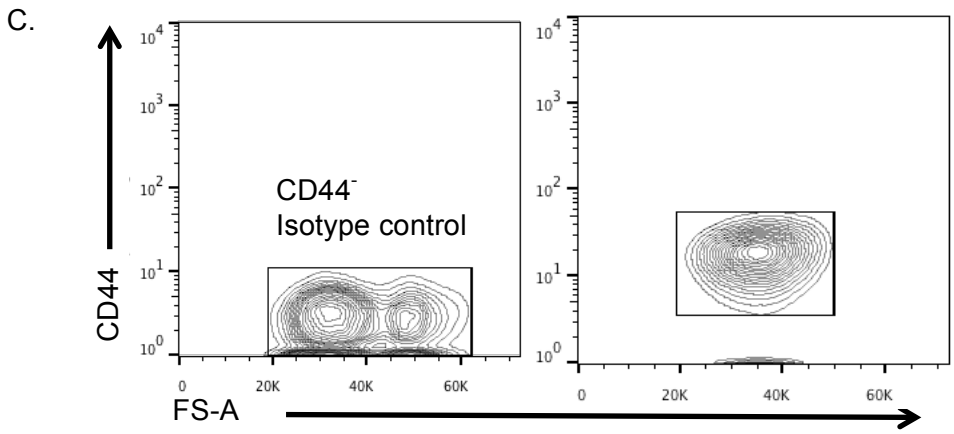

Figure 3.1 Two exclusively tissue resident erythroid populations can be identified by CD44 expression. A. Flow diagram of methodology used to generate data with the CD44 vd Ter119 gating strategy **B.** Representative FACS plots of the uninfected tissue sample (bone marrow. Representative plots for uninfected spleen can be found in the Appendix 8.1.2. The purple arrows indicate the sequential hierarchy of the gating strategy. Cells were gated successively as singlets and then as viable cells based on their impermeability to a viability dye. Leukocytes were removed from the viable population by excluding cells expressing the pan leukocyte marker CD45. The gate was set as $CD45^{-/low}$ due to the most immature stages of erythroblasts expressing a low level of CD45 (Gordon *et al.*, 2008). Granulocytes can be gated as $CD45^{low}$, to ensure all of these cells were removed from the population of interest cells negative for CD11b, a marker on granulocytes, were selected. Next erythroid cells were selected from the $CD11b^{-}$ population based on their expressed of the ubiquitous erythroid marker Ter119. $Ter119^{+}$ cells within the peripheral blood had a $CD44^{low}$ profile. The $CD44^{low}$ peripheral blood gate was transposed onto $Ter119^{+}$ cells from the tissue. Two additional $Ter119^{+}$ populations could be gated in the tissue samples based on CD44 expression and cell size (FS-A). These where called $CD44^{high}$ small and $CD44^{high}$ large. **C.** The left hand graph is a representative FACS plot of the CD44 isotype control. The right hand graph is a representative FACS plot of CD44 staining of $CD45^{-/low}$, $CD11b^{-}$, $Ter119^{+}$ cells in the peripheral blood.

3.2.2.2 Reliably Separating Nucleated and Enucleated Tissue Resident Erythroid Cells

In addition to the Ter119^{+}CD44^{low} population, the bone marrow and the spleen both contained a Ter119^{+}CD44^{high} population with low forward scatter (FS-A; small size) and a Ter119^{+}CD44^{high} population of larger cells (Figure 3.2B). Based on previous studies (Chen *et al.*, 2009; Liu *et al.*, 2013) these gates were termed early reticulocyte and erythroblast, respectively (Figure 3.3). The CD44^{high} large cells from uninfected bone marrow were cell sorted to determine whether the population exclusively contained nucleated erythroblasts. However, light microscopy of the sorted population revealed contamination with enucleated cells (Figure 3.3).

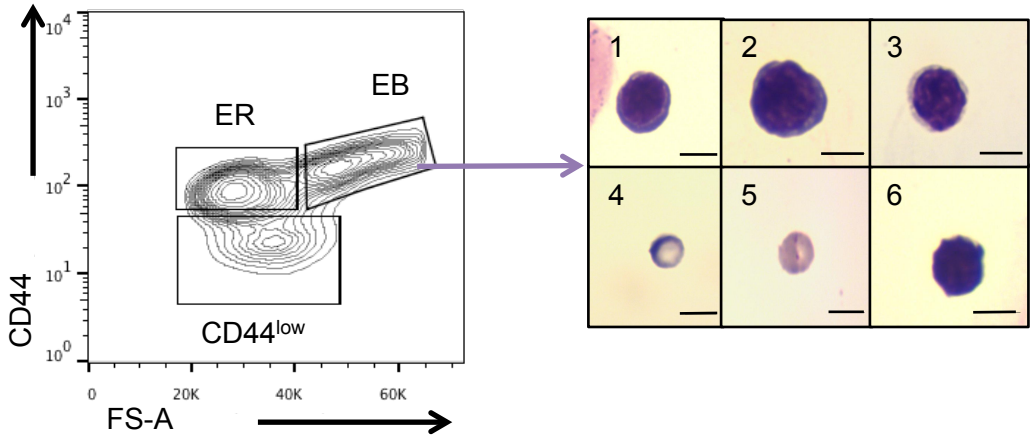

Figure 3.3 Erythroblasts and early reticulocytes could not be easily resolved. FACS plot shows uninfected bone marrow Viable, CD45$^{-/low}$, CD11b^{-}, Ter119^{+} cells gated against CD44 and FS-A. The CD44^{low} population was defined on the peripheral blood samples then transposed onto the tissue sample. The CD44^{high}, FS-A ^{low} (small) cells and the CD44^{high} large cells were termed early reticulocyte (ER) and erythroblasts (EB), respectively. Six representative images of cells sorted from the proposed erythroblasts (CD44 ^{high}, FS-A ^{high}) gate. Cells were stained with Giemsa and examined by light microscopy. This revealed that the gate was contaminated with enucleated cells (images 4 and 5). Scale bar 6 µm.

To circumvent this problem, a fluorescent DNA dye was included in the flow cytometry staining panel, allowing for the separation of DNA^+ and DNA^- cells in uninfected samples. However, as this methodology would be applied to infected tissues, the staining protocol was also tested on *P. berghei* infected blood and tissue samples. When the gating strategy, defined by the uninfected samples, was superimposed onto the infected samples DNA^+ staining of parasites in the peripheral blood was observed. This also affected the integrity of the gating strategy in the infected tissue samples, making it difficult to define enucleated and nucleated erythroid cells. However, the DNA staining protocol was optimised, through titrating the concentration and incubating at different temperatures, to ensure that the erythroid cell nucleus was stained but the intracellular parasite nucleus was not; the chosen staining condition was a 1:2000 concentration at 4°C (Figure 3.4 E).

A.

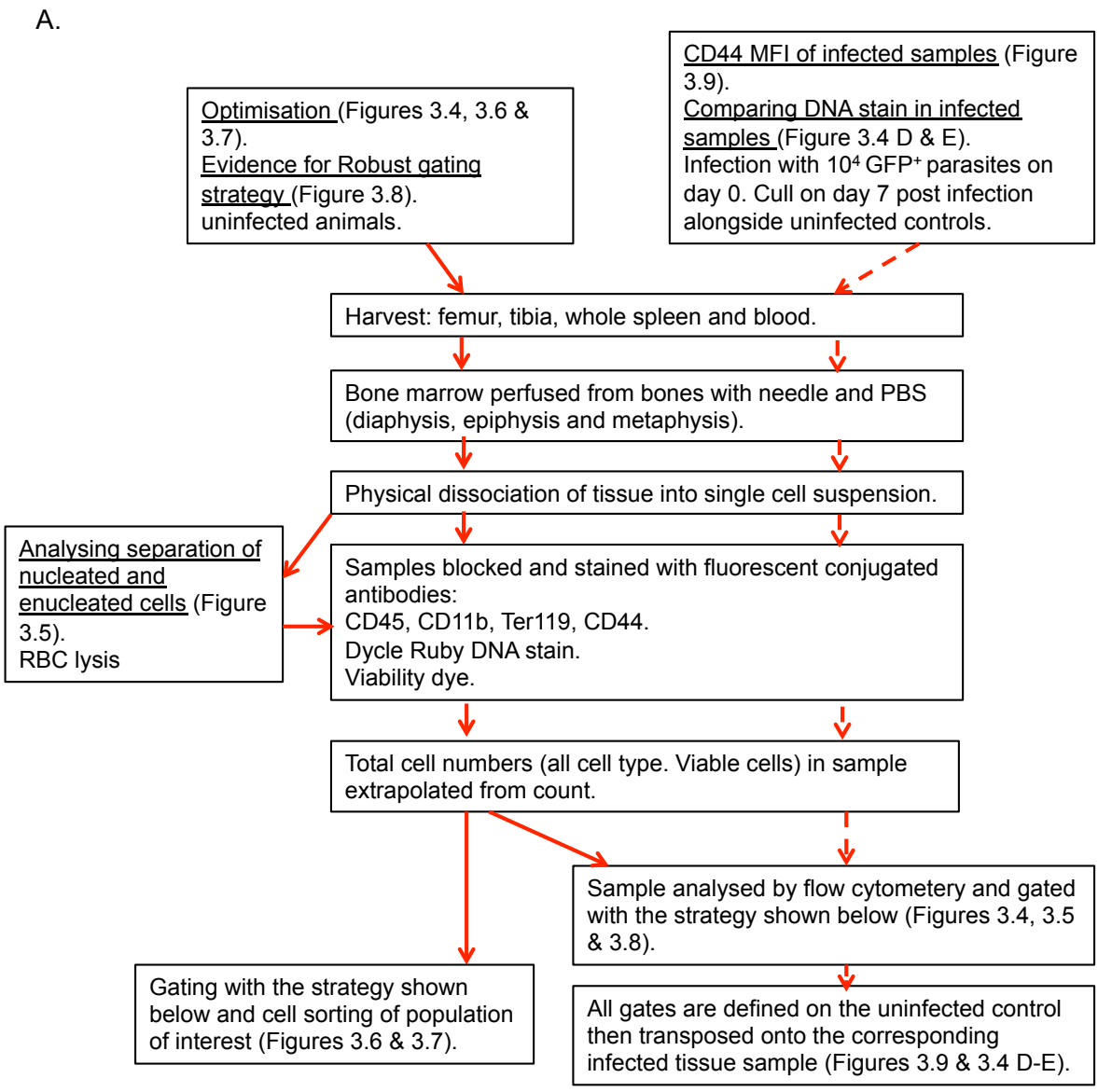

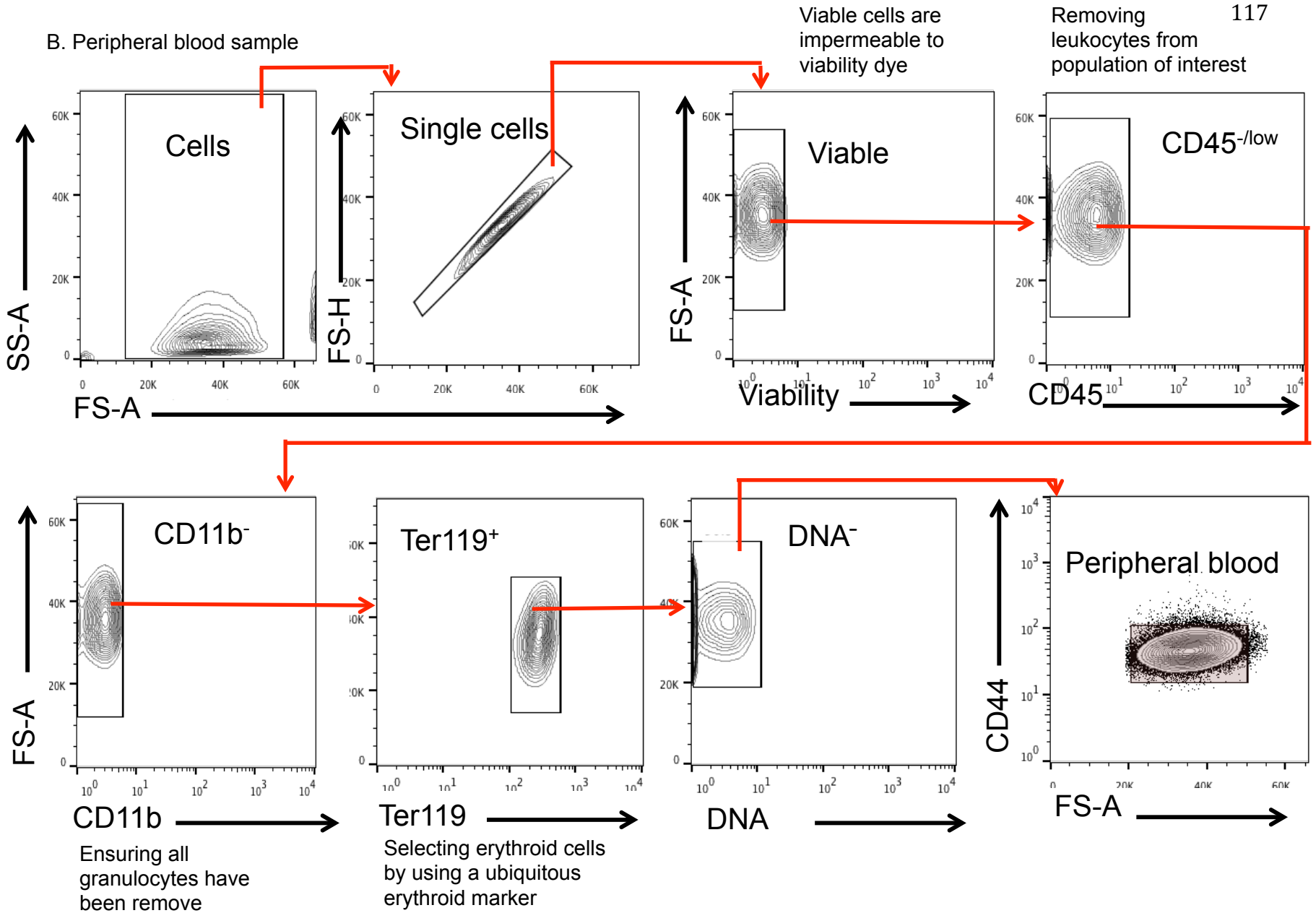
B. Peripheral blood sample
Cells
SS-A
FS-A
Single cells
FS-H
FS-A
Viable cells are impermeable to viability dye
Viable
FS-A
Viability
Removing leukocytes from population of interest
CD45-/low
CD45
CD11b-
FS-A
CD11b
Ensuring all granulocytes have been remove
Ter119+
Ter119
Selecting erythroid cells by using a ubiquitous erythroid marker
DNA-
DNA
Peripheral blood
CD44
FS-A

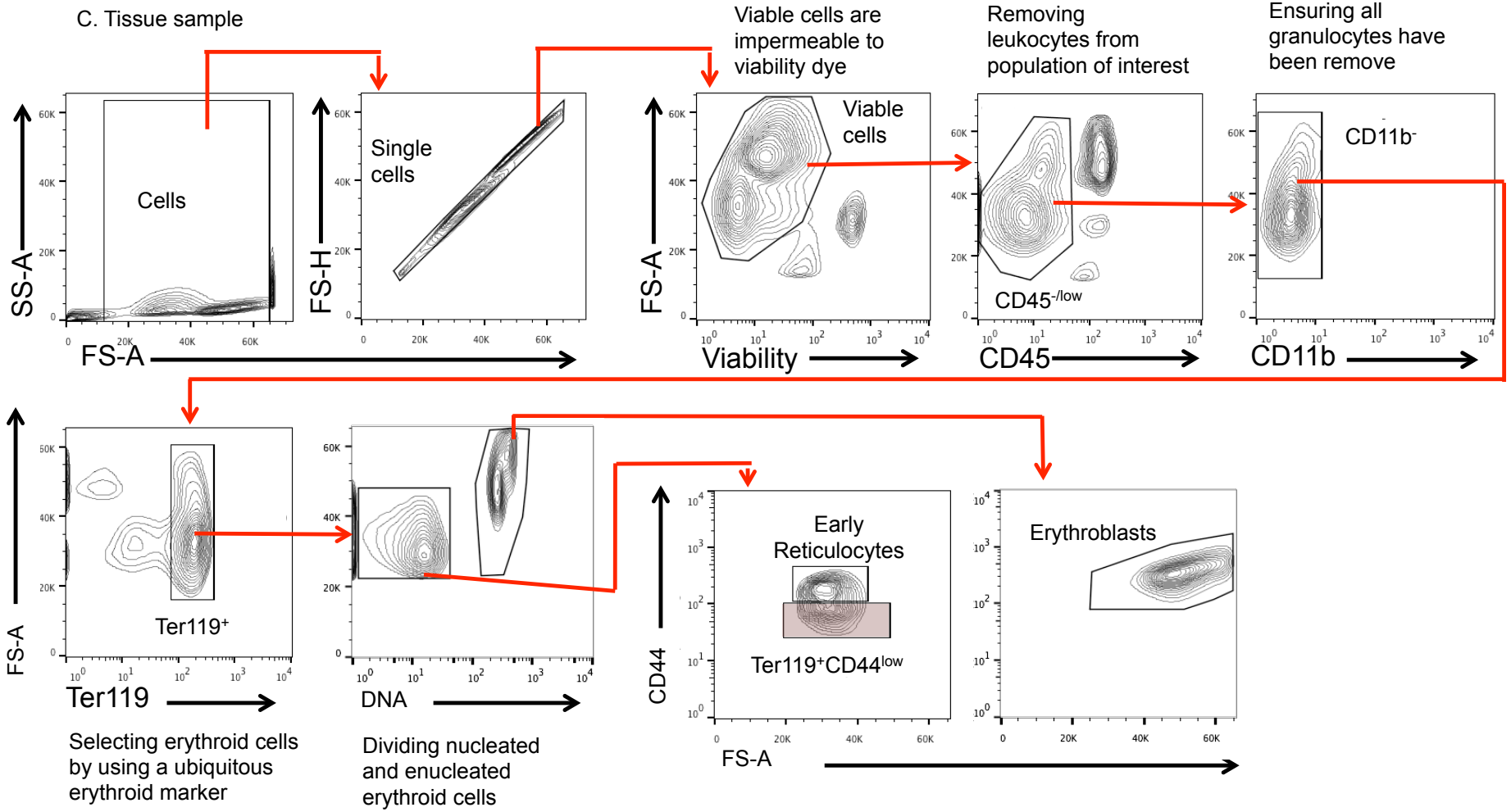
C. Tissue sample
Cells
SS-A
FS-A
Single cells
FS-H
Viable cells are impermeable to viability dye
Viable cells
FS-A
Viability
Removing leukocytes from population of interest
CD45-/low
CD45
Ensuring all granulocytes have been remove
CD11b-
CD11b
FS-A
Ter119+
Ter119
Selecting erythroid cells by using a ubiquitous erythroid marker
DNA
Dividing nucleated and enucleated erythroid cells
CD44
Early Reticulocytes
Ter119+CD44low
Erythroblasts
FS-A

D.

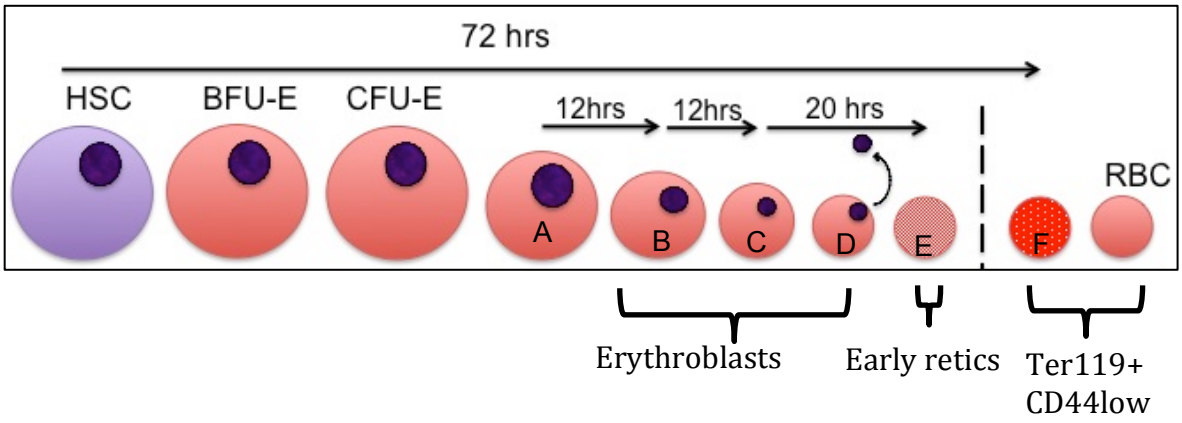
72 hrs
HSC
BFU-E
CFU-E
12hrs
12hrs
20 hrs
A
B
C
D
E
F
RBC
Erythroblasts
Early retics
Ter119+
CD44low

E.

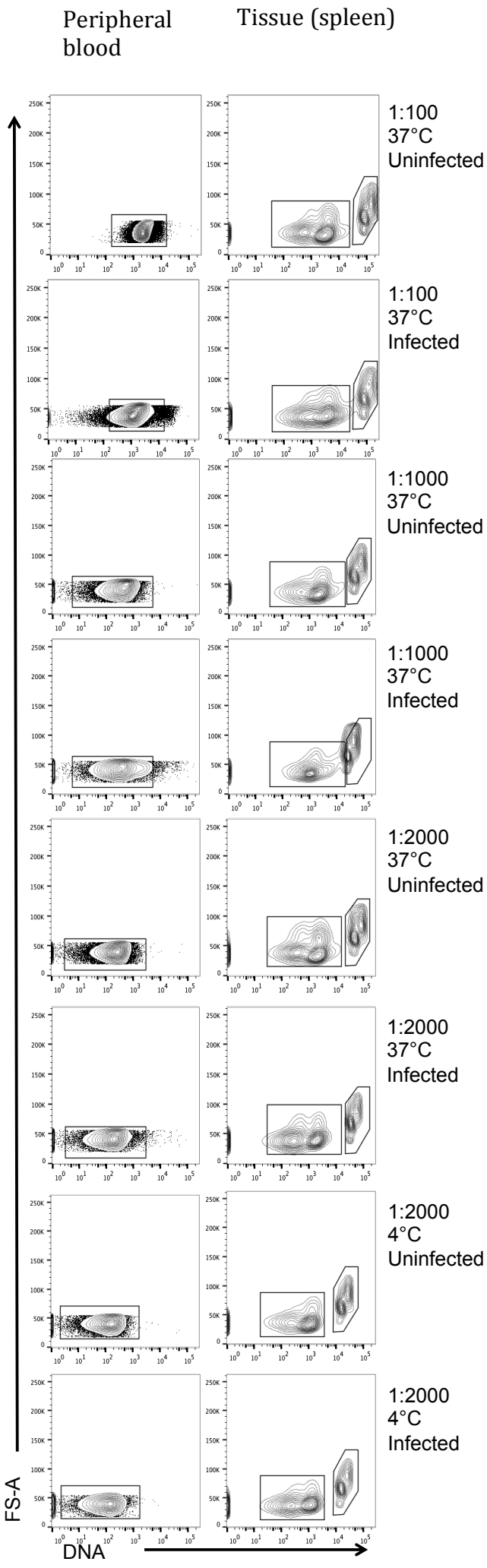
Peripheral blood
Tissue (spleen)
1:100 37°C Uninfected
1:100 37°C Infected
1:1000 37°C Uninfected
1:1000 37°C Infected
1:2000 37°C Uninfected
1:2000 37°C Infected
1:2000 4°C Uninfected
1:2000 4°C Infected
FS-A
DNA

Figure 3.4 Using a DNA stain to discriminate nucleated and enucleated erythroid cells allows resolution of a more distinct erythroblast population. This figure represents the gating strategy used throughout the rest of the study in order to identify erythroid cells. This will be further highlighted by the use of red arrows when extending the strategy. **A.** Flow diagram of methodology used to generate data using the CD44 vs Ter119 gating strategy. **B.** Representative FACS plots of uninfected peripheral blood and **C.** tissue sample (Bone marrow tissue). Samples were stained with 2.5 µM DyeCycle Ruby DNA stain at 4°C for 30 mins. Viable, $CD45^{-/low}$, $CD11b^{-}$, $Ter119^{+}$ cells were gated against DNA staining (DNA) and cell size (FS-A). In the peripheral blood sample all erythroid cells were DNA^{-}. The tissue samples contained DNA^{-} and DNA^{+} erythroid cells. The DNA^{-} population in the peripheral blood sample was gate against CD44 and cell size (FS-A) to reveal one $CD44^{low}$ population called 'peripheral blood'. Note the outliers included in the plot to highlight the homogeneity of the CD44 expression of peripheral blood erythroid cells. The $CD44^{low}$ 'peripheral blood' gate was imposed on the DNA^{-} cells in the tissues, to define the population called $Ter119^{+}CD44^{low}$ these two populations are tinted red in the diagram as both where considered to contain cells that were not tissue resident. The DNA^{-} cells in the tissues contained a second population that was $CD44^{high}$ small cells. Based on previous studies (Chen *et al.*, 2009; Liu *et al.*, 2013) these gates were termed early reticulocytes. The DNA^{+} cells in the tissue were also gated against CD44 and cell size (FS-A). This revealed a population of $CD44^{high}$ large erythroid cells that I termed erythroblasts based on previous studies (Chen *et al.*, 2009; Liu *et al.*, 2013). Only the early reticulocytes and erythroblast gate contained cells considered tissue resident **D**. Schematic indicating which developmental stages of erythroid cells that fall into the gates erythroblasts, early reticulocytes and $Ter119CD44^{low}$. CFU-E transform into A. pro-erythroblast, which then successively differentiate into B. basophilic erythroblast, C. polychromatic erythroblast and D. orthochromatic erythroblast. The orthochromatic stage enucleates to become an enucleated reticulocyte. The differentiation times in mice are marked above the cells (Chen et al., 2009; Filmanowicz and Gurney, 1961). E. Stage I-II reticulocytes mature within the tissue. F. Stage III-IV reticulocytes are within the circulation. The final differentiation stage is erythrocytes (RBC). The vertical dotted line indicates the separation between circulating and tissue resident stages. **E.** Representative FACS plots of DNA stain titration. Represented here are concentrations of 1:100, 1:1000, 1:2000 stained at 37°C and 1:2000 stained at 4°C. For each condition there is a representative plot for uninfected and infected peripheral blood and tissue (spleen), cells on these plots are $CD45^{-/low}$, $CD11b^{-}$, $Ter119^{+}$. Gates were set on the uninfected samples then imposed onto the corresponding infected sample. The only condition where intercellular parasites where not stained, as judged best by the peripheral blood plots, was the 1:2000 concentration stained at 4°C.

3.2.2.3 Evidence for Classification of Erythroid Stages

The most mature erythroblasts are small and have highly condensed nuclei. Therefore, it was important to ensure that these cells could be identified within the DNA^+ gate observed in tissue samples (Figure 3.4). To evaluate this, two samples were taken from an uninfected spleen. Erythrocyte lysis was performed on one of the samples to remove all enucleated cells (Figure 3.5). Through analysis of both samples by flow cytometry a total loss of the $Ter119^+DNA^-$ population was observed in the lysed sample, indicating that the $Ter119^+DNA^-$ population is a totally enucleated population. This was direct evidence that mature erythroblasts could be separated from enucleated erythrocyte populations on the basis of DNA staining.

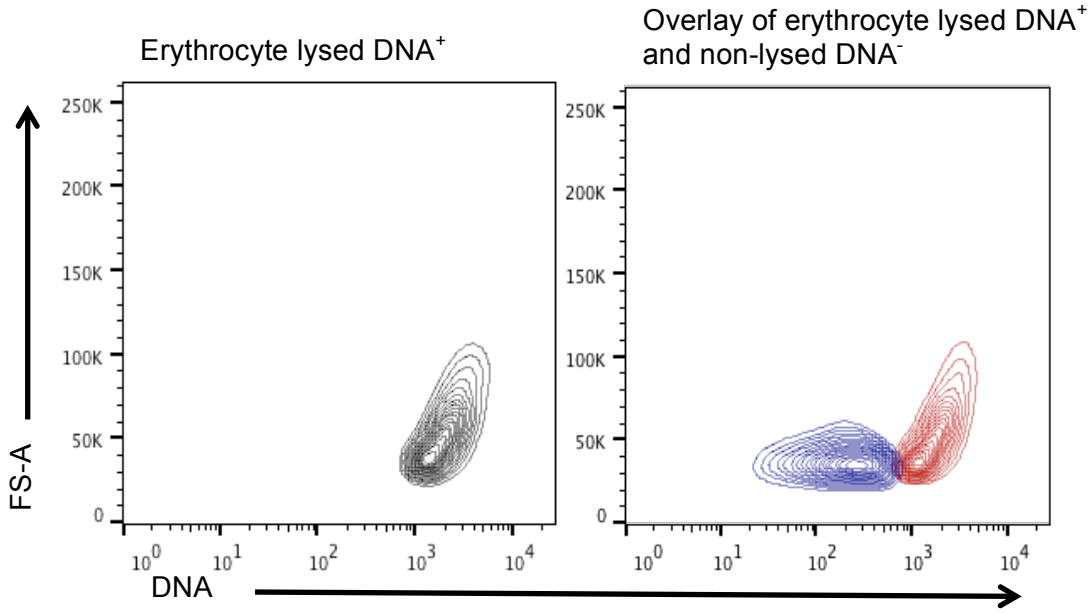

Figure 3.5. Nucleated and enucleated erythroid cells can be separated using a DNA stain. Both FACS plots showing viable, $CD45^{-/low}$, $cd11b^-$, $Ter119^+$ cells. Two samples were taken from an uninfected spleen, one was erythrocyte lysed to enrich for nucleated erythroid cells (left hand graph) and the other was not. The right hand graph shows DNA presence (identified with DyeCycle Ruby DNA stain) in the erythrocyte-lysed sample (red) can be clearly distinguished from the DNA^- population in the non-lysed sample (blue).

Moreover, nucleated cells were not observed in the sorted early reticulocyte population (Figure 3.4) when stained with Giemsa (Figure 3.6). The cell sorted viable, CD45$^{-/low}$, CD11b^{-}, Ter119^{+}, DNA^{-} peripheral blood cells and corresponding (Ter119^{+}CD44^{low}) population (Figure 3.4) in the bone marrow both contain cells notably paler than the early reticulocyte population (Figure 3.6), demonstrating the presence of mature erythrocytes and maturing reticulocytes in both locations (Lee *et al.*, 2013).

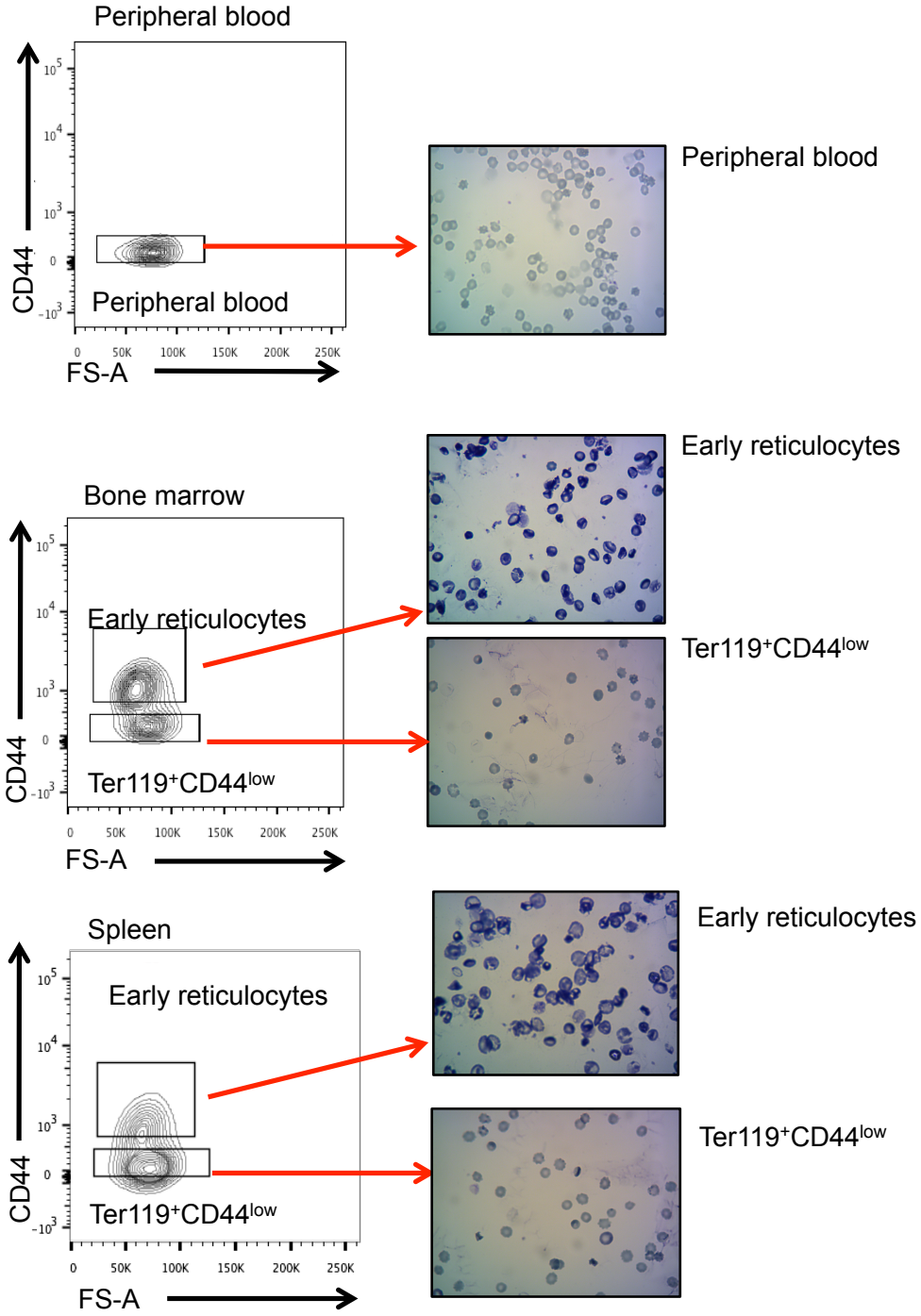

Figure 3.6 Ter119^{+}CD44^{low} cells in tissue samples are mature reticulocytes and erythrocytes. Viable, CD45$^{-/low}$, CD11b^{-}, Ter119^{+} DNA^{-} CD44^{low} cells were cell sorted from bone marrow and peripheral blood uninfected samples. All contain pale Giemsa stained cells. The sorted early reticulocyte population contained dark blue cells.

The Ter119^{+}CD44^{low} cells identified in tissue samples have the same cellular profile as the erythroid cells within peripheral blood, which is a heterogeneous population made up of stage III-IV reticulocytes and erythrocytes (Lim *et al.*, 2016). Reflecting this, it was inappropriate to label the tissue Ter119^{+}CD44^{low} population mature erythrocytes/ erythroid cells. Likewise, this population could not be referred to it as 'peripheral blood' as it was identified within tissue samples. There was not conclusive evidence that the tissue Ter119^{+}CD44^{low} gate contained an intra vascular (this will be examined further in 3.2.4) population, as such it could not be referred to as intravascular erythroid cells. Consequently, throughout this work the Ter119^{+}CD44^{low} population identified in tissue samples will be referred to as Ter119^{+}CD44^{low}.

3.2.2.4 Distinguishing Erythroblast Maturation Stages

An overlay of the DNA^{+} erythroblast population and the two DNA^{-} populations revealed that there is an overlap in cell size between enucleated early reticulocytes and erythroblasts (Figure 3.7A). This is supported by reported cell measurements of early reticulocytes and erythroblasts (Khurana, 2005) however, this has not been incorporated into flow based approaches previously. Moreover, the gradation in cell size in the erythroblast population was exploited to gate three sub-populations (large, intermediate and small) based on the 1:2:4 ratio previously and extensively defined by Liu *et al* (2013). The three erythroblast populations from uninfected bone marrow were cell sorted. Visualising the cells under light microscopy showed the populations contained exclusively nucleated cells and were not contaminated with enucleated cells (Figure 3.7B). Additionally, the images corroborate that the erythroblasts decrease in size during maturation. Nonetheless, as the gates are defined by an internal ratio to one another that may vary between replicates, and due to evidence in the literature that these gates do not define pure populations of any given erythroblast stage, the populations within the gates were referred to as immature, intermediate and mature (to reflect their decrease in size through maturation), rather than by stage names (e.g. orthoblast)

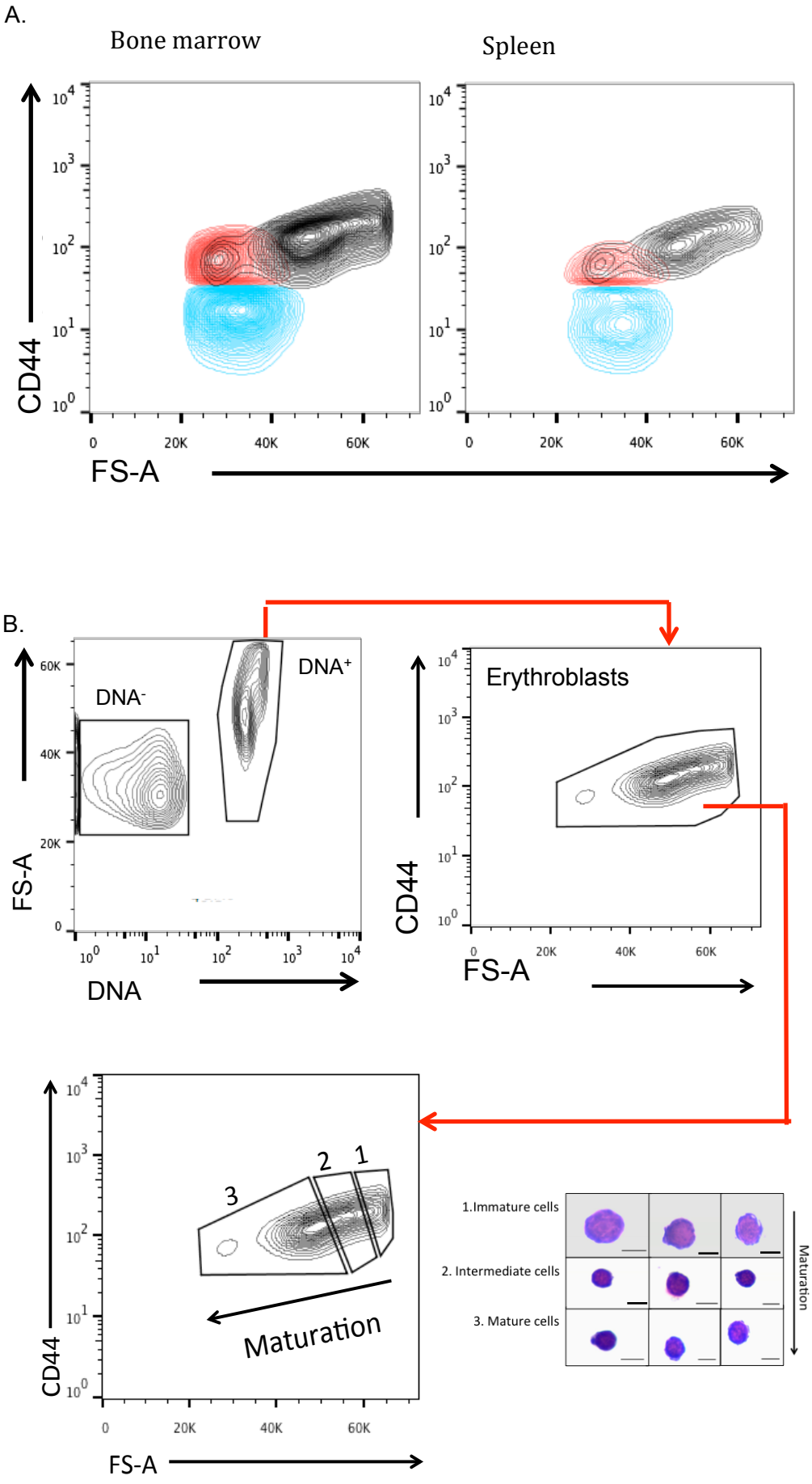
A.
Bone marrow
Spleen
CD44
FS-A
0
20K
40K
60K
B.
DNA-
DNA+
DNA
FS-A
Erythroblasts
CD44
FS-A
1
2
3
Maturation
1.Immature cells
2. Intermediate cells
3. Mature cells
Maturation

Figure 3.7 The stages of erythroblast maturity can be differentiated by cell size. A. Representative FACS plot overlay for uninfected bone marrow (plots for spleen tissue can be found in Figure 3.9). Viable, $CD45^{-/low}$, $CD11b^{-}$, $Ter119^{+}$ DNA^{-} were gated against CD44 and FS-A to identify the $Ter119^{+}CD44^{low}$ (blue) and early reticulocyte (green) populations. Viable, $CD45^{-/low}$, $CD11b^{-}$, $Ter119^{+}$ DNA^{+} were gated against CD44 and FS-A to identify the erythroblast population (red). The three erythroid populations were overlaid onto one another in Flowjo software. **B.** Representative FACS plots from uninfected bone marrow. Viable, $CD45^{-/low}$, $CD11b^{-}$, $Ter119^{+}$ DNA^{+} erythroblasts were gated as immature, intermediate and mature, (labelled 1,2,3 respectively,) in a 1:2:4 ratio. To confirm their identity, cells were sorted, stained with May-Grunwald and examined by light microscopy. Three representative cells from each group are shown. Scale bar is 6 μm.

3.2.2.5 Comparison of Cell Identification by Flow Cytometry to Published Methods

It was important to ensure that the erythroid populations the modified, *Plasmodium*-compatible gating strategy identified were comparable with published observations. Previously Liu *et al* (2006) had calculated the proportion that each erythroid population contributed to the overall $Ter119^{+}$ population from the bone marrow and the spleen of uninfected BALB/c mice. In our work I observed that $Ter119^{+}CD44^{low}$ cells, early reticulocytes and erythroblasts (using the gating strategy outlined in Figure 3.4) contributed 46% ±10%, 15% ±6%, 37% ±16%, receptively to the total $Ter119^{+}$ population in the bone marrow and 86% ± 0.5%, 7% ± 5%, 6 ± 5%, receptively to the total $Ter119^{+}$ population in the spleen of naïve BALB/c mice (±SD) (Figure 3.8). These values were reflective of the graphical data presented by Liu *et al* (2006) in their study into homeostatic erythropoietic regulation in Blab/c mice, I therefore concluded that our gating strategy was a useful tool for identifying tissue resident erythroid populations.

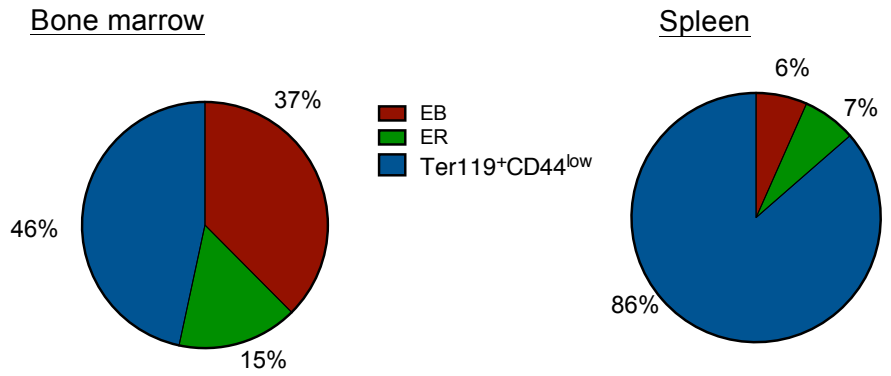

Figure 3.8 The average percentage contributions of erythroid cells to the total Ter119^{+} population. Erythroblasts (EB), Early Reticulocytes (ER) and Ter119^{+}CD44^{low} cells to total Ter119^{+} cell in the bone marrow and Spleen of BALB/c mice (n=9).

3.2.2.6 CD44 to Distinguish Erythroid Populations

The MFI of CD44 in uninfected and *P. berghei* infected peripheral blood, bone marrow and spleen samples was investigated. Samples were analysed by flow cytometry and gated according to the developed strategy (Figure 3.4). The MFI of CD44 was calculated for cells in the peripheral blood, early reticulocytes and erythroblast populations. There was no significant change in CD44 MFI between any of the erythroid populations during *P. berghei* infection compared with uninfected mice (Figure 3.9). This therefore makes CD44 a useful marker for defining erythroid populations during *Plasmodium* infection.

A

		Bone marrow		Spleen	
	peripheral blood	ER	EB	ER	EB
uninfected	19 ± 14	99 ± 60	180 ± 98	45.7 ± 19	128 ±177
infected	20 ± 14	100 ± 60	203 ± 126	45.9 ± 19	64 ± 37
	p = 0.8	p = 0.9	p = 0.3	p = 0.9	p = 0.14

B

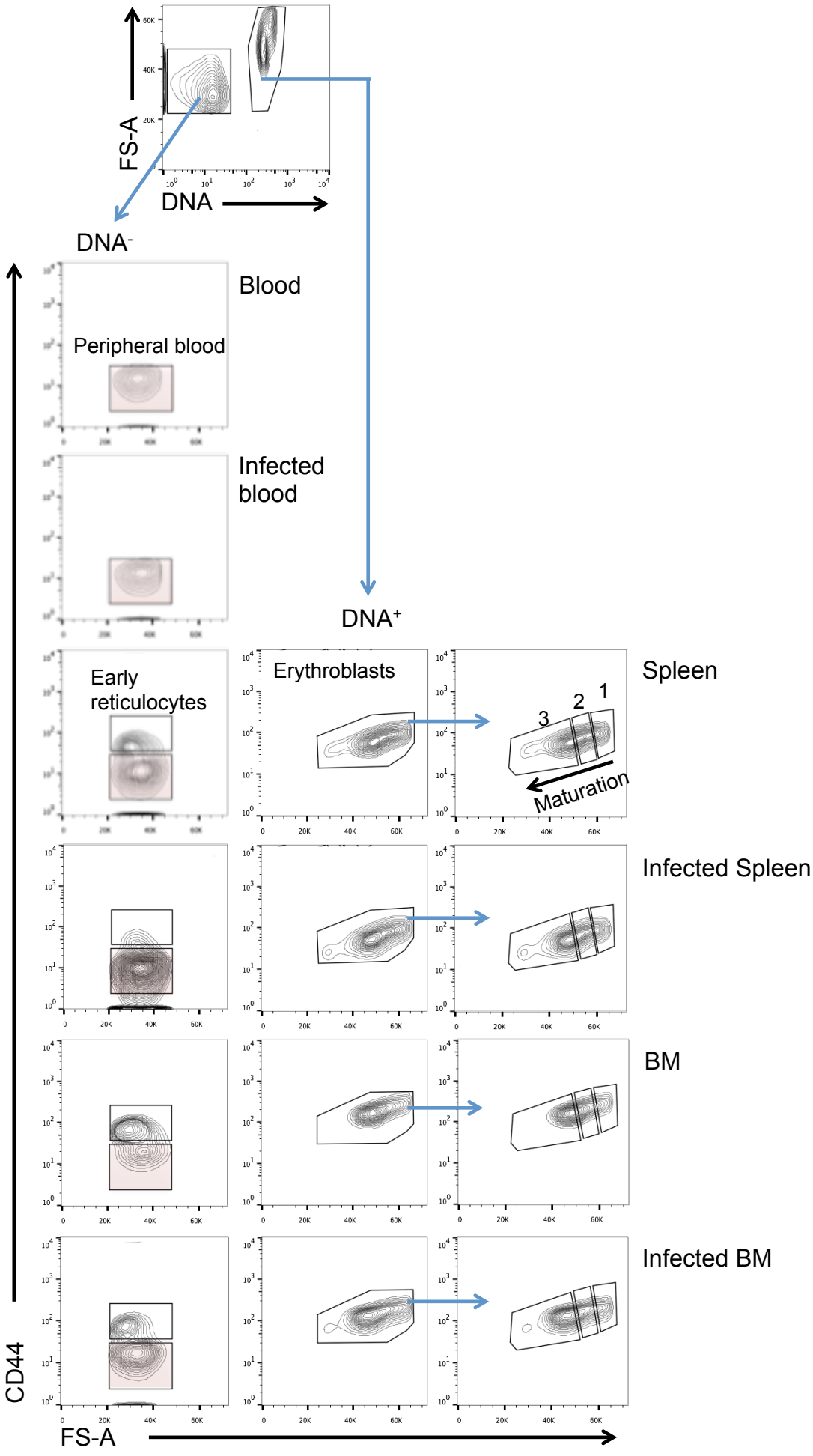
FS-A
DNA
DNA-
DNA+
Blood
Peripheral blood
Infected blood
Early reticulocytes
Erythroblasts
1
2
3
Maturation
Spleen
Infected Spleen
BM
Infected BM
CD44
FS-A

Figure 3.9 CD44 MFI. A. The table shows the average MFI of CD44 (± SD) of $CD45^{-/low}$, $CD11b^{-}$, $Ter119^{+}$ in circulating cells from the peripheral circulating blood, early reticulocytes (ER) and erythroblasts (EB) in both uninfected and *P. berghei* infected mice. The p values describe the difference between the CD44 MFI of the corresponding populations in the naïve and infected mice (n=3). **B.** Representative FACS plots from infected and uninfected tissue. Cells displayed on the plots are $CD45^{-/low}$, $CD11b^{-}$, $Ter119^{+}$. These cells were then gates as DNA^{+} or DNA^{-} (top plot). Both DNA^{+} and DNA^{-} were then gated CD44 vs FS-A. The plots displayed are 5% contort plots. There is a notable decrease in the number of early reticulocytes within the infected splenic early reticulocyte gate, this will be addressed later in Figure 3.23, however the decrease in cell numbers did not effect the MFI of the population as calculated in Figure 3.9 A.

3.2.3. Tissue Perfusion

The gating strategy defined tissue resident cells based on their CD44 expression and their absence from peripheral blood (Figure 3.4). It is a standard procedure to perform whole body perfusion to define extravascular cell populations, although this is subject to variable performance (Anderson *et al*. 2014). Therefore, the compatibility of tissue perfusion with my flow approach was tested. Whole body, post mortem perfusion was performed on uninfected mice. To confirm complete perfusion, samples from the vasculature were taken post-perfusion by venepuncture of a tail vein. Bone marrow was harvested from mice with visibly clear tail vein samples. Analysing the perfused bone marrow samples using our flow methodology (Figure 3.4) revealed the presence of residual $Ter119^{+}$ $CD44^{low}$ cells within the bone marrow compartment, which on average made up 5% ± 0.16% (n=3. ± SD) of total $Ter119^{+}$ population (Figure 3.10). As it is unprecedented to observe recirculation of erythroid cells into the bone marrow parenchyma (Itkin *et al.*, 2016), it was therefore concluded that these cells were present in the bone marrow vasculature and consequently that perfusion of this tissue was inefficient. I therefore decided not to perform tissue perfusion during my work. This was done in order to prevent the potential erroneous mis-interpretation of parasitised circulating erythroid cells infiltrating the bone marrow tissue during infection.

A.

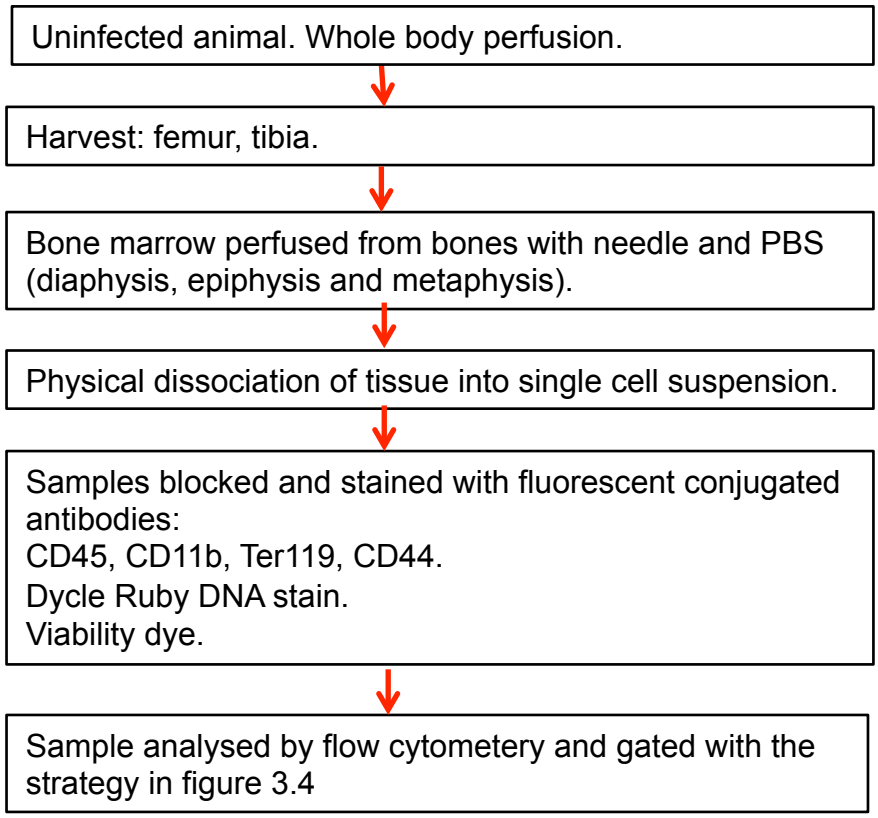
Uninfected animal. Whole body perfusion.
Harvest: femur, tibia.
Bone marrow perfused from bones with needle and PBS (diaphysis, epiphysis and metaphysis).
Physical dissociation of tissue into single cell suspension.
Samples blocked and stained with fluorescent conjugated antibodies:
CD45, CD11b, Ter119, CD44.
Dycle Ruby DNA stain.
Viability dye.
Sample analysed by flow cytometery and gated with the strategy in figure 3.4

B.

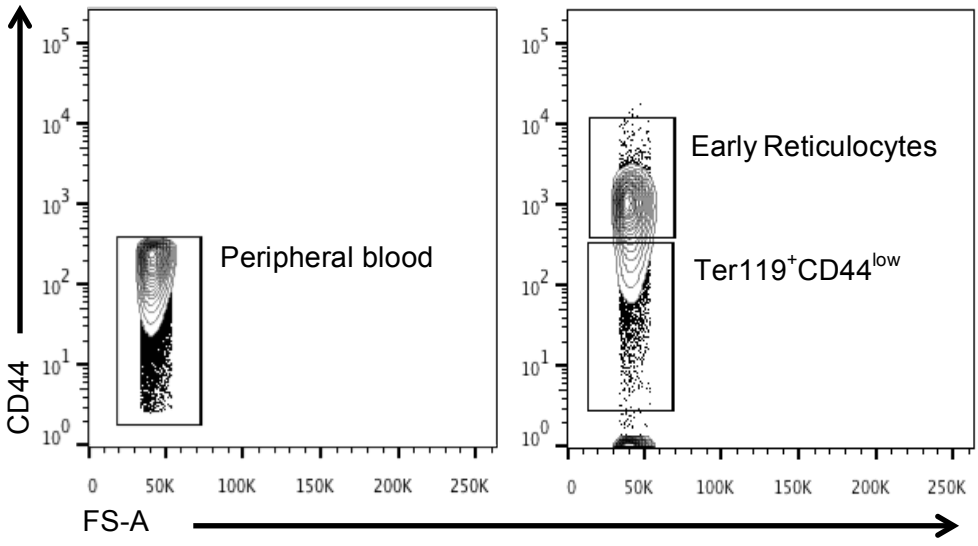
CD44
FS-A
Peripheral blood
Early Reticulocytes
Ter119+CD44low
0
50K
100K
150K
200K
250K

C.

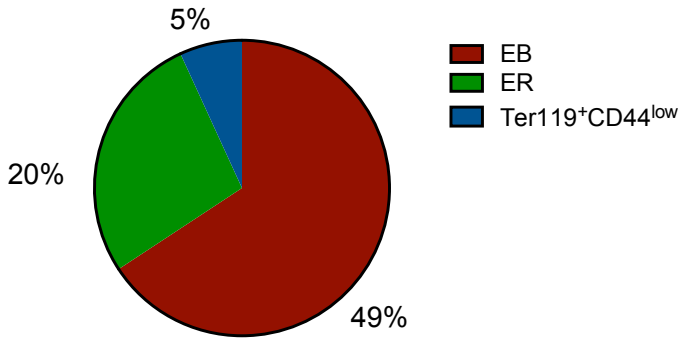

Figure 3.10 Perfusion leaves a residue of Ter119+CD44^{low} cells in the bone marrow. A. Flow diagram depicting the experimental procedure. **B.** Representative FACS plots of (viable, CD45$^{-/low}$, CD11b^{-}, Ter119^{+} DNA^{-}) peripheral blood before perfusion (left hand side) and (Viable, CD45$^{-/low}$, CD11b^{-}, Ter119^{+} DNA^{-}) early reticulocytes and Ter119^{+}CD44^{low} from the bone marrow after perfusion (right hand side). **C**. Pie chart shows the average percentage proportion of all Ter119+ cells in the bone marrow (n=3).

3.2.4. Intravascular Staining of Erythroid Cells

To further explore techniques to directly distinguish between extra- and intra-vascular cell populations, the use of an *in vivo* staining protocol was investigated (Pereira *et al.*, 2009; Anderson *et al.*, 2014). Injecting an erythroid targeting immunofluorescence label intravenously would stain erythroid cells within the vasculature but not within the extravascular spaces of tissue. Combining this with my flow-based approach (Figure 3.4) would allow for the determination between erythroid cell population that are within the vasculature and those that are not. Fluorescently conjugated anti-Ter119 IgG was intravenously (IV) introduced into uninfected mice 3 mins prior to organ and blood harvesting. The samples were stained *ex vivo* to comply with the flow-based approach and samples were examined through the gating strategy (Figure 3.4). The erythroid populations (peripheral blood, Ter119^{+}Cd44^{low}, early reticulocytes and erythroblasts) were then individually gated on a histogram with cell count on the y-axis and *in vivo* administered Ter119 on the x-axis. The histograms from each tissue sample were over-laid along with the *in vivo* stained peripheral blood (positive control) and a sample of peripheral blood from a animal that did not receive *in vivo* anti-Ter119 (negative control: FMO). Unsurprisingly due to the

murine splenic open circulation, staining of spleen extracted tissue resident erythroid cells was observed (Figure 3.11 A). However, it was also observed that bone marrow derived erythroid cells exhibited fluorescence intensity higher than the fluorescence minus one (FMO) negative control for the *in vivo* staining antibody (Figure 3.11 B).

A.

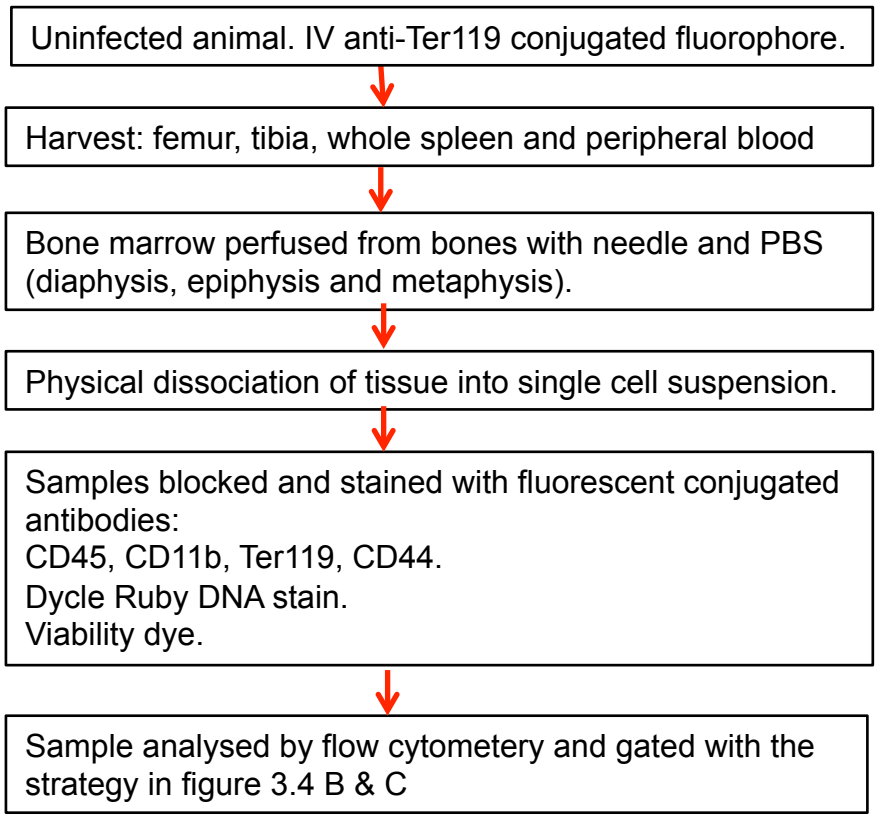

B.

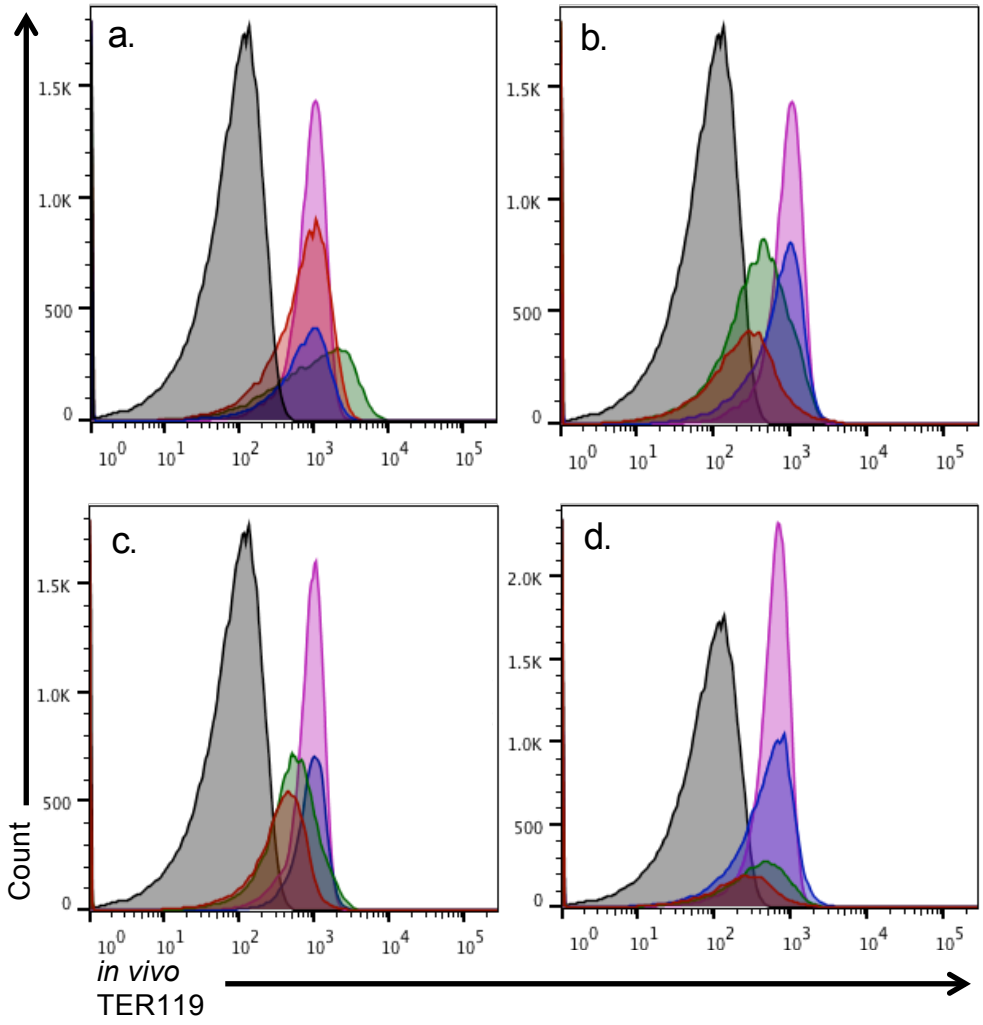

Figure 3.11 Early reticulocytes and erythroblasts in spleen and bone marrow are labelled by *in vivo* administration of Ter119 antibody. A. Flow diagram of experiment. **B.** In all plots the **black peaks** are *in vivo* Ter119 FMO, the **pink** are positive *in vivo* staining of peripheral blood, **indigo** are $Ter119^{+}CD44^{low}$ cells from the organ, the **green** are early reticulocytes and the **red** are erythroblasts. **a. and b.** spleen and bone marrow, respectively, from an animal injected with 3 µg Ter119- PE-Cy7. **c.** Bone marrow from an animal injected with 2 µg Ter119- pecy7. **d.** Bone marrow from an animal injected with 1 µg Ter119- pecy7.

This suggested that *in vivo* staining of the early reticulocytes and erythroblasts was due to leakage of the antibody into the bone marrow tissue. Therefore the approach was repeated using a second antibody specific to the stem cell growth factor receptor (c-Kit) which should only be expressed by Haemopoietic Stem Cells (HSC) found in the bone marrow parenchyma (Matsuoka *et al.*, 2011). The harvested blood and bone marrow were stained *ex vivo* and analysed by flow cytometry (Figure 3.12). A population of lineage$^-$, DNA$^+$, *ex vivo* c-Kit$^+$, sca1$^+$ cells where identified in the bone marrow, this cellular profile matches HSCs. An average of 45% ± 3% (n= 3) of these cells were positive for the *in vivo* injected c-kit antibody. HSC can mobilise and circulate throughout the body, thus a small fraction may be expected to stain with *in vivo* c-kit. However, as the peripheral blood was negative for *in vivo* c-kit staining, it can be concluded that injected antibody leaks into the bone marrow parenchyma.

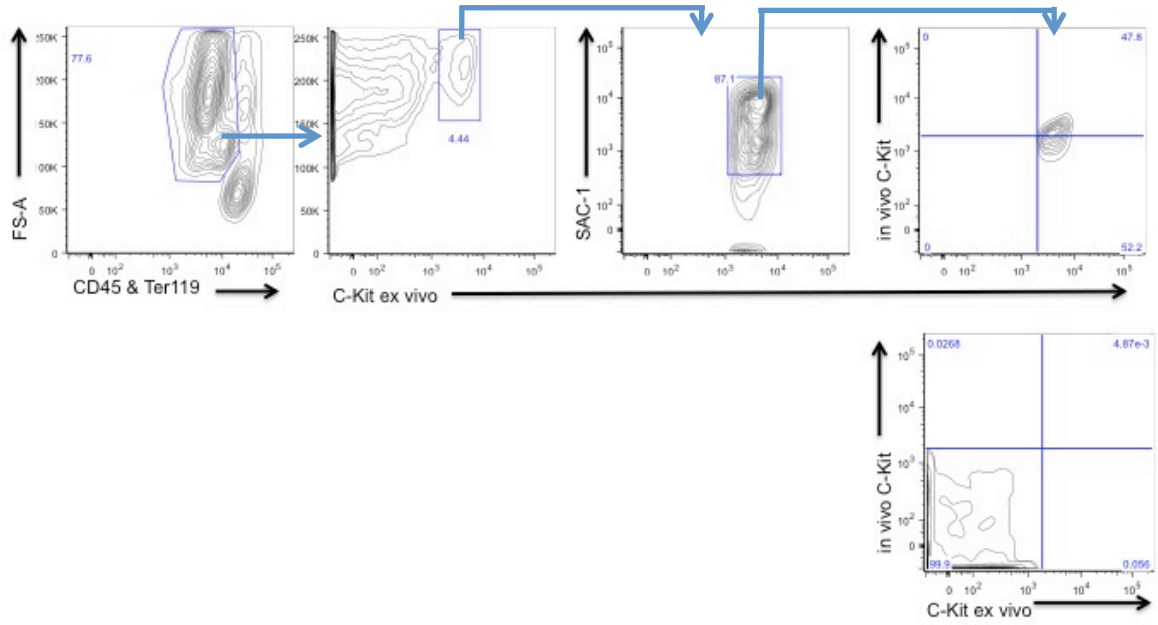

Figure 3.12 Bone marrow HSCs stain positive for *in vivo* administered c-Kit antibody. Top row: representative FACS plots showing the gating strategy to define *in vivo* positive c-Kit. Below: a representative FACS plot of peripheral blood staining negative for *ex vivo* and *in vivo* c-Kit.

As it has not directly proven that the cells within the early reticulocyte and erythroblast gates are within the extra-vascular tissue of the bone marrow, they will be referred to only as tissue resident cells.

3.2.5. Establishing the Model: Identifying Infected Cells

The optimised flow methodology was used to investigate the dynamics of the tissue resident infection during acute murine malaria. ECM resistant BALB/c mice were infected with parasites of a well-characterised *P. berghei* line (PbGFPko230p-SMCON: 507 clone1) that constitutively expresses GFP throughout its life-cycle (Janse *et al.*, 2006). For accuracy, the gates defining the GFP^+ cells were set using a negative control sample from mice infected with 10^4 parasites of a wild-type *P. berghei* line (HPtbb) (Figure 3.13 A). In parallel, a separate group was injected with 150 µl 1 x PBS. Bone marrow, spleen and peripheral blood were harvested on day 7 post-infection from the animals in these two groups as well as from uninfected animals (Figure 3.13). The mean blood parasitaemia of the HPtbb infected animals was 4% (Appendix 8.1.3). The flow analysis revealed that the erythroid GFP^- populations defined by the uninfected animal samples could be applied directly to the HPtbb and 1x PBS samples (groups n=3) (Figure 3.13). This showed that infection with *P. berghei* or injection of 1 x PBS does not mobilise granulated auto-fluorescent cells that may be misinterpreted as GFP^+ parasites in the 507 clone1 samples. As such, in the interests of reducing animal usage, the uninfected samples were used throughout this work as the negative control. Throughout this study, all gates were defined using the uninfected control samples and imposed onto the infected samples.

A

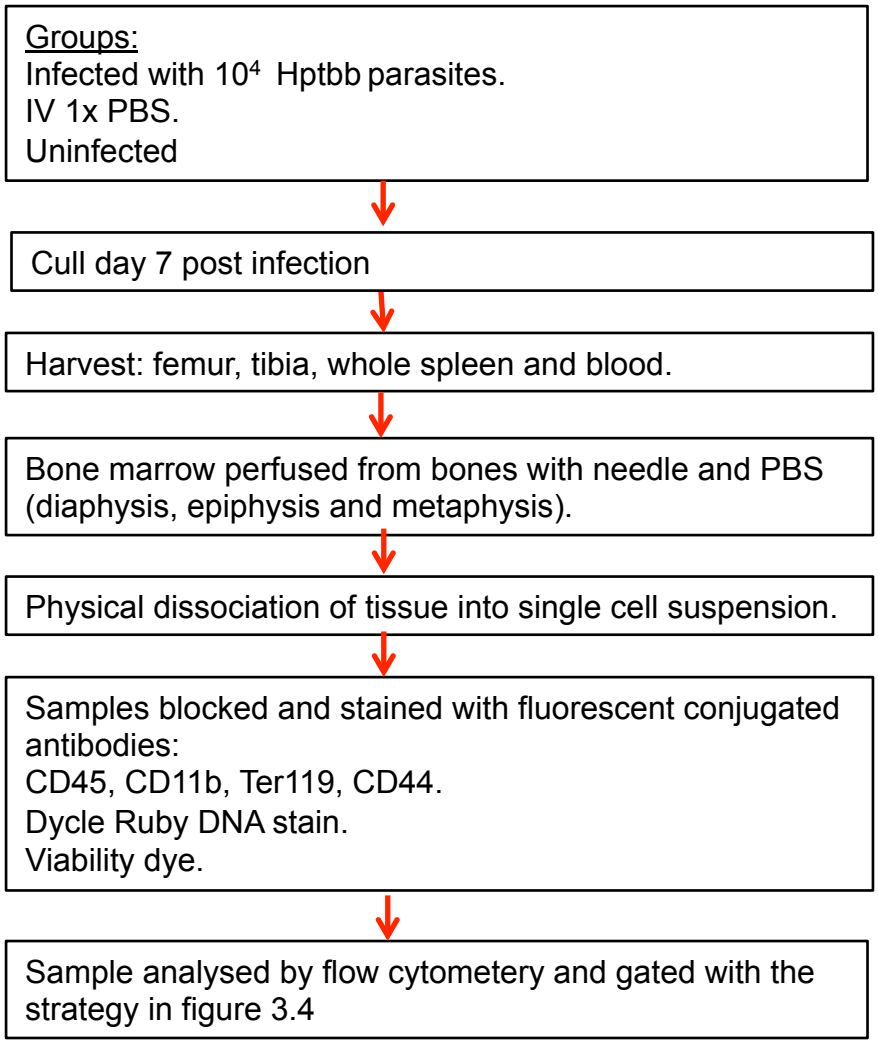
Groups:
Infected with 10^4 Hptbb parasites.
IV 1x PBS.
Uninfected
Cull day 7 post infection
Harvest: femur, tibia, whole spleen and blood.
Bone marrow perfused from bones with needle and PBS (diaphysis, epiphysis and metaphysis).
Physical dissociation of tissue into single cell suspension.
Samples blocked and stained with fluorescent conjugated antibodies:
CD45, CD11b, Ter119, CD44.
Dycle Ruby DNA stain.
Viability dye.
Sample analysed by flow cytometery and gated with the strategy in figure 3.4

B

.

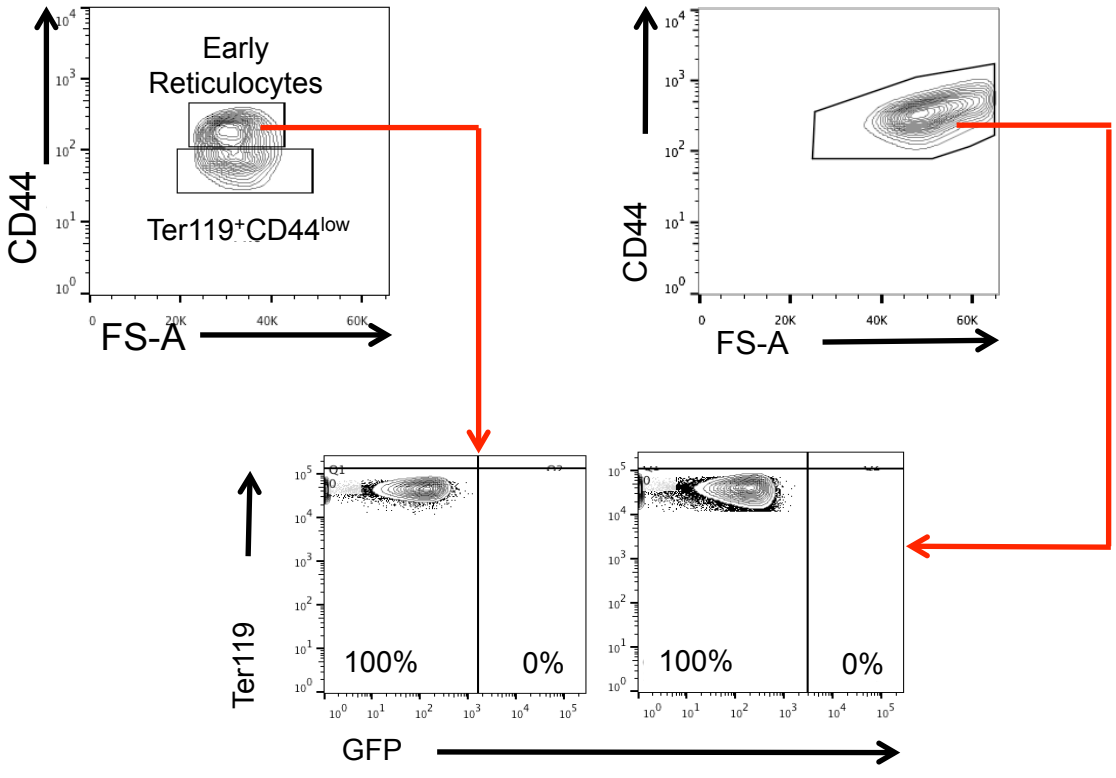
Early Reticulocytes
Ter119+CD44low
CD44
FS-A
CD44
FS-A
Ter119
GFP
100%
0%
100%
0%

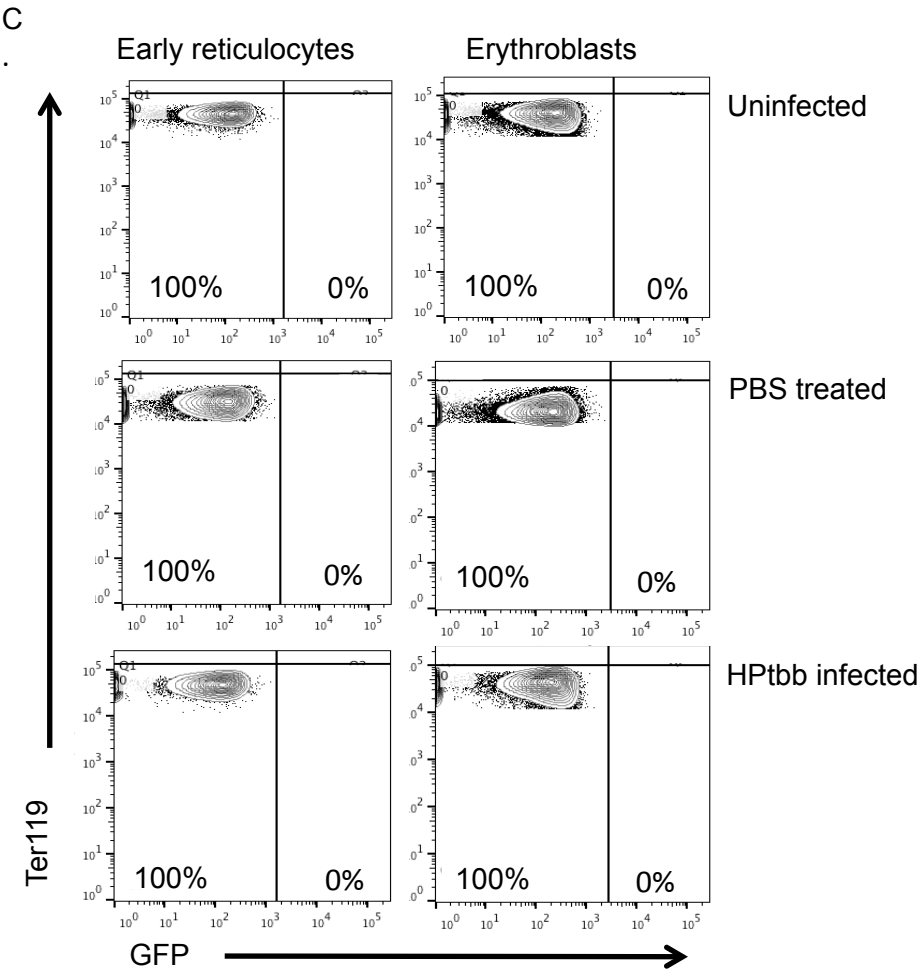

Figure 3.13 Wild type *P. berghei* Infection and PBS treatment do not result in aberrant GFP+ gating. A. Flow diagram of methodology used to generate data using the CD44 vd Ter119 gating strategy. **B.** Viable, $CD45^{-/low}$, $CD11b^{-}$, $Ter119^{+}$ DNA^{-} early reticulocytes and viable $CD45^{-/low}$, $CD11b^{-}$, $Ter119^{+}$ DNA^{+} erythroblasts where gated against Ter119 and GFP. **C.** Representative FACS plots from uninfected, PBS-treated and HPtbb (wild-type) *P. berghei* infected bone marrow. The gates show early reticulocytes do not spontaneously contain GFP due to infection or PBS treatment. Nor do viable $CD45^{-/low}$, $CD11b^{-}$, $Ter119^{+}$ DNA^{+} erythroblasts.

3.2.6. Establishing the Model: Patterns of Characterised *P. berghei* Accumulation.

Bone marrow, spleen and peripheral blood were harvested on day 7 post-infection with 10^4 asynchronous *P. berghei* 507 clone1 parasites (Figure 3.14).

Non-sequestering peripheral blood parasite stages were passaged from a donor animal to establish an asynchronous infections. Within asynchronous infections taken from or occurring within animals housed in standard day-night light conditions, 83 % ±4% of parasites undergo schizongy within the vasculature at 12-7 am and at the point of tissue harvest (9am) 91 % ±2% of asexual parasites were rings and early trophozoites within the peripheral blood (Figure 3.15A). This is directly reflective of the partly synchronized dynamics of *P. berghei* asynchronous infections characterised elsewhere (Franke-Fayard *et al.*, 2005; Mideo *et al.*, 2013). However, as the dynamics of *P. berghei* development within the tissue resident erythoid cells have yet to be directly established, this study restrained from making conclusion as to the parasite life stage beyond what is defined by the florescence markers: parasites are GFP+ and GFP MFI increases during asexual development and gametocyte maturation (Franke-Fayard *et al.*, 2004; Janse *et al.*, 2006).

The parasitaemia of the Ter119$^+$CD44^{low} cells extracted from the bone marrow tended to be higher in comparison to peripheral blood (Figure 3.15 C). The fluorescence intensity of GFP in the 507 clone1 parasite line peaks during female gametocytogenesis and in parallel, increases during asexual maturation (Franke-Fayard *et al.*, 2004; Janse *et al.*, 2006). The GFP MFI of the Ter119$^+$CD44^{low} cells extracted from the bone marrow and the spleen were not significantly higher than the peripheral blood, thus there is not an indication for a greater presence (combined or exclusively) of mature asexual parasites or gametocytes (Figure 3.15B) in any of the three populations.

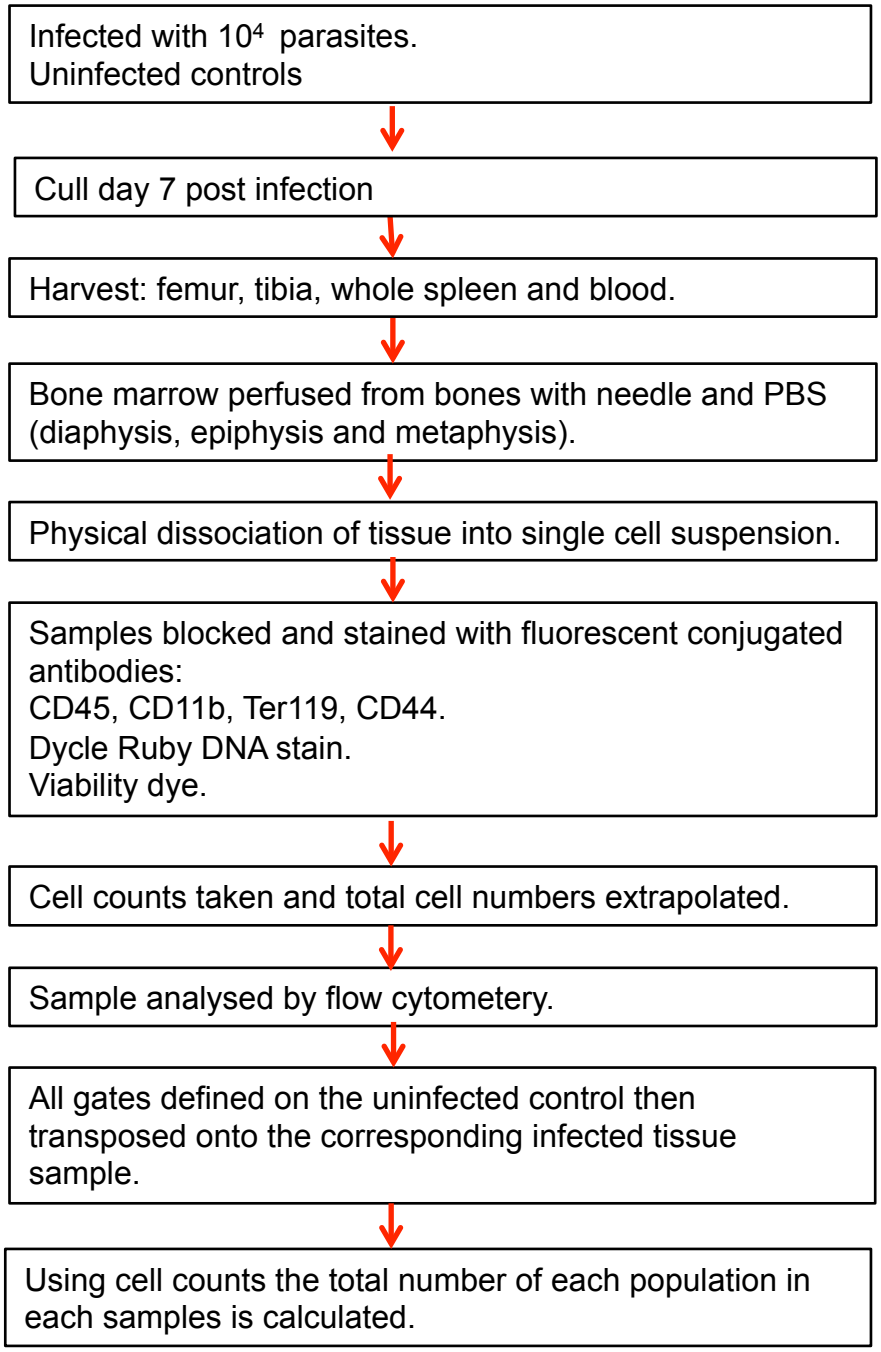

Figure 3.14. Finalised flow diagram of methodology used to investigate erythroid cell infection.

A

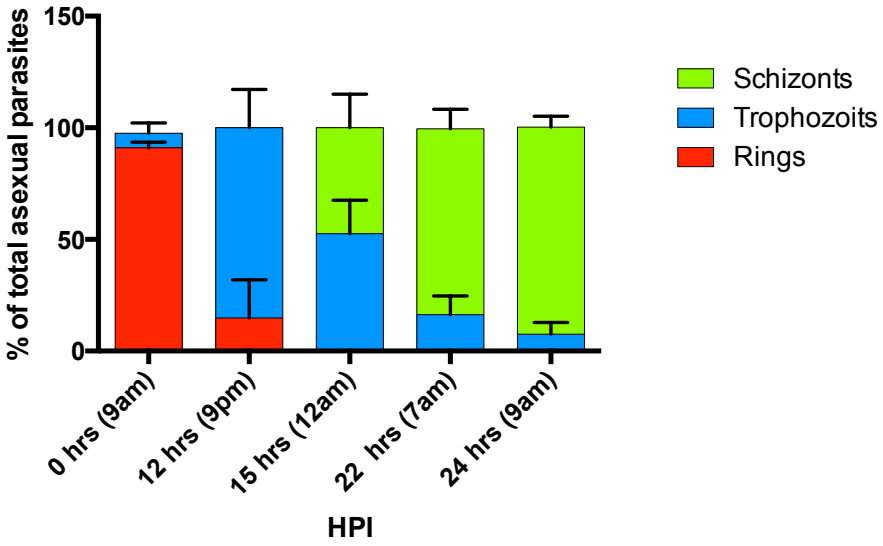
% of total asexual parasites
150
100
50
0
0 hrs (9am)
12 hrs (9pm)
15 hrs (12am)
22 hrs (7am)
24 hrs (9am)
HPI
Schizonts
Trophozoits
Rings

B

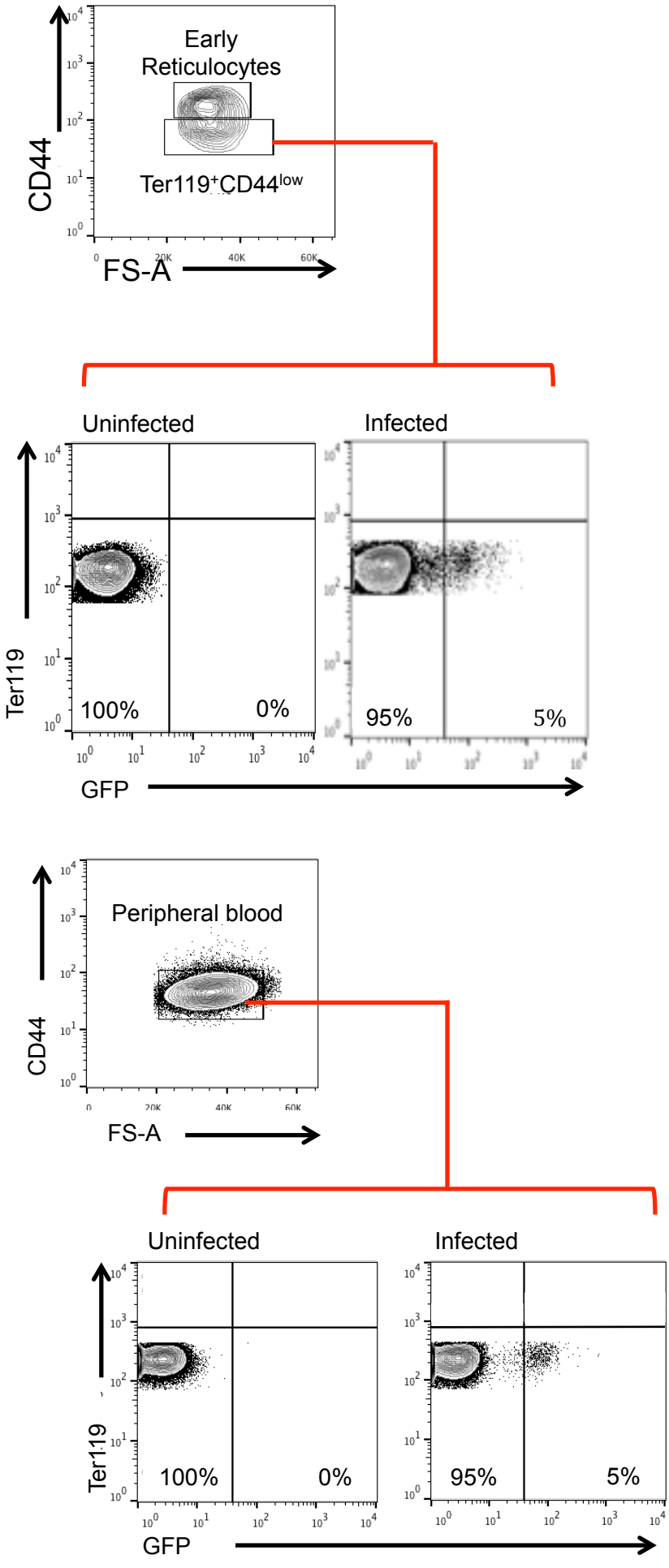
Early
Reticulocytes
Ter119+CD44low
CD44
FS-A
Uninfected
Infected
Ter119
100%
0%
95%
5%
GFP
Peripheral blood
CD44
FS-A
Uninfected
Infected
Ter119
100%
0%
95%
5%
GFP

C

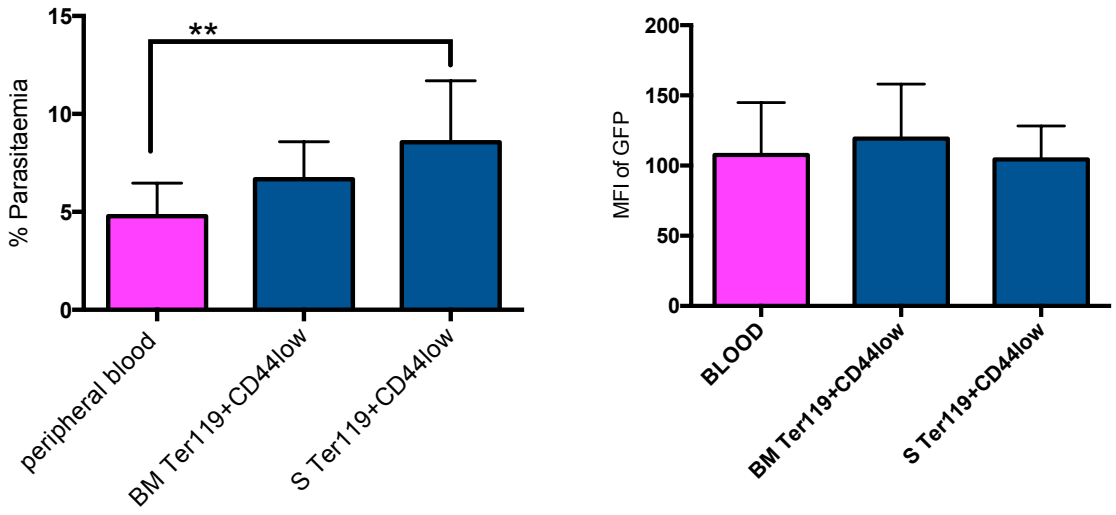

Figure 3.15 Selective accumulation of infected erythroid cells in the bone marrow and the spleen. A. Peripheral blood samples from the asynchronous infection of the 507 clone1 parasite line where cultured *in vitro* for 24 hrs and the proportion of each life stage calculated from Giemsa stained smears. HPI; hours post infection **B.** Representative FACS plots showing viable, $CD45^{-/low}$, $CD11b^{-}$, $Ter119^{+}$ DNA^{-} $Ter119^{+}CD44^{low}$ cells from bone marrow tissue (top) from uninfected and infected animals. Representative FACS plots showing viable, $CD45^{-/low}$, $CD11b^{-}$, $Ter119^{+}$ DNA^{-} peripheral blood cells from tissue (top) from uninfected and infected animals. **C.** The percentage parasitaemia (right) of the peripheral blood gate compared with the $Ter119^{+}CD44^{low}$ cells extracted from the bone marrow (BM) and spleen (S). The average MFI of GFP (left) in peripheral blood gate compared to $Ter119^{+}$ $CD44^{low}$ cells extracted from the bone marrow (BM) and spleen (S). Representative graphs (n=3) of three experimental repeats. Differences between the means tested using a one way ANOVA with multiple comparisons. Significant differences between groups or samples are indicated with asterisks, denoting as follows: * $p < 0.05$, ** $p < 0.01$. Error bars ± SD.

3.2.7. Erythroblasts are Susceptible to *P. berghei* Invasion *in vivo*

Both the bone marrow and the spleen harvested on day 7 post-infection with 10^4 asynchronous *P. berghei* 507 clone1 parasites (Figure 3.14) contained GFP^{+} erythroblasts (Figure 3.16). However, when the erythroblast population was sub-divided (as described in figure Figure 3.7), a significantly higher parasitaemia was

not detectable within the mature stage compared with the other stages. This suggested that *P. berghei* does not have a stage-specific preference for nucleated erythroid cells *in vivo* (Figure 3.17).

It should also be noted that the GFP^+ signal was detected in the $CD45^{-/low}$, $CD11b^-$ and $Ter119^+$ cell population, identified using a protocol for extracellular protein staining. Therefore, it can be concluded that the GFP^+ parasites are within erythroblasts that have not been phagocytosed.

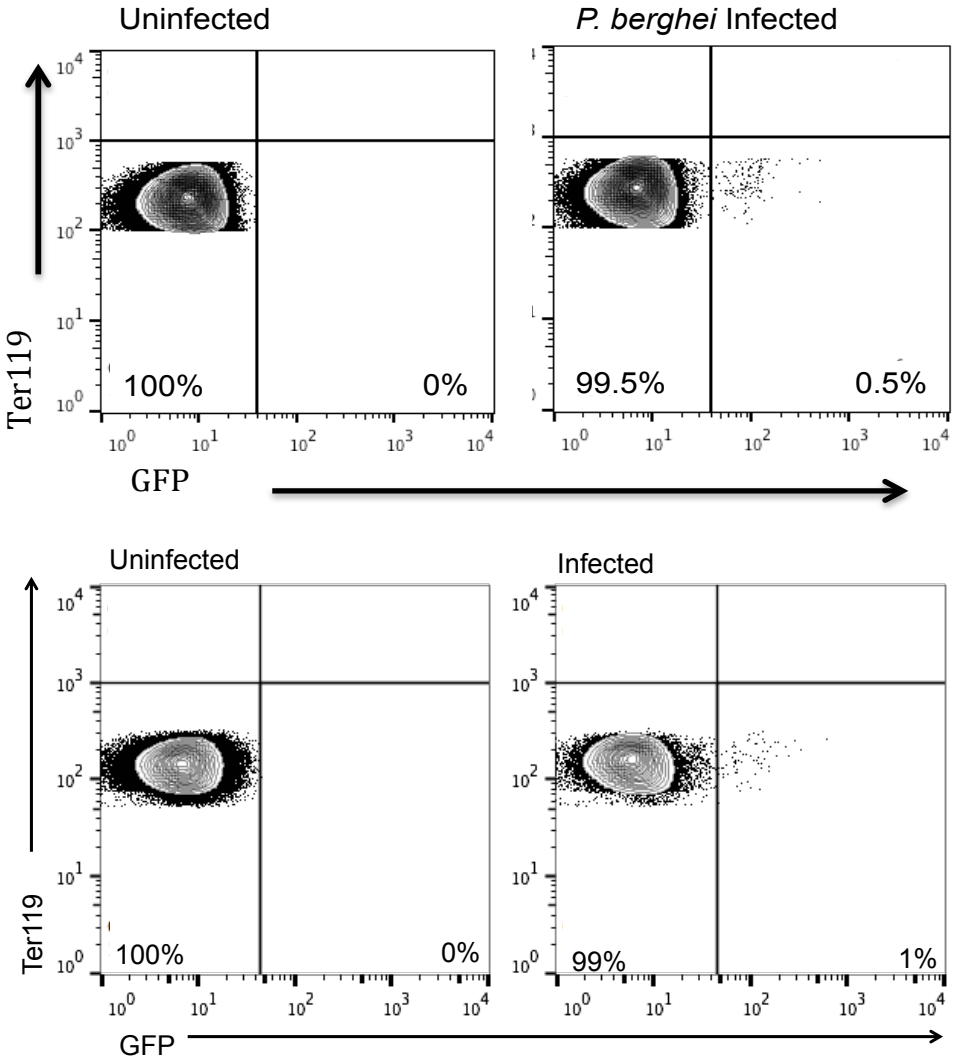

Figure 3.16 GFP^+ parasites were detected in erythroblasts in both tissues. Representative FACS plots from uninfected and infected animals showing viable $CD45^{-/low}$, $CD11b^-$, $Ter119^+$ DNA^+ (top row bone marrow; bottom row spleen) erythroblasts gated against Ter119 and GFP.

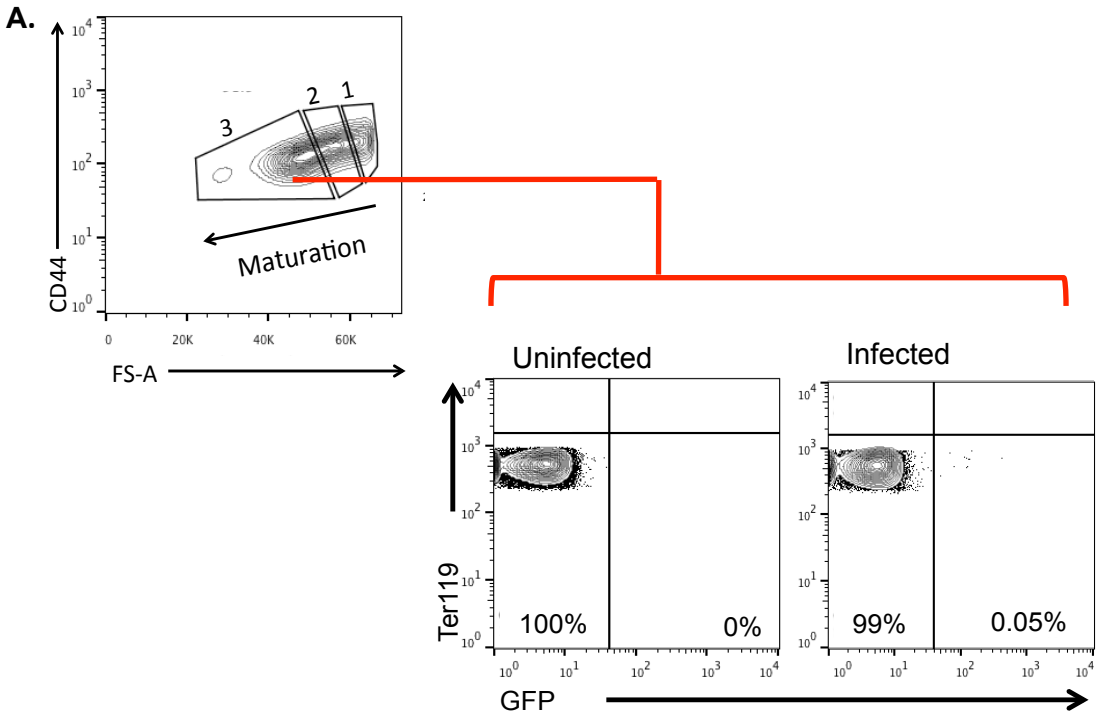

B

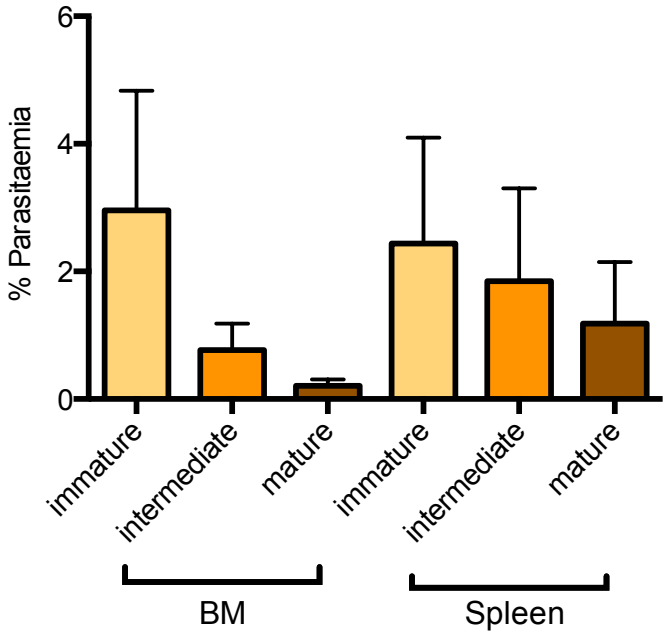

Figure 3.17 *P. berghei* does not show a preference for a particular erythroblast stage. A. Representative FACS plots from uninfected and infected animals showing viable CD45$^{-/low}$, CD11b^{-}, Ter119^{+} DNA^{+} erythroblasts gate 3 (mature. Plot from bone marrow) gated against Ter119 and GFP. **B.** Mice were injected with 10^4 *P. berghei* 507 clone1 and culled on day 7-post infection. The bone marrow and spleen were harvest and analysed by flow cytometry. Through this analysis the erythroblast populations in both tissues were sub gated into the previously defined maturation stages. The cells in each of these gates were then gated against Ter119 and GFP to calculate the parasitaemia of each maturation stage. Bone marrow (BM) and spleen of BALB/c mice Error bars ± SD. n = 9.

3.2.8. The Highest Observed Parasitaemia was in Splenic Early Reticulocytes

Both spleen and bone marrow (Figure 3.14) contained *P. berghei* infected (GFP^+) early reticulocytes (Figure 3.18). There was a significantly higher parasitaemia in early reticulocytes compared with erythroblasts (as a whole population). Moreover, the parasitaemia of splenic early reticulocytes was significantly higher compared with all other tissue resident erythrocyte populations (Figure 3.19A). The relative selectivity index of *P. berghei* for bone marrow (BM) and spleen-derived early reticulocytes (ER) and erythroblasts (EB) was calculated. The fold increase in parasitaemia was calculated relative to the tissue resident erythroid population containing the lowest parasitaemia. This revealed a BM EB: BM ER: spleen EB: spleen ER selectivity ratio of 1:12:3:26 (Figure 3.19B).

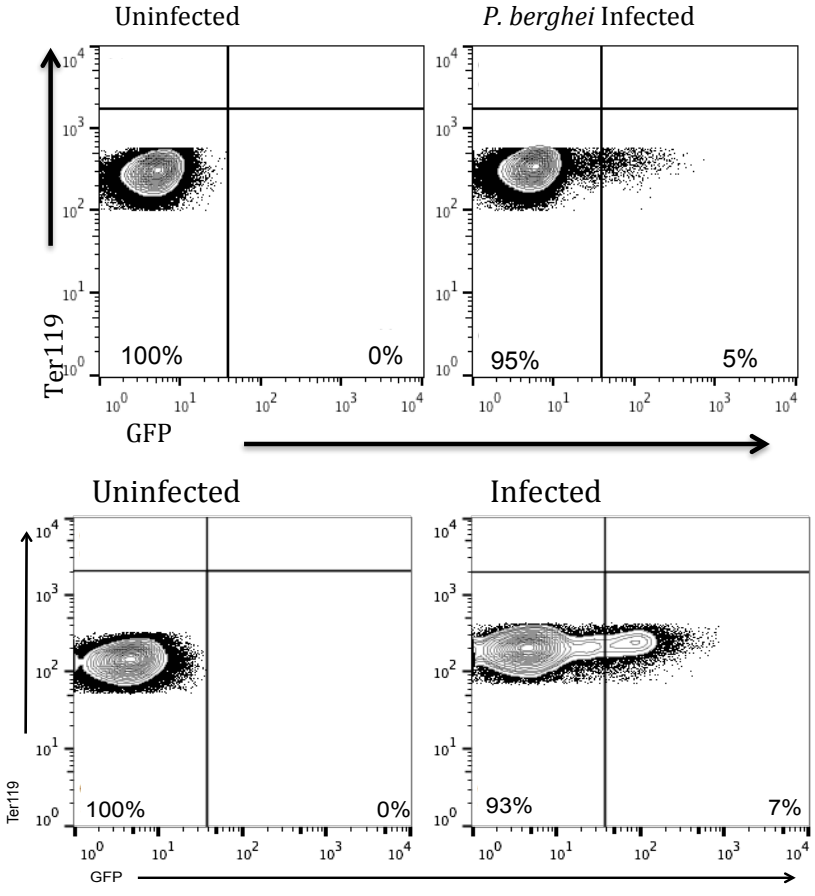

Figure 3.18 GFP^+ parasites were detected in early reticulocytes in both tissues. Representative FACS plots (bone marrow top row; spleen bottom row) from uninfected and infected animals showing viable $CD45^{-/low}$, $CD11b^-$, $Ter119^+$ DNA^- early reticulocytes gated against Ter119 and GFP.

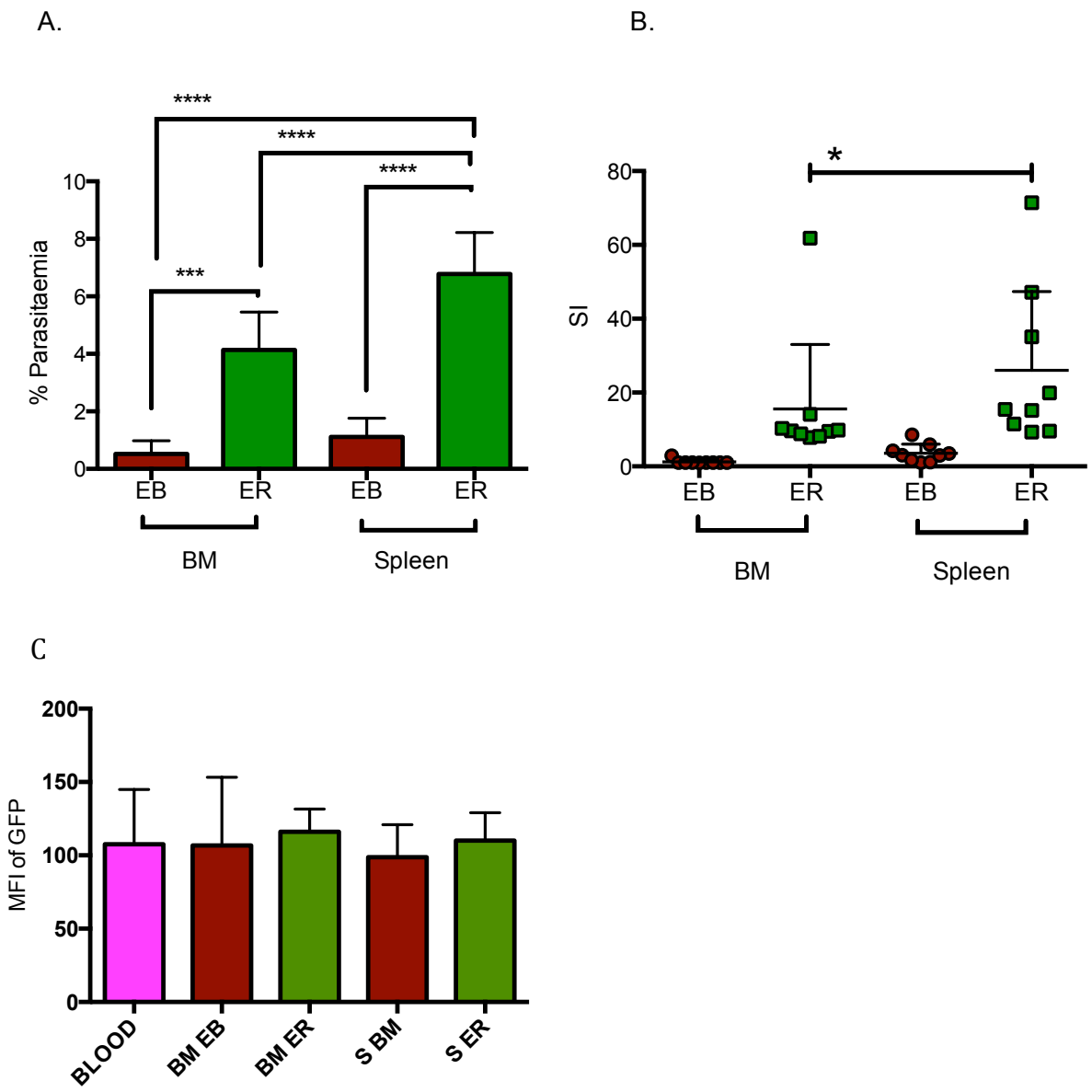

Figure 3.19 Splenic early reticulocytes have the highest *P. berghei* parasitaemia in BALB/c mice. Mice were injected with 10^4 *P. berghei* 507 clone1 and culled on day 7-post infection. The bone marrow and spleen were harvested and analysed by flow cytometry. **A.** The percentage parasitaemia in both erythroblasts (EB) and early reticulocytes (ER) in spleen and bone marrow. Error bars ± SD. n = 9. Differences between the means were tested using a one way ANOVA with multiple comparisons. **B.** Graph shows relative selectivity index (SI) for tissue resident erythroid cells. This was calculated for each animal by normalising the percentage parasitaemia as a fraction of the smallest parasitaemia. Error bars ± SD. n = 9. Difference between the means was tested with a paired t test. Significant differences between groups or samples are indicated with asterisks, denoting as follows: * $p < 0.05$, ** $p < 0.01$, *** $p < 0.001$, **** $p < 0.0001$. C. MFI of GFP in the tissue resident populations and the peripheral blood (n=3). Groups were not significantly different as judged by a one way ANOVA.

The intensity of GFP signal, expressed as MFI, was not significantly higher in cells extracted from either organ or the peripheral blood suggesting that the organs did not contained a higher proportion of mature parasites than the blood.

The parasitaemias of the early reticulocytes and the erythroblasts were not compared directly to the peripheral blood parasitaemia. *P. berghei* has a characterised tropism for circulating stage III-IV reticulocytes (Cromer *et al.*, 2006). These cells are reported to make up ~10% of the circulating erythroid population (Cromer *et al.*, 2006). However, our flow approach cannot distinguish between erythrocytes and circulating stage III-IV reticulocytes. Therefore, comparing a population of susceptible tissue resident erythroid cells with the circulating population that contains an assortment of susceptible and non-susceptible cells would bias our observations and possibly skew the results.

3.2.9. Conservative gating of GFP$^+$ cells

The uninfected samples were used as a FMO controls to define the gating for GFP$^+$ cells in each corresponding erythroid population. The GFP$^+$ gates were consistently defined on the uninfected control samples as containing 0% (no signal) of any given erythroid population. This was done to ensure the parasiteamia and whole cell numbers of parasites were defined by a GFP$^+$ gate containing parasites and not background fluorescence. Nonetheless, the conservative approach to defining the GFP$^+$ gate may have led to a proportion of GFP low young parasites being excluded from the analysis, as can be observed in Figure 3.18. The conservative gating practice was applied across all erythroid populations and the GFP signal of the parasites in each population was comparable (Figure 3.19 C). However, to ensure that the observation that splenic early reticulocytes contained the relative highest parasiteamia on day 7 pi (Figure 3.19) was not an artifact of conservative gating the plots were re-gated to include all potential parasites. This re-analysis of the data yielded a comparable result to the conservative gating strategy: splenic early reticulocytes contain the relatively higher parasiteamia compared to all other tissue resident populations (Figure 3.20).

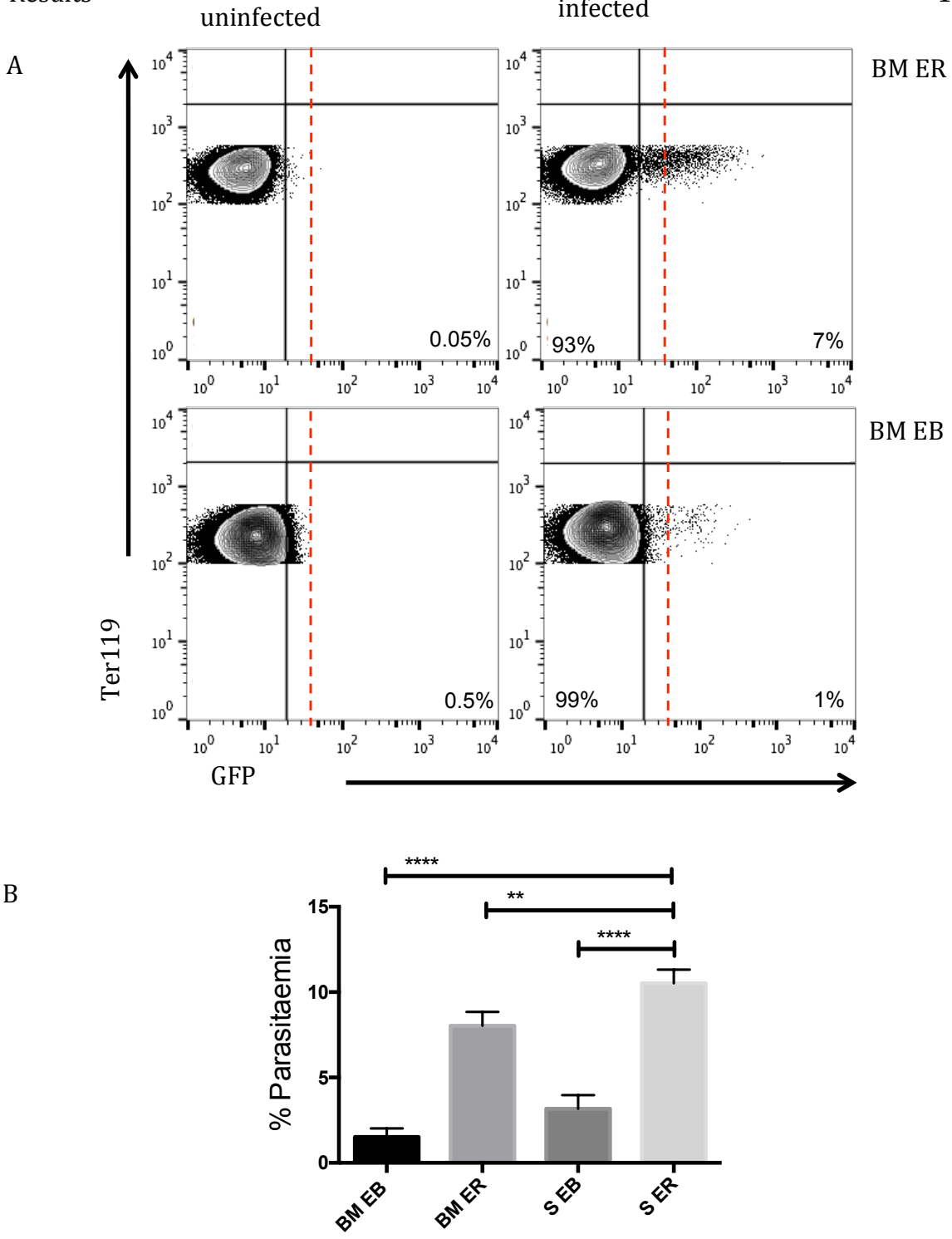

Figure 3.20 Re-analysis of GFP gating in tissue samples. A. representative FACS plots showing viable $CD45^{-/low}$, $CD11b^{-}$, $Ter119^{+}$ bone marrow early reticulocytes (BM ER) and erythroblasts (BM EB) gated against Ter119 and GFP. The red line represents the conservative gating strategy and the black line represents the re analysed gates. The percentages on the plots refer to the re analysed gates. **B**. Graph showing the parasiteamias generated from the re analysed plots. Bone marrow erythroblasts (BM EB) and early reticulocyts (BM ER) and the corresponding populations in the spleen (S EB and ER). The splenic early reticulocytes have the highest parasiteamia as judged by a one way ANOVA.

3.2.10. *P. berghei* May Undergo Schizogony in Erythroblasts

To confirm the presence of parasites within erythroblasts, nucleated GFP$^+$ splenocytes were cell sorted, then stained with anti-Ter119 and a DNA dye and visualised on a ImageStream flow cytometer. Although it was difficult to distinguish the lifecycle stages of the parasites, multinucleated GFP parasites, most probably schizonts were observed (Figure 3.21 D&F) indicating that parasites could multiply within erythroblasts.

A.

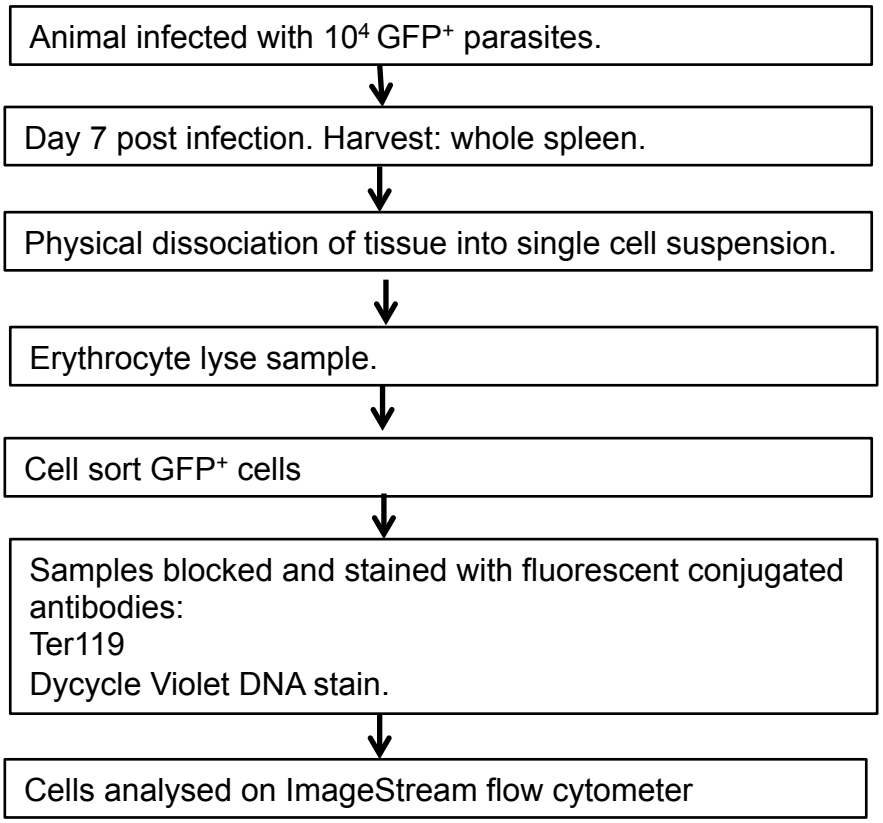

B

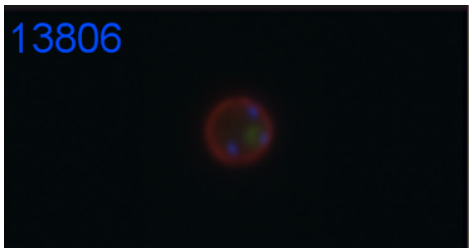

C.

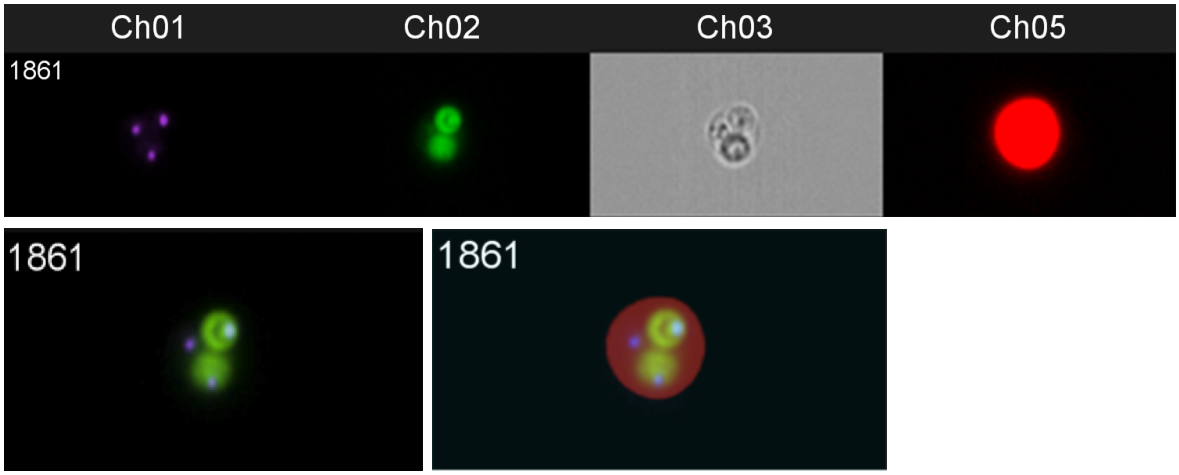
Ch01
Ch02
Ch03
Ch05
1861
1861
1861

D.

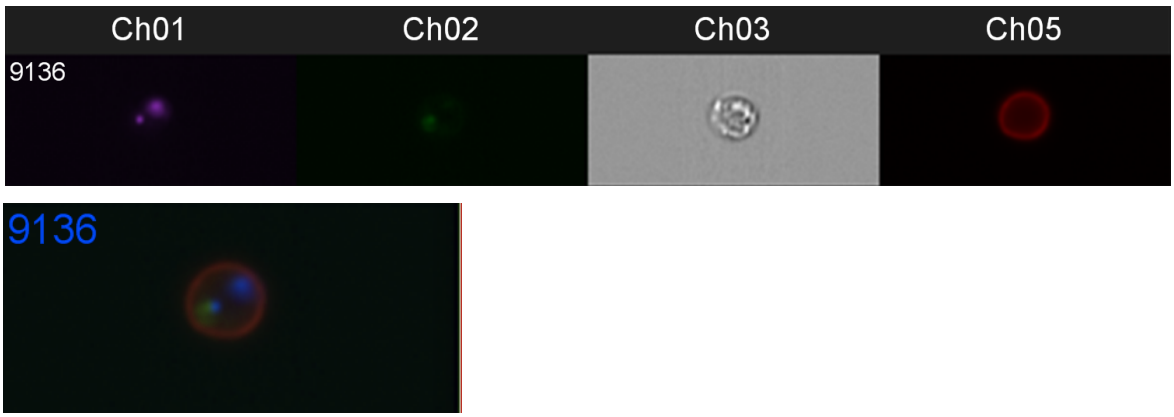
Ch01
Ch02
Ch03
Ch05
9136
9136

E.

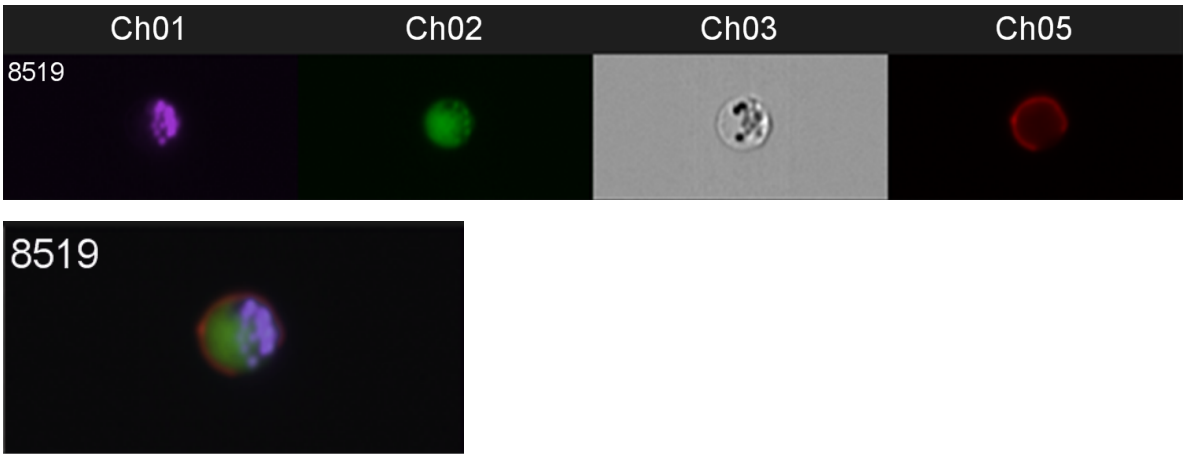
Ch01
Ch02
Ch03
Ch05
8519
8519

F.

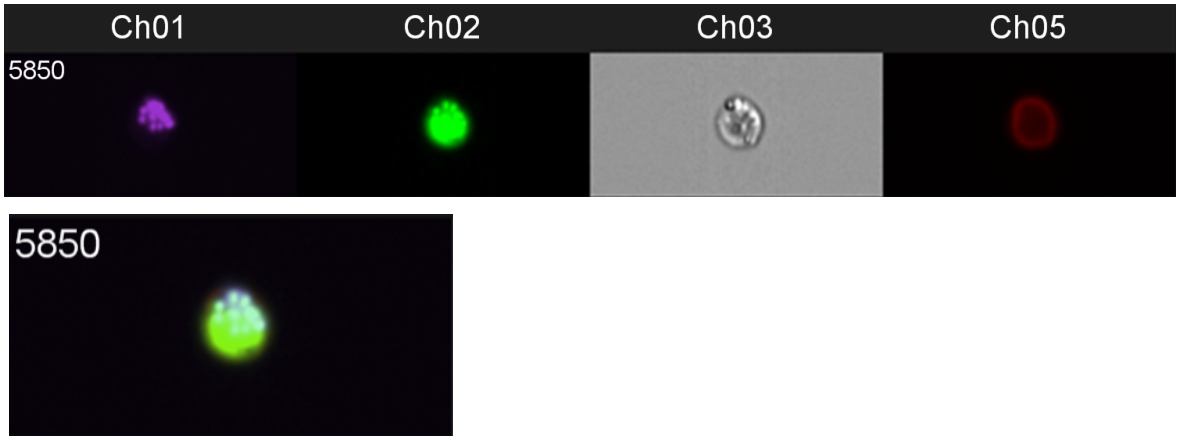

Figure 3.21 *P. berghei* parasitises erythroblasts. A. Flow diagram of the experiment. All panel images: Channel 1 (Ch01) DNA stain (dye cycle violet), Channel 2 (Ch02) GFP, Channel 3 (Ch03) bright field, Channel 5 (Ch05) anti- Ter119 APC. **B, D-F**: bottom single images: merge of Ch01, Ch02 and Ch05. **C**. Left hand single image: merge of Ch01 and Ch02. Right hand single image: merge of Ch01, Ch02 and Ch05. Number in the left hand corner indicates the position of image in the sequence of all images taken from the sample. Images taken from spleen samples (n=1).

3.2.11. Infected Erythroblasts and Early Reticulocytes can initiate *P. berghei* Infection

Using the flow based approached depicted in Figure 3.4 and the experimental procedure outlined in Figure 3.14, infected early reticulocytes and erythroblasts were cell sorted. 100 cells were then injected into separate uninfected mice to determine the viability and functionality of parasites they contained. A positive control of 100 GFP^+ parasites sorted from peripheral blood was set up in tandem. All mice had detectable parasitaemia by day 6 post-infection (n=1). This suggests that: 1. Both the early reticulocytes and erythroblasts contained asexual parasites, although the proportion of asexual and gametocytes were not quantified; 2. Both of these tissue resident erythroid cell populations are

permissive to *P. berghei* infection as both populations must have contained fully functioning asexual parasites that had undergone schizogony.

P. berghei has a characterised multiplication rate of 10x per 24 hrs. The parasitaemia detected on day 6 in both mouse groups was 0.1%. Therefore, the viable parasitaemia immediately after infection on day 0 was 0.000001%. As a BALB/c mouse contains 1ml of blood with 6 x 10^6 erythroid cells per µl, it would mean that 60 viable asexual parasites were injected into the mice on day 0.

3.2.12. Splenic Early Reticulocytes have the Highest Parasitaemia in a Mixed Genetic Background.

The *in vivo* spatial dynamics of *Plasmodium* cannot be fully appreciated in isolation. It is well established that the pathology of malaria is dependent on the interplay between parasite and host factors (Swanson *et al.*, 2016). Therefore, our model of tissue resident erythroid cell infection should be considered to be a closed but undefined system, with contributing elements deriving from the host response to infection. The BALB/c background is reportedly biased towards a particular adaptive immune response (Th2 response) (Fukushima *et al.*, 2006). To investigate whether the significant high parasitaemia observed in splenic early reticulocytes is dependent on the host genetics, the workflow depicted in Figure 3.14 was repeated in an outbred mouse strain (NIH). Again parasites where observed within erythroblasts and early reticulocytes of both organs, with splenic early reticulocytes containing the significantly highest parasitaemia compared to all other tissue resident erythroid populations (Figure 3.22 and Appendix 8.1.4). It should be noted that the parasiteamia in NIH tissue resident erythroid populations were not directly reflective of those observed in the BALB/c mice (Figure 3.19), nonetheless, like the BLAB/c mice, the highest parasiteamia was observed in the NIH splenic early reticulocytes.

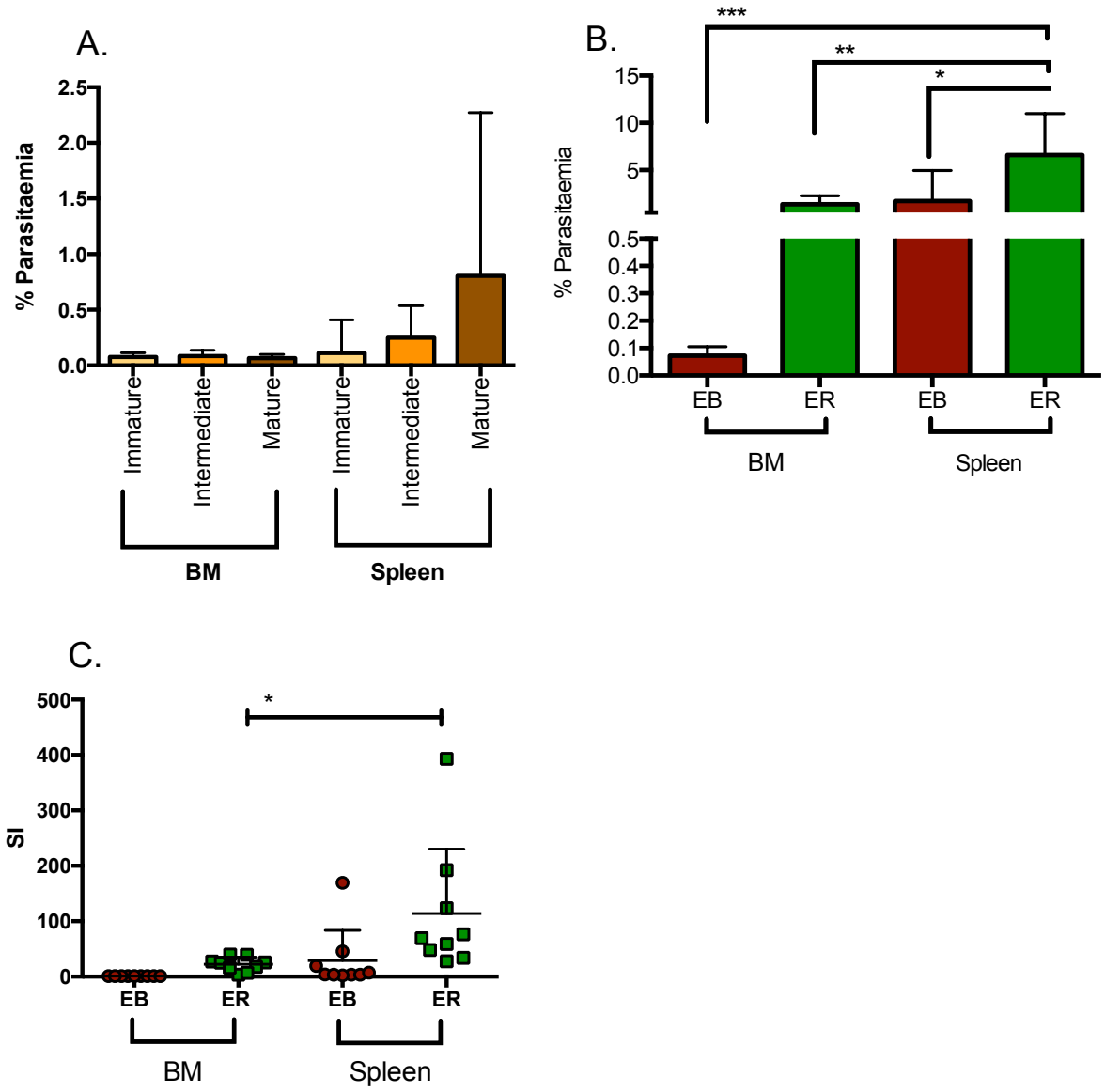

Figure 3.21 Host genetic background does not influence parasite preference for erythroblast and early reticulocytes. Mice were injected with 10^4 *P. berghei* 507 clone1 and culled on day 7-post infection. The bone marrow and spleen were harvested and analysed by flow cytometry. **A.** The percentage parasitaemia of erythroblast stages in the bone marrow (BM) and spleen in NIH outbred mice. Error bars ± SD. n = 6. **B.** Percentage parasitaemia of erythroblasts (EB) and early reticulocytes (ER) in the bone marrow (BM) and spleen in NIH mice. Error bars ± SD. n = 6. Differences between the means were tested using a one way ANOVA with multiple comparisons. **C.** Graph shows relative selectivity index for tissue resident erythroid cells. This was calculated for each animal by normalising the percentage parasitaemia as a fraction relative to the smallest parasitaemia. SI ratio of BM EB: BM ER: Spleen EB: Spleen ER is 1:22:29:114. Difference between the means was tested with a paired t test. Error bars ± SD. n = 6. Significant difference between groups or samples is indicated with asterisks, denoted as follows: * $p < 0.05$, ** $p < 0.01$, *** $p < 0.001$.

3.2.13. Splenic Early Reticulocytes Contain the Highest Parasite Burden

It is established that *Plasmodium* infection causes impaired murine splenic and bone marrow erythropoiesis leading to a decrease in erythroid progenitor populations (Maggio-Price, Brookoff and Weiss, 1985; Villeval, Lew and Metcalf, 1990; Chang, Tam and Stevenson, 2004). Similarly, the results generated using the workflow depicted in Figure 3.14 demonstrate a significant decrease in erythroblast numbers within the bone marrow of both BALB/c and NIH mice on day 7 post infection compared with the corresponding uninfected mice (Figure 3. 23 A&C). Furthermore, this effect was consistent with a trend observed in the spleen and independent of genetic background (Figure 3.23 B&D). An altered erythroblast stage ratio was also observed in the infected BALB/c spleen compared with the uninfected BALB/c spleen (Figure 3.23 G-H). This was not observed between the uninfected and infected NIH mice, which may be reflective of the NIH mice having a relatively increased erythropoietic response to EPO compared to BALB/c mice (Ohr, 1967).

The total parasite numbers (working under the assumption that each infected cell contains one parasite) in each tissue erythroid population were quantified. The greatest parasite population overall was observed in splenic early reticulocytes (Figure 3.23 I&J). This observed was consistent between the two genetic host backgrounds despite NIH mice having splenic and bone marrow pools of early reticulocytes quantifiably the same size in ($p = 0.7$), whereas they were different in Balb/c mice (* $p = 0.01$). Therefore, despite the host genetic background the greatest parasite burden was consistently observable within the splenic early reticulocytes.

A. Bone marrow: BALB/c

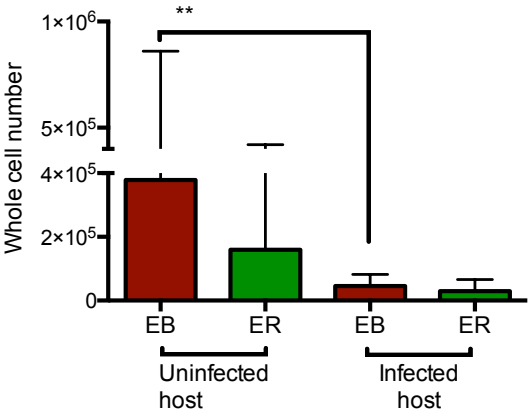

B. Spleen: BALB/c

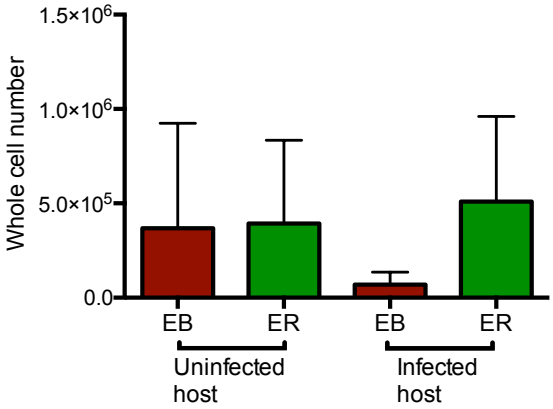

C. Bone marrow: NIH

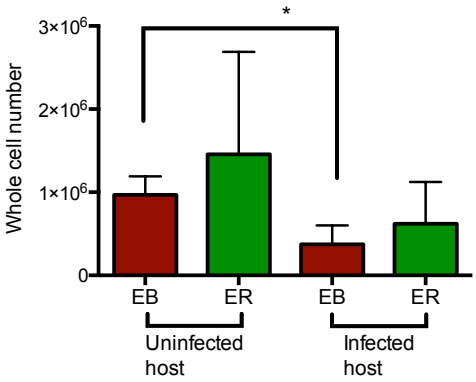

D. Spleen: NIH

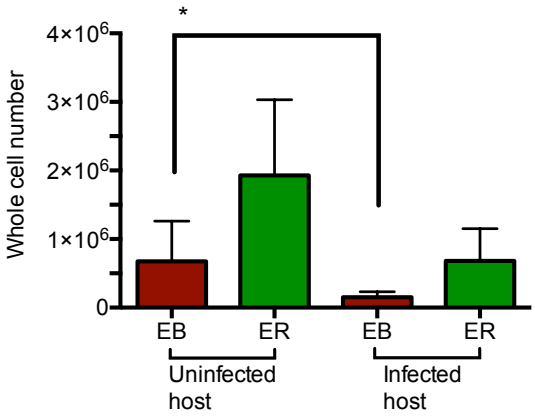

E. Infected BALB/c

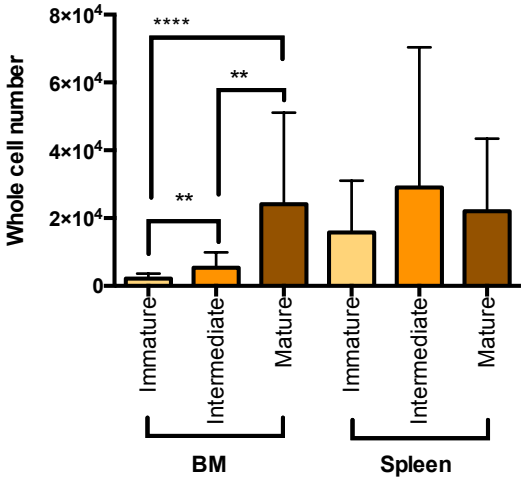

F. Infected NIH

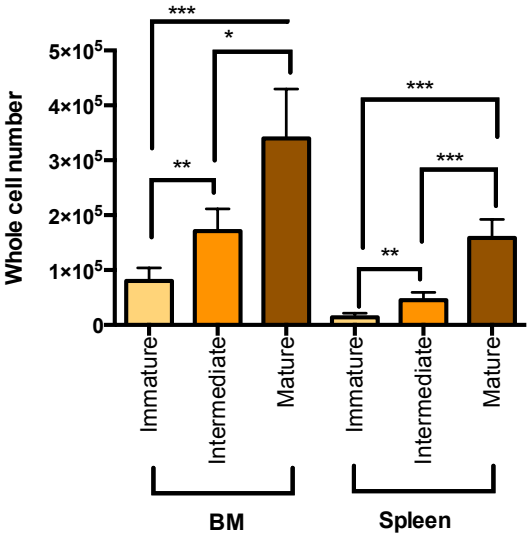

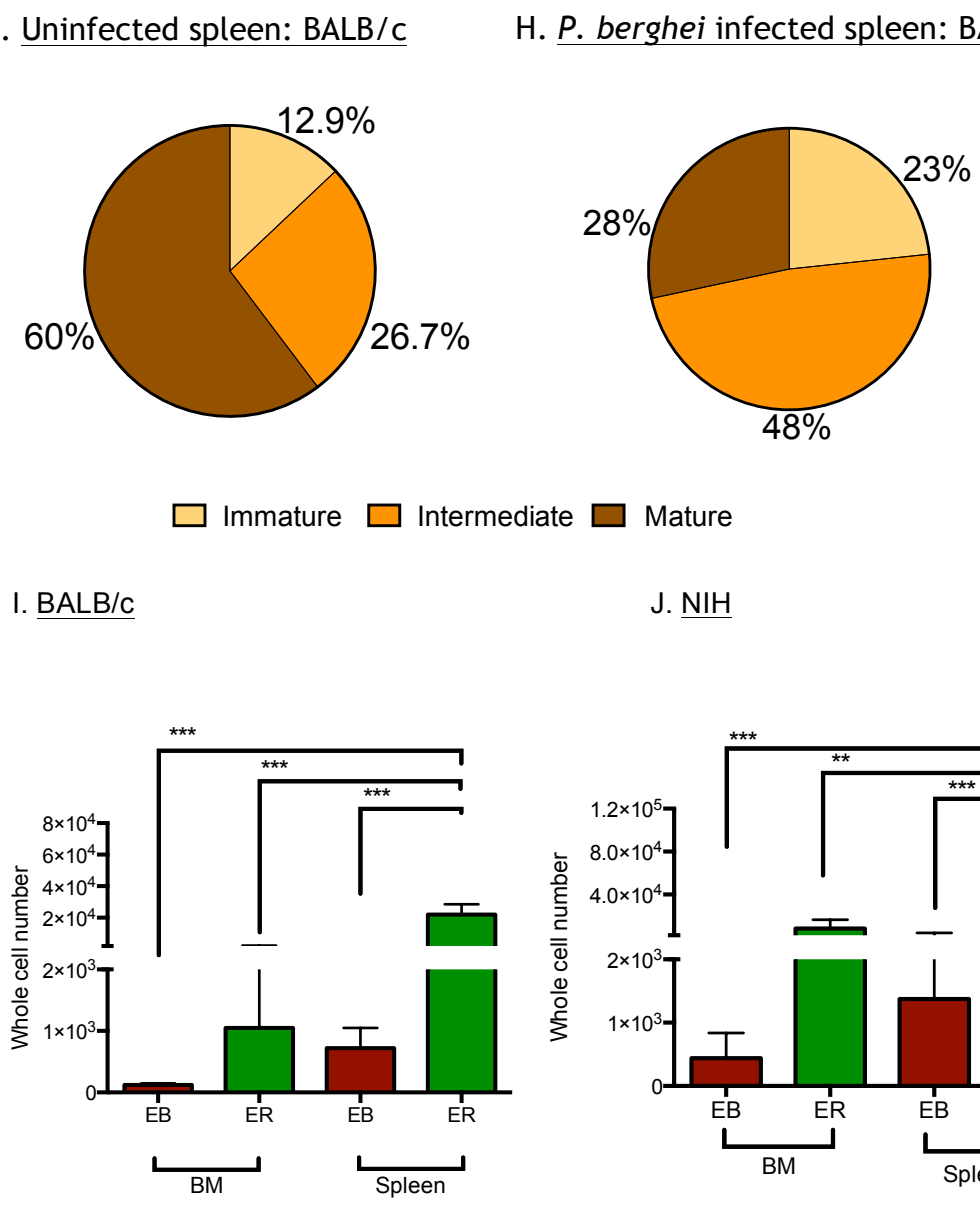

Figure 3.23. **Parasite burden and erythroid population size could be quantified.** Mice were injected with 10^4 *P. berghei* 507 clone1 and culled on day 7-post infection. The bone marrow and spleen were harvested and analysed by flow cytometry. Numbers of total erythroblasts (EB), though not early reticulocytes (ER) are reduced in bone marrow (**A & C**) and spleen (**B & D**) of infected mice. Error bars ± SD. Whole cell numbers of total erythroblast stages in infected bone marrow (BM) and spleen in BALB/c (**E**) and NIH mice (**F**). Error bars ± SD. Note the altered erythroblast stage ratio in the BALB/c spleen. Pie charts show the average proportion of each erythroblast stage in uninfected spleen (**G**) and infected spleen (**H**) of BALB/c mice. These charts demonstrate that on average, the proportion of the immature and intermediate erythroblasts doubles, whereas the mature proportion decreases by half. Total cell numbers of parasites in each erythroid population and of (**I**) BALB/c and (**J**) NIH mice. All BALB/c samples n = 9;. NIH all samples n=9. Differences between the means was tested using a one way ANOVA with multiple comparisons. Error bars ± SD

3.2.14. Results Summary

Work in this chapter successfully:

- Optimised a robust flow based methodology to identify different populations of erythroid cells.
- Observed *P. berghei* parasitising erythroblasts and early reticulocytes.
- Identified splenic early reticulocytes as containing the highest parasitaemia of tissue resident cells.
- Identified that splenic early reticulocytes contain the highest parasite burden of the tissue resident infection.

3.3. Discussion

The key discussion points are:

- Optimising the methodology:
    - The decreased abundance of CD71 during *P. berghei* infection is likely a by-product of a host response to inflammation.
    - Tissue perfusion was not performed during this investigation; therefore our results cannot be used to discuss the extra-vascularisation of mature erythrocytes.
- Identified *P. berghei* susceptible erythroid cells:
    - In contrast to *P. falciparum*, all erythroblasts were susceptible to *P. berghei* infection. This may indicate a difference in how the merozoites of the two species interact with the host cytoskeleton.
    - *P. berghei* may preferentially invade splenic early reticulocytes.
    - The quantified significant parasite burden in splenic early reticulocytes will have implications for antimalarial pharmacokinetics.

3.3.1. *Plasmodium* Induced Erythroid Cell Changes make CD71 an Unreliable Marker

Currently *Plasmodium* studies routinely use a combination of CD71 and Ter119 to resolve different erythroid populations (Martín-jaular *et al.*, 2013; Lelliott *et al.*, 2014; Lelliott, Mcmorran and Foote, 2015). Here a significant decrease in CD71 abundance was observed on the splenic early reticulocyte and erythroblasts extracted from *P. berghei* infected mice. A similar decrease has previously been observed in *P. vivax* cultures with matured human cord blood (Malleret *et al.*, 2015). To our knowledge the only incidence in uninfected mice when CD71 abundance fluctuates is during stress erythropoiesis, such as the response to anaemia or moving to high altitude. Stress erythropoiesis increases CD71 abundance before returning it to basal levels (Porpiglia *et al.*, 2012). It can therefore be suggested that the decrease in CD71 abundance I observed in infected mice is due to the presence of *Plasmodium*, rather than natural homoeostatic regulations. Under homeostatic conditions, CD71 is lost from the erythroid cell surface during terminal maturation (Chen *et al.*, 2009). It could therefore be suggested that *Plasmodium* infection increases the maturation rate

of its host cell. However, the abundance of CD44 also decreases during homeostatic erythroid maturation and there was not an observable difference in CD44 abundance on tissue resident erythroid cells between infected and uninfected samples in this study.

A recent transcriptional analysis of *P. falciparum*-infected erythroblasts revealed that infected cells down-regulate a number of genes (Tamez *et al.*, 2011). The down-regulated genes included some involved in clathrin-mediated endocytosis signalling (Tamez *et al.*, 2011). Interestingly CD71 facilitates the internalisation of iron through this pathway, although Tamez *et al* (2011) did not comment on effects *Plasmodium* infection has on erythroid heme biosynthesis. Significantly, by single cell, rather than population analysis, I showed that decreased CD71 abundance occurs on a population level, on both parasitised and non- parasitised cells *in vivo*. There is evidence in the literature that CD71 abundance is a proxy mediator of hepcidin suppression, with high CD71 leading to decreased hepcidin levels (Keel *et al.*, 2015). Hepcidin is protein released from cells in the liver and regulates the entry of iron into the circulation through interactions with gut enterocytes. Hepcidin production is increased by inflammatory cytokines, leading to a decrease in serum iron (Rossi, 2005). It is well documented that *Plasmodium* infection induces production of inflammatory cytokines (Mbengue *et al.*, 2016). As such, my observation of decreased CD71 abundance during infection could be linked to a global down-regulation of iron absorption due to inflammation induced expression of hepcidin (Cavill, 2002). Thus it may be a host response aimed at starving a parasite that requires iron for a number of biological processes including DNA synthesis. There is some clinical evidence associating iron deficiency with protection against malaria (Scholl, Tripathi and Sullivan, 2005; Clark, Goheen and Cerami, 2014). Our work would therefore recommend that future *Plasmodium* studies do not use CD71 as a marker for erythroid maturation.

3.3.2. Identifying Tissue Resident Erythroid Cells

In this study I optimised a CD44 based gating strategy to identify *P. berghei* infected erythroid cells in the bone marrow and the spleen. The advantage of using a flow-based approach, as opposed to histology, is that it is sensitive enough to distinguish discrete erythroid populations based on the quantitative

abundance of cellular markers. In this work I defined the early reticulocyte and erythroblast populations based on their absence from peripheral blood. However flow cytometry cannot distinguish between intra- and extra-vascular cell populations. Attempts in this work to adapt an *in vivo* intra-vascular staining technique were unsuccessful due to vascular leakage of the fluorescently conjugated antibody. Although, Pereira *et al* (2009) selectively labelled, as shown by histology sections, intra sinusoidal B cells in the murine bone marrow, my results directly reflect substantial evidence that bone marrow sinusoids are highly permeable (Sarin, 2010; Itkin *et al.*, 2016). Despite the incompatibility of the intra-vascular staining protocol with my methodology, tissue perfusion to remove vascular erythroid cells was not carried out in this work. Upon combining tissue perfusion with my flow approach I found an observable residual population of $Ter119^{+}$ $CD44^{low}$ cells within the bone marrow that previous studies have shown cannot be resident in extravascular spaces (Chen *et al.*, 2009; Muzykantov, 2011; Liu *et al.*, 2013). This is reflective of the strong evidence in the $CD8^{+}$ T cell literature that the post mortem perfusion of tissue is an unreliable process (Galkina *et al.*, 2005; Anderson *et al.*, 2012, 2014). As I did not want inefficient tissue perfusion to be misinterpreted as mature erythroid cells occupying extravascular spaces, I did not perform this procedure in my workflow. Nonetheless, my methodology allows us to study the infection of tissue resident early reticulocytes and erythroblasts *ex vivo* for the first time, moreover my approach will facilitate future studies investigating the pathology of malaria anaemia.

3.3.3. The Infection of Tissue Resident Erythroid Cells

In this work populations of *P. berghei* infected tissue resident cells were identified as $CD45^{-/low}$, $CD11b^{-}$, establishing that these infected cells were not within phagocytes. Moreover, infected early reticulocytes and erythroblasts were able to establish infection in uninfected animals, therefore these populations of host cells are permissive to functional asexual development.

3.3.4. *Plasmodium* Invasion of Nucleated Cells.

The observation of *P. berghei* within erythroblasts extracted from erythropoietic tissues is directly reflective of the observations that *P. falciparum, P. vivax* and *P. yoelii* can parasitise erythroblast populations in their hosts (Ru *et al.*, 2009; Tamez *et al.*, 2009; Imai *et al.*, 2013). Moreover, I observed parasites within all stages of erythroblast maturation. Immature erythroblasts undergo cell division, which is coupled with differentiation, in order to reach maturity (Chen *et al.*, 2009). I did not detect a significant difference in parasitaemia between the three erythroblast sub-gates, this therefore indicates that all stages of erythroblasts are susceptible to merozoite invasion and *P. berghei* does not have a preference for a particular stage. This is in contrast to *in vitro* work that observed that erythroid cells are only susceptible to *P. falciparum* from the orthochromatic stage (Tamez *et al.*, 2009). Orthochromatic cells are the smallest, most mature erythroblast and thus would not appear in our immature or intermediate erythroblast gates, in which I observed *P. berghei* infection.

The *Plasmodium* merozoite utilises a number of host receptors in order to gain entry into the host cell. The ligand-receptor interactions, which are well characterised in *P. falciparum* and *P. vivax*, remain undefined between the host cell and *P. berghei*. Both *P. vivax* and *P. falciparum* have the ability to interact with multiple host receptors in order to gain entry into the cell. These interactions, for *P. falciparum* at least, are redundant apart from the ones with the host receptors Basigin (CD147) and CD55 (Egan *et al.*, 2015). Both CD147 and CD55 are expressed at high levels on early erythroblasts (Bony *et al.*, 1999; Noji *et al.*, 2001). Therefore it would seem that erythroblast susceptibility to *P. falciparum* is not correlated with essential merozoite receptor expression.

Merozoite invasion, which has been characterised predominantly in *P. falciparum*, is believed to also involve interactions with the dynamic cytoskeleton of the erythrocyte, mediated by the defined parasite ligand-receptor's CR1 and GPA (Glodek *et al.*, 2010; Chais *et al.*, 2011; Koch and Baum, 2015; Zuccala *et al.*, 2016). This may be the precluding factor defining erythroblast susceptibility to *P. falciparum*. In contrast the only defined ligand-receptor interaction *P. vivax* makes with the host cell is PvDBP binding to the Duffy antigen. The downstream effects of this binding on the host cytoskeleton

has not been defined and it is believed to be unable to initiate intracellular signals when bound to CXC chemokines (Apostolakis *et al.*, 2011). The Duffy antigen is detectable on the erythroid cell surface by immunoblotting from the basophilic stage (Chen *et al.*, 2009). Directly correlated with Duffy detection, an *ex vivo* transmission electron microscopy study observed *P. vivax* in all erythroblast stages from the basophilic stage onwards (Ru *et al.*, 2009).

Taken together, this evidence indicates that *P. berghei*, like *P. vivax*, may not require the full assembly of the terminally differentiated erythroid cytoskeleton to gain entry into its host cell. Nonetheless, it must be noted that patients with genetic conditions resulting in both disordered spectrin arrangement and abnormal erythrocyte rigidity are still susceptible to *P. falciparum* infection within endemic malaria areas (Boctor and Dorion, 2008; Muley, Lakhani and Parekh, 2011; Makani *et al.*, 2017). As such, in light of the evidence that *Plasmodium* can invade nucleated and less deformable cells, the investigation into merozoite invasion should be extended to ensure any developed therapeutics also target the tissue resident infection.

3.3.5. *P. berghei* Preferentially Parasitises Early Reticulocytes

Erythropoiesis leads to the enucleation of erythroblasts resulting in the formation of reticulocytes. The maturation of reticulocytes is divided into four stages, with stages I-II residing within the erythropoietic tissue. To our knowledge, this work is the first time tissue resident reticulocytes have been studied *ex vivo* in the context of a *Plasmodium* infection. Malleret *et al*. (2015) previously observed that *P. vivax* has a preference for early reticulocytes differentiated in culture from human cord blood. Nonetheless, their study lacked anatomical context and a comprehensive definition of circulating and tissue resident reticulocytes.

Here I observed the highest parasitaemia of the tissue resident *P. berghei* infection within the early reticulocytes of both the bone marrow and the spleen. Erythropoiesis is a dynamic process with the cell successively maturing through the various erythroid stages. However, as I only sampled at one time point, the results presented in this chapter are a static snapshot of infection. As such, my

observations cannot directly rule out that *P. berghei* preferentially invades erythroblasts prior to day 7-post infection and that the host cell matures into reticulocytes in parallel to parasite development. In fact, *in vitro* work has directly shown that infected erythroblasts can enucleate and therefore mature into reticulocytes (Tamez *et al.*, 2009; Joice *et al.*, 2014). Nonetheless, the literature is conspicuously silent on whether infection in preceding erythroblast stages disrupted cell division and therefore maturation. In this study I observed that the erythroblasts of both tissues have the same expression of GFP compared with the early reticulocyte population. This observation can be discussed in the context of infected erythroblast being observed, using the image stream, to contain multinucleated parasites that suggested the presence of schizonts; thus would suggest that early reticulocytes contain schizonts as well. As stated previously, the fluorescence intensity of GFP in the 507 clone1 parasite line peaks during female gametocytogenesis and in parallel, increases during asexual maturation (Franke-Fayard *et al.*, 2004; Janse *et al.*, 2006). Therefore the higher the expression of GFP, the more mature the parasites are within an erythroid population. This suggests that the parasites within the erythroblast population are at the same or at more progressed maturation stage then the parasites in the early reticulocytes. This therefore implies there is not a linear model of merozoite invasion and ring development within erythroblasts that differentiate into early reticulocytes in parallel to parasite development. Moreover, this will be re-addressed in chapter 4.

3.3.6. Anaemia and Tissue Resident Parasite Burden

Malaria causes decreased erythroid cell numbers and altered stage distribution, resulting in anaemia (Yap and Stevenson, 1992; Lamikanra *et al.*, 2015). On day 7-post infection I observed a decrease in the numbers of erythroblasts in the bone marrow and the spleen compared with uninfected animals. As a result, the erythroid population containing the highest parasitaemia is not indicative of the erythroid population that contains the highest parasite burden in terms of whole numbers. To our knowledge this is the first study that has quantified the parasite burden (number of infected cells) in tissue resident erythroid cells. I identified that the erythroid population contributing the highest burden in tissue

resident infection mirrors the parasites cellular preference. The splenic early reticulocytes contain the greatest number of parasites in comparison to all other tissue resident erythroid cells. This has important implications for the pharmacokinetics of antimalarial drugs. In order to successfully resolve a malaria infection all parasites must be targeted. If the organs containing tissue resident infection present barriers that result in differential partitioning of drugs into tissue from the blood, this may lead to recrudescence and sub-optimal dosing.

3.4. Summary

In this chapter I optimised a method to resolve tissue resident erythroid cells using a flow-based approach. I then combined this with a *P. berghei* infection and observed that the greatest parasitaemia of tissue resident infection was consistently within the splenic early reticulocytes.

4 The Largest Tissue Resident Gametocyte Population Lies in the Splenic Early Reticulocytes.

4.1 Introduction

The postnatal erythropoietic tissue of the bone marrow and the spleen contain developing erythroid cells, which includes erythroblasts and stage I-II reticulocytes. A wide scale histological screen of autopsy tissue from malaria patients observed a significant enrichment of *P. falciparum* immature gametocytes within the parenchyma of the bone marrow (Joice *et al.*, 2014). In the aforementioned study, the authors concluded that immature gametocytes were parasitising mature erythroid cells (reticulocyte stage III-IV or erythrocytes), based on the absence of CD71 expression on the host cell. Evidence was presented in the previous results chapter showing that CD71 was down regulated during *P. berghei* infection, in agreement with previous studies in *P. vivax* (Malleret *et al.*, 2015), highlighting that CD71 is not a reliable marker of erythroid development during *Plasmodium* infection. Nonetheless, a hypothesis was constructed around the findings of Joice et al (2014) theorising that immature gametocyte infected circulating erythroid cells could home to, and migrate across the bone marrow sinusoidal endothelium (Nilsson *et al.*, 2015). Recent intravital imaging has observed the translocation of parasitised mature reticulocytes out of the vasculature into the bone marrow tissue after intravenous injection with synchronous and purified *P. berghei* ring stages (De Niz, submitted; Marti Lab, Glasgow, 2016). Although the authors could not definitively define the ring stages as early gametocytes, they did observe the transmigration of mature *P. berghei* gametocytes out of the bone marrow into the vasculature at subsequent points during infection. Nonetheless, the authors did not make observations concerning host cell maturation; a young ring stage parasite within a reticulocyte translocating into the bone marrow should emerge back into circulation as a mature parasite within a mature and aged erythrocyte. This therefore sustains the possibility that the authors observed mature gametocytes emerging into the blood stream in stage III reticulocytes after having undergone gametocytogenesis within a tissue resident erythroid cell. Moreover, they observed the ready translocation of merozoites into the bone

marrow parenchyma and the extra vascular presence of schizonts (De Niz, submitted). Consequently, the formation of gametocytes *de novo* within tissue resident erythroid cells remains a feasible and complementary model of gametocyte extravascularisation.

P. falciparum gametocytes undergo a protracted development, resulting in discrete morphologies that allow various maturation points to be easily classified into stages. Therefore, the absence of the immature stages of *P. falciparum* gametocytes from the peripheral blood is highly conspicuous. The developing gametocytes of parasite species within the sub-genus of *Plasmodium*, such as *P. berghei* and *P. vivax*, are morphologically indistinguishable from asexual trophozoites. As such, the dynamics of *P. berghei* gametocytes within the host are under-investigated and it is unclear whether they serve as a useful model for human gametocyte extravascularisation.

Here a parasite line will be developed in order to specifically identify *P. berghei* gametocytes using flow cytometry. As such, the aims of this chapter are:

- Construct a $PbGFP_{CON}/RFP_{GAM}$ parasite line.
- Characterise the $PbGFP_{CON}/RFP_{GAM}$ parasite line.
- Investigate spatial dynamics of gametocytes within tissue resident infection.
- Numerically investigating the preferential invasion of early reticulocytes by *P. berghei*.

4.2 Results

4.2.1 Construction of the $PbGFP_{CON}/RFP_{GAM}$ parasite line

In order to visualise *P. berghei* maturing gametocytes a fluorescent protein was placed under the control of a recently identified promoter (PBANKA_101870) that has early gametocyte activity (Sinha *et al.*, 2014). The commercially available gene encoding red fluorescent protein (RFP) was PCR amplified from a previously constructed plasmid, pG0161 (Dr. Katie Hughes; unpublished). The open reading frame in the pG306 plasmid was then exchanged with the *rfp* sequence (Sinha *et al.*, 2014). This brought *rfp* under the transcriptional control of the early gametocyte promoter (PBANKA-101870) creating plasmid pG403. The plasmid also contained a positive (pyrimethamine resistance) and negative (5-fluorocytosine (5-FC) sensitivity) drug selection cassette flanked by homologous sequence designed to facilitate sequence excision. The vector was linearised and then incorporated into the genome of the *P. berghei* 507 clone 1 parasite line at a silent locus (P230p) through double homologous recombination (Janse *et al.*, 2006). This created the parasite line G1137. Naïve mice were infected intravenously with G1137 immediately after the parasite transfection (day 0).

Incorporation of the vector into the parasite genome was positively selected by the administration of 70 µg/ ml pyrimethamine to the animal's drinking water on day 1. The peripheral blood was harvested when the parasitaemia was at an appropriate level (<1%). Correct integration of the vector into the parasite genome was confirmed by PCR (Figure 4.1). The parasite line was then cloned through limiting dilution to create $G1137cl_2$. The clonal line was negatively selected *in vivo* through the administration of 1.5 mg/ ml 5-FC to the animal's drinking water on day 1 post infection (pi). This selects parasites in which excision of the vector-derived drug selection cassette from the parasite genome has occurred via the recombination of the flanking homologous sequences. Excision of the drug selection cassette was confirmed by PCR (Figure 4.1 and Appendix 8.2.1) and $G1137cl_2$ was cloned through limiting dilution to create $PbGFP_{CON}/RFP_{GAM}$. This parasite line undergoes schizogony at 21-22 hrs-post invasion (hpi) and has a gametocytaemia directly reflective of the parental parasite line (Appendix 8.2.2).

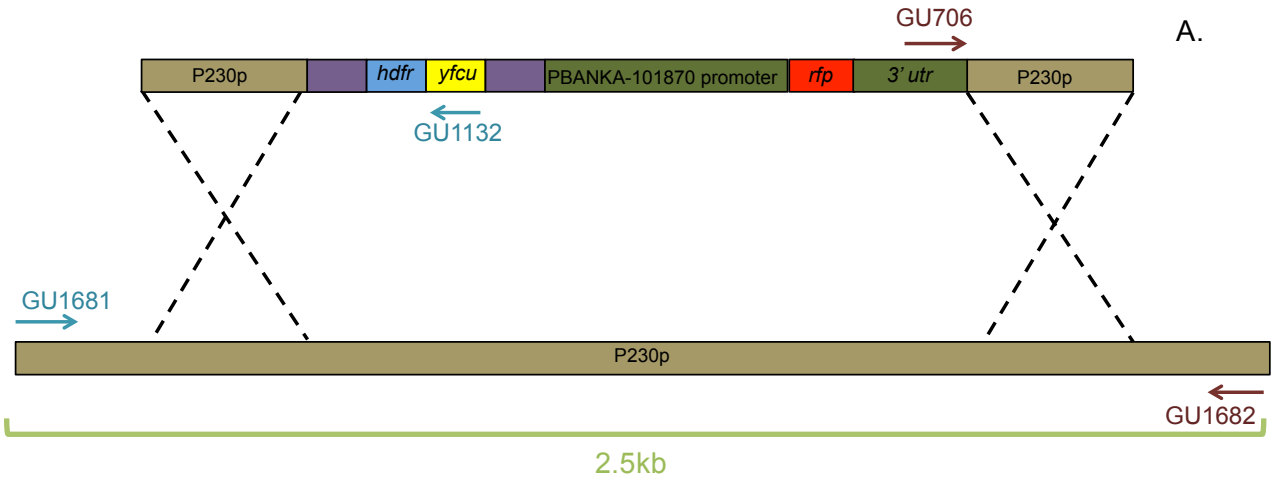
A.
GU706
P230p
hdfr
yfcu
PBANKA-101870 promoter
rfp
3' utr
P230p
GU1132
GU1681
P230p
GU1682
2.5kb

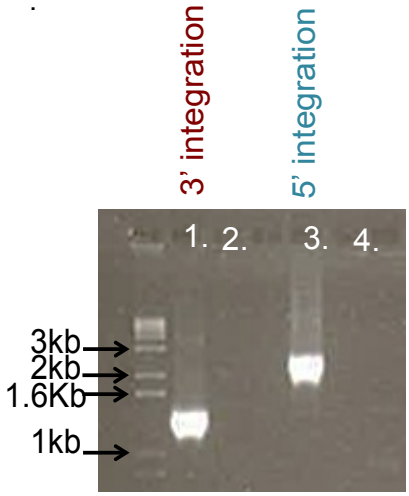
B.
3' integration
5' integration
1. 2. 3. 4.
3kb
2kb
1.6Kb
1kb

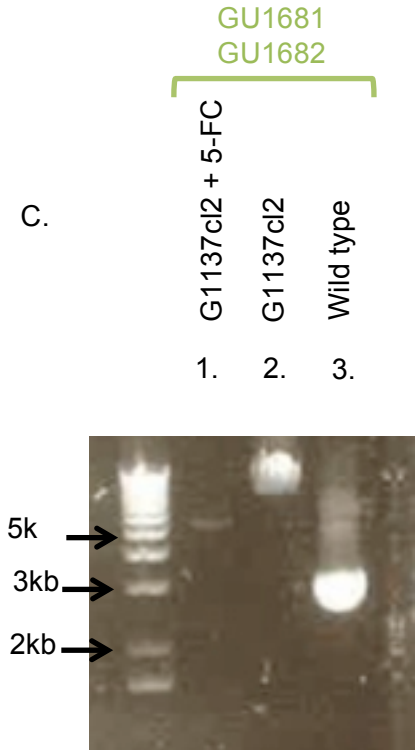
GU1681
GU1682
C.
G1137cl2 + 5-FC
G1137cl2
Wild type
1. 2. 3.
5k
3kb
2kb

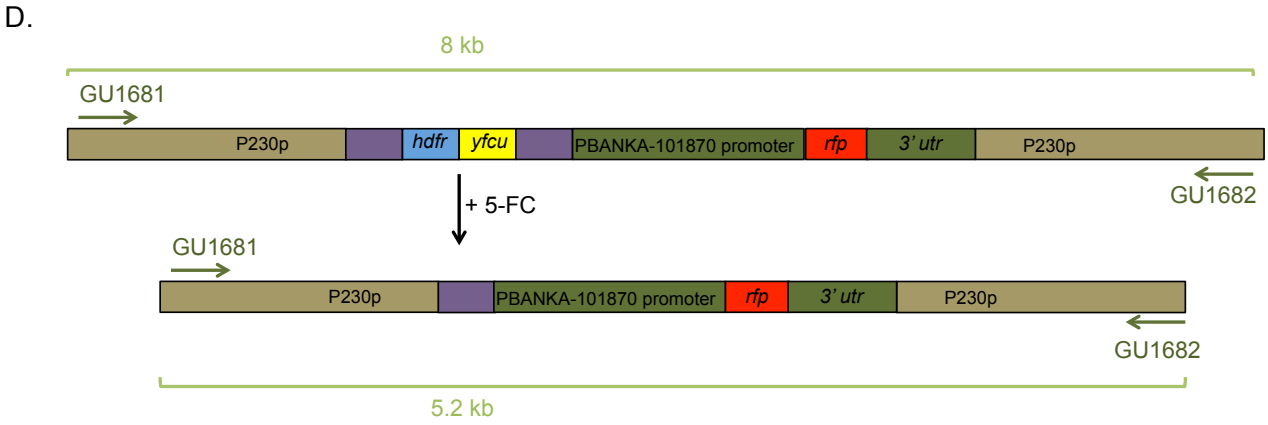
D.
8 kb
GU1681
P230p
hdfr
yfcu
PBANKA-101870 promoter
rfp
3' utr
P230p
GU1682
+ 5-FC
GU1681
P230p
PBANKA-101870 promoter
rfp
3' utr
P230p
GU1682
5.2 kb

Figure 4.1 Construction of the $PbGFP_{CON}/RFP_{GAM}$ line. A. Schematic showing the homologous recombination event that introduces the linearised vector into the parasite genome. Primers used to check integration by PCR are depicted and colour-coded as 3' integration (red) and 5' integration (blue). Green line indicated the size of the wild type P230p locus. Purple boxes are regions of homologous sequence in the vector, under 5-FC selection pressure these regions drive the excision of the drug selection cassette **B.** PCR gel showing integration of vector into the parasite genome. Lane 1 contains PCR reaction using G1137 genomic DNA. Primers are colour-coded to the schematic in A. correct 3' integration and 5' integration gives bands 1.4 Kb and 2 kb respectively. The ladder is located in the left hand lane and labeled. **C**. PCR gel showing removal of drug selection cassette after 5-FC treatment. Genomic DNA from $G1137cl_2$ parasites after treated with 5-FC, $G1137cl_2$ before treatment and wild type parasites with no vector integration at the P230p locus was used as templates in a reaction with primers spanning the P230p locus. Excision of the drug selection cassette should generate a band 5.2 Kb in length. No excision of the drug selection cassette will generate a band 8 Kb in length. Amplification of endogenous wild type locus will produce a band 2.5 Kb in length. The ladder is located in the left hand lane and labeled. **D.** Schematic showing the excision of the drug selection cassette under 5-FC pressure. The primers and band fragment length are colour-coded to the gel in C.

4.2.2 Characterising PbGFP$_{CON}$/RFP$_{GAM}$

Samples of peripheral blood from animals infected with asynchronous PbGFP$_{CON}$/RFP$_{GAM}$ were analysed by flow cytometry. Comparison of RFP/GFP expression produced four cell populations: GFP/RFP double negative uninfected erythrocytes, GFP^{+} cells, GFP^{+} RFP^{+} cells and GFP^{++} RFP^{+} cells (Figure 4.2).

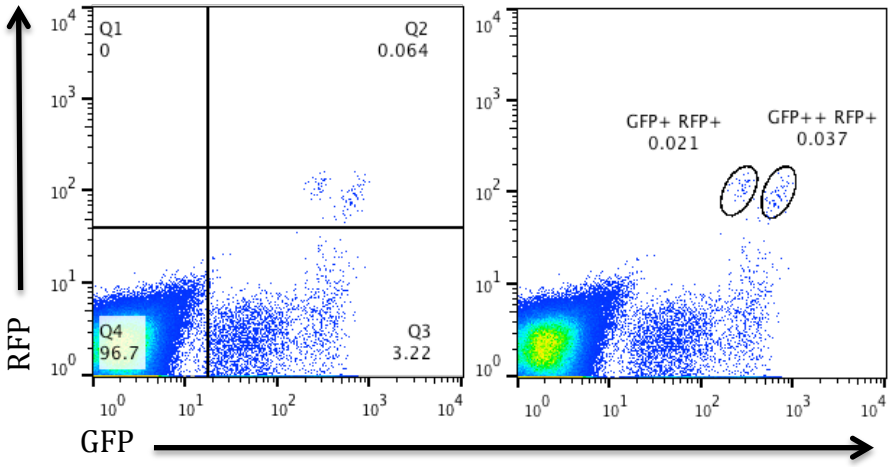

Figure 4.2 PbGFP$_{CON}$/RFP$_{GAM}$ contains two RFP^{+} populations. Representative FACS plots of peripheral blood. Resolving cell populations based on GFP and RFP expression reveals two RFP^{+} populations with different intensities of GFP expression (left). These cells were gated separately as GFP^{+} RFP^{+} cells and GFP^{++} RFP^{+} cells.

The fluorescence dynamics of GFP under the control of the eef1-alpha promoter have been previously characterised throughout the life cycle of *P. berghei*. Female gametocytes have a GFP MFI three times higher than the male gametocytes (Franke-Fayard *et al.*, 2004). The GFP MFI of our GFP^{+} RFP^{+} cells and GFP^{++} RFP^{+} cells was quantified as 428 relative fluorescence units (RFU) and 1086 RFU, respectively. This led to the speculation that these populations were exclusively male and female gametocytes. This was confirmed by cell sorting the two populations from a gametocyte-enriched, synchronised peripheral blood infection, performed at 48 hpi. The two gametocyte populations were activated and visualised by light microscopy. The GFP^{+} RFP^{+} sample contained exclusively exflagellating male gametes and the GFP^{++} RFP^{+} contained exclusively extracellular, activated female gametes (Figure 4.3).

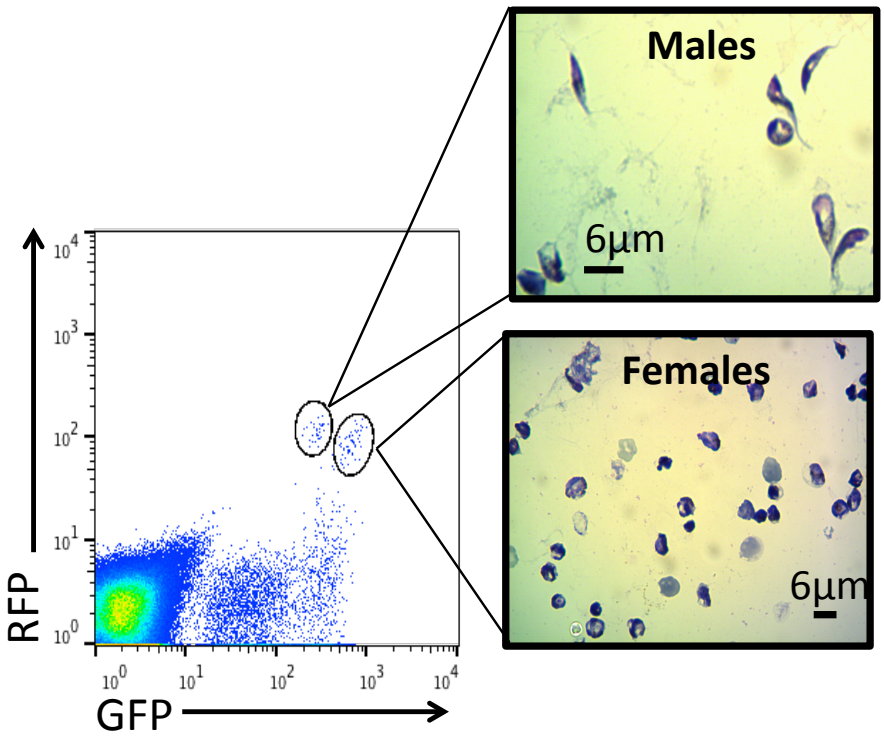

Figure 4.3 Distinguishing male and female gametocyte populations. The two GFP^+RFP^+ populations were cell sorted and then activated. Representative photos from the male and female gametocyte populations are shown. The two populations contained exclusively male or female gametes when Giesma stained and examined under light microscopy.

Next, the dynamics of RFP under the control of the early gametocyte promoter were investigated. The parasite line was characterised *in vitro* in order to circumvent gametocyte accumulation outwith the peripheral blood. As *P. berghei* schizonts do not spontaneously undergo merozoite egress *in vitro*, a donor mouse was used initially to stimulate re-invasion *in vivo*. Highly enriched synchronized schizonts were injected IV into the donor animal and the peripheral blood was harvested 10 mins post injection. Any residual mature gametocytes were removed by magnetic column sorting and samples were taken at specific time points from the newly invaded blood. RFP fluorescence was observed from 8 hpi and by 12 hpi the GFP^+RFP^+ $GFP^{++}RFP^+$ populations were distinguishable (Figure 4.4 and Appendix 8.2.3). The *rfp* promoter was active throughout the remaining developmental stages of maturing and mature gametocytes (Appendix 8.2.4).

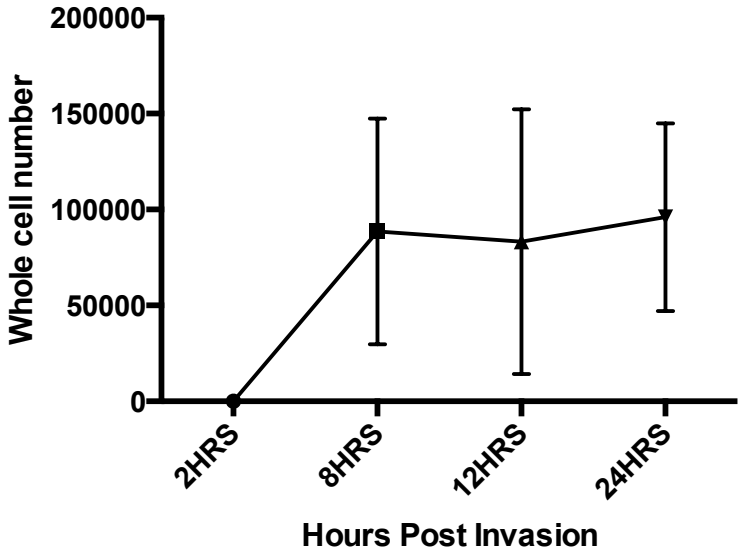

Figure 4.4 RFP was detectable from 8 hrs post invasion. Samples were taken at each time point from *in vitro* culture. The RFP expression in GFP postive cells was monitored by flow cytomotery. Graph showing the mean numbers of RFP positive gametocytes during the synchronized *in vitro* development of $PbGFP_{CON}/RFP_{GAM}$. Error bars ± SD. n = 3.

However, due to the hypothesis in the literature that immature gametocytes home to or develop in the bone marrow (Nilsson *et al.*, 2015), I felt the initial results were perhaps ambiguous as a result of the *in vivo* re-invasion step. Therefore, mature, synchronised schizonts were mechanically lysed to introduce re-invasion *in vitro*. Prior to this, residual mature gametocytes had been labelled with anti Ter119 IgG therefore ensuring they could be excluded from the analysis. Samples taken at specific time points were analysed by flow cytometry. Again RFP fluorescence was detected from 8 hpi and further demonstrated that this was not detectable at 6 hpi (Figure 4.5).

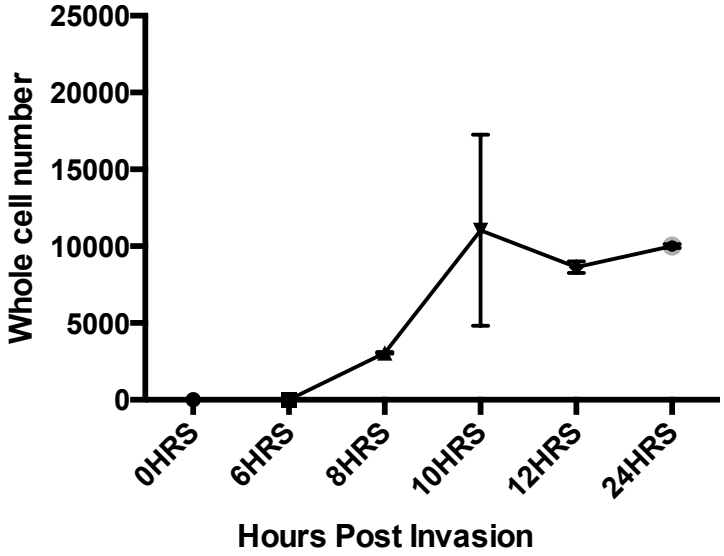

Figure 4.5 RFP was detectable from 8 hrs post invasion. Samples were taken at each time point from *in vitro* culture. The RFP expression in GFP postive cells was monitored by flow cytomotery. Graph showing the mean number of RFP positive gametocytes during synchronized *in vitro* development of $PbGFP_{CON}/RFP_{GAM}$. Error bars ± SD. n = 3.

4.2.3 Asexual Parasites and Gametocytes can be Separated in an Asynchronous Infection

During an asynchronised infection with $PbGFP_{CON}/RFP_{GAM}$ there is a GFP^+ RFP^- population that has a similar GFP MFI to the GFP^+RFP^+ population (Figure 4.2). To ensure this population is not composed of gametocytes at < 8 hpi, 100 asynchronous GFP^+RFP^- cells were sorted and injected into an uninfected mouse. These parasitised cells were able to establish an infection in peripheral blood that was detectable on Giemsa smears 6 days pi (n=1). This confirmed that GFP^+RFP^- populations contain asexual parasites; therefore ensuring asexual and sexual cells could be distinguished robustly.

4.2.4 Reproducible Infection Dynamics

The $PbGFP_{CON}/RFP_{GAM}$ parasite line was subsequently combined with the flow based approach established in the previous chapter to observe the temporal and spatial dynamics of *P. berghei* gametocytes within tissue resident erythroid cells *in vivo* (Figure 4.6A). Both BALB/c and NIH outbred mice were infected with 10^4

asynchronous parasites (9 am). As shown in the previous results chapter, the majority of asynchronous parasites undergo schizogony within the peripheral blood at 12-7 am and at the point of tissue harvest, the majority of parasites were ring or early trophozoite stages (as judged by examination of Giesma stain blood smears) within the peripheral blood (Figure 3.15 A). However, as the dynamics of parasite development within tissue resident erythroid cells have yet to be directly established, I focused my analysis on parasite life stage defined by the fluorescence markers: RFP^+ cells were gametocytes. RFP^- cells were asexual and the GFP MFI increased during asexual maturation.

Peripheral blood, bone marrow and spleen were harvested every 24 hrs (9 am) up to and including day 7 pi (Figure 4.6A). The parasitaemia (total GFP^+ cells) of the $Ter119^+CD44^{low}$ cells extracted from the spleen of BALB/c mice was significantly higher than the parasitaemia of the peripheral blood, beginning at day 5 pi (Figure 4.6; * $p < 0.05$), consistent with the results in the previous chapter (day 7 pi). Moreover, the splenic $Ter119^+CD44^{low}$ population contained a higher proportion of gametocytes than the peripheral blood. This occurred as early as day 4 pi (Figure 4.7). The observations in NIH mice were also consistent with the results in the previous chapter, where a non-significant difference between the parasitaemia of the tissue extracted $Ter119^+CD44^{low}$ cells and the peripheral blood in NIH mice was detected on day 7 pi (Figure 4.6 and Appendix 8.2.5).

A.

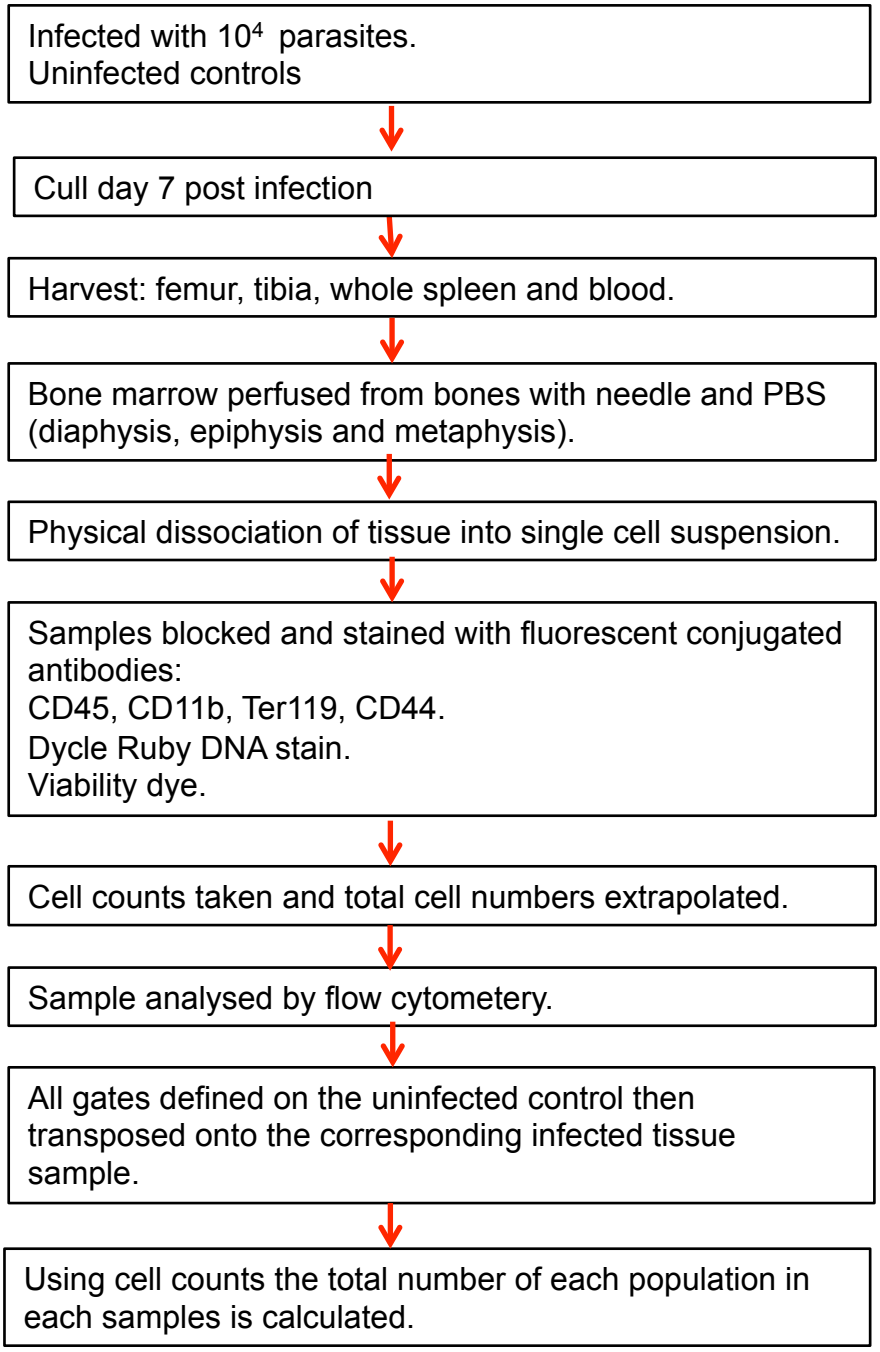
Infected with 10^4 parasites.
Uninfected controls
Cull day 7 post infection
Harvest: femur, tibia, whole spleen and blood.
Bone marrow perfused from bones with needle and PBS (diaphysis, epiphysis and metaphysis).
Physical dissociation of tissue into single cell suspension.
Samples blocked and stained with fluorescent conjugated antibodies:
CD45, CD11b, Ter119, CD44.
Dycle Ruby DNA stain.
Viability dye.
Cell counts taken and total cell numbers extrapolated.
Sample analysed by flow cytometery.
All gates defined on the uninfected control then transposed onto the corresponding infected tissue sample.
Using cell counts the total number of each population in each samples is calculated.

B.
BALB/c

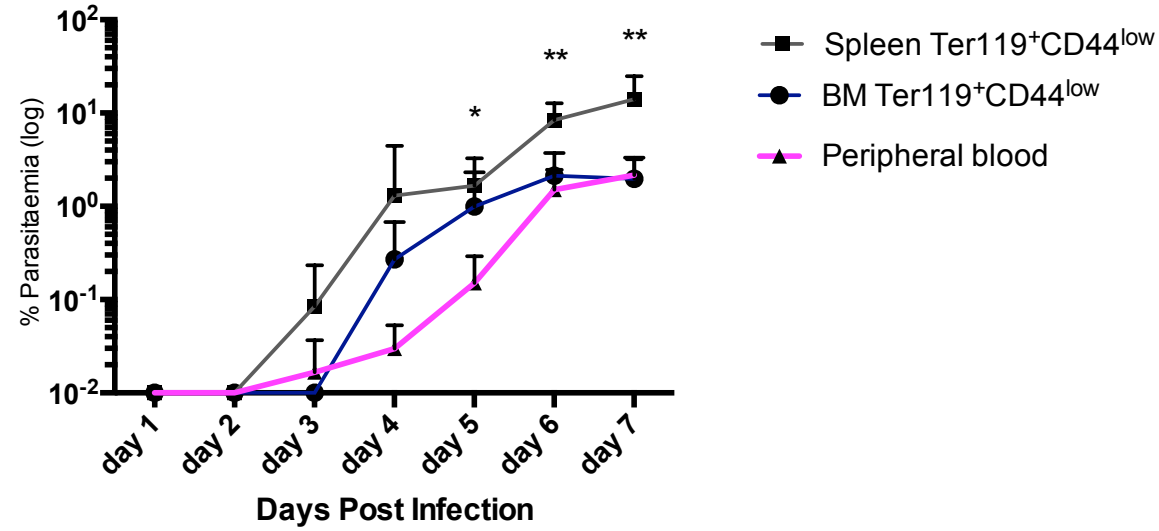

C. NIH

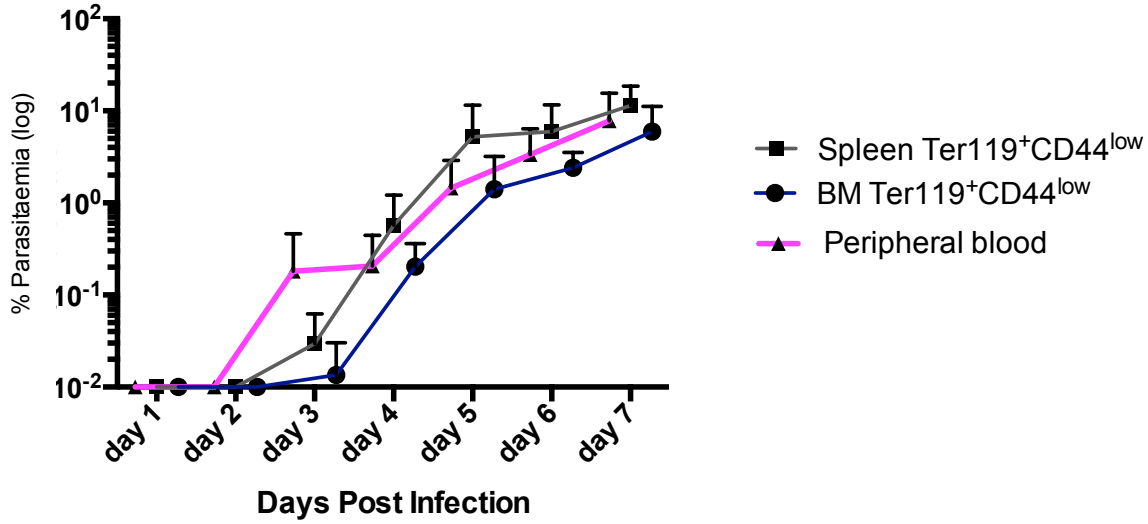

Figure 4.6 Parasitaemia of Ter119$^+$CD44^{low} cells across a 7 day infection. A. Flow diagram depicting the experimental protocol**. B.** BALB/c mice. All time points n=9; day 7 n=8. The parasitaemia in the splenic extracted Ter119$^+$CD44^{low} cells was significantly higher compared to the peripherial blood from day 5 pi **C.** NIH mice. All times points n =6. There was no difference in parasitaemia between the tissue and blood groups across infection. Significant differences between a tissue group and peripheral blood at a given time point was investigated with a one way ANOVA comparing the mean of each group. Significanct differences in parasitaemia compared with the peripheral blood are indicated with asterisks, denoting as follows: * $p < 0.05$, ** $p < 0.01$. Error bars ± SD

A. BALB/c

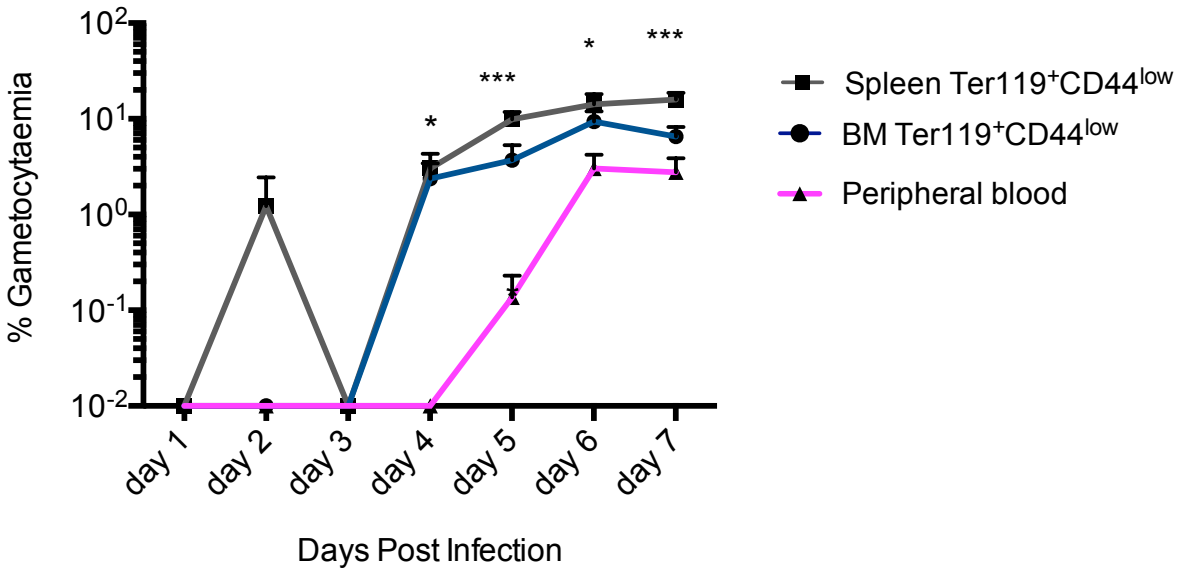
% Gametocytaemia
10^2
10^1
10^0
10^{-1}
10^{-2}
*
***
*
***
day 1
day 2
day 3
day 4
day 5
day 6
day 7
Days Post Infection
Spleen Ter119+CD44low
BM Ter119+CD44low
Peripheral blood

B.

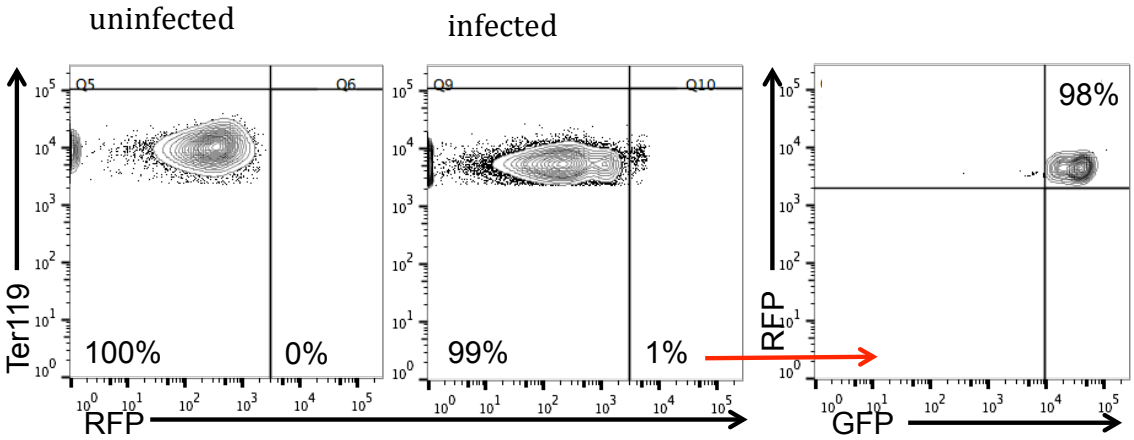
uninfected
infected
Ter119
RFP
Q5
Q6
100%
0%
Q9
Q10
99%
1%
98%
GFP

C.

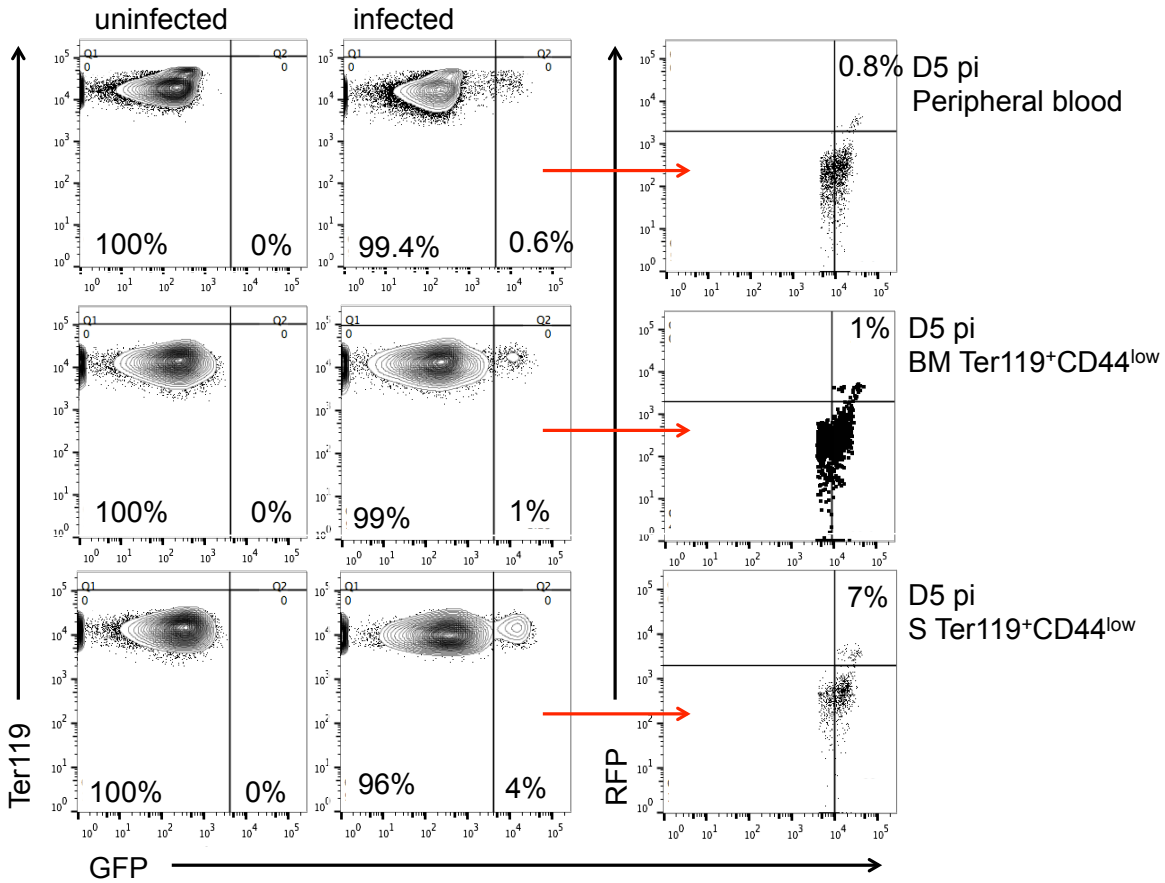

Figure 4.7 Gametocytaemia of Ter119^{+}CD44^{low} cells across a 7 day infection. A. BALB/ c mice. All time points n=9; day 7 n=8. The gametocytaemia in the splenic extracted Ter119^{+}CD44^{low} cells was significantly higher from day 4 pi compared to the peripheral blood. Significant differences between a tissue group and peripheral blood at a given time point was investigated with a one way ANOVA comparing the mean of each group. Significanct differences in parasitaemia compared with the peripheral blood are indicated with asterisks, denoting as follows: * $p < 0.05$, ** $p < 0.01$, *** $p < 0.001$. Error bars ± SD. **B**. Defining the RFP^{+}GFP^{+} gate. CD45$^{-/low}$, CD11b^{-}, Ter119^{+} RFP^{+} cells were identified within infected samples (gated defined by uninfected control). RFP^{+} cells were then gated RFP vs GFP to define where they sit on the graph. **C**. GFP^{+} cells in infected samples where gated RFP vs GFP. The RFP^{+}GFP^{+} were identified with the gate defined in figure 4.7 B in order to calculate the percentage of the RFP^{+}GFP^{+} cells within the GFP^{+} population. The plots displayed are representative FACS plots from day 5 post infection (D5 pi).

GFP$^+$ parasites were observable within early reticulocytes and erythroblasts of the bone marrow and spleen from as early as day 3 pi. Moreover, splenic early reticulocytes had the highest parasitaemia and highest parasite burden compared with any other tissue resident erythroid population from as early as day 5 pi (Figure 4.8 and Appendix 8.2.6). As discussed in the previous results chapter, the parasitaemia of the tissue resident erythroid cells (early reticulocytes and erythroblasts) was not compared with the peripheral blood.

It should also be noted that all parasites were within viable erythroid cells that had not been internalised by phagocytes (CD45$^-$ and CD11b$^-$ cellular phenotype). Taken together, the dynamics of the GFP$^+$ parasite populations showed that the model generates reproducible results, and moreover the PbGFP$_{CON}$/RFP$_{GAM}$ parasite line displays infection dynamics reflective of the parental line.

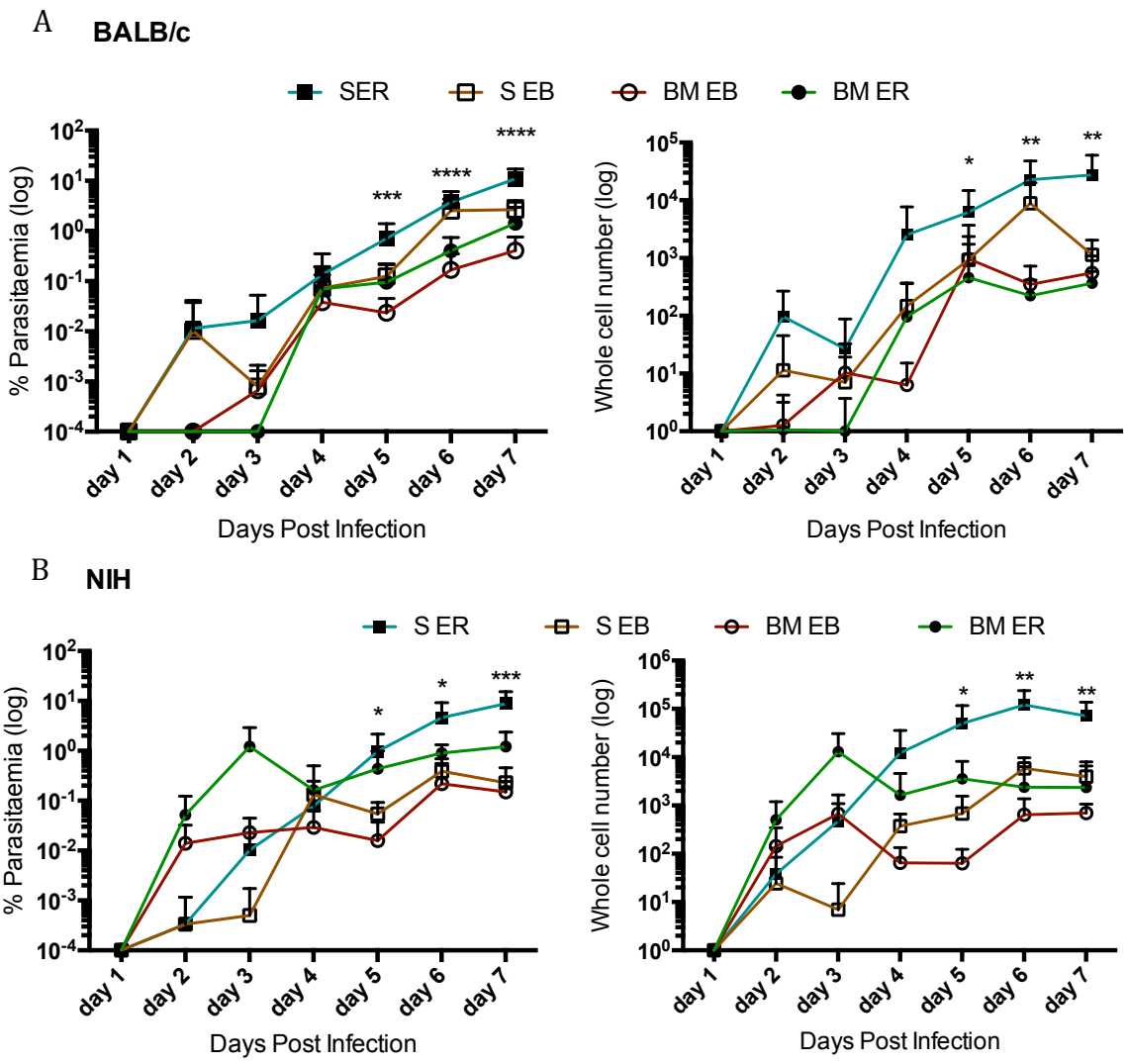

Figure 4.8 Parasitaemia and parasite burden of tissue resident erythroid cells across a 7 day infection. Left graphs show parasitaemia; Right graphs show whole cell numbers of parasites for **A.** BALB/ c mice. All time points n=9; day 7 n=8. There is a significant difference between the erythroid groups in terms of both percentage parasitaemia and parasite whole cell numbers from day 5 pi. **B.** NIH mice. All time points n =6. There is a significant parasite burden between the erythoid groups from day 5 pi. Mean values at each time point were compared using a one way ANOVA without multiple comparisons and significant differences between groups or samples are indicated with asterisks, denoting as follows: * $p < 0.05$, ** $p < 0.01$, *** $p < 0.001$, **** $p < 0.0001$. S ER; splenic early reticulocytes. S EB; splenic erythroblasts. BM ER; bone marrow early reticulocytes. BM EB; bone marrow erythroblasts. Error bars ± SD.

4.2.5 Gametocyte Enrichment in Splenic Early Reticulocytes Transcends Host Genetics

The relative enrichment of gametocytes within the individual tissue resident erythroid populations was investigated during a simulated natural infection (Figure 4.6A). Gametocytaemia was calculated as the percentage of RFP^+ cells in the total GFP^+ cell population, therefore gametocyte enrichment was normalised for varying parasite burden. This analysis revealed a difference in gametocytaemia between the two early reticulocyte populations, where splenic early reticulocytes were significantly enriched for gametocytes on day 5 and day 7 pi in both host backgrounds (BALB/c * $p = 0.0113$ and * $p = 0.0370$, respectively. NIH *** $p = 0.0004$ and * $p = 0.018$, respectively. Paired t test). Furthermore, as speculated in the previous results chapter, this population was significantly enriched for gametocytes compared with peripheral blood from as early as day 5 pi (Figure 4.9). The relative fold increase in the gametocytaemia of the splenic early reticulocyte population compared with peripheral blood was calculated for each individual mouse on days 5,6 and 7 pi (Figure 4.9). From this, the ratio of gametocytaemia for peripheral blood and splenic early reticulocytes was calculated as 1:11, 1:17 and 1:16 (BALB/c mice) on days 5, 6, and 7 pi, respectively and 1:4, 1:8 (NIH) on days 6 and 7 pi, respectively. BALB/c and NIH mice both displayed similar enrichment of gametocytes in early splenic reticulocytes compared with peripheral blood.

A. BALB/c

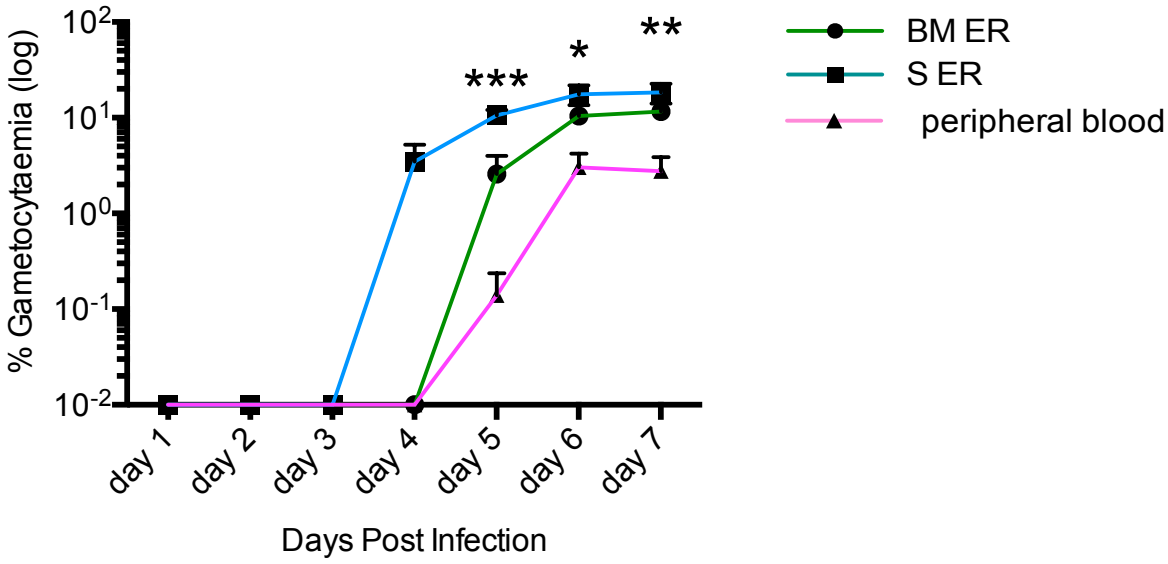
% Gametocytaemia (log)
10^2
10^1
10^0
10^{-1}
10^{-2}
***
*
**
day 1
day 2
day 3
day 4
day 5
day 6
day 7
Days Post Infection
BM ER
S ER
peripheral blood

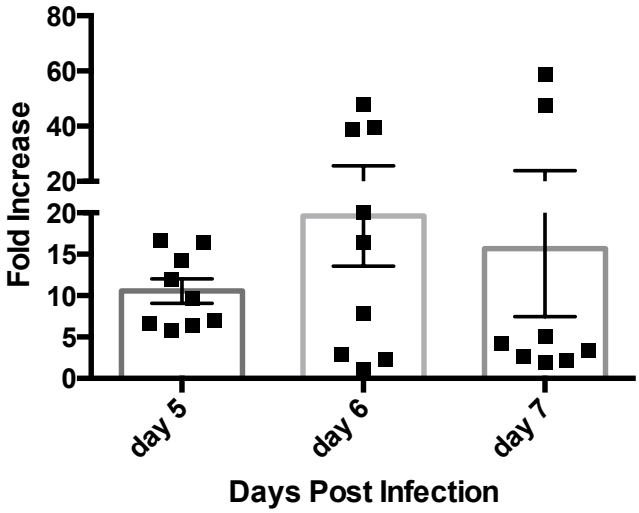
Fold Increase
80
60
40
20
20
15
10
5
0
day 5
day 6
day 7
Days Post Infection

B. NIH

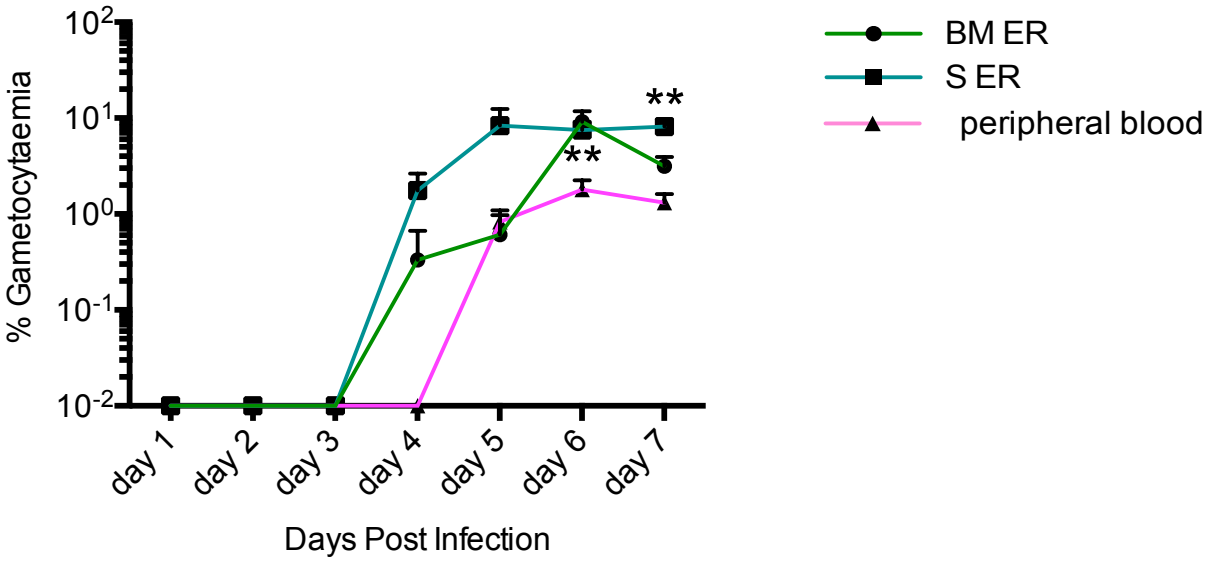
% Gametocytaemia
10^2
10^1
10^0
10^{-1}
10^{-2}
**
**
day 1
day 2
day 3
day 4
day 5
day 6
day 7
Days Post Infection
BM ER
S ER
peripheral blood

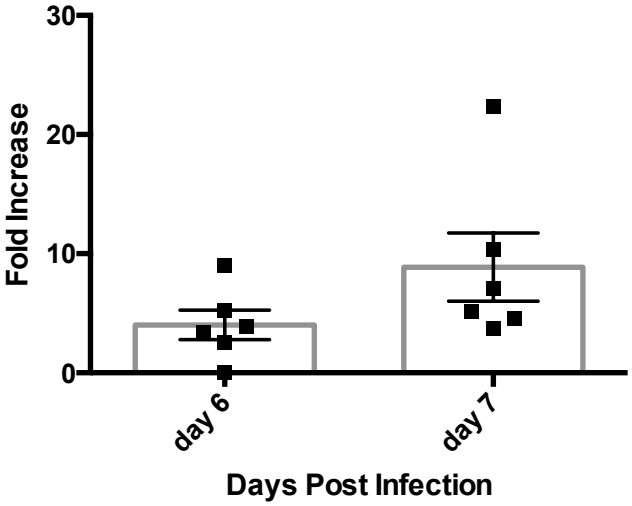
30
20
10
0
Fold Increase
day 6
day 7
Days Post Infection

C

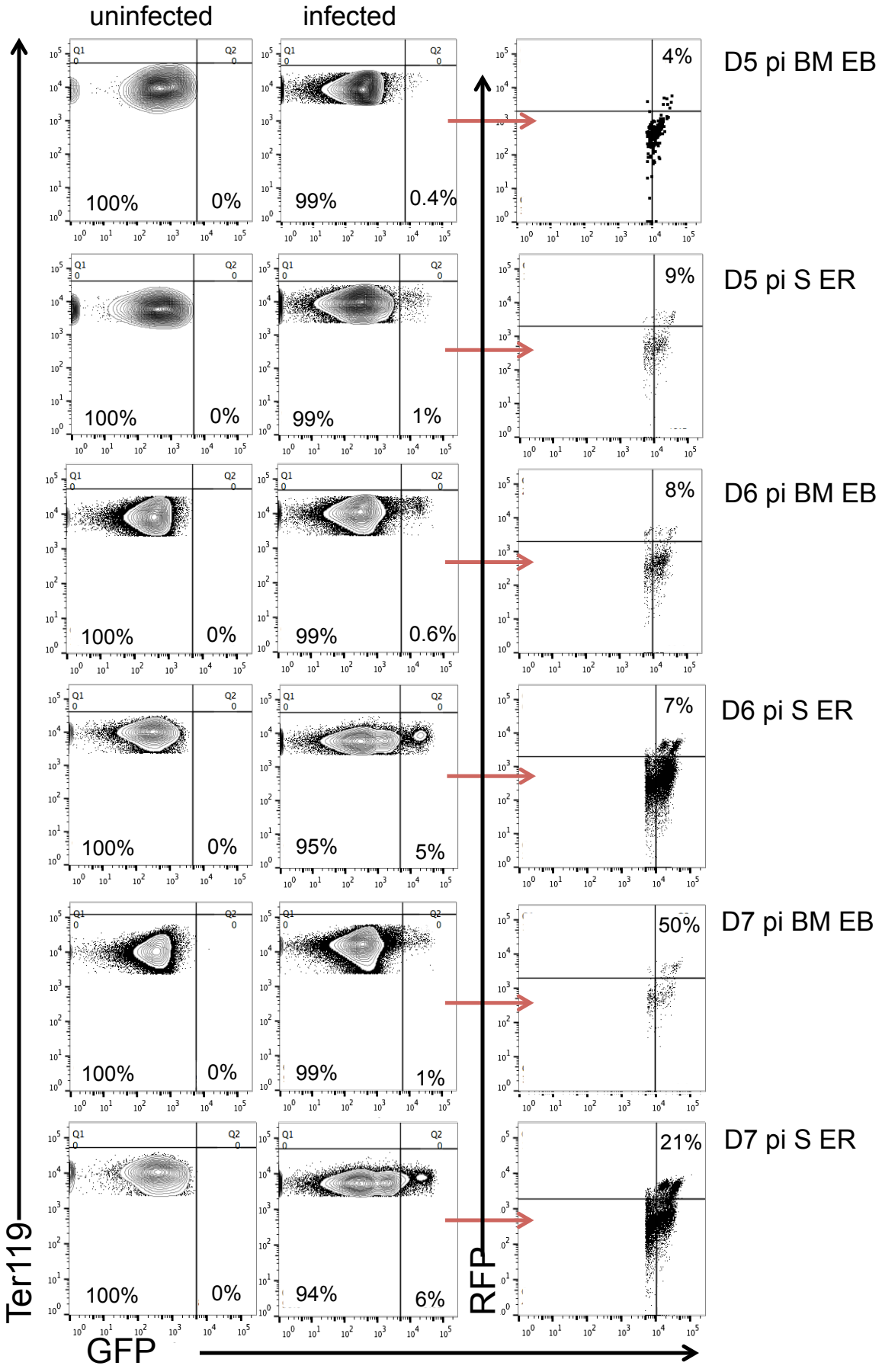
uninfected
infected
D5 pi BM EB
D5 pi S ER
D6 pi BM EB
D6 pi S ER
D7 pi BM EB
D7 pi S ER
100%
0%
99%
0.4%
4%
100%
0%
99%
1%
9%
100%
0%
99%
0.6%
8%
100%
0%
95%
5%
7%
100%
0%
99%
1%
50%
100%
0%
94%
6%
21%
Ter119
GFP
RFP

Figure 4.9 Gametocytaemia of early reticulocytes and peripheral blood across a 7 day infection. A. BALB/ c mice. Gametocytaemia was significantly higher within splenic early reticulocytes compared to the peripheral blood from day 5 pi. All time points n=9; day 7 n=8. **B.** NIH mice. Gametocytaemia was significantly higher within splenic early reticulocytes compared to the peripheral blood from day 6 pi. All time points n =6. Significant differences between splenic early reticulocytes and peripheral blood samples are indicated with asterisks, denoting as follows: * $p < 0.05$, ** $p < 0.01$. Significance values were generated from a one way ANOVA comparing the means of the tissue groups to the mean of the peripheral blood. BM ER; bone marrow early reticulocytes. S ER; splenic early reticulocytes. Error bars ± SD. **C**. Representative FACS plots showing $CD45^{-/low}$, $CD11b^{-}$, $Ter119^{+}$ cells from the populations with the highest gametocyteamia (splenic early reticulocytes; S ER) and the lowest gametocyteamia (bone marrow erythroblasts; BM EB). Cells where gated as either erythroblasts or early reticulocytes (see Figure 3.4), then gated as GFP^{+}, the GFP^{+} cells where then gated RFP vs GFP. Plots are from day 5 post infection (D5 pi) to day 7 post infection (D7 pi).

4.2.6 Erythroblasts are not a Niche for Consistent Gametocytogenesis

There was no significant difference in gametocytaemia between splenic and bone marrow erythroblasts on any day pi. Moreover, there was no significant difference between the gametocyte enrichment of erythroblasts of either organ and the peripheral blood at any time point. This reflects the high variability in erythroblast gametocytaemia between individuals and in relation to the infection of other erythroid populations. For example, within one independent experimental repeat (n=3) gametocytaemia was measured as 18% ± 22% (SD) (range 44% - 0%) within BALB/c splenic erythroblasts on day 7 pi (Appendix 8.2.8).

4.2.7 The Spleen Contains the Highest Gametocyte and Asexual Burden

Next, the tissue resident erythroid populations that contained the majority of the gametocyte burden was examined (Figure 4.10) (workflow depicted in Figure 4.6A).

A. BALB/c

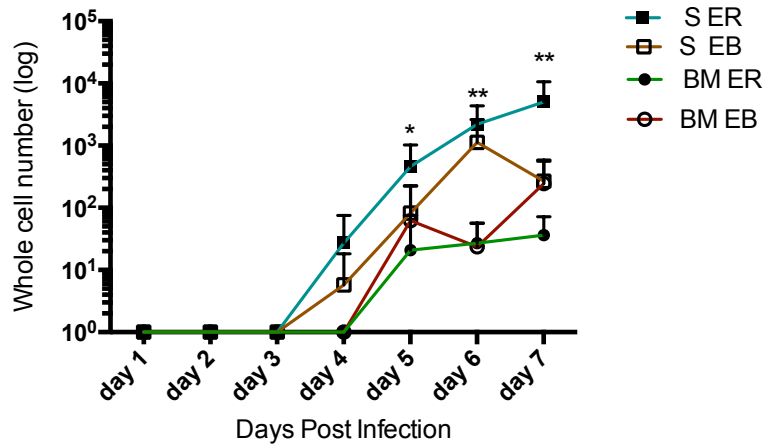

B. NIH

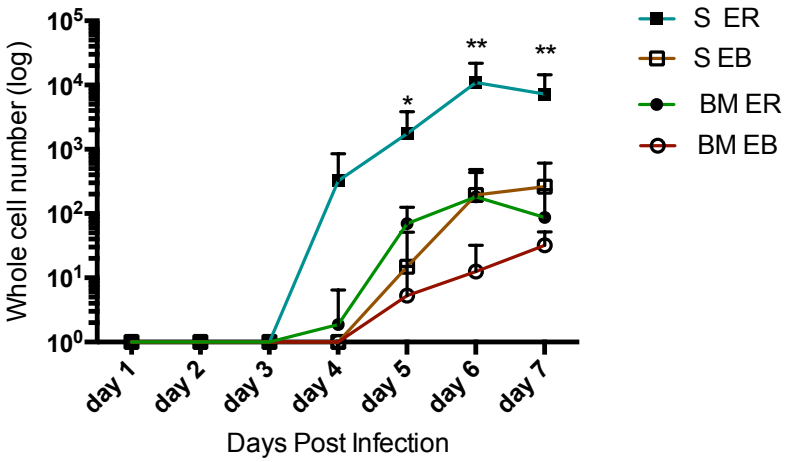

Figure 4.10 Gametocyte numbers in erythroblasts and early reticulocytes across a 7 day infection. A. BALB/ c mice. All time points n=9; day 7 n=8. **B.** NIH mice. All time points n =6. Both mouse backgrounds had a significantly higher number of gametocytes within the splenic early reticulocytes compared with all over groups from day 5 pi. Significant differences between groups are indicated with asterisks, denoting as follows: * $p < 0.05$, ** $p < 0.01$. Significance values were generated from a one way ANOVA comparing all groups. S ER; splenic early reticulocytes. S EB; splenic erythroblasts. BM ER; bone marrow early reticulocytes. BM EB; bone marrow erythroblasts. Error bars ± SD.

The $PbGFP_{CON}/RFP_{GAM}$ parasite line also allowed for the accurate quantification of the burden of asexual parasites (GFP^{+} RFP^{-}) within the tissue resident populations (Figure 4.11).

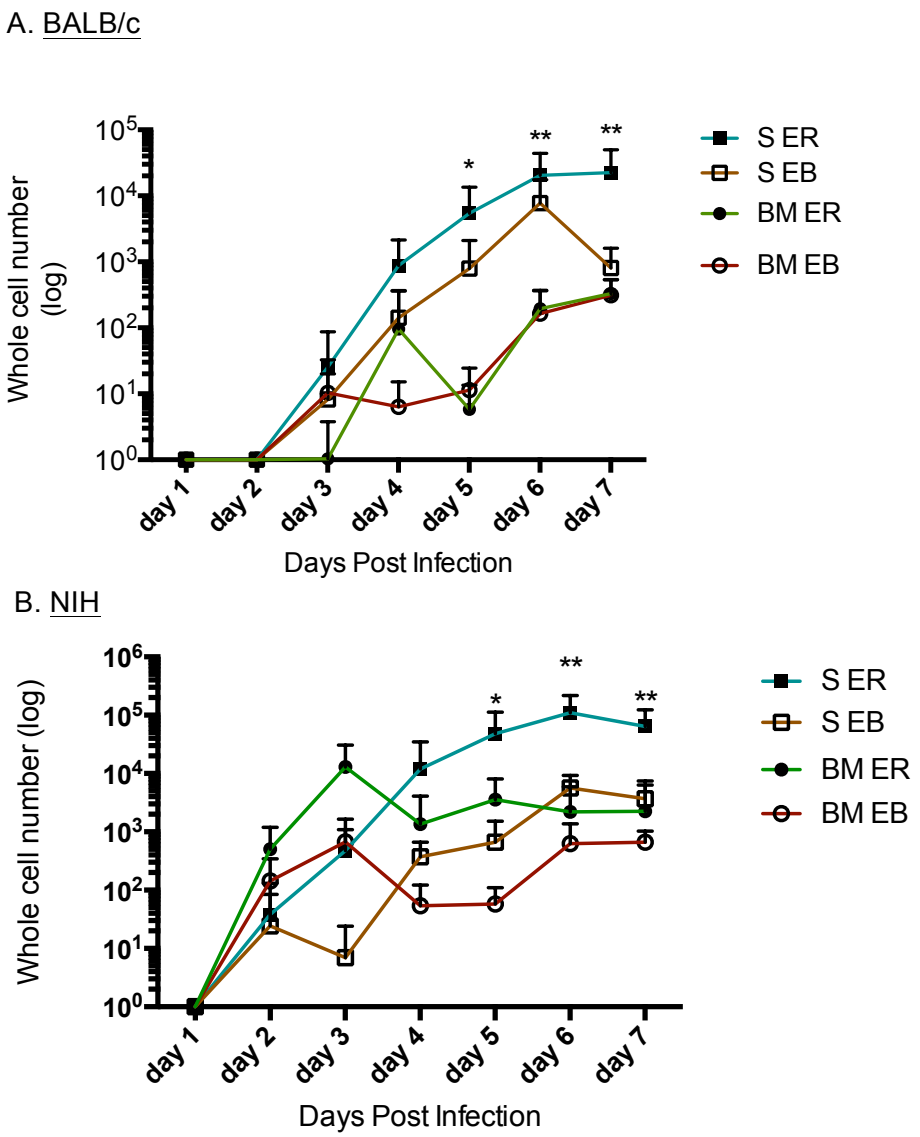

Figure 4.11 Asexual parasite numbers in of erythroblasts and early reticulocytes across a 7 day infection. A. BALB/c mice. All time points n=9; day 7 n=8. **B.** NIH mice. All time points n =6. Both mouse backgrounds had a significantly higher number of asexual parasites within the splenic early reticulocytes compared to all over groups from day 5 pi. Significant differences between groups are indicated with an asterisk (* $p < 0.05$). Significance values were generated from a one way ANOVA comparing all groups. S ER; splenic early reticulocytes. S EB; splenic erythroblasts. BM ER; bone marrow early reticulocytes. BM EB; bone marrow erythroblasts. Error bars ± SD.

There is a significant difference from day 5 pi in the number of asexual and sexual parasites observed within the four tissue resident populations, with the splenic tissue resident populations (SER and SEB) containing the greatest number of both types of parasites (Figure 4.10 & Figure 4.11). Interestingly, within the splenic populations the early reticulocytes contained sexual parasites compared to the splenic erythroblasts from day 5 pi within the NIH mice (Paired t test. d5 pi $p = 0.001$, d pi $p = 0.04$, d7 pi $p = 0.04$) and the BALB/c mice (Paired t test. d5 pi $p = 0.03$, d pi $p = 0.04$, d7 pi $p = 0.03$).

4.2.8 Variation in the Size of Bone Marrow and Splenic Early Reticulocytes

Whilst the splenic and bone marrow pools of early reticulocytes in NIH mice were quantifiably the same size, in BALB/c mice they were significantly different (Figure 4.12). Therefore, despite the host genetic background, the greatest sexual and asexual parasite burden was consistently observable within the splenic early reticulocytes compared with all other tissue resident cells.

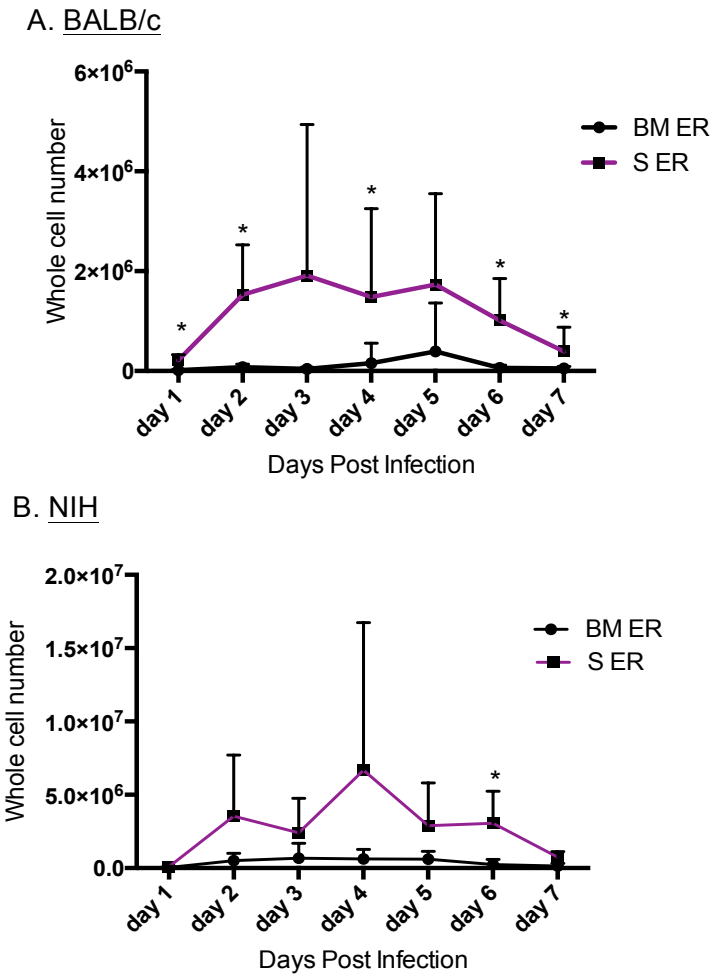

Figure 4.12 Whole cell numbers of bone marrow and splenic early reticulocytes across a 7 day infection. A. BALB/ c mice. All time points n=9; day 7 n=8. Significant differences in numbers bone marrow and splenic early reticulocytes were observed, except at days 3 and 5 ($p = 0.06$ and $p = 0.07$, respectively) **B.** NIH mice. All time points n =6. At all time points erythroblast and early reticulocyte populations are not significantly different. Statistical analysis at each time point was performed using an unpaired t test and significant differences are indicated with asterisks, denoting as follows: * $p < 0.05$. BM ER; bone marrow early reticulocytes. S ER; splenic early reticulocytes. Error bars ± SD.

4.2.9 Splenic Early Reticulocytes and Peripheral Blood Contain Similar Numbers of Gametocytes

A higher proportion of splenic early reticulocytes contain gametocytes than any other erythroid population within the body from day 5 pi (Figure 4.9). This population also contains the greatest number of gametocytes within the tissue resident infection from day 5 pi (Figure 4.10). However, the relevance of splenic early reticulocyte gametocytes to parasite transmission remains unclear. Therefore, the total number of gametocytes in the peripheral blood was compared with the total number of gametocytes in splenic early reticulocytes (Figure 4.13). Proportionally, there was a trend for preferential gametocyte location towards the peripheral blood as the infection progressed. This trend was exhibited in both mice strains (Figure 4.14). This could possibly suggest that gametocytes are initially formed within the tissue resident erythroid population before migrating into and accumulating within the peripheral blood. However, due to the dynamics of the promoter controlling *rfp* expression it is not possible to conclude whether the gametocytes within the tissue resident population are early gametocytes which would then go on to populate the peripheral blood as mature gametocytes.

A

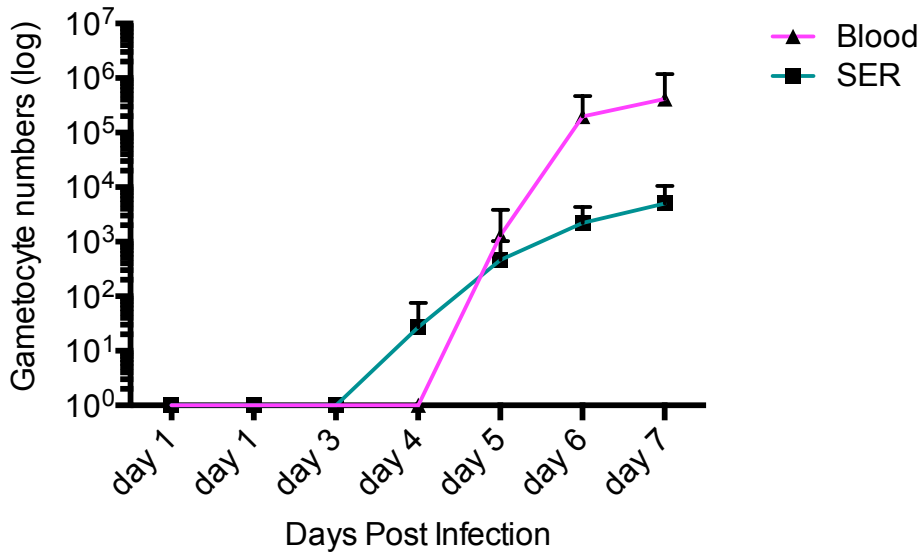

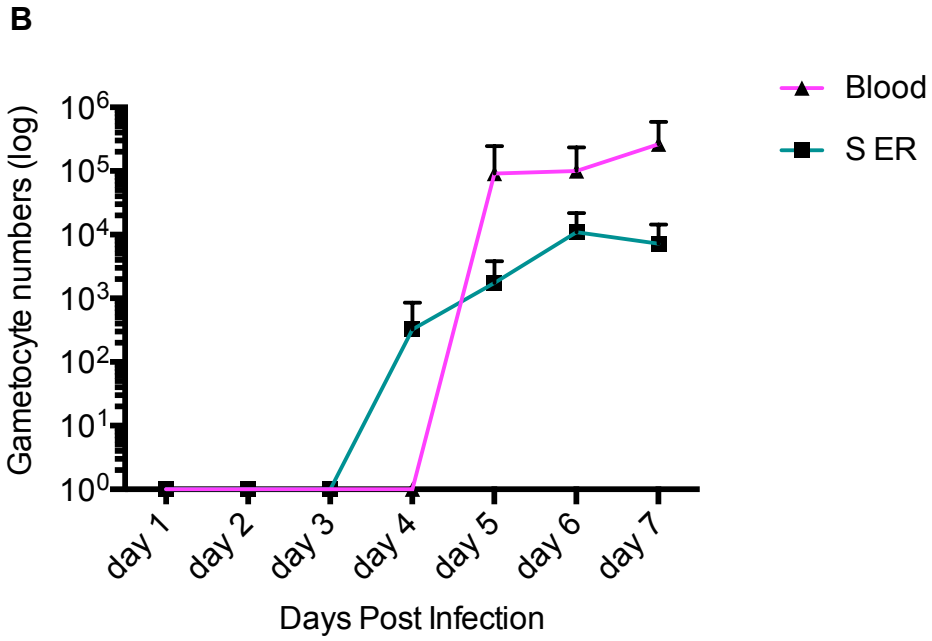

Figure 4.13 Gametocyte numbers in the peripheral blood and splenic early reticulocytes across a seven day infection. A. BALB/ c mice. All time points n=9; day 7 n=8. **B.** NIH mice. All time points n =6. Statistical analysis was performed using a one way ANOVA comparison. Error bars ± SD.

A. BALB/c

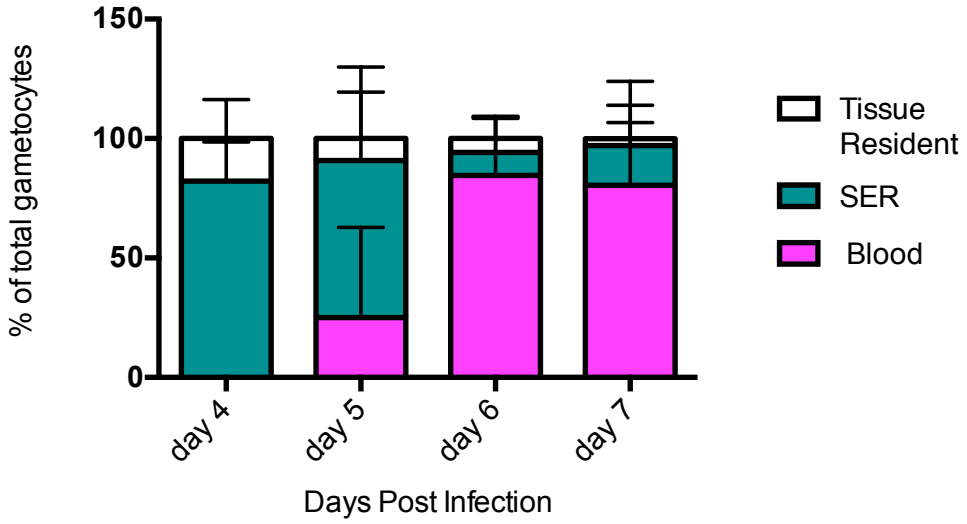

B. NIH

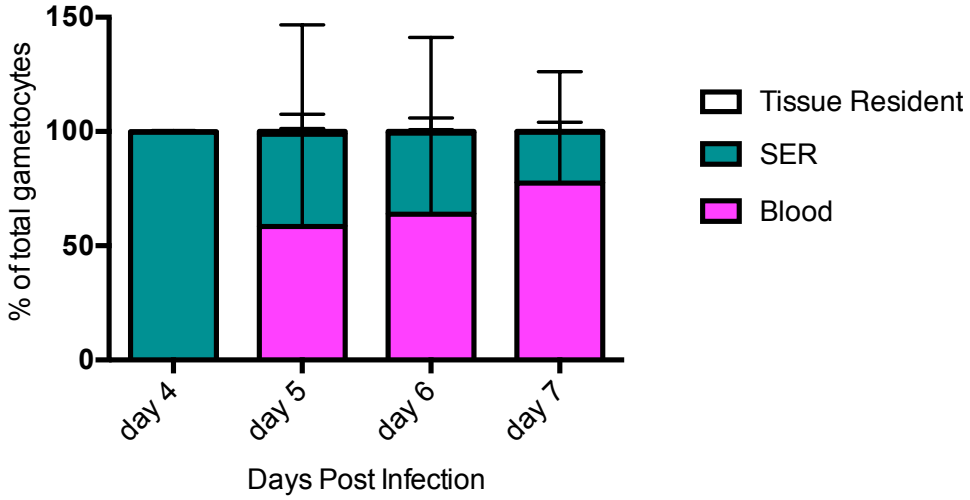

Figure 4.14 Proportion of total gametocytes in the peripheral blood and splenic early reticulocytes A. BALB/ c mice. All time points n=9; day 7 n=8. **B.** NIH mice. All time points n =6. Error bars ± SD. SER; splenic early reticulocytes. Tissue resident population is the combined number of parasites in the bone marrow early reticulocytes, erythroblasts and splenic erythroblasts.

4.2.10 Invasion of Splenic Early Reticulocytes

The suggestion that splenic early reticulocytes are the tissue resident erythroid stage for preferential *P. berghei* invasion and gametocyte formation was tested experimentally (workflow depicted in Figure 4.6A).

The *P. berghei* asexual life cycle is 22 – 24 hrs. In an asynchronous infection schizogony occurs for the majority of asexual parasites in the peripheral blood population at 12-7 am. In this study, samples were taken from the bone marrow, spleen and peripheral blood at 24 hr intervals at 9 am when the majority of asexual parasite forms were rings and early trophozoites in the peripheral blood. It takes 36 hrs for the most immature erythroblasts to mature into early reticulocytes (Chen *et al.*, 2009). Therefore, if the temporal dynamics of asexual

maturation in tissue resident erythroid cells is reflective of the 22-24 hrs life cycle in the peripheral blood, all asexual parasites will have undergone egress from immature erythroblasts before reaching the early reticulocyte compartment. It takes 20 hrs for the intermediate erythroblasts to mature into early reticulocytes (Chen *et al.*, 2009). Under normal maturation dynamics, a ring stage parasite in an intermediate or mature erythroblast would have developed and undergone egress within 24 hrs. As such, parasites observed in the erythroblast population at any given time point of this experiment would have not contributed to the early reticulocyte population at the ensuing time point.

Nonetheless, there is no evidence that *P. berghei* parasites develop at the same rate or undergo the same synchronicity as observed in the peripheral blood. Therefore, the combined total number of $GFP^{+}RFP^{-}$ parasites in the intermediate and mature splenic erythroblasts at each 24 hr time point was calculated. The percentage contribution this total made to the quantified parasite burden in the splenic early reticulocytes at each ensuing time point was determined. Here <13% of the parasites observed within splenic early reticulocytes could be the result of an invasion event occurring within a splenic erythroblast population (Figure 4.15).

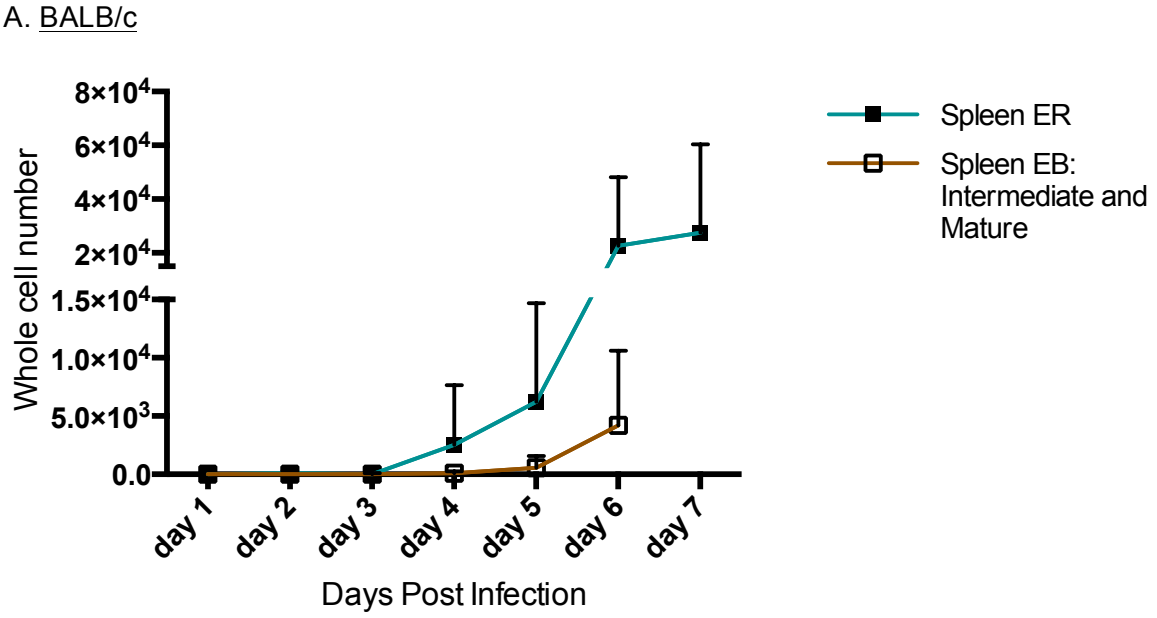

B. NIH

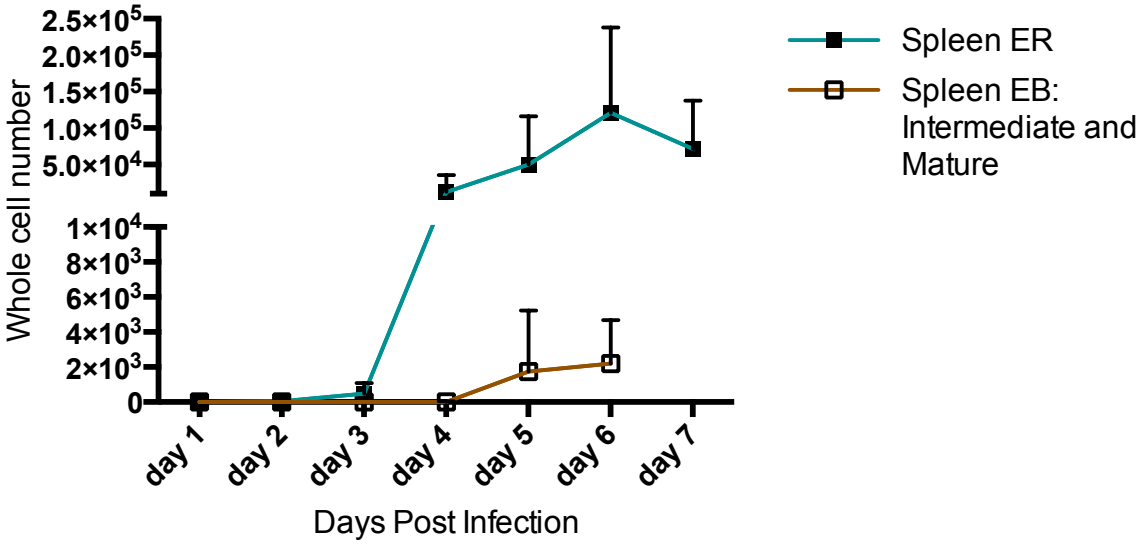

Figure 4.15 Percentage contribution of splenic EB parasites to the splenic ER parasite population 24 hours later. Plotted on the graph are the mean ± SD whole cell numbers of GFP^+RFP^- splenic early reticulocytes (ER) and the mean ± SD whole cells numbers of GFP^+RFP^- splenic intermediate and mature erythroblasts (EB)**.** Tables show the percentage contribution the parasitised splenic intermediate and mature erythroblasts make to the parasitised splenic early reticulocytes population at the ensuing time point ± SD. **A**. BALB/c mice. All time points n=9; day 7 n=8. **B**. NIH mice. All time points n=6.

Days pi	Contribution of EB to ER parasites % (± SD)
Day2	0
Day3	0
Day4	0
Day5	9.92 ±14
Day6	0.8 ± 0.8
Day7	5.81 ± 5

Gametocyte maturation of *P. berghei* takes 26-27 hrs and the gametocytes are stable for a further 10-11 hrs. Therefore gametocytes within the intermediate or mature splenic erythroblast population at any given time point, could contribute to the gametocyte population in the splenic early reticulocytes at the ensuing 24 hr time point. I calculated the percentage contribution the total number of RFP^+ gametocytes in the intermediate and mature erythroblasts made to the gametocyte burden in the early reticulocytes at each ensuing time point (Figure 4.16). Here <25 % of the gametocytes observed within splenic early reticulocytes could be the result of an invasion and gametocyte conversion event occurring within a splenic erythroblast population. Therefore the majority of gametocytes observed within early reticulocytes were formed within this erythroid population and not the preceding erythroblast population.

A. BALB/c

Days pi	Contribution of EB to ER gametocytes % (± SD)
Day2	0
Day3	0
Day4	0
Day5	0.8 ± 2.3
Day6	1.6 ± 2.6
Day7	25 ± 24

B. NIH

Days pi	Contribution of EB to ER gametocytes % (± SD)
Day2	0
Day3	0
Day4	0
Day5	0
Day6	0.6 ± 0.1
Day7	10 ± 19

Figure 4.16. Percentage contribution of splenic EB gametocytes to the splenic ER gametocyte population 24 hours later. Tables show the percentage contribution the RFP^+ splenic intermediate and mature erythroblasts make to the RFP^+ splenic early reticulocytes population at the ensuing time point ± SD. **A**. BALB/c mice. All time points n=9; day 7 n=8. **B**. NIH mice. All time points n=6.

4.2.11 Invasion of Bone Marrow Early Reticulocytes

The bone marrow early reticulocyte and erythroblast data generated from the time course did not mirror the splenic data discussed above. The parasitised (GFP^+) erythroblast population in the bone marrow was equal or greater than the parasitised early reticulocyte population at the ensuing time point (Appendix 8.2.9) and on each corresponding day (Figure 4.11: BALB/c all time points NS. NIH all time points NS). Nonetheless, as the gametocytaemia (GFP^+RFP^+) in the erythroblast population was less than the gametocytaemia of early reticulocyte population at the ensuing time point, it likely that the early reticulocytes are the site of preferential gametocyte formation in the bone marrow (Appendix 8.2.10). Therefore, although it is difficult to conclude as to the dynamic of bone marrow erythroid invasion and development, it would seem that the early reticulocytes universally provide a niche for gametocyte formation within tissue resident erythroid cells.

Together the data in this chapter suggests that splenic early reticulocytes are the tissue resident erythroid population preferentially invaded by *P. berghei* and that subsequently these cells selectively promote gametocyte formation.

In this chapter I successfully:

- Developed a parasite line that can distinguish male and female gametocytes from asexual parasites at >8-12 hrs post invasion.
- Identified that splenic early reticulocytes have the highest gametocytaemia in the host.
- Identified that *P. berghei* preferentially invades splenic early reticulocytes and not the preceding erythroblast population.
- Identified that *P. berghei* gametocytes preferentially form within early reticulocytes and not the preceding erythroblast population.

4.3 Discussion

The key discussion points are:

- The development of the $PbGFP_{CON}/RFP_{GAM}$ reporter line for young gametocytes.
- The preferential invasion by *P. berghei* of early reticulocytes within the spleen may be due to the stress regulation of the splenic erythroblasts.
- The preferential invasion of splenic early reticulocytes compared to all other tissue resident erythroid population may be due to accessibility.
- Early reticulocytes may be the "Goldilocks" niche for gametocyte conversion.

4.3.1 Generating the Gametocyte Reporter Line

In the previous chapter, I established that *P. berghei* parasitises erythroblasts and early reticulocytes to different degrees both within an organ and between organs on day 7 pi. As these parasitised cells could establish an infection in naïve mice, a percentage of erythroblasts and early reticulocytes must contain asexual cells. In this chapter, I wanted to quantify the gametocyte burden of these tissue resident cells. In order to achieve this aim I constructed a parasite line that allowed me to identify gametocytes from an early developmental stage. Moreover, in successfully generating $PbGFP_{CON}/RFP_{GAM}$ I have created a tool that easily revolves sexual parasites from asexual parasites, whilst at the same time defining gender specific populations. To our knowledge, this parasite line offers gender discrimination at the earliest developmental time point available in the *P. berghei*.

4.3.2 *P. berghei* Preferentially Invades Early Reticulocytes Compared with Erythroblasts in the Spleen, a Dynamic Not Mirrored in the Bone Marrow

In the previous chapter, GFP MFI was used to infer the life stage of parasites within early reticulocytes and erythroblasts at a single time point. Through inferring that both tissue resident populations contained parasites at the same maturation stage, it was suggested that the parasites observed in early

reticulocytes on day 7 pi were not a result of invasion events within erythroblasts on day 6 pi. As such, it was postulated that *P. berghei* preferentially invades early reticulocytes in both tissues. Here, this assertion was numerically justified for the splenic erythroid populations, but not the bone marrow, with data derived from 24 hr time intervals across a 7 day infection. The random sampling of mice in two (NIH) or three (BALB/c) independent experiments generated reproducible data with regard to the proportions of parasitaemia and gametocytaemia between the splenic early reticulocytes and other erythroid compartments.

4.3.3 Parasite Preference due to Host Cell Metabolism

P. berghei has a characterised tropism for stage III- IV reticulocytes within peripheral blood. There is evidence that such tropism benefits the parasite through access to the greater metabolic capabilities of the circulating reticulocyte compared with the erythrocyte (Srivastava *et al.*, 2015). A recent preliminary screen comparing the metabolomics of reticulocytes (stage I-IV) extracted from human cord blood revealed a continual decrease in metabolite concentrations during reticulocyte maturation to erythrocytes (Malleret *et al.*, 2013). These data indicate that tissue resident reticulocytes are more nutrient rich than the erythroid cells in circulation. Nonetheless, the results of a transcriptional comparison between polychromatic and orthochromatic erythroblasts suggest that earlier erythroid stages are even more metabolically active than reticulocytes and mature RBC (Tamez *et al.*, 2011). As such, parasitising erythroblasts might be comparatively more beneficial for parasite growth. While this might explain the invasion dynamics implied by the bone marrow data, it does not explain the observed preference of *P. berghei* for splenic reticulocytes over splenic erythroblasts.

4.3.4 Physical Accessibility of Early Reticulocytes and Erythroblasts

It should be acknowledged that the architecture of the erythropoetic tissue in the spleen and the bone marrow are different. As such, physical accessibility to the different maturation stages of erythroid cells may be an influencing factor for the difference in parasite selectivity for early reticulocytes between the two tissues. However, there is evidence that erythroid maturation correlates with peri-sinusoidal localisation in the bone marrow; with the most mature cells

being closer to the sinus endothelium (Yokoyama *et al.*, 2003). Therefore, parasites (free merozoites or schizont infected erythrocytes) migrating into the bone marrow would have disproportionate access to early reticulocytes compared with erythroblasts. In contrast, studies observing erythroblast islands within the human and mouse spleen have not commented on the spatial arrangement of maturing tissue resident erythroid cells (Palitzsch *et al.*, 1987; Deiwick, 1992). However, when taking into consideration that the endothelium-free, open circulation within the splenic red pulp would not differentially restrain parasite access to erythroblasts versus reticulocytes, it seems unlikely that physical accessibility is a driving factor for the different erythroid cell selectivity observed between the two tissues.

4.3.5 Erythroblast Apoptosis and the Parasite's Preference in the Spleen for Early Reticulocytes

It has been demonstrated that *Plasmodium*-infected erythroblasts can present parasite derived peptides via MHC class I, stimulating a $CD8^+$ cytotoxic T cell response (Imai *et al.*, 2013). Moreover, this interaction stimulates apoptosis of the erythroblast via the Fas pathway (Imai *et al.*, 2015a). Apoptosis pathways result in the fragmentation of DNA and the permeabilisation of the mitochondria. During reticulocyte maturation the cell undergoes mitochondrial disruption, nonetheless, this event is not accompanied by cell death as the apoptotic machinery is also undergoing degradation (Koury *et al.*, 2005). Moreover, reticulocytes do not display Fas (Liu *et al.*, 2006). Although reticulocytes do display MHC class I, it is down regulated during maturation (Carayon *et al.*, 2011; Imai *et al.*, 2013; Martín-Jaular *et al.*, 2016). As such, the preference of *P. berghei* for splenic early reticulocytes over splenic erythroblasts may stem from the continued expression by the latter of proteins involved in apoptosis and immune surveillance pathways. Nonetheless, as the data implies that *P. berghei* does not preferentially invade an erythroid age class within the bone marrow, it might be the case that a significant proportion of *P. berghei* parasites invade splenic erythroblasts but were not observed in this work due to immune regulatory driven apoptotic events occurring to a greater extent in the spleen than in the bone marrow prior to sampling. Although, it should be noted that there is no evidence of difference in erythroblast driven immune responses between the two tissues (Imai *et al.*, 2013).

On the other hand, the homeostatic regulation of splenic and bone marrow derived erythroblasts is well documented to be different. During basal conditions the splenic erythroblasts and erythroid progenitors undergo a higher rate of apoptosis compared with the corresponding populations in the bone marrow (Liu *et al.*, 2006; Varricchio *et al.*, 2012). Moreover, during erythropoetic stress responses the cell surface apoptotic markers Fas and FasL are down-regulated to a greater extent by the splenic erythroblasts than the bone marrow erythroblasts (Liu *et al.*, 2006). Consequently, splenic erythroblasts inhabit a distinctively different niche to bone marrow erythroblasts *in vivo*. This might be a factor fuelling the parasite's preferential tropism for early reticulocytes in one tissue and not the other, although how factors involved in regulating the host's stress erythropoetic influence parasite selectivity remains to be investigated.

4.3.6 Parasites Preferentially Invade Splenic Early Reticulocytes Compared to those in the Bone Marrow

Within this work I observed that *P. berghei* preferentially invades splenic early reticulocytes compared with all other tissue resident erythroid populations. Although variation in erythroblast regulation may influence the difference in the parasites selectivity for erythroid age classes within the two tissues, there is no evidence that splenic early reticulocytes and bone marrow early reticulocytes are different. As such, in order to explain the parasite's preference for early reticulocytes in spleen versus bone marrow, the accessibility of the two erythropoietic tissues, due to the different anatomical structure of the organs, should be taken in account again (Steiniger, Bette and Schwarzbach, 2011; Itkin *et al.*, 2016). As mentioned above, the blood in the murine spleen empties into the red pulp where it drains through the splenic cords before re-entering the closed circulation. In contrast, the tissue of the bone marrow and the cells within the vasculature are separated by endothelium (Steiniger, Bette and Schwarzbach, 2011; Itkin *et al.*, 2016). Therefore, it is possible that the parasite preferentially invades splenic reticulocytes *in vivo* due to the relative ease of access. Nonetheless, it should be taken into account that the perisinusoidal niche of erythropoiesis in the bone marrow is a high reactive oxygen species (ROS) environment, whereas the splenic cords are an acidotic and hypoxic

environment (Steiniger, Bette and Schwarzbach, 2011; Itkin *et al.*, 2016). Although early reticulocytes are enucleated they retain a residual mitochondrial metabolism and an active TCA cycle (Malleret *et al.*, 2013; Srivastava *et al.*, 2015, 2016), however, the environmental differences between the two niches implies that the metabolism of the splenic early reticulocytes may be more dependent on glycolysis then the bone marrow early reticulocytes. Nonetheless, the features of the cell's metabolism driving parasite selectivity remain to be investigated.

4.3.7 Preferential Gametocyte Formation in Early Reticulocytes Compared to Erythroblasts

In this chapter, I combined the newly generated parasite line with our previously described flow based approach and observed that the highest gametocytaemia within each tissue was detectable within the early reticulocyte population. Sampling every 24 hrs allowed me to determine that the majority of these gametocytes had undergone invasion and subsequent commitment within the early reticulocyte and not the preceding erythroblast population in both tissues. Moreover, the highest gametocyteamia within the host was observable within splenic early reticulocytes. Considering that the spleen is an interface for the circulatory and immune systems, and that mature asexual stages of *P. berghei* display defined parasite-derived proteins, it is likely that the clearance of asexually parasitised early reticulocytes is greater in relation to gametocytes (Engwerda, Beattie and Amante, 2005; Imai *et al.*, 2013, 2015b). Although it should be noted that antibodies in the plasma of malaria patients have indicated the existence and immune recognition of gametocyte specific antigens (Dinko et al., 2012; Saeed et al., 2008). Based solely on proportional data, it could be argued that the splenic early reticulocytes may seem to have the highest gametocyte enrichment due to the relatively higher clearance of asexual parasites. However, in this work I also quantified the tissue resident erythroid population containing the highest asexual and total parasite burdens as the splenic early reticulocytes. Taken together these data suggested that a relatively elevated clearance of asexual parasitised early reticulocytes does not occur, and therefore cannot explain the selective enrichment of gametocytes

within this population. Splenic early reticulocytes therefore represent the tissue resident population where preferential gametocyte formation occurs.

The transcription factor AP2G has been identified as the master regulator for initiating *Plasmodium* gametocytogenesis (Sinha *et al.*, 2014). Downstream events during gametocytogenesis are accompanied by a shift in parasite metabolism away from rapid fermentation glycolysis towards the more efficient TCA cycle and oxidative phosphorylation. This metabolic transition is associated with development within a relatively nutrient deprived environment (MacRae *et al.*, 2013; Salcedo-Sora *et al.*, 2014; Srivastava *et al.*, 2016). It has recently been demonstrated that *ap2g* is regulated in a similar manner to *var* genes, with gametocyte commitment being plastic up to the trophozoite stage (Dr Robyn Kent. unpublished;(Brancucci *et al.*, 2014; Coleman *et al.*, 2014). It would therefore be tempting to theorise that the host cell's metabolic profile influences signaling pathways upstream of *ap2g* transcription within newly invaded merozoites, promoting a parasite shift towards oxidative phosphorylation. However, studies have shown that cord blood derived early reticulocytes and circulating stage III-IV reticulocytes retain residual mitochondrial metabolism and an active TCA cycle and therefore have a more enriched metabolic profile than erythrocytes (Malleret *et al.*, 2013; Srivastava *et al.*, 2015, 2016). Therefore early reticulocytes provide a more metabolically enriched environment for the parasite then erythrocytes (Malleret *et al.*, 2013; Srivastava *et al.*, 2015, 2016). Nonetheless, it should be taken into account, as mentioned above, that the splenic early reticulocytes may have a more glycolytic based metabolism due to their local niche which is believed to be hypoxic, but this remains to be investigated. As such, the gametocyte stimulating factors provided by the host cell metabolism and immature status are yet to be directly studied.

4.3.8 Gametocytes in the Splenic Early Reticulocytes and the Peripheral Blood

The dynamics of the gametocyte-specific fluorescence proxy in the $PbGFP_{CON}/RFP_{GAM}$ parasite line was defined in this chapter with the RFP signal distinguishing gametocytes from 8 hpi. This parasite line was used in an

asynchronous infection to determine the gametocyte dynamics of tissue resident erythroid cells. The methodology used meant that the whole cell numbers of gametocytes in the peripheral blood could be quantified in tandem with the quantification of erythroid populations. Calculating the proportional distribution of total gametocytes within the host indicated that there was a trend for sexual cells to be formed in the tissue resident erythroid population prior to being observed within the peripheral blood. Nonetheless, the maturation stages of the gametocytes within either population could not be determined, therefore the biological relevance to transmission of gametocyte formation outwith the peripheral blood cannot be determined. This can be addressed by further work using a synchronised infection across 24 hrs. The workflow for this experiment would be as follows: a known amount of highly synchronised and purified schizonts in erythrocytes stained with anti-Ter119 IgG would be intravenously injected into mice in order to undergo merozoite egress and re-invasion. The fluorescent conjugated antibody will identify residual schizonts and mature gametocytes from the previous cycle. Samples of peripheral blood will be taken at 0 hpi and then at 8 hpi when the tissue of three mice will be harvested at random. The RFP^+ signal in the peripheral blood and the tissue resident erythroid cells will be quantified by flow cytometry of tissues sampled from mice at 12, 15 and 18 hpi. If the splenic early reticulocytes are the location of gametocyte formation in the host then it would be expected that at 8 hpi a greater number of RFP^+ cells will be observed within this population compared with the peripheral blood. As gametocyte maturation progresses it would be expected that the ratio of RFP^+ cells in the splenic early reticulocytes compared to the peripheral blood would skew positively in favour of the latter population. This would indicate that gametocytes leave the tissue and enter the peripheral blood. This point is important, as although the previous results chapter demonstrated that sorted parasitised early reticulocytes and erythroblasts were permissible to functional parasite development, it has yet to be shown that parasitised tissue resident erythroid cells can leave the tissue join the peripheral blood.

4.4 Summary

In this chapter I developed a parasite line that discriminates sexual cells from asexual parasites early in their development. I coupled this with our previously optimised flow based methodology and observed that *P. berghei* preferentially invades and preferentially forms gametocytes within splenic early reticulocytes compared to all other tissue resident erythroid populations.

5 Artemisinin Treatment Failure and Tissue Resident Erythroid Infection.

5.1 Introduction

The initial steps in evaluating the effectiveness of antimalarial drugs and novel antimalarial compounds are carried out *in vitro* with parasitised mature erythrocytes (Traore *et al.*, 2015). This directly reflects the dogma that effective malaria treatment correlates with the concentration of active drug within the blood stream (White, 2013). The data in the previous chapters of this thesis demonstrate that *P. berghei* can parasitise both nucleated and enucleated tissue resident erythroid cells of the bone marrow and the spleen. The infection dynamics described by this work may confound effective chemotherapy and represent a route for malaria recrudescence and generation of drug resistance. A recent study carried out on circulating erythroid cells linked the metabolic enrichment of the host cell to an increase in IC_{50} of antimalarials targeting the metabolic pathways of *Plasmodium* (Srivastava *et al.*, 2015). Studies have demonstrated that early reticulocytes and erythroblasts are more metabolically enriched than circulating erythroid cells (Tamez *et al.*, 2011; Malleret *et al.*, 2013; Srivastava *et al.*, 2015). It is therefore likely that the IC_{50} of a drug may be further increased in relation to parasitised tissue resident erythroid cells (Srivastava *et al.*, 2015).

Currently the WHO advocates ACTs as front line therapy against all species-specific malarias (WHO, 2015). ARTs are pro-drugs that are activated by the end products of parasite metabolism (Klonis, Creek and Tilley, 2013). There are emerging reports from the field documenting the treatment failures of both ARTs mono and worryingly even ACTs combined therapies due to the recrudescence of infection (Chang *et al.*, 2016).

In this chapter the $PbGFP_{CON}/RFP_{GAM}$ parasite line was combined with an established recrudescence assay in order to:

- Identify parasitised tissue resident erythroid cells that may fuel infection recrudescence after ART treatment.

- Investigate any effects ART has on the tissue resident erythroid cell populations.

5.2 Results

5.2.1 Parasitised Splenic Early Reticulocytes May be a Source of Infection Recrudescence

The Peters "4 day suppressive test" was used, as previously described, to ascertain recrudescence after treatment with ART (Figure 5.1) (Vega-Rodríguez *et al.*, 2015). ART doses ranged from 1 mg/kg through to previously reported curative doses (10-40 mg/kg) (Janse *et al.*, 1994; Vega-Rodríguez *et al.*, 2015) Mice infected with 10^6 $PbGFP_{CON}/RFP_{GAM}$ parasites on day 0 where treated with ART beginning 1 hpi, and daily until day 3 pi (Figure 5.2).

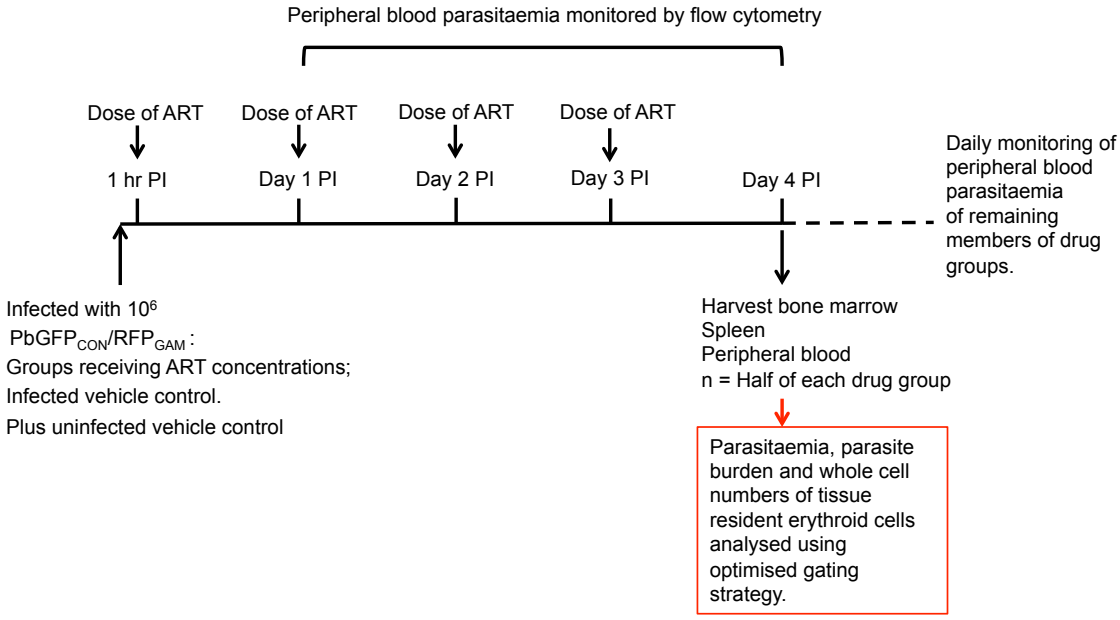

Figure 5.1. Work flow of the Peters 4 day suppressive test. PI; post infection.

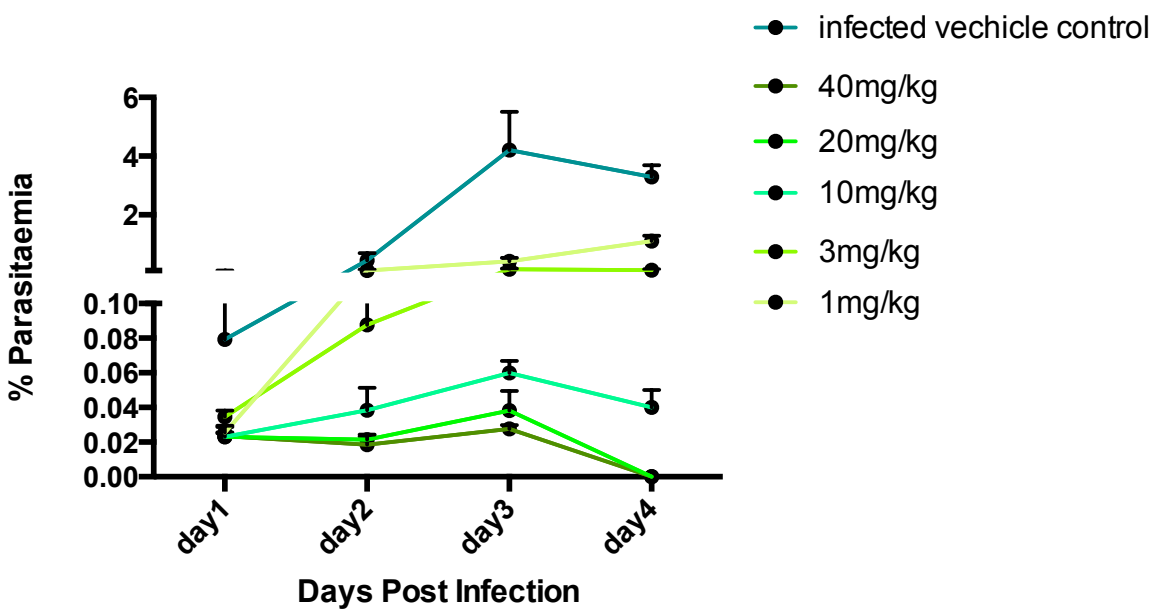

Figure 5.2 Impact of ART treatment doses on daily parasitaemia. BALB/c mice were infected with the PbGFP$_{CON}$/RFP$_{GAM}$ parasite line and treated daily with the indicated doses of ART. Blood parasitaemia of animals was monitored daily by flow cytometry and mice dosed with 20mg/kg and 40mg/kg ART had undetectable parasitaemia by day 4 post infection. n=7. Error bars ±SD.

On day 4 pi peripheral blood, bone marrow and spleen were harvested from animals from each group. As expected, the peripheral parasitaemia of all drug-treated groups was significantly attenuated compared with the infected vehicle control (Figure 5.3A). As such, the ART IC$_{50}$ for peripheral blood was calculated on day 4 pi as 0.04 mg/kg (Figure 5.3B). Due to the dynamics of the fluorescent proxies in the PbGFP$_{CON}$/RFP$_{GAM}$ parasite line it was determined that the 10 mg/kg – 1mg /kg ART treated groups contained asexual (GFP^{+}RFP^{-}) parasites, therefore assuring us the analysis was not based on degrading gametocytes (Figure 5.3C).

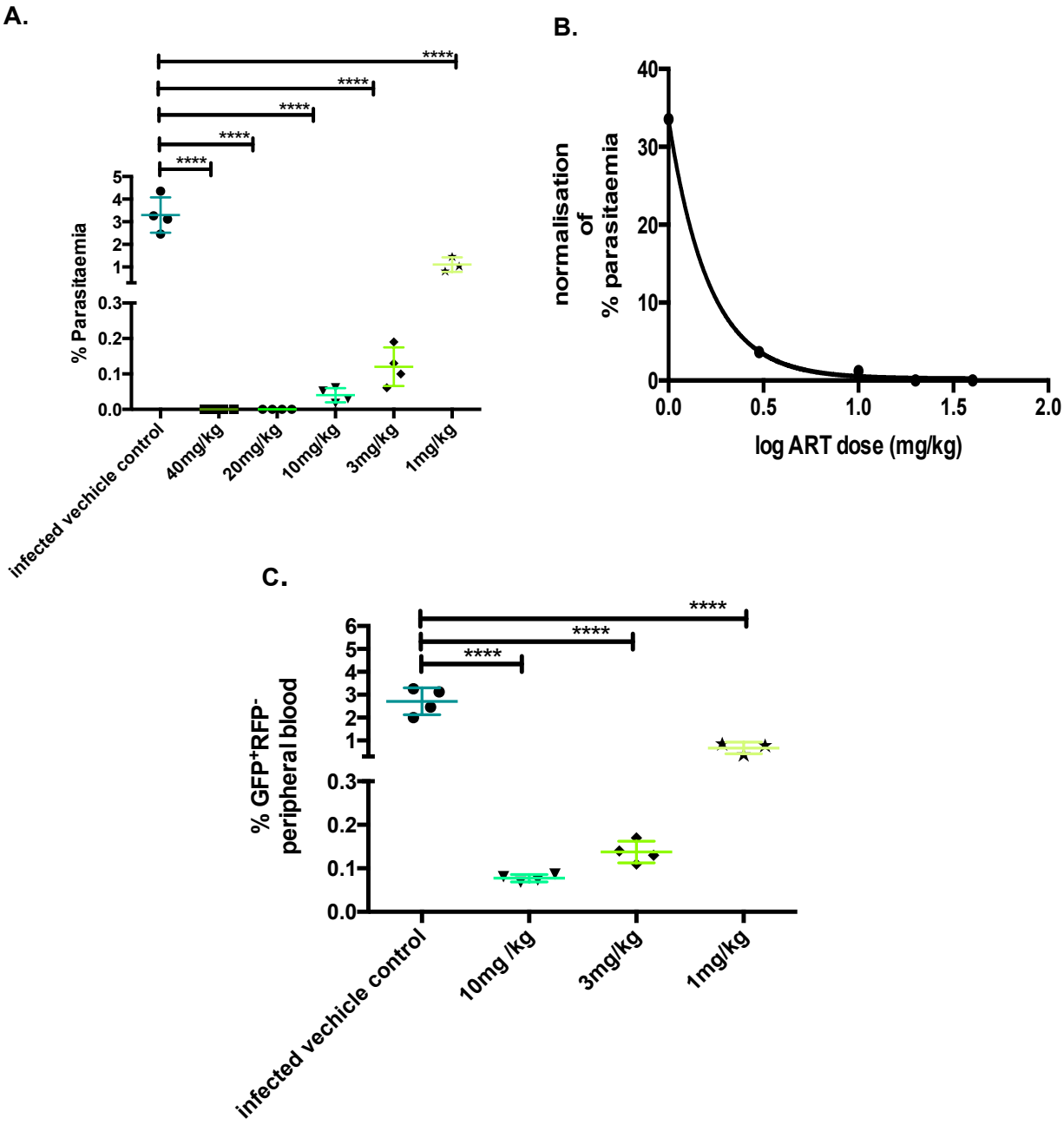

Figure 5.3 Parasites were undetectable in the peripheral blood of BALB/c mice dosed with ART at 20 mg/ kg and 40 mg/kg A. Peripheral blood parasitaemia at day 4 pi of BALB/c mice dosed with different ART concentrations. n = 4; 1 mg/kg n = 3. ±SD **B.** The IC_{50} of ART was calculated as 0.04mg/kg for the blood infection parasitaemia of the groups dosed. **C.** Percentage of peripheral blood containing $GFP^{+}RFP^{-}$ asexual parasites. n = 4; 1 mg/kg n = 3. ±SD. Drug dose concentrations displayed on the x-axis. The groups were compared using a one-way ANOVA with multiple comparisons. Significant difference between groups or samples is indicated with asterisks, denoting as follows: **** $p < 0.0001$.

Despite being unable to detect parasites within the peripheral blood by flow cytometry, mice from both the 20 mg/kg and 40 mg/kg groups contained parasitised splenic early reticulocytes (Figure 5.4A). Unsurprisingly, the administration of all concentrations of ART attenuated splenic early reticulocyte parasitaemia and parasite whole numbers compared with the infected vehicle control (Figure 5.4B). Nonetheless, the dose dependent attenuation was lost beyond 1 mg/kg. GFP^+ parasites could not be detected within splenic erythroblasts or any tissue resident erythroid population in bone marrow. Incidentally, the IC_{50} for bone marrow tissue resident erythroid cells was calculated as 0.0019 mg/ kg (Appendix 8.3.1).

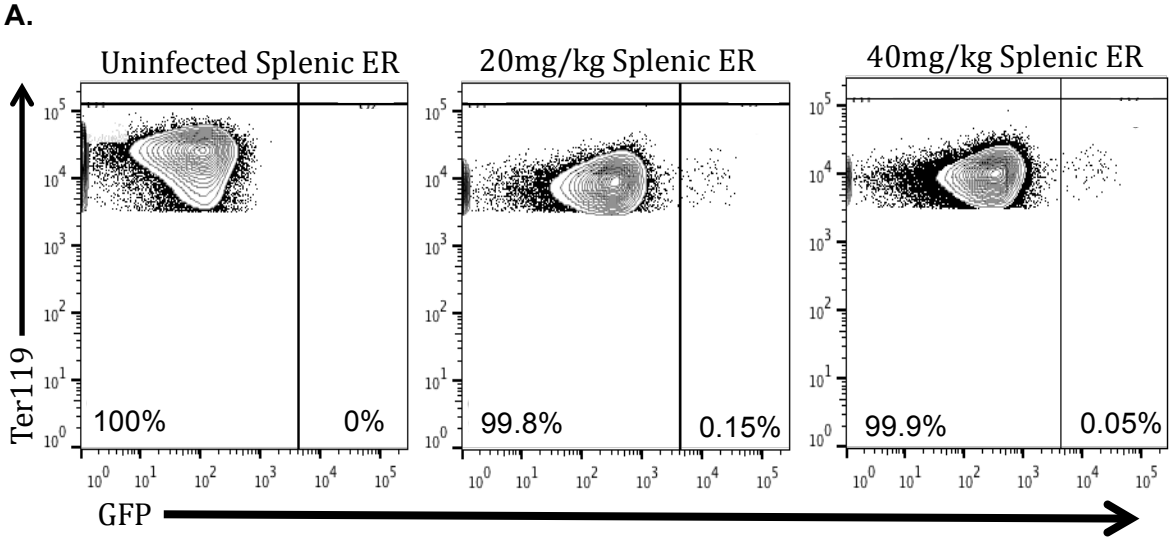

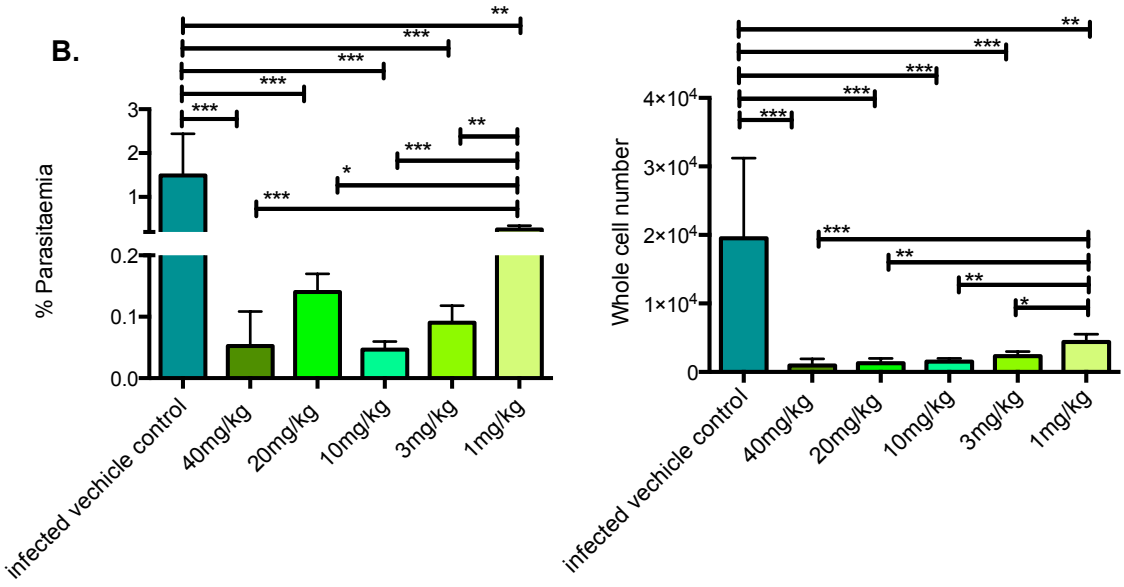

Figure 5.4 GFP$^+$ parasites were detectable within splenic early reticulocytes of BALB/c mice after ART treatment. ER; early reticulocyte. **A.** Representative FACS plots showing splenic early reticulocytes from the uninfected vehicle control, 20 mg/kg ART dosed group and the 40 mg/kg ART dosed group harvested on day 4 pi. Note the GFP$^+$ parasites in the drug-dosed animals. **B.** The percentage parasitaemia and whole cell numbers of parasites within the splenic early reticulocytes of infected mice treated with ART. The splenic early reticulocyte parasitaemia and parasite whole numbers are not significantly different between the 3 mg/kg – 40 mg/kg groups. n = 4; infected vehicle control and 1 mg/kg n = 3. ±SD. Drug dose concentrations displayed on the x-axis. The groups were compared using a one-way ANOVA with multiple comparisons. Significant difference between groups or samples is indicated with asterisks, denoting as follows: * $p < 0.05$, ** $p < 0.01$, *** $p < 0.001$. BALB/c mice.

The splenic early reticulocytes were colonised by both sexual and asexual parasites (Figure 5.5A&C). Through quantifying the number of gametocytes within the splenic early reticulocyte population it was determined that ART treatment does not stimulate an increase in sexual cells (Figure 5.5B). The significantly increased gametocytaemia of early reticulocytes observed in mice treated with 20 mg/kg is likely due to the degradation of asexual parasites rather than an increased gametocyte conversion rate (Appendix 8.3.2).

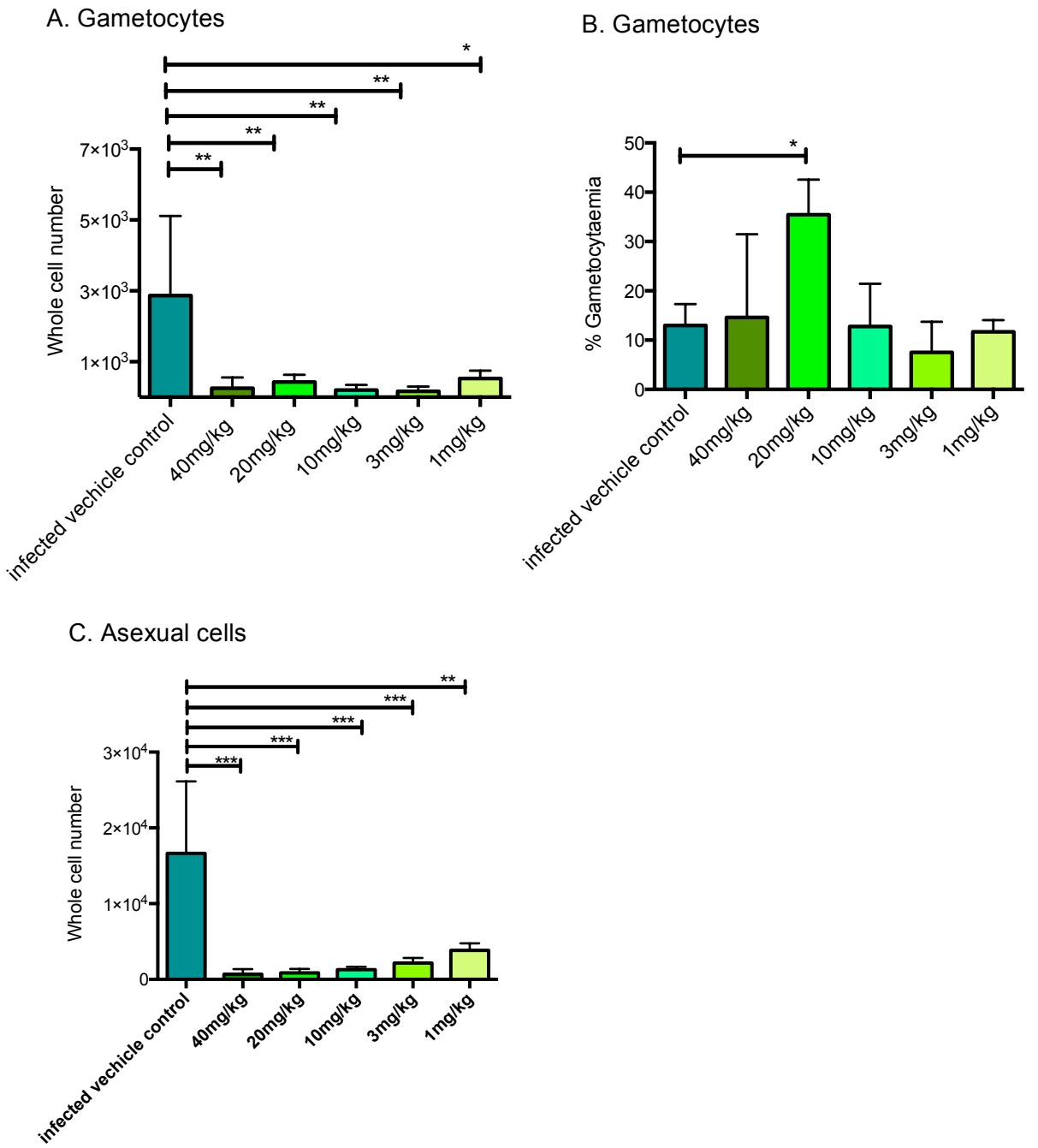

Figure 5.5 ART treatment does not increase gametocytogenesis within early reticulocytes of BALB/c mice. A. Whole cell numbers of gametocytes within the splenic early reticulocyte population of infected BALB/c mice treated with ART**. B.** Gametocytaemia of splenic early reticulocytes. **C.** Whole cell numbers of asexual parasites within the splenic early reticulocytes. Mean values ± SD are shown for n = 4, except infected vehicle control and 1 mg/kg n = 3. Drug dose concentration displayed on the x-axis. The groups were compared using a one-way ANOVA with multiple comparisons. Significant differences between groups or samples is indicated with asterisks, denoting as follows: * $p < 0.05$, ** $p < 0.01$, *** $p < 0.001$.

The remaining mice in the 20 mg/kg and 40 mg/kg (n=3) dosed groups experienced recrudescence of infection from day 6 pi (72 hrs after final drug dose). On day 6 pi the average parasitaemia of mice in the 40 mg/kg dosing group was 0.0006% (Figure 5.6). When taking into account that the average BALB/c mouse contains 1ml of blood with 6 $x10^6$ erythroid cells/µl, it can be extrapolated that the mice on average contained 36,000 parasites on day 6. *P. berghei* has a x 10 replication rate/ 24 hrs (Janse, 2014), as such, it can be extrapolated that on day 4 the mice would need to contain 360 asexual parasites. On average the mice contained 683 ± 341 asexual parasites in the splenic early reticulocytes on day 4 (Figure 5.5C and Appendix 8.3.3). As such, the hypothesis that the recrudescence in the 40mg/kg group is due solely to the survival of parasites in the tissue resident erythroid cells is mathematically sound.

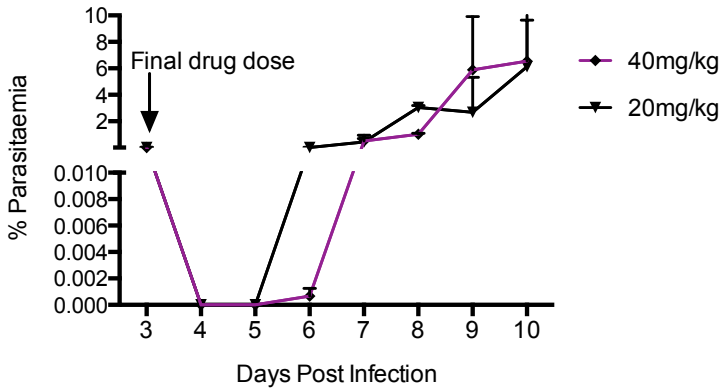

Figure 5.6 Recrudescence of infection after ART treatment. Parasitaemia of BALB/c mice dosed with 40 mg/kg and 20 mg/kg ART. n=3. Error bars ± SD.

5.2.2 ART Treatment Promotes Splenic Erythropoiesis in *P. berghei* Infected Mice

Using the flow-based approach I was also able to investigate the effects ART treatment has on erythropoiesis. The samples investigated here were harvested from mice on day 4 post-infection after treatment under the modified Peters "4 day suppressive test" (Figure 5.1).

A significantly higher proportion of tissue resident erythroid cells were nucleated erythroblasts in the spleens of mice treated with doses of ART between 1- 10 mg/kg compared with the uninfected vehicle control. This was reflective of the erythropoietic dynamics stimulated by the untreated *P. berghei* infection (infected vehicle control) (Figure 5.7A). When the populations of splenic tissue resident erythroid cells were quantified it became apparent that treatment with non-curative doses of ART between 3 – 10 mg/kg significantly increased the number of early reticulocytes and erythroblasts compared with untreated *P. berghei* infection (infected vehicle control) (Figure 5.7B). In contrast, when mice were treated with 40 mg/kg the stimulatory effects of ART on erythropoiesis were significantly reduced compared with 10 mg/kg (whole cell numbers of reticulocytes ** $p = 0.011$; whole cell numbers of erythroblasts **** $p = <0.0001$) (Figure 5.7B). Nonetheless, treatment of infected mice with 40 mg/kg maintained greater levels of erythropoiesis than uninfected mice that were similar to that observed in untreated infection control mice. (Figure 5.7 A&B). However, treatment with this concentration of ART resulted in altered stage distribution of splenic erythroblasts, with a significant lower number of mature erythroblasts compared to the intermediate group (Figure 5.7C&D). This is in stark contrast to the 1:2:4 ratio of immature: intermediate: mature erythroblasts observed under steady state conditions and thus implies dysregulation of erythropoiesis.

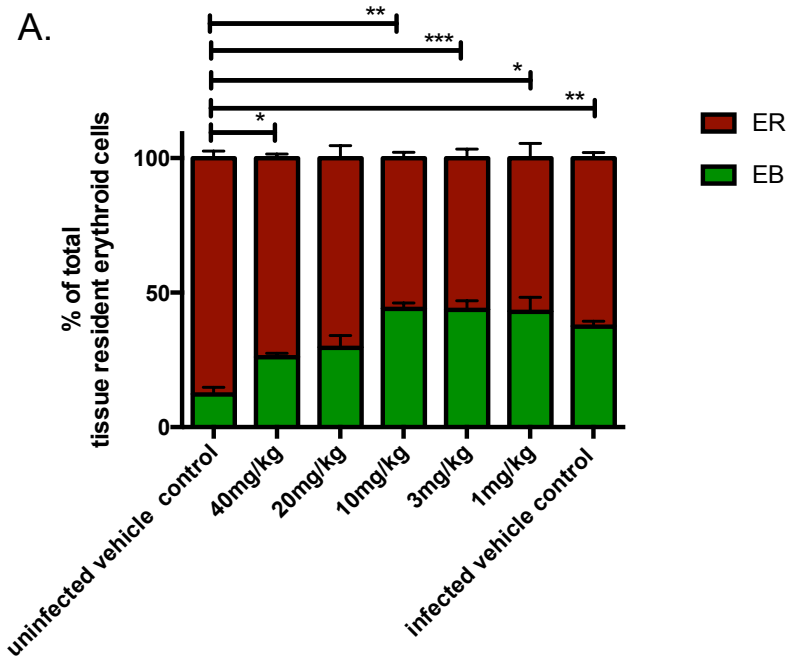
A.
**
***
*
**
*
100
50
0
% of total
tissue resident erythroid cells
ER
EB
uninfected vehicle control
40mg/kg
20mg/kg
10mg/kg
3mg/kg
1mg/kg
infected vehicle control

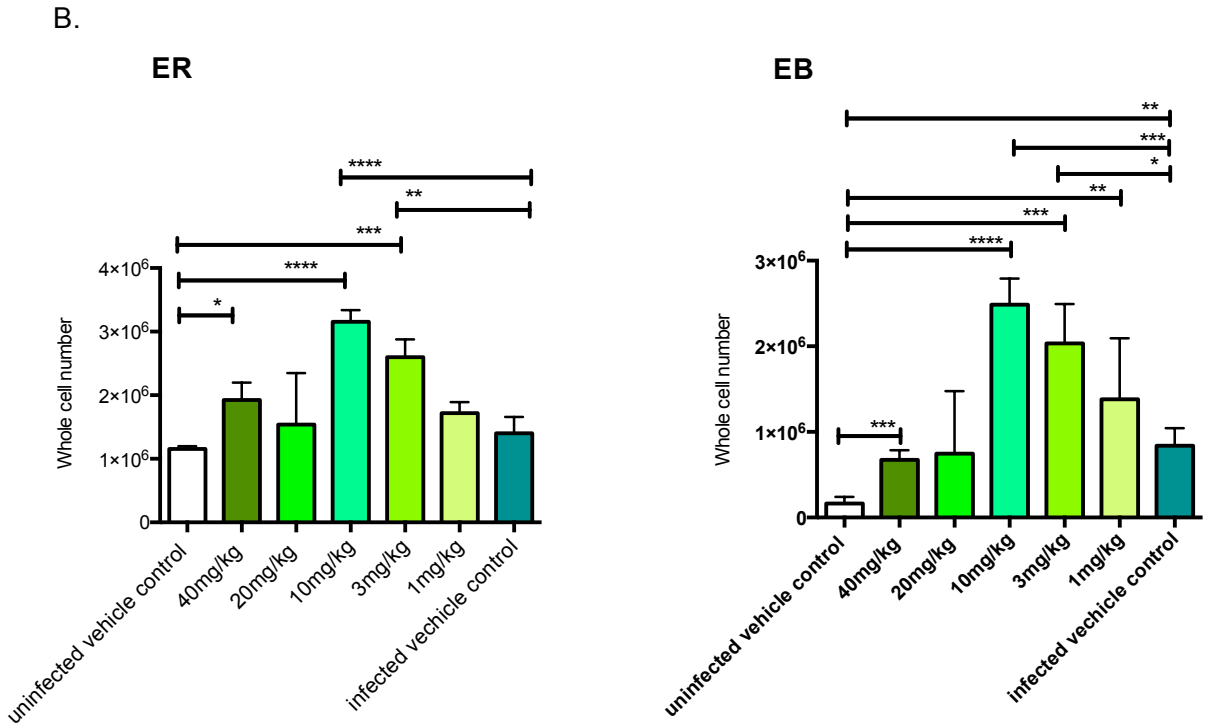
B.
ER
EB
Whole cell number
4×10^6
3×10^6
2×10^6
1×10^6
0
uninfected vehicle control
40mg/kg
20mg/kg
10mg/kg
3mg/kg
1mg/kg
infected vechicle control

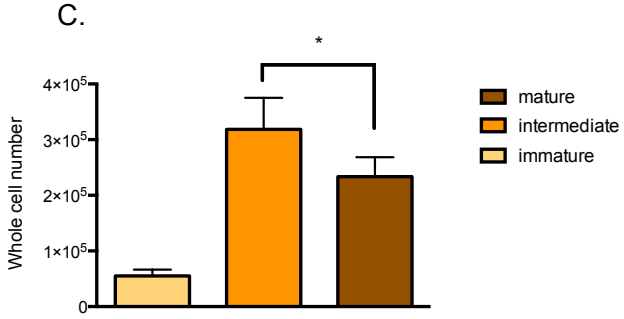
C.
Whole cell number
4×10^5
3×10^5
2×10^5
1×10^5
0
mature
intermediate
immature

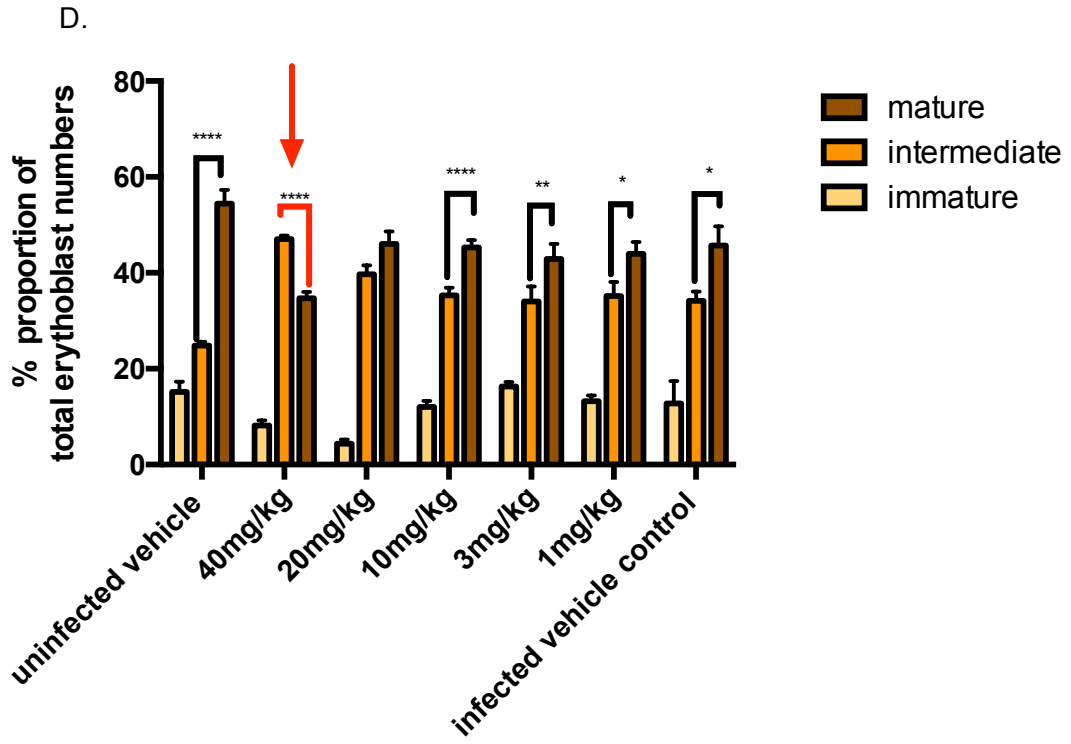

Figure 5.7 ART treatment stimulates splenic erythropoiesis in a dose dependent manner in infected mice. ER; early reticulocyte. EB; Erythroblast. **A.** The proportion of splenic tissue resident erythroid cells that are erythroblasts (EB) is significantly increased in BALB/c mice infected with *P. berghei* compared with the uninfected vehicle control. **B.** Whole cell numbers of splenic early reticulocytes (ER; left) and whole cell numbers of splenic erythroblasts (right). **C.** Whole cell numbers of splenic erythroblast stages. **D.** Proportion of total splenic erythroblasts falling within the immature, intermediate and mature gates. Drug dose concentration displayed on the x-axis. The groups were compared using a one-way ANOVA with multiple comparisons. Values shown are means of n = 4 except infected vehicle control and 1 mg/kg n= 3. ±SD. Significant differences between groups or samples is indicated with asterisks, denoting as follows: * $p < 0.05$, ** $p < 0.01$, *** $p < 0.001$, **** $p < 0.0001$.

5.2.3 ART Administration Promotes Splenic Erythropoiesis in Uninfected Mice

Next it was investigated whether the stimulating effects observed after ART treatment were independent of *P. berghei* infection. To do this, four daily doses of ART were administered to uninfected mice. Bone marrow and spleen tissue was harvested 24 hrs after the final drug dose. Quantifying the populations of tissue resident erythroid cells demonstrated a significant increase in both splenic early reticulocytes and erythroblasts in animals dosed with 40 mg/kg compared

with the vehicle control (Figure 5.8). Moreover, treatment with this concentration of ART did not result in altered stage distribution of splenic erythroblasts (Figure 5.8). This suggested that ART treatment stimulates erythropoiesis in a dose dependent manner independently of *P. berghei* infection.

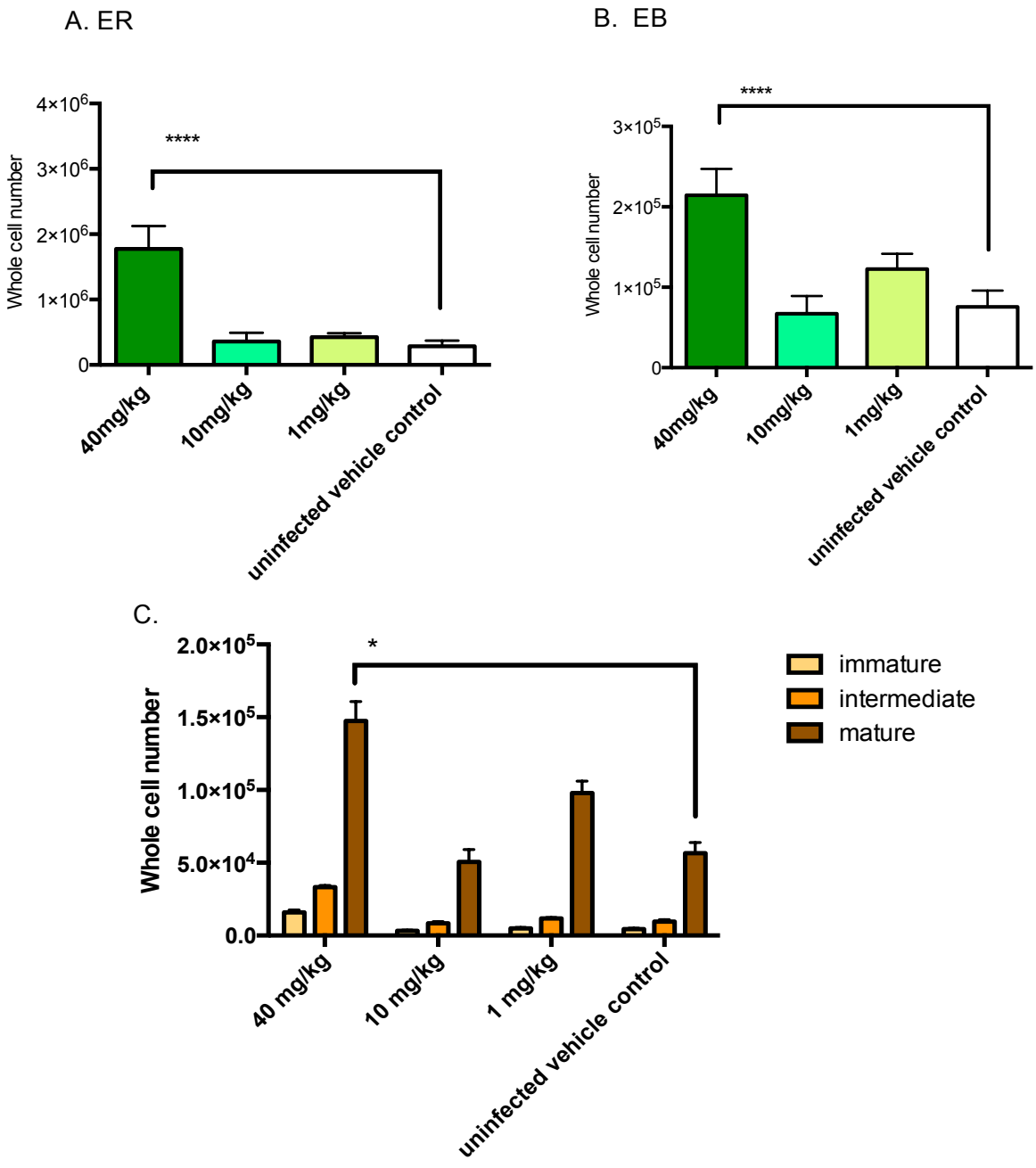

Figure 5.8 ART administration results in the increased numbers of splenic early reticulocytes and erythroblasts in uninfected BALB/c. ER; early reticulocyte. EB; Erythroblast.**A**. Whole cell numbers of early reticulocytes. **B**. Whole cell numbers of erythroblasts. **C**. Whole cell numbers of splenic erythroblast stages. n= 4. ±SEM. Drug dose concentration displayed on the x-axis. The groups were compared using a one-way ANOVA with multiple comparisons. Significant difference between groups or samples is indicated with asterisks, denoting as follows: * $p < 0.05$, ** $p < 0.01$, *** $p < 0.001$, **** $p < 0.0001$. BALC/c mice.

5.2.4 ART Administration does not Promote Erythropoiesis in the Bone Marrow.

To investigate whether the impact of ART on erythropoiesis was tissue specific, we also analysed bone marrow samples after treatment. No significant increase in erythroid cells was observed in *P. berghei* infected mice given four consecutive daily doses of ART compared with untreated or uninfected controls (Figure 5.9).

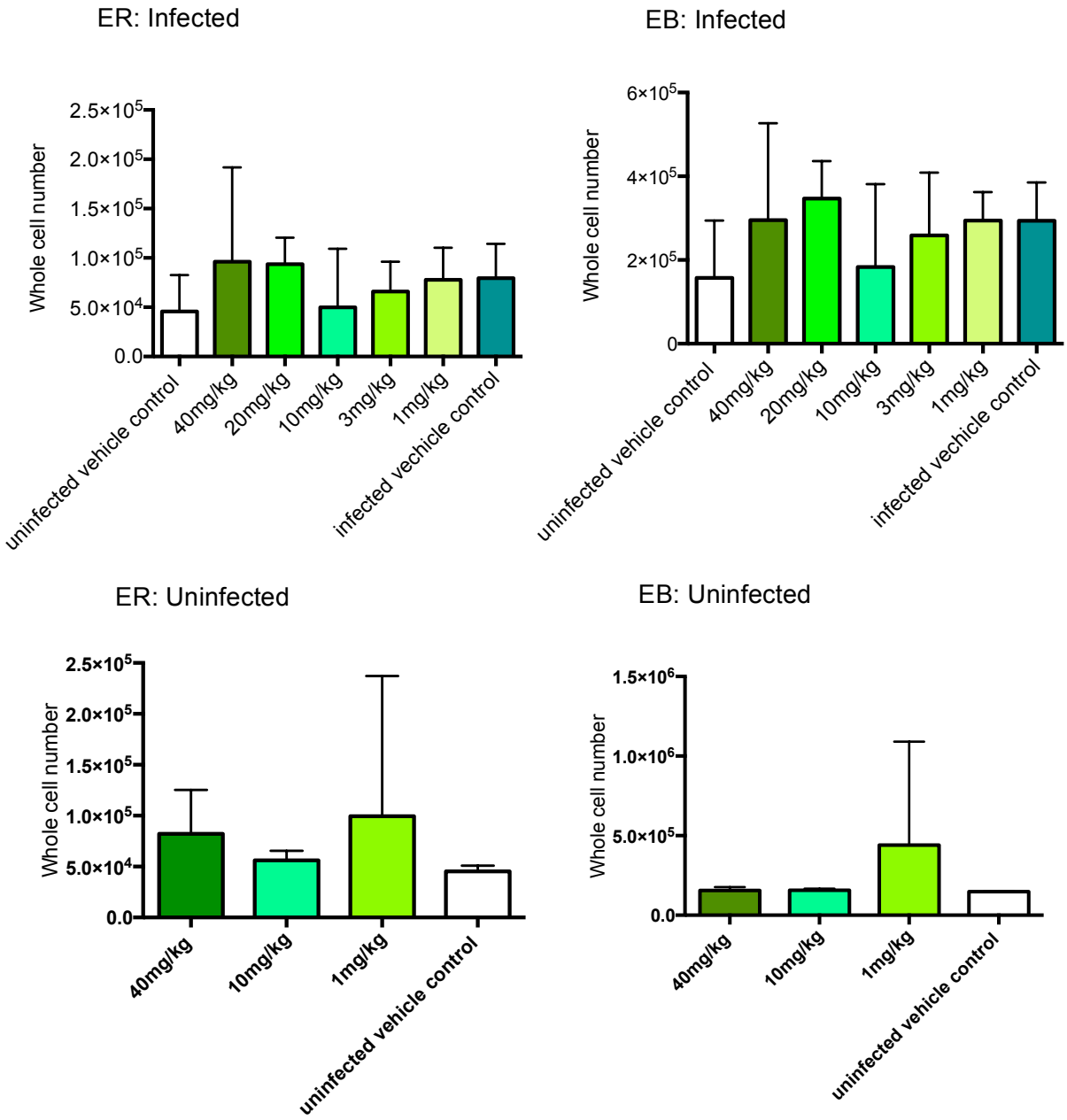

Figure 5.9 ART treatment does not stimulate erythropoiesis in the bone marrow of BALB/c mice. ER; early reticulocyte. EB; Erythroblast. Whole cell numbers of bone marrow early reticulocytes (left; top) and whole cell numbers of bone marrow erythroblasts

(right; top) from infected mice. n = 4; infected vehicle control and 1 mg/kg n = 3. Whole cell numbers of bone marrow early reticulocytes (left; top) and whole cell numbers of bone marrow erythroblasts (right; top) from uninfected mice. n=4 of all groups. Drug dose concentration displayed on the x-axis. The groups were compared using a one-way ANOVA with multiple comparisons. Error bars ±SD.

5.2.5 Chloroquine or Pyrimethamine Administration does not Promote Splenic Erythropoiesis

To investigate whether the stimulating effects of ART on splenic erythropoiesis are exclusive to this class of antimalarial, mice were infected with 10^6 $PbGFP_{CON}/RFP_{GAM}$ parasites and treated with either CQ or PYR under the previously mentioned Peters "4 day suppressive test" regime (Figure 5.1). Under CQ treatment, the numbers of early reticulocytes in the spleen of animals administered with the curative dose, 10 mg/kg, were the same as the uninfected vehicle control (Figure 5.10A). Compared with untreated *P. berghei* infection, CQ doses of either 3mg/ kg or 1mg/ kg had no impact on splenic early reticulocyte numbers (Figure 5.10B). In contrast, the whole numbers of splenic erythroblasts in the drug treated groups did not differ from either the uninfected or infected vehicle control (Figure 5.10B). Under PYR treatment (Figure 5.10C) the whole cell numbers of either splenic early reticulocyte or splenic erythroblasts were not significantly different to the infected vehicle control (Figure 5.10D).

A.

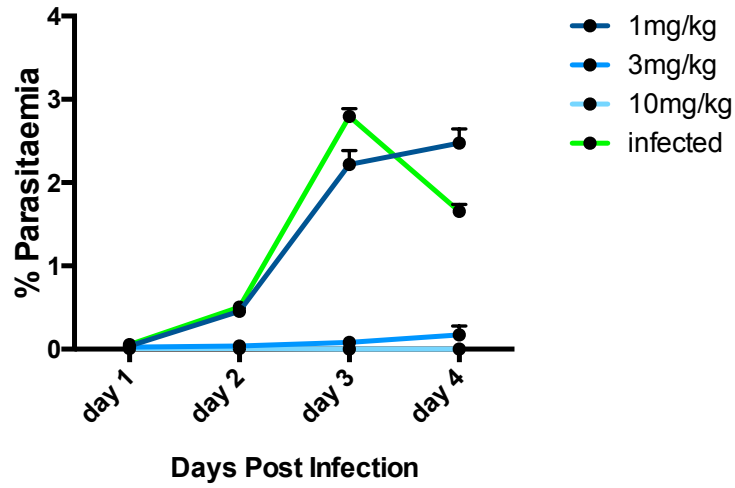

B.

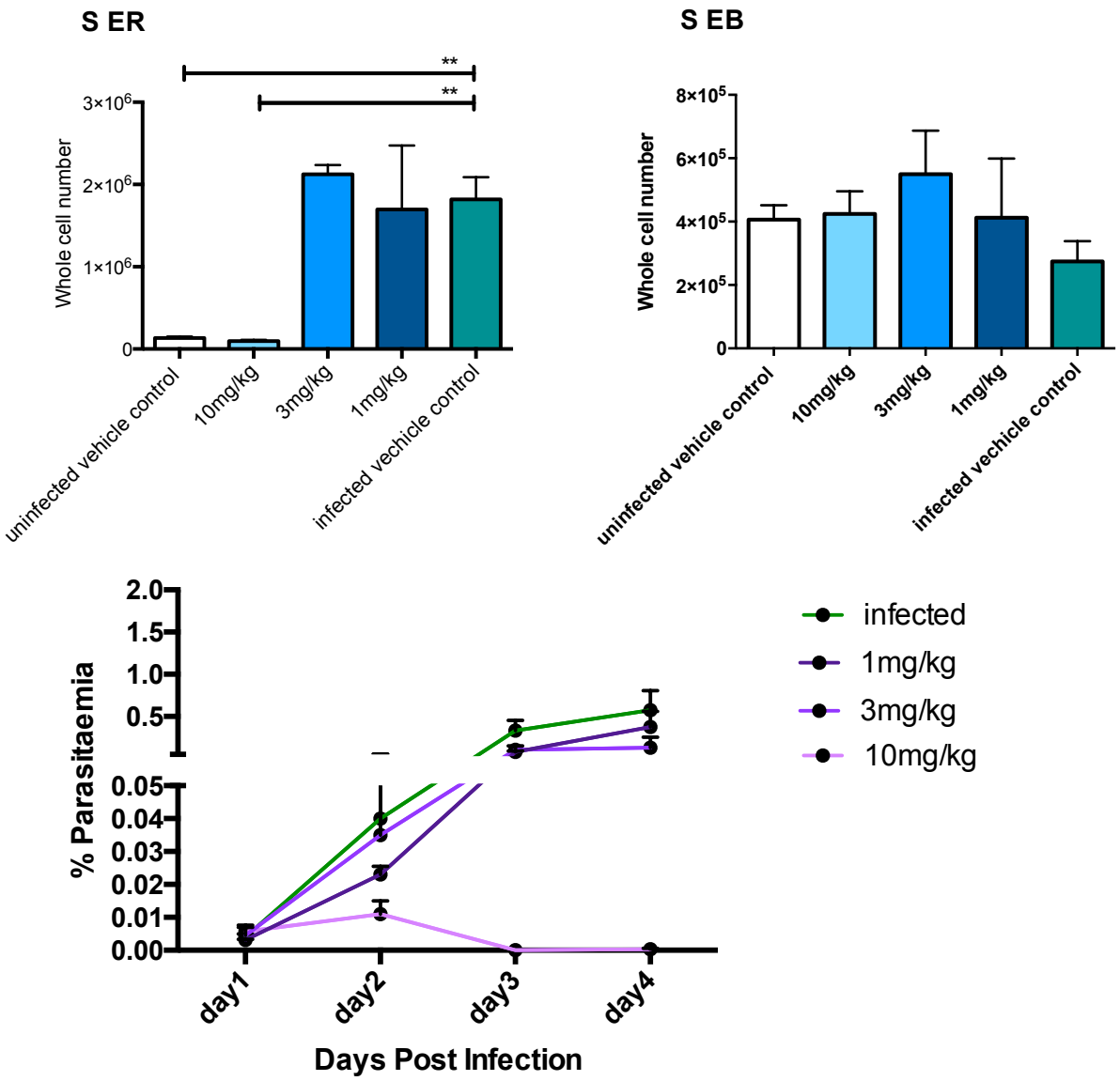
S ER
Whole cell number
3×10^6
2×10^6
1×10^6
0
**
**
uninfected vehicle control
10mg/kg
3mg/kg
1mg/kg
infected vechicle control
S EB
Whole cell number
8×10^5
6×10^5
4×10^5
2×10^5
0
uninfected vehicle control
10mg/kg
3mg/kg
1mg/kg
infected vechicle control
% Parasitaemia
2.0
1.5
1.0
0.5
0.05
0.04
0.03
0.02
0.01
0.00
day1
day2
day3
day4
Days Post Infection
infected
1mg/kg
3mg/kg
10mg/kg

D.

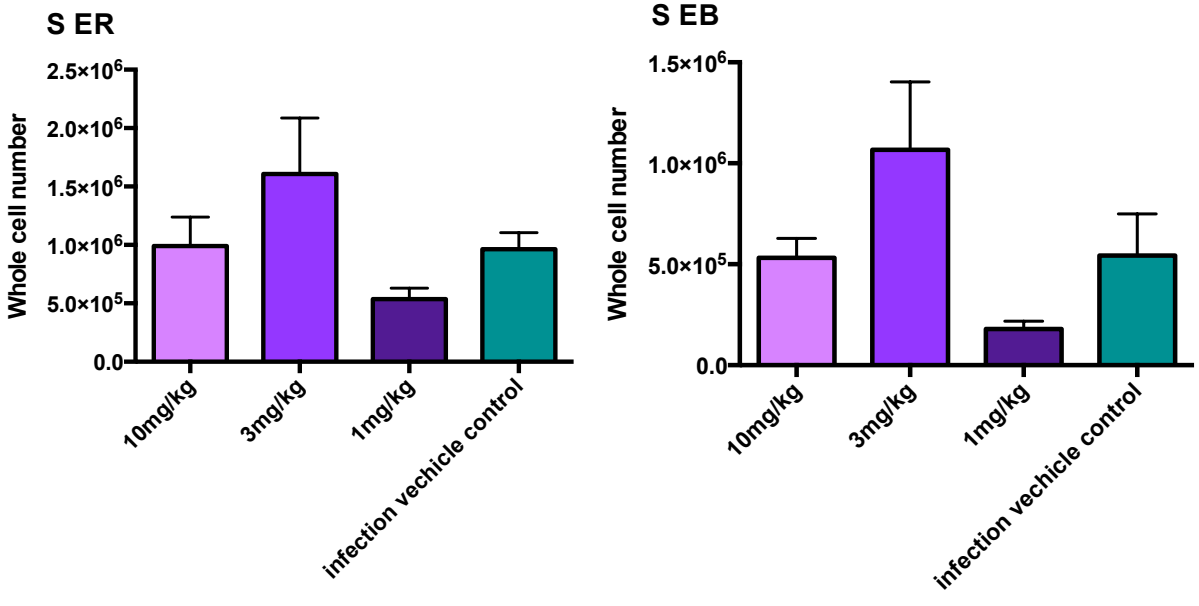
S ER
Whole cell number
2.5×10^6
2.0×10^6
1.5×10^6
1.0×10^6
5.0×10^5
0.0
10mg/kg
3mg/kg
1mg/kg
infection vechicle control
S EB
Whole cell number
1.5×10^6
1.0×10^6
5.0×10^5
0.0
10mg/kg
3mg/kg
1mg/kg
infection vechicle control

Figure 5.10 CQ or PYR treatment does not stimulate splenic erythropoiesis. ER; early reticulocyte. EB; Erythroblast. **A.** Parasitaemia of animals dosed with CQ. **B**. Whole cell numbers of splenic early reticulocytes (left) and whole cell numbers of splenic erythroblasts (right; top) from infected mice dosed with CQ. n = 3. **C**. Parasitaemia of animals dosed with PYR. **D**. Whole cell numbers of splenic early reticulocytes (left) and whole cell numbers of splenic erythroblasts (right; top) from infected mice dosed with PYR. n = 3. Drug dose concentration displayed on the x-axis. The groups were compared using a one-way ANOVA with multiple comparisons. Error bars ±SD.

5.3 Discussion

5.3.1 Recrudescence of Infection Despite Undetectable Parasites in Peripheral Blood

The phenomenon of antimalarial drug resistance initially emerged in Thailand in 1957 in the form of CQ resistant *P. falciparum* (White, 2013). The prominent use of CQ was replaced by alternative synthetic antimalarials, which in turn fuelled treatment specific failure. The global use of ARTs began in the 1990s. Artemisinin treatment reduces parasite burden very rapidly (Miller *et al.*, 2013) and ART monotherapies have been tested with duration as short as 2 consecutive days (Nguyen Duy Sy *et al.*, 1993). Although 50 % of patients under this regime suffered recrudescence of infection, regimes of the same ART concentration but administered for 7 days also suffered recrudescence (Nguyen Duy Sy *et al.*, 1993). To tackle the high ART monotherapy treatment failure and to prevent a surge in ART residence, the WHO recommends a ACT treatment duration of three consecutive days (World Health Organisation, 2015). Nonetheless, treatment failure of ACT combined therapies, due to infection recrudescence following initial blood clearance, were reported as early as 2000 (Packard, 2000). In this chapter I have shown that after four daily administrations of ART at 20 mg/kg or 40 mg/kg, previously reported IC_{90} values in BALB/c mice (Janse *et al.*, 1994; Vega-Rodríguez *et al.*, 2015), GFP^{+} parasites are undetectable by flow cytometry in the peripheral blood but readily apparent in splenic early reticulocytes. It is interesting to note that the disparity between parasite persistence within bone marrow and spleen after drug treatment is unlikely to be due to the pharmacokinetics of ART. Multiple studies have observed radiolabeled (^{14}C) ART reaches relatively higher concentrations (14% of total radioactivity) in the spleen across 192 hrs after a single dose of 3mg/kg compared to all other sampled tissues (Li *et al.*, 2006; Xie *et al.*, 2009).

It is important to acknowledge that although flow cytometry is highly sensitive at detecting rare events (Domingo *et al.*, 2010), the peripheral blood parasitaemia of the mice treated with 20 mg/kg or 40mg/kg may have been below the level of detection by this method. The ability of a single parasitised erythrocyte to establish an infection is the basis for the use of limiting dilution during the acquisition of clonal parasite lines. However, the asexual numbers

shown here to be present in the splenic early reticulocytes on day 4 could generate the blood stage parasite numbers on day 6, it is reasonable to argue that the recrudescence of infection witnessed on days 6 and 7 may be the result of a residual peripheral blood parasitaemia. In future work this concern may be circumvented through the use of RT-PCR against parasite specific markers in peripheral blood samples. Work assessing technical approaches for the detection of minimal residual disease (MRD) have shown that PCR-based studies are >1-log more sensitive than flow cytometry (Domingo *et al.*, 2010). I chose to use flow cytometry in this study as it allowed us to define the erythroid populations that contained parasites after drug treatment, a characterisation that could not be made with RT-PCR. However, the sensitivity of flow cytomety prevents us from identifying the persistent splenic early reticulocyte infection as the sole source of the recrudescing infection following ART treatment.

Interestingly, multiple reports have stated that post ART treatment, recrudescing parasites are not resistant to ART in vitro and re-administration of ART to patients is effective in clearing the recrudesced infection (Looareesuwan *et al.*, 1997; Ittarat *et al.*, 2003; Cheng, Kyle and Gatton, 2012). In this study I did not test the viability and drug sensitivity of the parasites within the splenic early reticulocytes. But this is the next logical step in the experimental workflow. This could be achieved by cell sorting the asexual (GFP^+RFP^-) infected splenic early reticulocytes from the 20 mg/kg and 40 mg/kg ART dosed mice. These cells could then be injected into uninfected mice to establish new infections, which could then be treated with the same drug concentration as the primary infection.

A prominent hypothesis in the field to how drug sensitive parasites can survive treatment is ART-induced dormancy, whereby some parasites within a population can suspend their growth during drug administration only to resume it after drug clearance (Bwijo *et al.*, 1997; Cheng, Kyle and Gatton, 2012). This theory has supporting evidence *in vitro* (Bwijo *et al.*, 1997) and *in vivo* (LaCrue *et al.*, 2011) where dormant parasites, morphologically identified as ring stages with unusually condensed cytoplasm and nucleus, have been observed after ART treatment (Teuscher *et al.*, 2010). In this work I did not visualise the splenic infected early reticulocytes and therefore cannot comment on whether they

displayed a dormant morphology. Nonetheless, there is evidence that the maturation stage of the host cell may affect treatment outcome. Srivastava *et al* (2015) showed that the effects of drugs that target the parasites intermediary metabolism are compensated by the relatively ready availability of host derived metabolites in mature reticulocytes compared to erythrocytes, this effect could be potentially amplified in the more nutrient rich immature tissue resident reticulocytes. Thus in future work I need to identify whether parasites within splenic early reticulocytes are arrested or growing in a protective environment. This could be achieved by analysing the population with the same gating strategy on an Imagestream opposed to standard flow cytometry. The images generated will attest to whether the parasites are ring stages with unusual morphology or parasites developing through their life cycle.

5.3.2 ART Stimulating Erythropoiesis in a Dose Dependent Manner

The enhanced survival of parasites within splenic early reticulocytes post ART treatment may perpetuate infection through recrudescence and arguably may also create a cradle for drug resistance. Exacerbating this phenomenon, I observed that ART doses between 3- 10 mg/kg stimulated erythropoiesis in the spleen of *P. berghei* infected mice, thus enlarging the resource for parasite survival. It is established within the literature that ARTs treatment leads to haemolysis in both humans and mice, a well defined trigger for the stimulation of stress erythropoiesis (Jaureguiberry *et al.*, 2014; Arguin, 2017). Nonetheless, the delayed onset time of ART associated haemolysis, > 1 week post parasite clearance, would suggest that the stimulatory effects I observed under 3 – 10mg/ kg treatment were due to a more immediate erythropoietic dynamics (Jaureguiberry *et al.*, 2014; Arguin, 2017). Moreover, administrating ART to uninfected mice suggested that splenic erythropoiesis is amplified in a dose-dependent manner independent of malarial infection. Furthermore, this effect is likely drug class dependent as treatment with CQ or PYR did not elicit the same significant increase in tissue resident splenic erythroid cells.

The murine spleen is the predominant site of stress erythropoiesis, which is regulated differently to basal erythropoiesis. It has been shown that stress erythropoiesis, but not basal erythropoiesis, is regulated via the glucocorticoid

(GC) receptor and this protein is essential for the expansion of erythroid progenitors (BFU-E) (Bauer *et al.*, 1999). There is evidence that ART up-regulates this receptor on different cell lineages *in vivo* (Bauer *et al.*, 1999; Wu *et al.*, 2011). ARTs also have been shown to possess anti-cancer, anti-viral and anti-inflammatory activities (Krishna *et al.*, 2008; Cheng *et al.*, 2011). Artesunate inhibits and blocks the production of inflammatory cytokines from stimulated macrophages by the inhibition of the PI3K/Akt signaling pathway in a dose dependent manner (Xu *et al.*, 2007; Li *et al.*, 2008). Of particular interest is the noted suppression of TNF-alpha and IL-6, both of which are negative feed back regulators of erythropoiesis secreted by the central erythroblast island macrophage (Xu *et al.*, 2007; Li *et al.*, 2008). It is therefore tempting to speculate that the significantly increased splenic tissue resident erythroid cell populations I observed after treatment of infected and uninfected mice, was due to ART targeting pathways in the stress erythropoietic pathway in a dose dependent manner. I detected dysregulation of postnatal splenic erythropoiesis only after the administration of 40 mg/kg to *P. berghei* infected mice. This can be linked to the observations that ART effects human developmental erythropoieisis *in vitro* in a dose dependent manner (Finaurini *et al.*, 2010). The same authors later showed this was the result of a dose dependent disruption of cell cycle progression (Finaurini *et al.*, 2012). Taken together, the dose dependent effects I observe during ART treatment of *P. berghei* are likely due to the balance between the de-repression of erythropoiesis and the disruption of erythroid maturation.

5.4 Summary

In this chapter observed persistent parasitism of the erythropoietic tissue and an unprecedented expansion of this niche under treatment with artemisinin concentrations that elicit clearance of the peripheral blood infection.

6. General Discussion; Relevance to Human Disease.

The overarching narrative of the work in this thesis is (Figure 7.1):

- *P. berghei* can invade the tissue resident erythroid cells located in the murine bone marrow and spleen.
- This cell population provides a niche for the highest gametocyte conversion rates in the body.
- It also provides a protective niche during treatment with ART doses that clear the peripheral blood infection.

These observations extend the asexual life that classically has been considered to be within circulating erythrocytes and maturing reticulocytes (Figure 7.1).

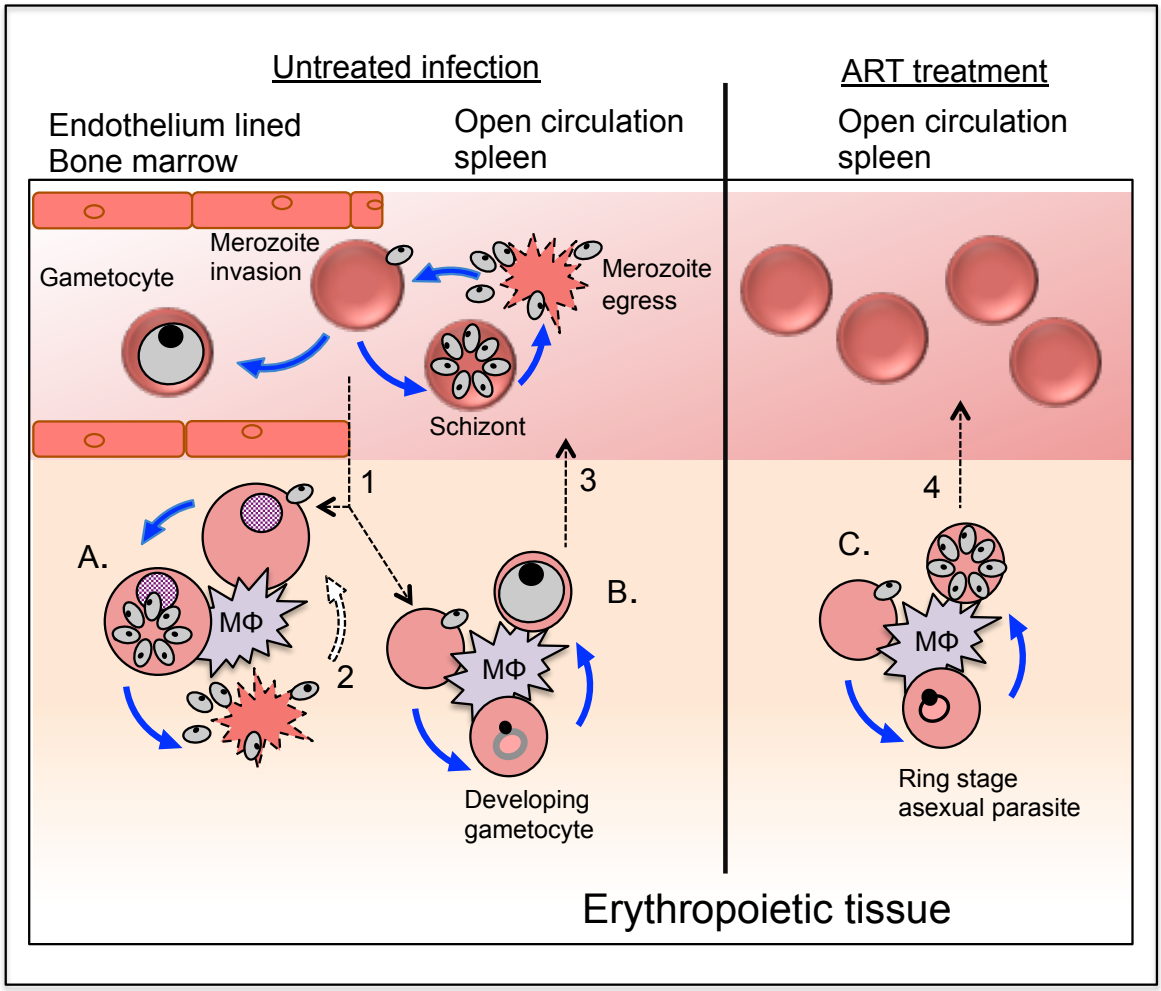

Figure 7.1 Summary of thesis observations. Blue arrows are events suggested by this work. Dotted arrows are events indirectly observed to occur. MΦ: central 'nurse' macrophage. The *Plasmodium* life cycle (untreated infection), carried out in erythrocytes and maturing reticulocytes, is depicted in an endothelium lined blood vessel (top left; bone marrow) and the non-endothelium lined splenic red cords (top left; open circulation spleen). The observations made in this work suggest that: **A**. Merozoites can invade erythroblasts and early reticulocytes; these infected cells are permissive to *P. berghei* therefore schizonts can form and merozoites can undergo egress. **B**. Merozoites can invade tissue resident erythroid cells and develop as gametocytes, with the most consistent gametocytaemia being observed in early reticulocytes. **C**. Under ART treatment that cures the peripheral blood infected, a population of parasites within splenic early reticulocytes are not cleared. 1. Dotted lines indicate the migration of parasites into the erythropoietic tissue. The establishment of a tissue resident infection is dependent on a merozoite invading tissue resident erythroid cells, as such, a migration event must occur, however work in this thesis has not established that mechanism or parasite stage. 2. The establishment of a cryptic cycle within the tissue from merozoites released from tissue resident erythroid cells. 3. The migration of parasite infected stage III reticulocytes into circulation. 4. The infected tissue resident population may lead to disease

recrudescence, as judged by detectible parasites within the peripheral blood, due to the maturation and release of the infected early reticulocytes into circulation.

6.1 Relevance to Human Infective *Plasmodium*

There are five species of *Plasmodium* that cause human malaria, but the greatest morbidly and mortality is caused by just two of these species, *P. vivax* and *P. falciparum*, respectively. *Plasmodium* merozoites initiate entry to their host cell through a series of hierarchal ligand-receptor interactions (Weiss, Crabb and Gilson, 2016). The repertoire of ligands expressed by the parasite govern its tropism for a particular maturation stage of erythroid cell development (Han *et al.*, 2016; Lim *et al.*, 2016). Both *P. vivax* and *P. falciparum*, like *P. berghei,* can invade reticulocytes within the peripheral blood (Lim *et al.*, 2016). Furthermore, *P. falciparum* and *P. vivax* have also been observed to invade nucleated erythroid progenitors (Ru *et al.*, 2009; Tamez *et al.*, 2009) and *P. falciparum* has directly been shown to accumulate within the parenchyma of the bone marrow (Farfour *et al.*, 2012; Joice *et al.*, 2014). Joice *et al* (2014) observed that the majority of extravascular parasites within the bone marrow reside within enucleated cells. CD71 is expressed on erythroid cells and down regulated during maturation. Due to the low expression levels of CD71 on the observed infected cells Joice et al (2014) postulated that they could be erythrocytes that had been infected within the vasculature and then migrated, by undefined mechanisms, across the endothelium into the tissue (Joice *et al.*, 2014). The work presented in this thesis demonstrated that the murine infective parasite, *P. berghei* can invade tissue resident erythroid cells. My work is the first time that parasite burden, alongside parasite preference for the different maturation stages of erythroid cells has been measured *in vivo*. Reflecting the observation made by Joice *et al* (2014), my work showed that the highest parasite burden is observable within the enucleated tissue resident erythroid populations: the early reticulocytes. Moreover, I showed that during infection CD71 is down-regulated in the stress erythropoietic tissue, which in humans is believed to be located to an extent in the bone marrow, (Palitzsch *et al.*, 1987; Nandakumar, Ulirsch and Sankaran, 2016). This evidence suggests that the highly parasitised erythroid population previously observed within the extra vascular spaces of the bone marrow (Joice *et al* (2014) were most likely early reticulocytes and perhaps not transmigratory erythrocytes.

Moreover, through calculating gametocytaemia within erythroid cell compartments *in vivo,* I observed that the highest gametocyte conversion rates occur within the early reticulocyte population. Again, this directly reflects the *ex vivo* observations of Joice *et al* (2014) that the immature gametocytes of *P. falciparum* are observable within an enucleated extra vascular population within the bone marrow. Therefore, I have provided evidence that my murine model is directly comparable with the observations made in the human host. Furthermore, although my data does not exclude a role for immature gametocyte infected erythrocytes directly transmigrating into the bone marrow, it does give considerable weight to the hypothesis that extracellular merozoites or schizont parasitised erythrocytes infiltrate haematopoietic tissue, whereby the proceeding invasion event into early reticulocytes triggers gametocyte formation.

6.2 Human Definitive Erythropoiesis

As mentioned above, I identified murine splenic early reticulocytes as the erythroid cell niche with highest parasite burden and the greatest gametocyte conversion.

In contrast to the mammalian bone marrow, blood flow in the murine spleen and the open circulation of the human spleen is not bound by vascular endothelium. Inward blood flow in each situation empties into the red pulp where it drains through the splenic cords before re-entering the closed circulation (Steiniger, Bette and Schwarzbach, 2011). Therefore, the erythroid pool in the murine spleen is arguably more accessible than the bone marrow pool and this may explain parasite preference. Furthermore, the expansion and maturation of the erythroid pool within the murine spleen is governed by stress erythropoiesis signalling within a hypoxic environment, compared with the constitutive nature of murine bone marrow erythropoiesis (Reichardt *et al.*, 1998; Bauer *et al.*, 1999).

In contrast to the mouse, the erythropoiesis in humans has defined as predominantly residing in the bone marrow (Nandakumar, Ulirsch and Sankaran,

2016). This would mean that both stress and basal erythropoiesis occur in parallel within the same low hypoxic environment, and consequently the parasite would need to transmigrate out of the vasculature in order to access either erythroid pool. However, it should be noted that extramedullary haematopoiesis (EMH) has been observed within human spleens during disease, such as myeloproliferative disorders, lymphomas, leukaemias and notably beta thalassemia, a hemoglobinapathy under stablising selection in malaria endemic regions (Freedman and Saunders, 1981; Bird *et al.*, 2016). It has even been observed within the spleens of the 'healthy' controls in a multi-organ histology screen of autopsy samples taken from patients with terminal cirrhotic livers (Palitzsch *et al.*, 1987). Splenomegaly is a common feature of human malaria resulting from architectural remodelling and accumulation of parasitised erythrocytes (Engwerda, Beattie and Amante, 2005). Such gross distortions may have masked any the role splenic EMH plays in perpetuation of the *Plasmodium* life cycle and commitment to gametocytogenesis. Moreover, in the *Plasmodium* literature the cellular marker CD71 is used to demark immature erythroid cells (Martín-jaular *et al.*, 2013; Lelliott *et al.*, 2014; Lelliott, Mcmorran and Foote, 2015). As discussed previously, I have shown that CD71 is down regulated in stress erythropoieitic tissue during *Plasmodium* infection, therefore making it an unreliable marker for separating tissue resident from mature erythroid cells in circulation. This, coupled with the open circulation of the splenic cords, may have led histological examinations of the spleen to misinterpret tissue resident infected early reticulocytes as mature circulating erythrocytes (Joice *et al.*, 2014).

Human EMH is not restricted to the spleen, it has been reported within the paravertebral area, intracranial area, liver sinusoids and lymph nodes and is a well-recognised complication of conditions with ineffective hematopoiesis, such as in patients with beta thalassemia (Baden, 2013; Lanigan and Fordham, 2017; Ricchi, 2017; Varshney *et al.*, 2017). These observations imply a wide range of non-bone marrow niches have the capability to support erythropoiesis within the human. Consequently, the observation in this thesis that niches of extramedullary erythropoiesis contribute to significant tissue resident parasite burden and are a source of recrudescence maybe directly relevant to human malaria.

6.3 ART and Malaria Transmission

Work presented in this thesis demonstrated that ART both de-represses and disrupts the expansion of the stress erythropoietic niche in mice in a dose dependent manner. Thus, it would seem that a front-line anti-malarial has the ability to fuel the expansion of the parasite's preferential tissue niche. Moreover, splenic early reticulocytes are the site of preferential gametocyte formation in the host, a feature reflected by the observation of both asexual and sexual parasites in this niche after ART treatment. Thus, the off-target effects of ART may incidentally provide parasites with a niche for evasion of chemotherapy, the evolution of drug resistance, whilst in parallel also promoting the transmission of both sensitive and any subsequent ART resistant parasites. As such, it would be interesting to tease out the dose dependent effects ART on erythroid expansion. The transcriptional changes ART induces directly or indirectly within erythroid cells could be investigated by performing RNAseq on cell-sorted erythroblasts from mice administered different concentrations of the drug. Comparing the transcriptomes from these groups will give an indication of the pathways ART effects and suggest approaches that may avoid these off target, counterprotective effects.

It is important to note that the regulation of human EMH has not been investigated (Paulson, Shi and Wu, 2011). Therefore it is impossible to conclude whether erythroid maturation is governed through similar anatomical, cellular and molecular processes as described in murine splenic stress erythropoiesis (Barminko, Reinholt and Baron, 2016). However, it would be interesting to examine bone marrow and spleen biopsies from malaria patients treated with ART to investigate whether a evident difference in expansion of erythroid cells is observable between the two tissues.

6.4 Conclusion

Taken together the findings reported in this thesis have shown that haematopoietic tissue is an important niche for perpetuating malaria transmission as well as disease recrudescence in the face of drug pressure, both

of which have implications for effective drug treatment and/or transmission control of human infection.

6.5 Further work

There are a number of further experimental routes that my established work could support. These can be broken down into three groups: investigating the infected immature erythroid cell dynamics; characterising the new parasite line; using my model for novel antimalarial screens and examining the evolution of drug resistance.

Further characterisation of the infected erythroid cells:

- Combining my flow-based approach with the $PbGFP_{CON}/RFP_{GAM}$ parasite line would allow for the purification of infected and uninfected immature erythroid cells. These could be used in workflow designed to investigate whether the parasite alters or arrest the maturation of the host cell and if the parasite itself is altered in its gene expression profile as a result of colonising increasingly immature (nucleated) cells of the erythroid lineage. Any alterations in parasite transcriptome in relation to parasitised host cell immaturity should be taken into account in the development of anti-malarials to ensure that parasites within both the circulation and the tissue resident niche are targeted.

Further characterisation of the $PbGFP_{CON}/RFP_{GAM}$ parasite line:

- The early onset of the RFP gametocyte specific promoter (8hrs post invasion) would allow for the purification of early gametocytes. These can then be used in a work flow designed to investigate early gametocyte deformability and the transcriptional profile of both male and female gametocytes.

A model for novel antimalarial screening and the evolution of drug resistance:

- By combining the flow-based approach for detecting immature erythroid cells with the $PbGFP_{CON}/RFP_{GAM}$ parasite line developed in this study, a model to directly test new antimalarials for their effects on erythropoiesis and parasite persistence might be developed. This approach might also be exploited to examine whether this niche offers conditions that might

promote the selection of drug-resistant parasites or enhance parasite transmission.

7. Appendix

8.1. Supplementary material: Chapter 3

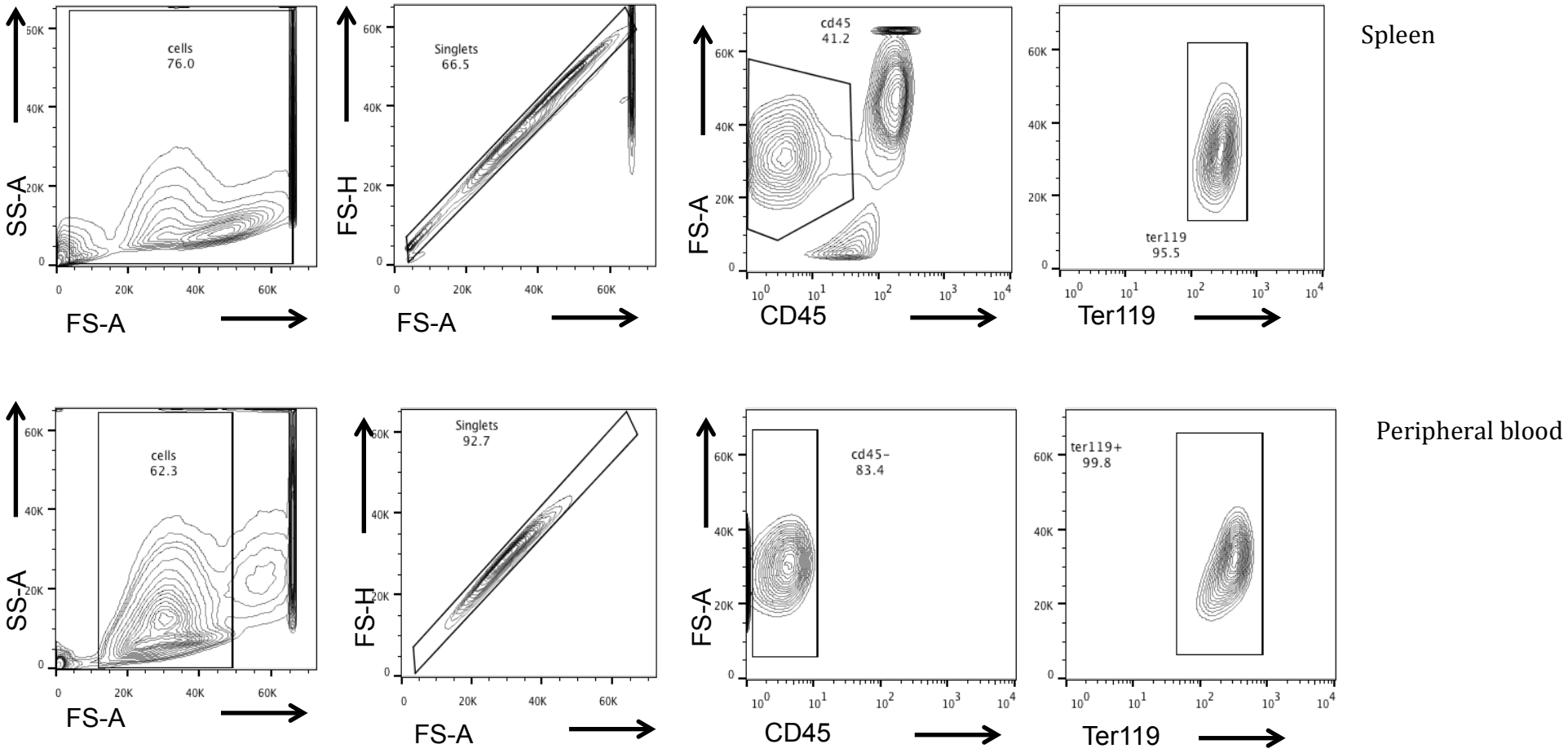

Figure 7.1.1 CD71 is an unreliable marker for resolving different erythroid populations during *P. berghei* infection. Spleen and peripherial blood representative FACS plots.

Spleen

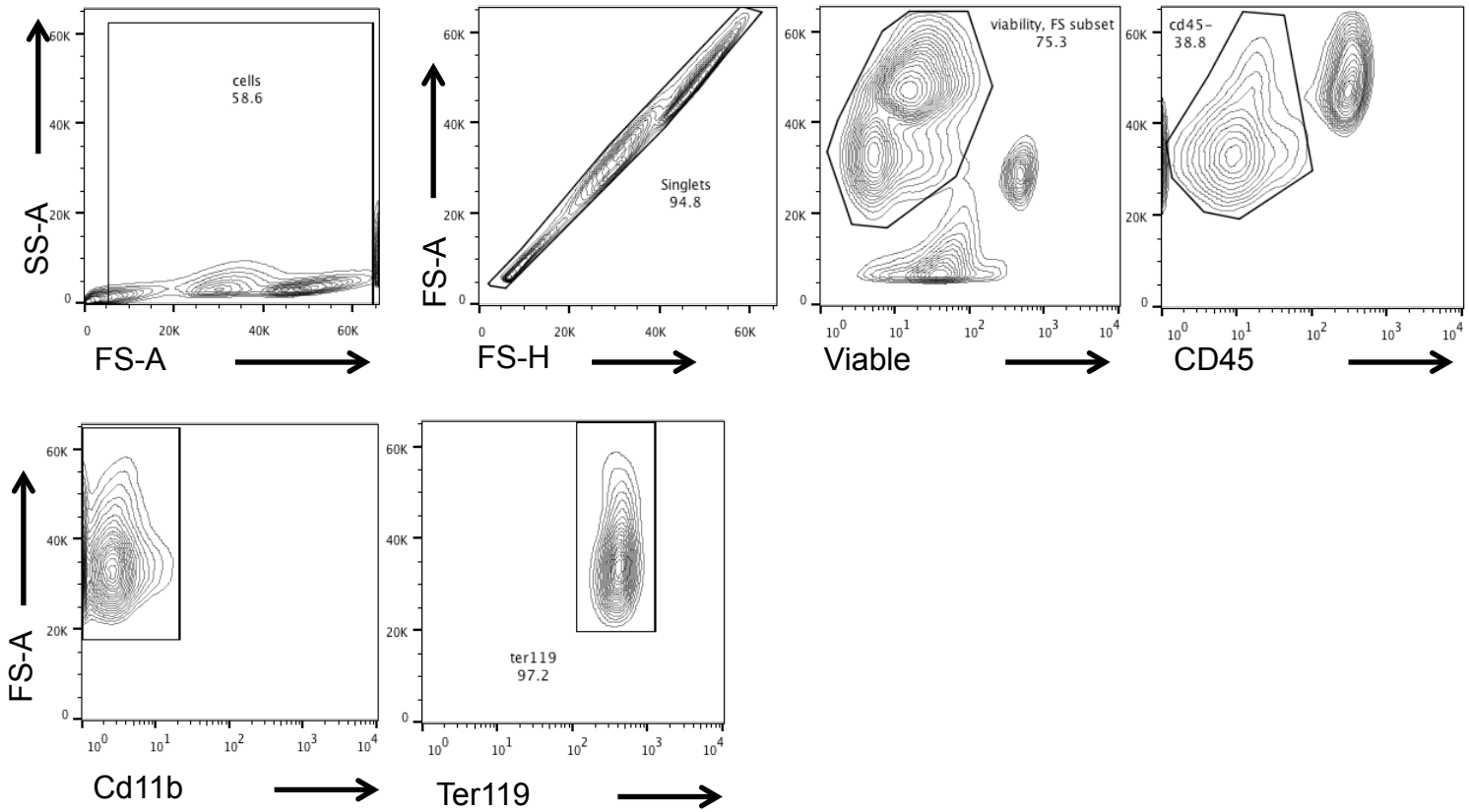

Figure 7.1.2 CD44 vs FS-A gating. Spleen and peripherial blood representative FACS plots.

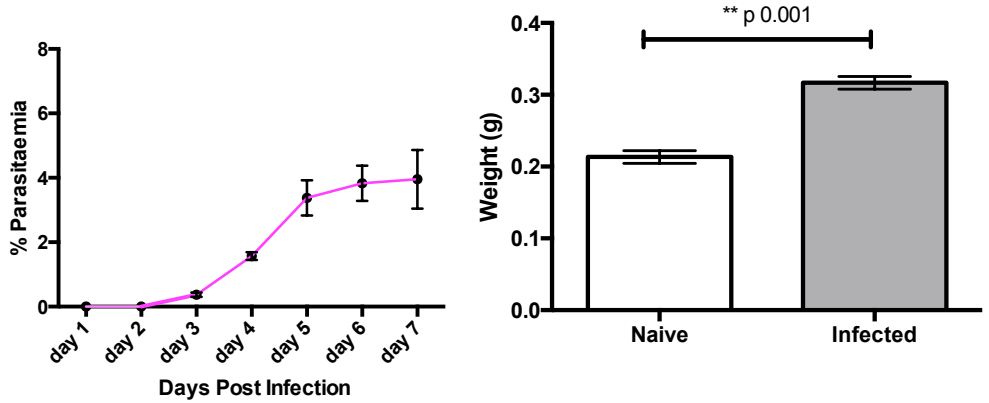

Figure 7.1.3 Peripheral blood parasiteamia (left) and spleen weight on day 7 post infection (right).n= 9. ±SD.

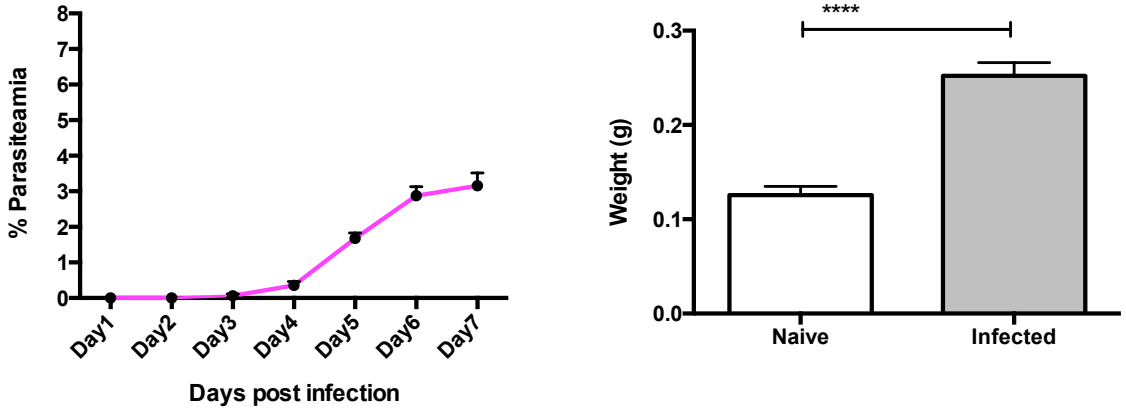

Figure 7.1.4 Peripheral blood parasiteamia (left) and spleen weight on day 7 post infection (right) NIH mice. N= 9. ± SD. Significant difference between groups or samples is indicated with asterisks, denoting as follows: * $p < 0.05$, ** $p < 0.01$, *** $p < 0.001$, **** $p < 0.0001$.

7.2 Supplementary material: Chapter 4

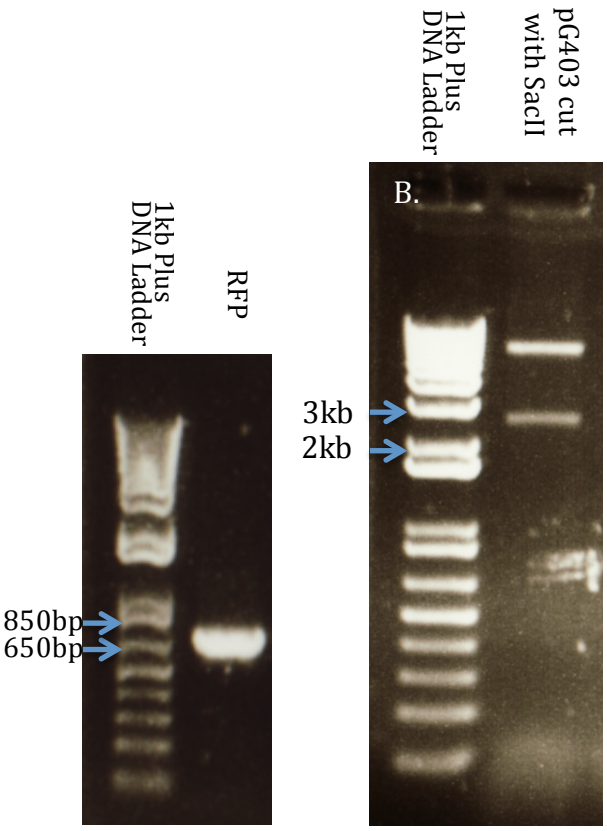

Figure 7.2.1 A. Gel showing amplified RFP fragment. Fragment is 650bp in size. **B.** linearization of pG403 plasmid with SacII. 2.5kb band corresponds to the excised Amp resistance gene. The larger band is the vector band bone to transfect into parasite genome.

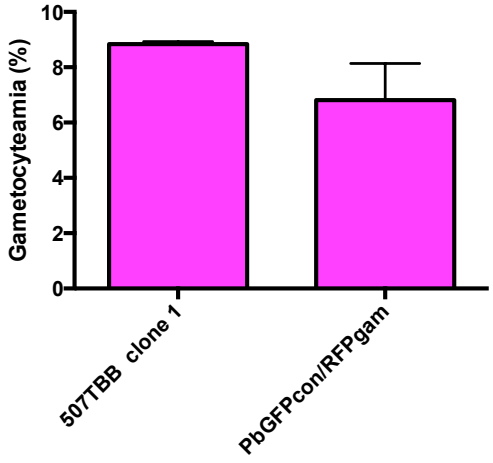

Figure 8.2.2 The Introduction of the RFP_{GAM} cassette does not effect gametocyteamia. ±SD

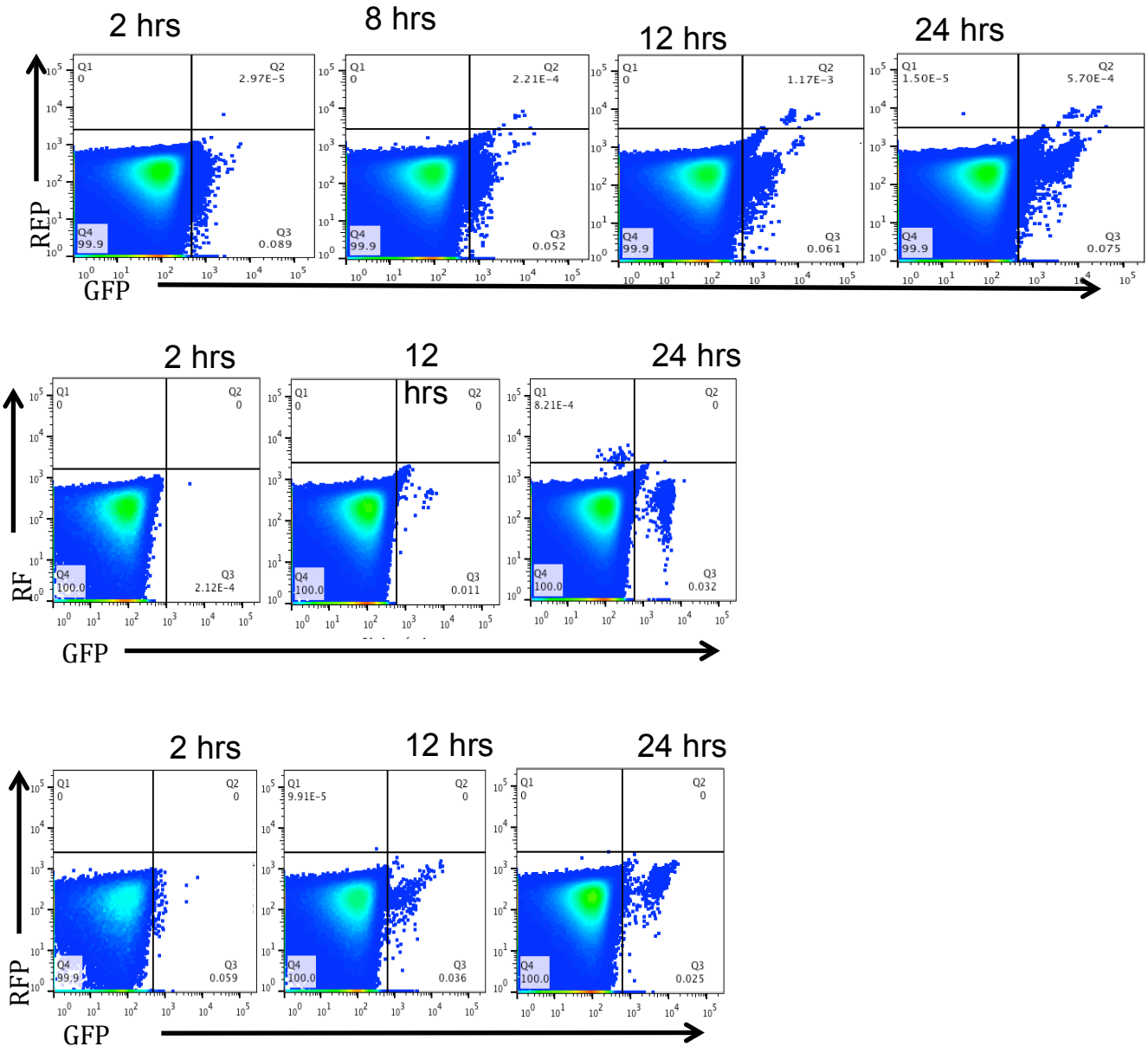

Figure 8.2.3 Representative FACS plots. Top row $PbGFP_{CON}/RFP_{GAM,}$ middle row characterized line 820tbb, bottom row characterized line 507 clon1. 820tbb line contains GFP and RFP fluorophore which are observable from 12hrs post invasion and 22hrs post invasion, respectively . This line was therefore a timing control. 507 clone 1 is the parental line to $PbGFP_{CON}/RFP_{GAM.}$ This line was a RFP-gating control.

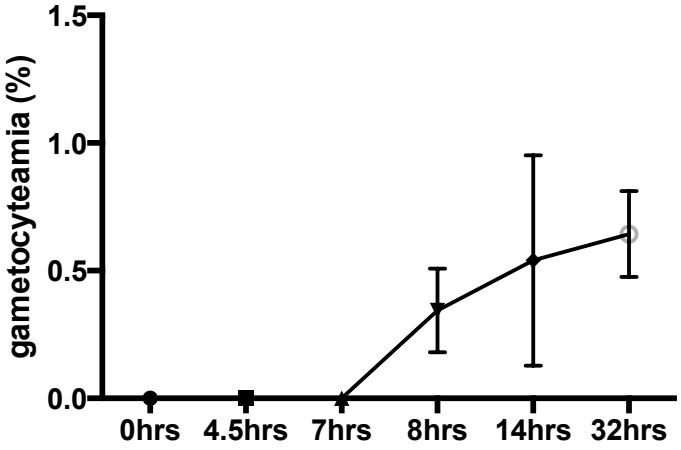

Figure 8.2.4 Gametocytaemia of synchronized PbGFP$_{con}$/RFP$_{GAM}$ in vitro culture. As P. berghei cannot re invade in vitro the gametocyteamia is reflective of the dynamics of the florescent proxy. Hours post invasion on the x-axis. Error bars are ± SD.

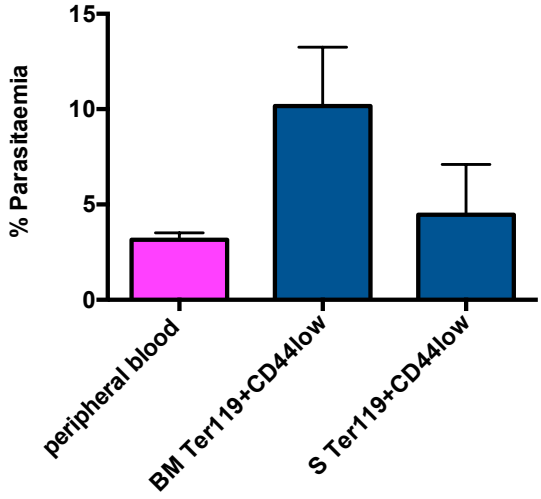

Figure 8.2.5 Parasitaemia of peripheral blood and tissue extracted Ter119^{+}CD44^{low} cells from NIH on day 7 post infection with parasite line 507 clone 1.

BALB/C

A.

	Day 5 pi			Day 6 pi			Day 7 pi		
	S EB	BM ER	BM EB	S EB	BM ER	BM EB	S EB	BM ER	BM EB
S ER	** p = 0.0065	** p = 0.0042	** p = 0.0013	NS = 0.3	*** p = 0.0002	**** p = 0.0001	**** p = 0.0001	**** p = 0.0001	**** p = 0.0001

B.

	Day 5 pi			Day 6 pi			Day 7 pi		
	S EB	BM ER	BM EB	S EB	BM ER	BM EB	S EB	BM ER	BM EB
S ER	NS p = 0.14	NS p = 0.12	NS p = 0.15	NS p = 0.17	** p = 0.009	** p = 0.009	* p = 0.016	* p = 0.013	* p = 0.012

NIH

C.

	Day 5 pi			Day 6 pi			Day 7 pi		
	S EB	BM ER	BM EB	S EB	BM ER	BM EB	S EB	BM ER	BM EB
S ER	NS p = 0.08	NS p = 0.07	NS p = 0.1	* p = 0.01	** p = 0.009	* p = 0.01	* p = 0.01	** p = 0.009	** p = 0.007

D.

	Day 5 pi			Day 6 pi			Day 7 pi		
	S EB	BM ER	BM EB	S EB	BM ER	BM EB	S EB	BM ER	BM EB
S ER	NS p = 0.1	NS p = 0.4	NS p = 0.08	* p = 0.02	NS p = 0.051	* p = 0.01	** p = 0.001	** p = 0.003	** p = 0.001

BALB/c

A

	Day 5 pi			Day 6 pi			Day 7 pi		
	S EB	BM ER	BM EB	S EB	BM ER	BM EB	S EB	BM ER	BM EB
S ER	NS p = 0.051	* p = 0.02	* p = 0.04	NS p = 0.3	** p = 0.006	** p = 0.006	** p = 0.01	** p = 0.009	** p = 0.006

NIH

B

	Day 5 pi			Day 6 pi			Day 7 pi		
	S EB	BM ER	BM EB	S EB	BM ER	BM EB	S EB	BM ER	BM EB
S ER	* p = 0.04	NS p = 0.051	* p = 0.04	* p = 0.01	* p = 0.01	* p = 0.01	* p = 0.01	* p = 0.01	* p = 0.01

BALB/c

C.

	Day 5 pi			Day 6 pi			Day 7 pi		
	S EB	BM ER	BM EB	S EB	BM ER	BM EB	S EB	BM ER	BM EB
S ER	NS p = 0.09	* p = 0.04	* p = 0.04	NS p = 0.1	* p = 0.01	* p = 0.01	** p = 0.01	** p = 0.01	** p = 0.01

NIH

D.

	Day 5 pi			Day 6 pi			Day 7 pi		
	S EB	BM ER	BM EB	S EB	BM ER	BM EB	S EB	BM ER	BM EB
S ER	NS p = 0.08	NS p = 0.07	NS p = 0.1	* p = 0.01	* p = 0.01	** p = 0.009	* p = 0.01	** p = 0.007	** p = 0.009

Figure 8.2.7

A & B. p values generated from ANOVA multiple comparisons of the whole cell numbers of gametocytes in the tissue resident erythroid cells.

C&D. p values generated from ANOVA multiple comparisons of the whole cell numbers of asexual parasites in the tissue resident erythroid cells.

A. BALB/c

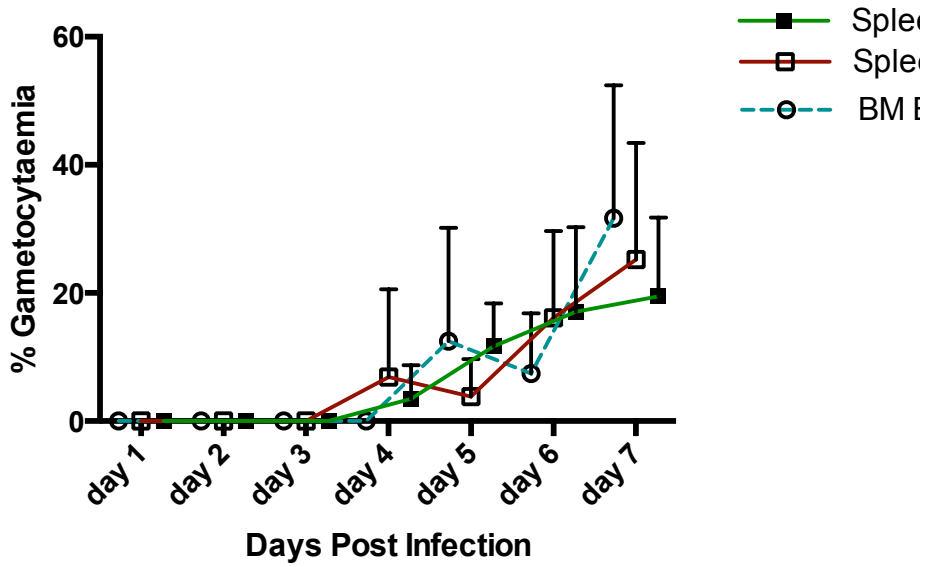

B. NIH

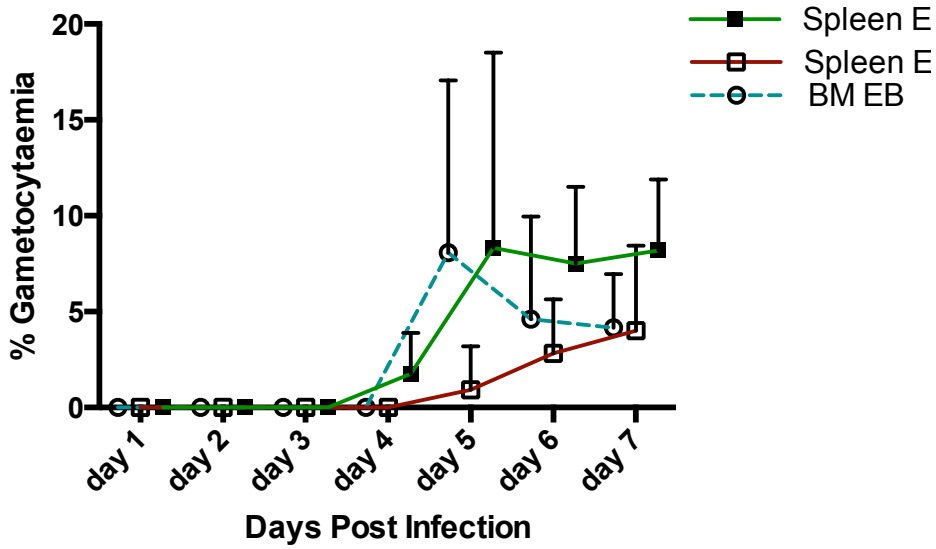

Figure 8.2.8 Gametocytaemia of erythroblastsa and splenic early re across a 7 day infection. The bars represent the data from the organs an lines infer continuous growth. **A.** BALB/ c mice. All time points n=9; day 7 mice. All time points n =6. Error bars ± SEM. Significant difference between s reticulocytes and peripheral blood samples is indicated with asterisks, denotin * $p < 0.05$, ** $p < 0.01$, *** $p < 0.001$, **** $p < 0.0001$. Significance generatec way ANOVA comparison. Significance represents comparison between the s reticulocytes and peripheral blood.

A. BALB/c

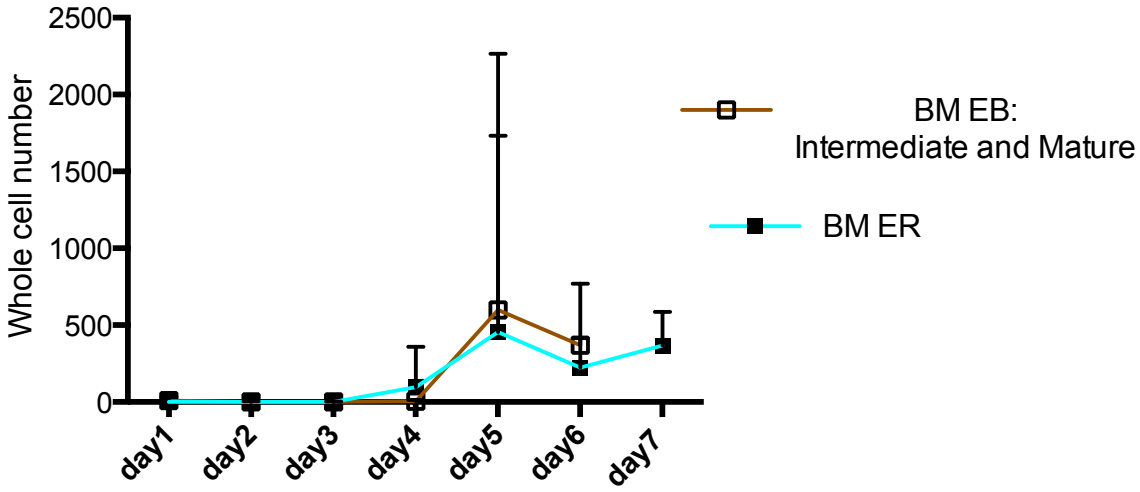

Days pi	Contribution of EB to ER parasites % (± SD)
Day2	0
Day3	0
Day4	0
Day5	103 ± 75
Day6	141 ± 107
Day7	163 ± 157

B. NIH

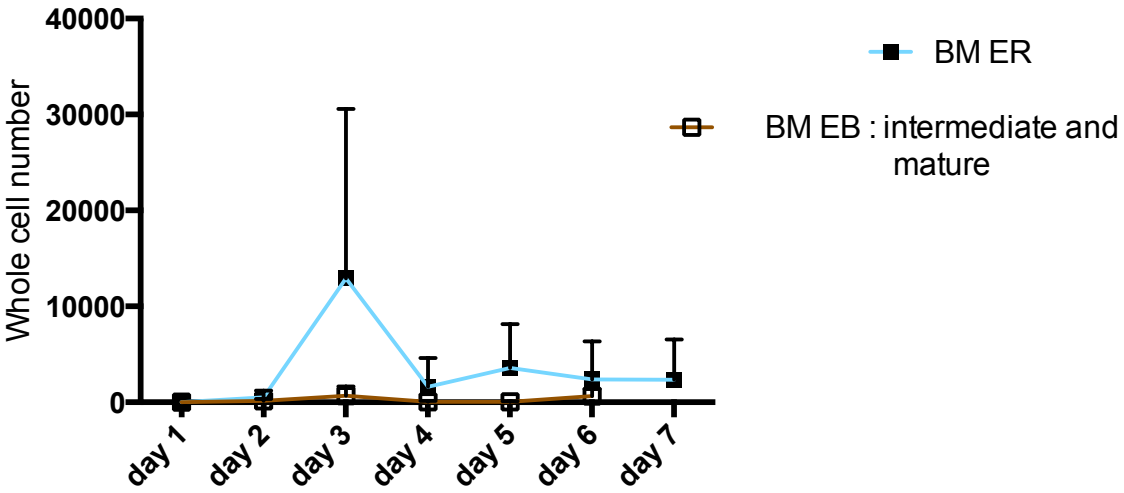

Days pi	Contribution of EB to ER parasites % (± SD)
Day2	0
Day3	0
Day4	0.07 ± 0.1
Day5	1.11 ± 2.73
Day6	87.49 ± 213
Day7	91 ± 112

Figure 8.2.9 Percentage contribution of bone marrow EB parasites to the bone marrow ER parasites population 24 hours later. Plotted on the graph are the mean ± SD whole cell numbers of $GFP^{+}RFP^{-}$ splenic early reticulocytes (ER) and the mean ± SD whole cells numbers of $GFP^{+}RFP^{-}$ splenic intermediate and mature erythroblasts (EB). Tables show the percentage contribution the parasitised splenic intermediate and mature erythroblasts make to the parasitized splenic early reticulocytes population at the ensuing time point ± SD. A. BALB/c mice. All time points n=9; day 7 n=8. B. NIH mice. All time points n=6.

A. BALB/c

Days pi	Contribution of EB to ER gametocytes % (± SD)
Day2	0
Day3	0
Day4	0
Day5	0
Day6	11 ± 21
Day7	34 ± 45

B. NIH

Days pi	Contribution of EB to ER gametocytes % (± SD)
Day2	0
Day3	0
Day4	0
Day5	0
Day6	1 ± 2
Day7	6 ± 11

Figure 8.2.10 Percentage contribution of splenic EB gametocytes to the splenic ER gametocyte population 24 hours later. Tables show the percentage contribution the RFP^+ splenic intermediate and mature erythroblasts make to the RFP^+ splenic early reticulocytes population at the ensuing time point ± SD. A. BALB/c mice. All time points n=9; day 7 n=8. B. NIH mice. All time points n=6.

8.2. Supplementary material: Chapter 5

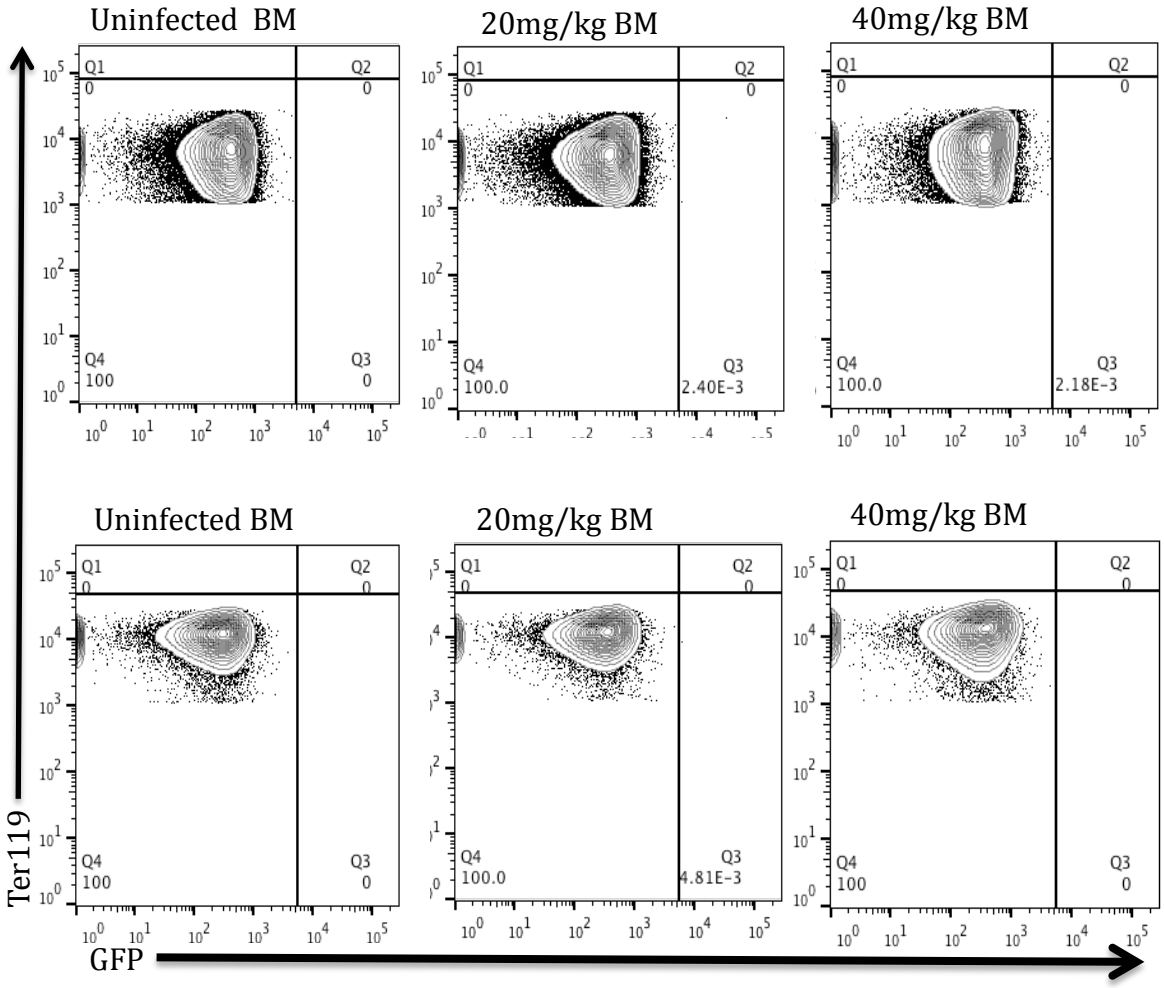

Figure 8.3.1 Representative FACS plots showing bone marrow early reticulocytes from the uninfected vehicle control, 20 mg/kg ART dosed group and the 40 mg/kg ART dosed group.

\

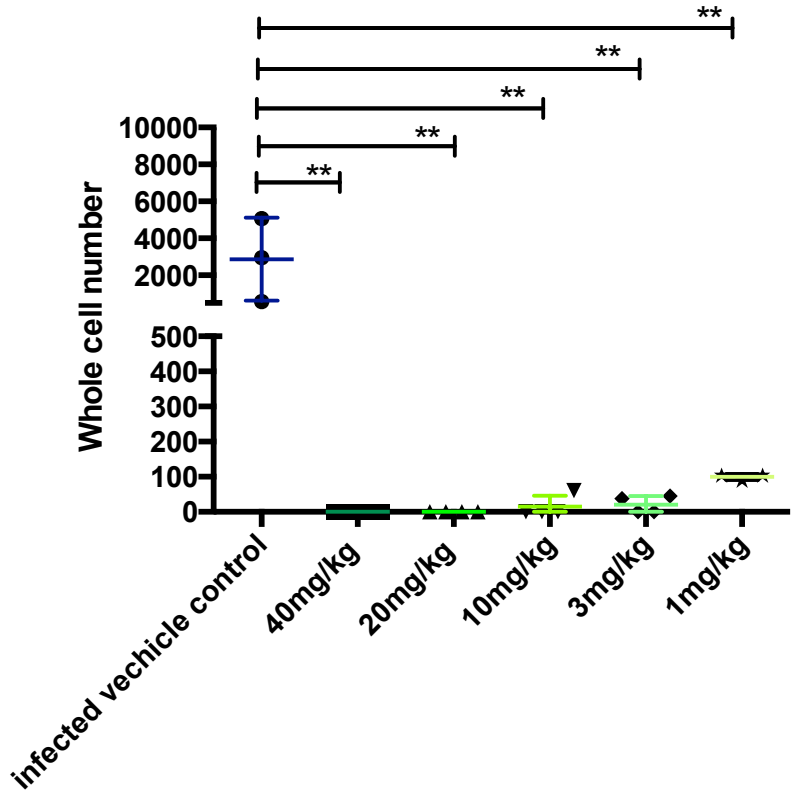

Figure 7.3.2 ART treatment does not increase gametocytogenesis within erythroblasts of BALB/c mice. Whole cell numbers of gametocytes within the splenic erythroblast population of infected BALB/c mice treated with ART.

Appendix 8.3.3

On day 6 pi the average parasitaemia of mice in the 20 mg/kg dosing group was 0.02%. When taking into account that the average BALB/c mouse contains 1ml of blood with 6 x10^6 erythroid cells/µl, it can be extrapolated that the mice on average contained 1200000 parasites on day 6. *P. berghei* has a x 10 replication rate/ 24 hrs (Janse, 2014), as such, it can be extrapolated that on day 4 the mice would need to contain 12000 asexual parasites. On average the mice contained 853 ± 700 asexual parasites in the splenic early reticulocytes on day 4 (Figure 5.5C).

9. References

Abdulsalam, A.H., N. Sabeeh, and B.J. Bain. 2010. Immature Plasmodium falciparum gametocytes in bone marrow. *Am. J. Hematol.* 85:943–943. doi:10.1002/ajh.21796.

Abrahamsen, J., R. Smaaland, S. Rb, L. Od, J.F. Abrahamsen, and O.D. Laerum. 1997. Circadian cell cycle variations of erythro- and myelopoiesis in humans. 333–345.

Acar, M., K.S. Kocherlakota, M.M. Murphy, J.G. Peyer, H. Oguro, C.N. Inra, C. Jaiyeola, Z. Zhao, K. Luby-phelps, and S.J. Morrison. 2015. Stem Cells Are Mainly Perisinusoidal. doi:10.1038/nature15250.

Aguilar, R., A. Magallon-Tejada, A.H. Achtman, C. Moraleda, R. Joice, P. Cisteró, C.S.N. Li Wai Suen, A. Nhabomba, E. Macete, I. Mueller, M. Marti, P.L. Alonso, C. Menéndez, L. Schofield, and A. Mayor. 2014a. Molecular evidence for the localization of plasmodium falciparum immature gametocytes in bone marrow. *Blood.* 123:959–966. doi:10.1182/blood-2013-08-520767.

Aguilar, R., C. Moraleda, A.H. Achtman, A. Mayor, L. Quintó, P. Cisteró, A. Nhabomba, E. Macete, L. Schofield, P.L. Alonso, and C. Menéndez. 2014b. Severity of anaemia is associated with bone marrow haemozoin in children exposed to Plasmodium falciparum. *Br. J. Haematol.* 164:877–887. doi:10.1111/bjh.12716.

Ahouidi, A.D., A. Amambua-Ngwa, G.A. Awandare, A.K. Bei, D.J. Conway, M. Diakite, M.T. Duraisingh, J.C. Rayner, and Z.A. Zenonos. 2016. Malaria Vaccine Development: Focusing Field Erythrocyte Invasion Studies on Phenotypic Diversity: The West African Merozoite Invasion Network (WAMIN). *Trends Parasitol.* 32:274–283. doi:10.1016/j.pt.2015.11.009.

Aingaran, M., R. Zhang, S.K. Law, Z. Peng, A. Undisz, E. Meyer, M. Diez-Silva, T. a. Burke, T. Spielmann, C.T. Lim, S. Suresh, M. Dao, and M. Marti. 2012. Host cell deformability is linked to transmission in the human malaria parasite Plasmodium falciparum. *Cell. Microbiol.* 14:983–993. doi:10.1111/j.1462-5822.2012.01786.x.

Aiuti, B. a, I.J. Webb, C. Bleul, and T. Springer. 1997. New Mechanism to Explain the Mobilization of CD34 ♀ Progenitors to Peripheral Blood. *In Vivo*

(Brooklyn). 185:111–20.

Allen, T., D. Gracieux, M. Talib, D. Tokarz, M. Hensley, J. Cores, A. Vandergriff, J. Tang, J. De Andrade, P.-U. Dinh, J. Ypder, and K. Cheng. 2017. Angiopellosis as an Alternative Mechanism of Cell Extravasation. 170–180.

An, X., M. Christine Lecomte, J.A. Chasis, N. Mohandas, and W. Gratzer. 2002. Shear-response of the spectrin dimer-tetramer equilibrium in the red blood cell membrane. *J. Biol. Chem.* 277:31796–31800. doi:10.1074/jbc.M204567200.

Anderson, J.M., S. Mao, B. Sam, C. Sopha, C.M. Chuor, C. Nguon, S. Sovannaroth, S. Pukrittayakamee, P. Jittamala, K. Chotivanich, K. Chutasmit, C. Suchatsoonthorn, C. V Plowe, K. Stepniewska, P.J. Guerin, A.M. Dondorp, N.P. Day, and N.J. White. 2014a. Spread of Artemisinin Resistance in. doi:10.1056/NEJMoa1314981.

Anderson, K.G., K. Mayer-Barber, H. Sung, L. Beura, B.R. James, J.J. Taylor, L. Qunaj, T.S. Griffith, V. Vezys, D.L. Barber, and D. Masopust. 2014b. Intravascular staining for discrimination of vascular and tissue leukocytes. *Nat. Protoc.* 9:209–222. doi:10.1038/nprot.2014.005.

Anderson, K.G., H. Sung, C.N. Skon, L. Lefrancois, A. Deisinger, V. Vezys, and D. Masopust. 2012. Cutting Edge: Intravascular Staining Redefines Lung CD8 T Cell Responses. *J. Immunol.* 189:2702–2706. doi:10.4049/jimmunol.1201682.

Angel, D.I., A. Mongui, J. Ardila, M. Vanegas, and M.A. Patarroyo. 2008. The Plasmodium vivax Pv41 surface protein: Identification and characterization. *Biochem. Biophys. Res. Commun.* 377:1113–1117. doi:10.1016/j.bbrc.2008.10.129.

Apostolakis, S., G.K. Chalikias, D.N. Tziakas, and S. Konstantinides. 2011. Erythrocyte Duffy antigen receptor for chemokines (DARC): diagnostic and therapeutic implications in atherosclerotic cardiovascular disease. *Acta Pharmacol. Sin.* 32:417–24. doi:10.1038/aps.2011.13.

Arguin, P.M. 2017. Case definition : postartemisinin delayed hemolysis A microRNA involved in the germinal center reaction. 124:157–159.

Arisue, N., T. Hashimoto, H. Mitsui, N.M.Q. Palacpac, A. Kaneko, S. Kawai, M. Hasegawa, K. Tanabe, and T. Horii. 2012. The plasmodium apicoplast genome: Conserved structure and close relationship of P. ovale to rodent malaria parasites. *Mol. Biol. Evol.* 29:2095–2099. doi:10.1093/molbev/mss082.

Babon, J.J., W.D. Morgan, G. Kelly, J.F. Eccleston, J. Feeney, and A.A. Holder. 2007. Structural studies on Plasmodium vivax merozoite surface protein-1. *Mol. Biochem. Parasitol.* 153:31–40. doi:10.1016/j.molbiopara.2007.01.015.

Badalà, F., K. Nouri-mahdavi, and D.A. Raoof. 2008. NIH Public Access. *Computer (Long. Beach. Calif).* 144:724–732. doi:10.1038/jid.2014.371.

Baden, L. 2013. Extramedullary Hematopoiesis in Thalassemia. 2017. doi:10.1056/NEJMicm1303084.

Baldwin, M.R., X. Li, T. Hanada, S.C. Liu, and A.H. Chishti. 2015. Merozoite surface protein 1 recognition of host glycophorin a mediates malaria parasite invasion of red blood cells. *Blood.* 125:2704–2711. doi:10.1182/blood-2014-11-611707.

Balogh, P. 2011. Developmental biology of peripheral lymphoid organs. *Dev. Biol. Peripher. Lymphoid Organs.* 1–177. doi:10.1007/978-3-642-14429-5.

Bannister, L.H., J.M. Hopkins, R.E. Fowler, S. Krishna, and G.H. Mitchell. 2000. A brief illustrated guide to the ultrastructure of Plasmodium falciparum asexual blood stages. *Parasitol. Today.* 16:427–433. doi:10.1016/S0169-4758(00)01755-5.

Bargieri, D., V. Lagal, N. Andenmatten, I. Tardieux, M. Meissner, and R. Ménard. 2014. Host Cell Invasion by Apicomplexan Parasites: The Junction Conundrum. *PLoS Pathog.* 10:1–9. doi:10.1371/journal.ppat.1004273.

Bargieri, D.Y., N. Andenmatten, V. Lagal, S. Thiberge, J.A. Whitelaw, I. Tardieux, M. Meissner, and R. Ménard. 2013. Apical membrane antigen 1 mediates apicomplexan parasite attachment but is dispensable for host cell invasion. *Nat. Commun.* 4:2552. doi:10.1038/ncomms3552.

Barminko, J., B. Reinholt, and M.H. Baron. 2016. Development and differentiation of the erythroid lineage in mammals. *Dev. Comp. Immunol.* 58:18–29. doi:10.1016/j.dci.2015.12.012.

Barnes, K.I., F. Little, P.J. Smith, A. Evans, W.M. Watkins, and N.J. White. 2006. Sulfadoxine-pyrimethamine pharmacokinetics in malaria: Pediatric dosing implications. *Clin. Pharmacol. Ther.* 80:582–596. doi:10.1016/j.clpt.2006.08.016.

Bártfai, R., W.A.M. Hoeijmakers, A.M. Salcedo-Amaya, A.H. Smits, E. Janssen-Megens, A. Kaan, M. Treeck, T.W. Gilberger, K.J. Franc ̧oijs, and H.G. Stunnenberg. 2010. H2A.Z demarcates intergenic regions of the Plasmodium falciparum epigenome that are dynamically marked by H3K9ac and

H3K4me3. *PLoS Pathog*. 6. doi:10.1371/journal.ppat.1001223.

Bartholdson, S.J., L.Y. Bustamante, C. Crosnier, S. Johnson, S. Lea, J.C. Rayner, and G.J. Wright. 2012. Semaphorin-7A Is an Erythrocyte Receptor for P. falciparum Merozoite-Specific TRAP Homolog, MTRAP. *PLoS Pathog*. 8. doi:10.1371/journal.ppat.1003031.

Baruch, D., B. Pasloske, H. Singh, X. Bi, X. Ma, M. Feldman, T. Taraschi, and R. Howard. 1995. Cloning the P . falciparum Gene Encoding PfEMPl , a Malarial Variant Antigen and Adherence Receptor on the Surface of Parasitized Human Erythrocytes. 92.

Bauer, A., F. Tronche, O. Wessely, C. Kellendonk, H.M. Reichardt, and P. Steinlein. 1999. The glucocorticoid receptor is required for stress erythropoiesis The glucocorticoid receptor is required for stress erythropoiesis. *Genes Dev*. 13:2996–3002. doi:10.1101/gad.13.22.2996.

Baum, J., T.W. Gilberger, F. Frischknecht, and M. Meissner. 2008. Host-cell invasion by malaria parasites: insights from Plasmodium and Toxoplasma. *Trends Parasitol*. 24:557–563. doi:10.1016/j.pt.2008.08.006.

Baum, J., D. Richard, J. Healer, M. Rug, Z. Krnajski, T.W. Gilberger, J.L. Green, A.A. Holder, and A.F. Cowman. 2006. A conserved molecular motor drives cell invasion and gliding motility across malaria life cycle stages and other apicomplexan parasites. *J. Biol. Chem*. 281:5197–5208. doi:10.1074/jbc.M509807200.

Baumgärtner, F., J. Jourdan, C. Scheurer, B. Blasco, B. Campo, P. Mäser, and S. Wittlin. 2017. In vitro activity of anti - malarial ozonides against an artemisinin - resistant isolate. *Malar. J*. 10–15. doi:10.1186/s12936-017-1696-0.

Bei, A.K., and M.T. Duraisingh. 2012. Functional analysis of erythrocyte determinants of Plasmodium infection. *Int. J. Parasitol*. 42:575–582. doi:10.1016/j.ijpara.2012.03.006.

Berendt, A.R., D.L. Simmons, J. Tansey, C.I. Newbold, and K. Marsh. 1989. Intercellular adhesion molecule-1 is an endothelial cell adhesion receptor for Plasmodium falciparum. *Nature*. 341:57–59. doi:10.1038/341057a0.

Bernabeu, M., F.J. Lopez, M. Ferrer, L. Martin-Jaular, A. Razaname, G. Corradin, A.G. Maier, H.A. del Portillo, and C. Fernandez-Becerra. 2012. Functional analysis of Plasmodium vivax VIR proteins reveals different subcellular localizations and cytoadherence to the ICAM-1 endothelial

receptor. *Cell. Microbiol.* 14:386–400. doi:10.1111/j.1462-5822.2011.01726.x.

Binh, T.Q., T.M.E. Davis, W. Johnston, L.T.A. Thu, R. Boston, P.T. Danh, and T.K. Anh. 1997. Glucose metabolism in severe malaria: Minimal model analysis of the intravenous glucose tolerance test incorporating a stable glucose label. *Metabolism.* 46:1435–1440. doi:10.1016/S0026-0495(97)90144-X.

Bird, E.M., U. Parameswaran, T. William, T.M. Khoo, M.J. Grigg, A. Aziz, J. Marfurt, T.W. Yeo, S. Auburn, N.M. Anstey, and B.E. Barber. 2016. Transfusion - transmitted severe Plasmodium knowlesi malaria in a splenectomized patient with beta - thalassaemia major in Sabah , Malaysia : a case report. *Malar. J.* 1–6. doi:10.1186/s12936-016-1398-z.

Black, C.G., J.W. Barnwell, C.S. Huber, M.R. Galinski, and R.L. Coppel. 2002. The Plasmodium vivax homologues of merozoite surface proteins 4 and 5 from Plasmodium falciparum are expressed at different locations in the merozoite. *Mol. Biochem. Parasitol.* 120:215–224. doi:10.1016/S0166-6851(01)00458-3.

Black, C.G., L. Wang, T. Wu, and R.L. Coppel. 2003. Apical location of a novel EGF-like domain-containing protein of Plasmodium falciparum. *Mol. Biochem. Parasitol.* 127:59–68. doi:10.1016/S0166-6851(02)00308-0.

Black, C.G., T. Wu, L. Wang, A.R. Hibbs, and R.L. Coppel. 2001. Merozoite surface protein 8 of Plasmodium falciparum contains two epidermal growth factor-like domains. *Mol. Biochem. Parasitol.* 114:217–226. doi:10.1016/S0166-6851(01)00265-1.

Blythe, J.E., Y.Y. Xue, C. Kuss, Z. Bozdech, A.A. Holder, K. Marsh, J. Langhorne, and P.R. Preiser. 2008. Plasmodium falciparum STEVOR proteins are highly expressed in patient isolates and located in the surface membranes of infected red blood cells and the apical tips of merozoites. *Infect. Immun.* 76:3329–3336. doi:10.1128/IAI.01460-07.

Boctor, F.N., and R.P. Dorion. 2008. Malaria and Hereditary Elliptocytosis. 35105. doi:10.1002/ajh.21018.

Bony, V., P. Gane, P. Bailly, and J.P. Cartron. 1999. Time-course expression of polypeptides carrying blood group antigens during human erythroid differentiation. *Br. J. Haematol.* 107:263–274. doi:bjh1721 [pii].

Bourin, P., A.F. Ledain, J. Beau, and D. Mille. 2009. In-vitro circadian rhythm of

murine bone marrow progenitor production. 528. doi:10.1081/CBI-120002677.

Branch, O.H., V. Udhayakumar, A.W. Hightower, A.J. Oloo, W.A. Hawley, B.L. Nahlen, P.B. Bloland, D.C. Kaslow, and A.A. Lal. 1998. A longitudinal investigation of IgG and IgM antibody responses to the merozoite surface protein-1 19-kilodalton domain of Plasmodium falciparum in pregnant women and infants: Associations with febrile illness, parasitemia, and anemia. *Am. J. Trop. Med. Hyg.* 58:211–219.

Brancucci, N.M.B., N.L. Bertschi, L. Zhu, I. Niederwieser, W.H. Chin, R. Wampfler, C. Freymond, M. Rottmann, I. Felger, Z. Bozdech, and T.S. Voss. 2014. Heterochromatin protein 1 secures survival and transmission of malaria parasites. *Cell Host Microbe*. 16:165–176. doi:10.1016/j.chom.2014.07.004.

Brochet, M., and O. Billker. 2016. Calcium signalling in malaria parasites. *Mol. Microbiol*. 100:397–408. doi:10.1111/mmi.13324.

Broxmeyer, H.E., C.M. Orschell, D.W. Clapp, G. Hangoc, S. Cooper, P.A. Plett, W.C. Liles, X. Li, B. Graham-Evans, T.B. Campbell, G. Calandra, G. Bridger, D.C. Dale, and E.F. Srour. 2005. Rapid Mobilization of Murine and Human Hematopoietic Stem and Progenitor Cells with AMD3100, a CXCR4 antagonist. *J. Exp. Med.* 201:1307–1318. doi:10.1084/jem.20041385.

Bruce, M.C., P. Alano, S. Duthie, and R. Carter. 1990. Commitment of the malaria parasite Plasmodium falciparum to sexual and asexual development. *Parasitology*. 100 Pt 2:191–200. doi:10.1017/S0031182000061199.

Buffet, P.A., I. Safeukui, G. Deplaine, V. Brousse, and V. Prendki. 2011. Review Article : The pathogenesis of Plasmodium falciparum ... The pathogenesis of Plasmodium falciparum malaria in humans : insights from splenic physiology Review Article : The pathogenesis of Plasmodium falciparum ... 117:381–392. doi:10.1182/blood-2010-04-202911.

Bunnik, E.M., A. Polishko, J. Prudhomme, N. Ponts, S.S. Gill, S. Lonardi, and K.G. Le Roch. 2014. DNA-encoded nucleosome occupancy is associated with transcription levels in the human malaria parasite Plasmodium falciparum. *BMC Genomics*. 15:347. doi:10.1186/1471-2164-15-347.

Buscaglia, C.., I. Coppens, W.. Hol, and V. Nussezweig. 2004. Sites of Interaction between Aldolase and Thrombospondin-related Anonymous Protein in Plasmodium. *Mol. Biol. Cell*. 15:3751–3737. doi:10.1091/mbc.E03.

Bwijo, B., M.H. Alin, N. Abbas, W. Wernsdorfer, and a Björkman. 1997. Efficacy of artemisinin and mefloquine combinations against Plasmodium falciparum. In vitro simulation of in vivo pharmacokinetics. *Trop. Med. Int. Health*. 2:461–467.

C.River. 2017. http://www.criver.com/products-services/basic-research/find-a-model/jax-mice-strain-nod-scid-gamma-(nsg).

Campos, F.M.F., B.S. Franklin, A. Teixeira-carvalho, A.L.S. Filho, S.C.O. De Paula, C.J. Fontes, C.F. Brito, and L.H. Carvalho. 2010. Augmented plasma microparticles during acute Plasmodium vivax infection. 1–8.

Carayon, K., K. Chaoui, E. Ronzier, I. Lazar, J. Bertrand-Michel, V. Roques, S. Balor, F. Terce, A. Lopez, L. Salom??, and E. Joly. 2011. Proteolipidic composition of exosomes changes during reticulocyte maturation. *J. Biol. Chem.* 286:34426–34439. doi:10.1074/jbc.M111.257444.

Carlton, J.M., J.H. Adams, J.C. Silva, S.L. Bidwell, H. Lorenzi, E. Caler, J. Crabtree, S. V Angiuoli, E.F. Merino, P. Amedeo, Q. Cheng, R.M.R. Coulson, B.S. Crabb, H.A. Del Portillo, K. Essien, T. V Feldblyum, C. Fernandez-Becerra, P.R. Gilson, A.H. Gueye, X. Guo, S. Kang'a, T.W.A. Kooij, M. Korsinczky, E.V.-S. Meyer, V. Nene, I. Paulsen, O. White, S.A. Ralph, Q. Ren, T.J. Sargeant, S.L. Salzberg, C.J. Stoeckert, S.A. Sullivan, M.M. Yamamoto, S.L. Hoffman, J.R. Wortman, M.J. Gardner, M.R. Galinski, J.W. Barnwell, and C.M. Fraser-Liggett. 2008. Comparative genomics of the neglected human malaria parasite Plasmodium vivax. *Nature*. 455:757–63. doi:10.1038/nature07327.

Carvalho, B.O., S.C.P. Lopes, P.A. Nogueira, P.P. Orlandi, D.Y. Bargieri, Y.C. Blanco, R. Mamoni, J.A. Leite, M.M. Rodrigues, I.S. Soares, T.R. Oliveira, G. Wunderlich, M.V.G. Lacerda, H.A. del Portillo, M.O.G. Araújo, B. Russell, R. Suwanarusk, G. Snounou, L. Rénia, and F.T.M. Costa. 2010. On the Cytoadhesion of *Plasmodium vivax* –Infected Erythrocytes. *J. Infect. Dis.* 202:638–647. doi:10.1086/654815.

Castillo, A.I., M. Andreína Pacheco, and A.A. Escalante. 2017. Evolution of the merozoite surface protein 7 (msp7) family in Plasmodium vivax and P. falciparum: A comparative approach. *Infect. Genet. Evol.* 50:7–19. doi:10.1016/j.meegid.2017.01.024.

Cavill, I. 2002. Erythropoiesis and iron. *Best Pract. Res. Clin. Haematol.* 15:399–409. doi:10.1016/S1521-6926(02)90004-6.

Cesta, M.F. 2006a. Normal Structure , Function , and Histology of the Spleen. 455–465. doi:10.1080/01926230600867743.

Cesta, M.F. 2006b. Normal structure, function, and histology of the spleen. *Toxicol. Pathol.* 34:455–65. doi:10.1080/01926230600867743.

Chais, A.J., M.E. Reid, R.H. Jensen, N. Mohandas, and J.A. Chasis. 2011. A : by Glycophorin Signal Transduction and Cytoplasmic Role of Extracellular Process in a Modulatable Domains. 107:1351–1357.

Chang, H.-H., E. Meibalan, J. Zelin, R. Daniels, A.C. Eziefula, E.C. Meyer, F. Tadesse, L. Grignard, R.C. Joice, C. Drakeley, D.F. Wirth, S.K. Volkman, C. Buckee, T. Bousema, and M. Marti. 2016. Persistence of Plasmodium falciparum parasitemia after artemisinin combination therapy: evidence from a randomized trial in Uganda. *Sci. Rep.* 6:26330. doi:10.1038/srep26330.

Chang, K.H., and M.M. Stevenson. 2004. Malarial anaemia: Mechanisms and implications of insufficient erythropoiesis during blood-stage malaria. *Int. J. Parasitol.* 34:1501–1516. doi:10.1016/j.ijpara.2004.10.008.

Chang, K.H., M. Tam, and M.M. Stevenson. 2004. Inappropriately low reticulocytosis in severe malarial anemia correlates with suppression in the development of late erythroid precursors. *Blood.* 103:3727–3735. doi:10.1182/blood-2003-08-2887.

Chasis, J.A., and N. Mohandas. 2009. Erythroblastic islands : niches for erythropoiesis ASH 50th anniversary review Erythroblastic islands : niches for erythropoiesis. *Cell.* 112:470–478. doi:10.1182/blood-2008-03-077883.

Cheeseman, I.H., B.A. Miller, S. Nair, S. Nkhoma, A. Tan, J.C. Tan, S. Al Saai, A.P. Phyo, C.L. Moo, K.M. Lwin, R. Mcgready, E. Ashley, M. Imwong, K. Stepniewska, P. Yi, A.M. Dondorp, M. Mayxay, P.N. Newton, N.J. White, F. Nosten, M.T. Ferdig, and T.J.C. Anderson. 2012. A Major Genome Region Underlying Artemisinin Resistance in Malaria. 1481.

Chen, K., J. Liu, S. Heck, J. a Chasis, X. An, and N. Mohandas. 2009. Resolving the distinct stages in erythroid differentiation based on dynamic changes in membrane protein expression during erythropoiesis. *Proc. Natl. Acad. Sci. U. S. A.* 106:17413–17418. doi:10.1073/pnas.0909296106.

Cheng, C., W.E. Ho, F.Y. Goh, S.P. Guan, L.R. Kong, W.Q. Lai, B.P. Leung, and W.S.F. Wong. 2011. Anti-malarial drug artesunate attenuates experimental allergic asthma via inhibition of the phosphoinositide 3-kinase/Akt pathway.

PLoS One. 6. doi:10.1371/journal.pone.0020932.

Cheng, Q., D.E. Kyle, and M.L. Gatton. 2012. Artemisinin resistance in plasmodium falciparum: A process linked to dormancy? *Int. J. Parasitol. Drugs Drug Resist*. 2:249–255. doi:10.1016/j.ijpddr.2012.01.001.

Cheng, Y., Y. Wang, D. Ito, D.H. Kong, K.S. Ha, J.H. Chen, F. Lu, J. Li, B. Wang, E. Takashim, J. Sattabongkot, T. Tsuboi, and E.T. Han. 2013. The plasmodium vivax merozoite surface protein 1 paralog is a novel erythrocyte-binding ligand of p. vivax. *Infect. Immun.* 81:1585–1595. doi:10.1128/IAI.01117-12.

Chinappi, M., A. Via, P. Marcatili, and A. Tramontano. 2010. On the mechanism of chloroquine resistance in Plasmodium falciparum. *PLoS One*. 5. doi:10.1371/journal.pone.0014064.

Chotivanich, K., R. Udomsangpetch, R. Suwanarusk, S. Pukrittayakamee, P. Wilairatana, J.G. Beeson, N.P.J. Day, and N.J. White. 2012. Plasmodium vivax adherence to placental glycosaminoglycans. *PLoS One*. 7:1–7. doi:10.1371/journal.pone.0034509.

Chow, A., M. Huggins, J. Ahmed, D. Hashimoto, D. Lucas, Y. Kunisaki, S. Pinho, M. Leboeuf, C. Noizat, N. van Rooijen, M. Tanaka, Z.J. Zhao, A. Bergman, M. Merad, and P.S. Frenette. 2013. $CD169^{+}$ macrophages provide a niche promoting erythropoiesis under homeostasis and stress. *Nat. Med.* 19:429–36. doi:10.1038/nm.3057.

Chow, A., D. Lucas, A. Hidalgo, S. Méndez-Ferrer, D. Hashimoto, C. Scheiermann, M. Battista, M. Leboeuf, C. Prophete, N. van Rooijen, M. Tanaka, M. Merad, and P.S. Frenette. 2011. Bone marrow CD169+ macrophages promote the retention of hematopoietic stem and progenitor cells in the mesenchymal stem cell niche. *J. Exp. Med.* 208:261–271. doi:10.1084/jem.20101688.

Chris J Janse, J.R.& A.P.W. 2006. High-efficiency transfection and drug selection of genetically transformed blood stages of the rodent malaria parasite Plasmodium berghei. *Nat. Protoc.* 1:614–623. doi:10.1038/nprot.2006.88.

Claessens, A., W.L. Hamilton, M. Kekre, T.D. Otto, A. Faizullabhoy, J.C. Rayner, and D. Kwiatkowski. 2014. Generation of Antigenic Diversity in Plasmodium falciparum by Structured Rearrangement of Var Genes During Mitosis. *PLoS Genet*. 10. doi:10.1371/journal.pgen.1004812.

Clark, J.T., S. Donachie, R. Anand, C.F. Wilson, H.G. Heidrich, and J.S. McBride.

1989. 46-53 Kilodalton glycoprotein from the surface of Plasmodium falciparum merozoites. *Mol. Biochem. Parasitol.* 32:15–24. doi:10.1016/0166-6851(89)90125-4.

Clark, M.A., M.M. Goheen, and C. Cerami. 2014. Influence of host iron status on Plasmodium falciparum infection. 5:1–12. doi:10.3389/fphar.2014.00084.

Claser, C., B. Malleret, K. Peng, N. Bakocevic, S.Y. Gun, B. Russell, L.G. Ng, and L. Rénia. 2014. Rodent Plasmodium-infected red blood cells: Imaging their fates and interactions within their hosts. *Parasitol. Int.* 63:187–194. doi:10.1016/j.parint.2013.07.012.

Coleman, B.I., U. Ribacke, M. Manary, A.K. Bei, E.A. Winzeler, D.F. Wirth, and M.T. Duraisingh. 2012. Nuclear repositioning precedes promoter accessibility and is linked to the switching frequency of a plasmodium falciparum invasion gene. *Cell Host Microbe*. 12:739–750. doi:10.1016/j.chom.2012.11.004.

Coleman, B.I., K.M. Skillman, R.H.Y. Jiang, L.M. Childs, L.M. Altenhofen, F.C. Kafsack, M. Marti, M. Llina, M. Ganter, Y. Leung, I. Goldowitz, C.O. Buckee, and M.T. Duraisingh. 2014. Article A Plasmodium falciparum Histone Deacetylase Regulates Antigenic Variation and Gametocyte Conversion. 177–186. doi:10.1016/j.chom.2014.06.014.

Combes, V., N. Coltel, M. Van Eck, G.E. Grau, and G. Chimini. 2005. ABCA1 Gene Deletion Protects against Cerebral Malaria Potential Pathogenic Role of Microparticles in Neuropathology. 166:295–302. doi:10.1016/S0002-9440(10)62253-5.

Cortés, A. 2008. Switching Plasmodium falciparum genes on and off for erythrocyte invasion. *Trends Parasitol.* 24:517–524. doi:10.1016/j.pt.2008.08.005.

Cowman, A.F., D.L. Baldi, J. Healer, K.E. Mills, R.A. O'Donnell, M.B. Reed, T. Triglia, M.E. Wickham, and B.S. Crabb. 2015. Functional analysis of proteins involved in Plasmodium falciparum merozoite invasion of red blood cells. *FEBS Lett.* 476:84–88. doi:10.1016/S0014-5793(00)01703-8.

Crabb, B.S., B.M. Cooke, J.C. Reeder, R.F. Waller, S.R. Caruana, K.M. Davern, M.E. Wickham, G. V Brown, R.L. Coppel, and a F. Cowman. 1997. Targeted gene disruption shows that knobs enable malaria-infected red cells to cytoadhere under physiological shear stress. *Cell.* 89:287–296. doi:10.1016/S0092-8674(00)80207-X.

Craig, A.G., G.E. Grau, C. Janse, J.W. Kazura, D. Milner, J.W. Barnwell, G. Turner, and J. Langhorne. 2012. The role of animal models for research on severe malaria. *PLoS Pathog.* 8. doi:10.1371/journal.ppat.1002401.

Cromer, D., K.J. Evans, L. Schofield, and M.P. Davenport. 2006. Preferential invasion of reticulocytes during late-stage Plasmodium berghei infection accounts for reduced circulating reticulocyte levels. *Int. J. Parasitol.* 36:1389–1397. doi:10.1016/j.ijpara.2006.07.009.

Cyrklaff, M., C.P. Sanchez, N. Kilian, C. Bisseye, J. Simpore, F. Frischknecht, and M. Lanzer. 2010. Reports 28. 1048.

Day, K.P., R.E. Hayward, D. Smith, and J.G. Culvenor. 1998. CD36-dependent adhesion and knob expression of the transmission stages of Plasmodium falciparum is stage-specific. *Mol. Biochem. Parasitol.* 93:167–177. doi:Doi 10.1016/S0166-6851(98)00040-1.

Dearnley, M.K., J. a. Yeoman, E. Hanssen, S. Kenny, L. Turnbull, C.B. Whitchurch, L. Tilley, and M.W. a. Dixon. 2012. Origin, composition, organization and function of the inner membrane complex of Plasmodium falciparum gametocytes. *J. Cell Sci.* 125:2053–2063. doi:10.1242/jcs.099002.

Decherf, G., S. Egée, H.M. Staines, J.C. Ellory, and S.L. Thomas. 2004. Anionic channels in malaria-infected human red blood cells. *Blood Cells, Mol. Dis.* 32:366–371. doi:10.1016/j.bcmd.2004.01.008.

Degefa, T., A. Zeynudin, E. Zemene, D. Emana, and D. Yewhalaw. 2016. High Prevalence of Gametocyte Carriage among Individuals with Asymptomatic Malaria: Implications for Sustaining Malaria Control and Elimination Efforts in Ethiopia. *Hum. Parasit. Dis.* 8:17–25. doi:10.4137/HPD.S34377.

Deiwick, A. 1992. Extramedullary Erythropoiesis in Human Liver Grafts. 689–696.

Van Dijk, M.R., C.J. Janse, J. Thompson, A.P. Waters, J.A.M. Braks, H.J. Dodemont, H.G. Stunnenberg, G.J. Van Gemert, R.W. Sauerwein, and W. Eling. 2001. A central role for P48/45 in malaria parasite male gamete fertility. *Cell.* 104:153–164. doi:10.1016/S0092-8674(01)00199-4.

Van Dijk, M.R., B.C.L. Van Schaijk, S.M. Khan, M.W. Van Dooren, J. Ramesar, S. Kaczanowski, G.-J. Van Gemert, H. Kroeze, H.G. Stunnenberg, W.M. Eling, R.W. Sauerwein, A.P. Waters, and C.J. Janse. 2010. Three Members of the 6-cys Protein Family of Plasmodium Play a Role in Gamete Fertility. *PLoS Pathog.* 6:1–13. doi:10.1371/journal.ppat.1000853.

Dinko, B., T. Bousema, and C.J. Sutherland. 2012. Recognition of Plasmodium falciparum gametocyte surface antigens by plasma antibodies in asymptomatic Ghanaian school children. *Malar. J.* 11:P24. doi:10.1186/1475-2875-11-S1-P24.

Dluzewski, a R., G.H. Mitchell, P.R. Fryer, S. Griffiths, R.J. Wilson, and W.B. Gratzer. 1992. Origins of the parasitophorous vacuole membrane of the malaria parasite, Plasmodium falciparum, in human red blood cells. *J. Cell Sci.* 102 (Pt 3:527–532.

Dolznig, H., P. Bartunek, K. Nasmyth, E.W. Müllner, and H. Beug. 1995. Terminal differentiation of normal chicken erythroid progenitors: shortening of G1 correlates with loss of D-cyclin/cdk4 expression and altered cell size control. *Cell Growth Differ.* 6:1341–1352. doi:papers2://publication/uuid/389B090C-23B0-460F-82D6-F834406C9B67.

Domingo, E., C. Moreno, A. Sánchez-Ibarrola, C. Panizo, J.A. Páramo, and J. Merino. 2010. Enhanced sensitivity of flow cytometry for routine assessment of minimal residual disease. *Haematologica.* 95:691–692. doi:10.3324/haematol.2009.018911.

Drenckhahn, D., and J. Wagner. 1986. Stress Fibers in the Splenic Sinus Endothelium Insitu - Molecular-Structure, Relationship To the Extracellular-Matrix, and Contractility. *J. Cell Biol.* 102:1738–1747. doi:10.1083/jcb.102.5.1738.

Duffier, Y., A. Lorthiois, P. Cisteró, F. Dupuy, G. Jouvion, L. Fiette, D. Mazier, A. Mayor, C. Lavazec, and A. Moreno Sabater. 2016. A humanized mouse model for sequestration of Plasmodium falciparum sexual stages and in vivo evaluation of gametocytidal drugs. *Sci. Rep.* 6:35025. doi:10.1038/srep35025.

Duffy, M.F., S.A. Selvarajah, G.A. Josling, and M. Petter. 2014. Epigenetic regulation of the plasmodium falciparum genome. *Brief. Funct. Genomics.* 13:203–216. doi:10.1093/bfgp/elt047.

Duffy, M.F., J. Tang, F. Sumardy, H.H.T. Nguyen, S.A. Selvarajah, G.A. Josling, K.P. Day, M. Petter, and G. V. Brown. 2016. Activation and clustering of a *Plasmodium falciparum var* gene are affected by subtelomeric sequences. *FEBS J.* 284:237–257. doi:10.1111/febs.13967.

Duffy, M.F., and W.H. Tham. 2007. Transcription and coregulation of multigene families in Plasmodium falciparum. *Trends Parasitol.* 23:183–186.

doi:10.1016/j.pt.2007.02.010.

Duraisingh, M.T., T. Triglia, S.A. Ralph, J.C. Rayner, J.W. Barnwell, G.I. McFadden, and A.F. Cowman. 2003. Phenotypic variation of Plasmodium falciparum merozoite proteins directs receptor targeting for invasion of human erythrocytes. *EMBO J.* 22:1047–57. doi:10.1093/emboj/cdg096.

Duval, L., M. Fourment, E. Nerrienet, D. Rousset, S.A. Sadeuh, S.M. Goodman, N. V Andriaholinirina, M. Randrianarivelojosia, R.E. Paul, V. Robert, F.J. Ayala, and F. Ariey. 2010. African apes as reservoirs of Plasmodium falciparum and the origin and diversification of the Laverania subgenus. *Proc. Natl. Acad. Sci. U. S. A.* 107:10561–10566. doi:10.1073/pnas.1005435107.

Dvorak, J., L.H. Miller, W. Whitehouse, and T. Shiroishi. 1975. Invasion of erythrocytes by malaria merozoites. 748–750.

Egan, E.S., R.H.Y. Jiang, M.A. Moechtar, N.S. Barteneva, M.P. Weekes, L. V Nobre, S.P. Gygi, J.A. Paulo, C. Frantzreb, Y. Tani, J. Takahashi, S. Watanabe, J. Goldberg, A.S. Paul, C. Brugnara, D.E. Root, R.C. Wiegand, J.G. Doench, and M.T. Duraisingh. 2015. A forward genetic screen identifies erythrocyte CD55 as essential for Plasmodium falciparum invasion. *Science*. 348:711–4. doi:10.1126/science.aaa3526.

Eksi, S., B. Czesny, G.J. Van Gemert, R.W. Sauerwein, W. Eling, and K.C. Williamson. 2006. Malaria transmission-blocking antigen, Pfs230, mediates human red blood cell binding to exflagellating male parasites and oocyst production. *Mol. Microbiol.* 61:991–998. doi:10.1111/j.1365-2958.2006.05284.x.

El-Assaad, F., J. Wheway, A. Mitchell, J. Lou, N. Hunt, V. Combes, and G.E.R. Grau. 2013. Cytoadherence of Plasmodium berghei -Infected Red Blood Cells to. 81:3984–3991. doi:10.1128/IAI.00428-13.

Ellyard, J.I., D.T. Avery, C.R. Mackay, and S.G. Tangye. 2005. Contribution of stromal cells to the migration, function and retention of plasma cells in human spleen: Potential roles of CXCL12, IL-6 and CD54. *Eur. J. Immunol.* 35:699–708. doi:10.1002/eji.200425442.

Engwerda, C.R., L. Beattie, and F.H. Amante. 2005. The importance of the spleen in malaria. *Trends Parasitol.* 21:75–80. doi:10.1016/j.pt.2004.11.008.

Etienne-Manneville, S. 2004. Actin and microtubules in cell motility: Which one

is in control? *Traffic*. 5:470–477. doi:10.1111/j.1600-0854.2004.00196.x.

Fairlamb, A.H., N.A.R. Gow, K.R. Matthews, and A.P. Waters. 2016. Europe PMC Funders Group Drug resistance in eukaryotic microorganisms. 1:1–33. doi:10.1038/nmicrobiol.2016.92.Drug.

Farfour, E., F. Charlotte, C. Settegrana, M. Miyara, and P. Buffet. 2012. The extravascular compartment of the bone marrow: a niche for Plasmodium falciparum gametocyte maturation? *Malar. J.* 11:285. doi:10.1186/1475-2875-11-285.

Farrell, A., S. Thirugnanam, A. Lorestani, J.D. Dvorin, K.P. Eidell, D.J.P. Ferguson, B.R. Anderson-White, M.T. Duraisingh, G.T. Marth, and M.-J. Gubbels. 2012. A DOC2 protein identified by mutational profiling is essential for apicomplexan parasite exocytosis. *Science (80-.).* 335:218–21. doi:10.1126/science.1210829.

Fearon, R.M.P., D. Reiss, L.D. Leve, D.S. Shaw, L. V. Scaramella, J.M. Ganiban, and J.M. Neiderhiser. 2015. HHS Public Access. *Dev. Psychopathol*. 27:1251–1265. doi:10.1017/S0954579414000868.Child-evoked.

Feller, T., P. Thom, N. Koch, H. Spiegel, O. Addai-Mensah, R. Fischer, A. Reimann, G. Pradel, R. Fendel, S. Schillberg, M. Scheuermayer, and H. Schinkel. 2013. Plant-based production of recombinant plasmodium surface protein Pf38 and evaluation of its potential as a vaccine candidate. *PLoS One*. 8. doi:10.1371/journal.pone.0079920.

Fernandez-Becerra, C., O. Pein, T.R. De Oliveira, M.M. Yamamoto, A.C. Cassola, C. Rocha, I.S. Soares, C.A. De Bragança Pereira, and H.A. Del Portillo. 2005. Variant proteins of Plasmodium vivax are not clonally expressed in natural infections. *Mol. Microbiol*. 58:648–658. doi:10.1111/j.1365-2958.2005.04850.x.

Ferrer, M., L. Martin-Jaular, M. De Niz, S.M. Khan, C.J. Janse, M. Calvo, V. Heussler, and H.A. Del Portillo. 2014. Imaging of the spleen in malaria. *Parasitol. Int*. 63:195–205. doi:10.1016/j.parint.2013.08.014.

Filippi, M.D. 2016. Mechanism of Diapedesis: Importance of the Transcellular Route. 129. 1st ed. Elsevier Inc. 25-53 pp.

Filmanowicz, E., and C. Gurney. 1961. Studies on Erythropoiesis.

Finaurini, S., N. Basilico, Y. Corbett, S. D'Alessandro, S. Parapini, P. Olliaro, R.K. Haynes, and D. Taramelli. 2012. Dihydroartemisinin inhibits the human erythroid cell differentiation by altering the cell cycle. *Toxicology*. 300:57–

66. doi:10.1016/j.tox.2012.05.024.

Finaurini, S., L. Ronzoni, A. Colancecco, A. Cattaneo, M.D. Cappellini, S.A. Ward, and D. Taramelli. 2010. Selective toxicity of dihydroartemisinin on human CD34+ erythroid cell differentiation. *Toxicology*. 276:128–134. doi:10.1016/j.tox.2010.07.016.

Fischer, K., T. Marti, B. Rick, D. Johnson, J. Benting, S. Baumeister, C. Helmbrecht, M. Lanzer, and K. Lingelbach. 1998. Characterization and cloning of the gene encoding the vacuolar membrane protein EXP-2 from Plasmodium falciparum. *Mol. Biochem. Parasitol*. 92:47–57. doi:10.1016/S0166-6851(97)00224-7.

Florens, L., M.P. Washburn, J.D. Raine, R.M. Anthony, M. Grainger, J.D. Haynes, J.K. Moch, N. Muster, J.B. Sacci, D.L. Tabb, A.A. Witney, D. Wolters, Y. Wu, M.J. Gardner, A.A. Holder, R.E. Sinden, J.R. Yates, and D.J. Carucci. 2002. A proteomic view of the Plasmodium falciparum life cycle. *Nature*. 419:520–6. doi:10.1038/nature01107.

Flueck, C., R. Bartfai, J. Volz, I. Niederwieser, A.M. Salcedo-Amaya, B.T.F. Alako, F. Ehlgen, S.A. Ralph, A.F. Cowman, Z. Bozdech, H.G. Stunnenberg, and T.S. Voss. 2009. Plasmodium falciparum heterochromatin protein 1 marks genomic loci linked to phenotypic variation of exported virulence factors. *PLoS Pathog*. 5. doi:10.1371/journal.ppat.1000569.

Flygare, J., V.R. Estrada, C. Shin, S. Gupta, and H.F. Lodish. 2011. HIF1?? synergizes with glucocorticoids to promote BFU-E progenitor self-renewal. *Blood*. 117:3435–3444. doi:10.1182/blood-2010-07-295550.

Fonager, J., E.M. Pasini, J.A.M. Braks, O. Klop, J. Ramesar, E.J. Remarque, I.O.C.M. Vroegrijk, S.G. Van Duinen, A.W. Thomas, S.M. Khan, M. Mann, C.H.M. Kocken, C.J. Janse, and B.M.D. Franke-fayard. 2012. Reduced CD36-dependent tissue sequestration of Plasmodium -infected erythrocytes is detrimental to malaria parasite growth in vivo. 209:93–107. doi:10.1084/jem.20110762.

Franca, C.T., W.Q. He, J. Gruszczyk, N.T.Y. Lim, E. Lin, B. Kiniboro, P.M. Siba, W.H. Tham, and I. Mueller. 2016. Plasmodium vivax Reticulocyte Binding Proteins Are Key Targets of Naturally Acquired Immunity in Young Papua New Guinean Children. *PLoS Negl. Trop. Dis*. 10:1–17. doi:10.1371/journal.pntd.0005014.

Franke-Fayard, B., J. Fonager, A. Braks, S.M. Khan, and C.J. Janse. 2010.

Sequestration and tissue accumulation of human malaria parasites: Can we learn anything from rodent models of malaria? *PLoS Pathog.* 6. doi:10.1371/journal.ppat.1001032.

Franke-Fayard, B., C.J. Janse, M. Cunha-Rodrigues, J. Ramesar, P. Büscher, I. Que, C. Löwik, P.J. Voshol, M. a M. den Boer, S.G. van Duinen, M. Febbraio, M.M. Mota, and A.P. Waters. 2005. Murine malaria parasite sequestration: CD36 is the major receptor, but cerebral pathology is unlinked to sequestration. *Proc. Natl. Acad. Sci. U. S. A.* 102:11468–11473. doi:10.1073/pnas.0503386102.

Franke-Fayard, B., H. Trueman, J. Ramesar, J. Mendoza, M. Van Der Keur, R. Van Der Linden, R.E. Sinden, A.P. Waters, and C.J. Janse. 2004. A Plasmodium berghei reference line that constitutively expresses GFP at a high level throughout the complete life cycle. *Mol. Biochem. Parasitol.* 137:23–33. doi:10.1016/j.molbiopara.2004.04.007.

Freedman, M.H., and E.F. Saunders. 1981. Hematopoiesis in the human spleen. *Am. J. Hematol.* 11:271–5. doi:10.1001/archinte.1983.00350070037004.

Fukushima, A., T. Yamaguchi, W. Ishida, K. Fukata, T. Taniguchi, F.T. Liu, and H. Ueno. 2006. Genetic background determines susceptibility to experimental immune-mediated blepharoconjunctivitis: Comparison of Balb/c and C57BL/6 mice. *Exp. Eye Res.* 82:210–218. doi:10.1016/j.exer.2005.06.010.

Gaehtgens, P., F. Schmidt, and G. Will. 1981. Comparative Rheology of Nucleated and Non-Nucleated Red Blood Cells. *Pfltigers Arch.* 390:278–282. doi:10.1007/BF00658276.

Galinski, M.R., P. Ingravallo, C. Corredor-Medina, B. Al-Khedery, M. Povoa, and J.W. Barnwell. 2001. *Plasmodium vivax* merozoite surface proteins-3beta and-3gamma share structural similarities with *P. vivax* merozoite surface protein-3alpha and define a new gene family. *Mol. Biochem. Parasitol.* 115:41–53. doi:S0166-6851(01)00267-5 [pii].

Galinski, M.R., C.C. Medina, P. Ingravallo, and J.W. Barnwell. 1992. A reticulocyte-binding protein complex of plasmodium vivax merozoites. *Cell.* 69:1213–1226. doi:10.1016/0092-8674(92)90642-P.

Galkina, E., J. Thatte, V. Dabak, M.B. Williams, K. Ley, and T.J. Braciale. 2005. Preferential migration of effector CD8+ T cells into the interstitium of the normal lung. *J. Clin. Invest.* 115:3473–3483. doi:10.1172/JCI24482.

Gao, X., K. Gunalan, S.S.L. Yap, and P.R. Preiser. 2013. Triggers of key calcium signals during erythrocyte invasion by Plasmodium falciparum. *Nat. Commun.* 4:2862. doi:10.1038/ncomms3862.

Gao, X., K.P. Yeo, S.S. Aw, C. Kuss, J.K. Iyer, S. Genesan, R. Rajamanonmani, J. Lescar, Z. Bozdech, and P.R. Preiser. 2008. Antibodies targeting the PfRH1 binding domain inhibit invasion of Plasmodium falciparum merozoites. *PLoS Pathog.* 4. doi:10.1371/journal.ppat.1000104.

Gardner, M.J., N. Hall, E. Fung, O. White, M. Berriman, R.W. Hyman, J.M. Carlton, A. Pain, K.E. Nelson, S. Bowman, I.T. Paulsen, K. James, J. a Eisen, K. Rutherford, S.L. Salzberg, A. Craig, S. Kyes, M.-S. Chan, V. Nene, S.J. Shallom, B. Suh, J. Peterson, S. Angiuoli, M. Pertea, J. Allen, J. Selengut, D. Haft, M.W. Mather, A.B. Vaidya, D.M. a Martin, A.H. Fairlamb, M.J. Fraunholz, D.S. Roos, S. a Ralph, G.I. McFadden, L.M. Cummings, G.M. Subramanian, C. Mungall, J.C. Venter, D.J. Carucci, S.L. Hoffman, C. Newbold, R.W. Davis, C.M. Fraser, and B. Barrell. 2002. Genome sequence of the human malaria parasite Plasmodium falciparum. *Nature*. 419:498–511. doi:10.1038/nature01097.

Gardner, M.J., N. Hall, E. Fung, O. White, M. Berriman, W. Richard, J.M. Carlton, A. Pain, K.E. Nelson, S. Bowman, T. Ian, K. James, J.A. Eisen, K. Rutherford, S.L. Salzberg, S. Kyes, M. Chan, V. Nene, S.J. Shallom, J. Peterson, S. Angiuoli, M. Pertea, J. Allen, D. Haft, M.W. Mather, A.B. Vaidya, D.M.A. Martin, and H. Alan. 2013. Europe PMC Funders Group Genome sequence of the human malaria parasite Plasmodium falciparum. 419:3–9. doi:10.1038/nature01097.Genome.

Gaur, D., and C.E. Chitnis. 2011. Molecular interactions and signaling mechanisms during erythrocyte invasion by malaria parasites. *Curr. Opin. Microbiol.* 14:422–428. doi:10.1016/j.mib.2011.07.018.

Gaur, D., C.E. Chitnis, and V.S. Chauhan. 2016. Advances in malaria research.

Gething, P.W., I.R.F. Elyazar, C.L. Moyes, D.L. Smith, K.E. Battle, C.A. Guerra, A.P. Patil, A.J. Tatem, R.E. Howes, M.F. Myers, D.B. George, P. Horby, H.F.L. Wertheim, R.N. Price, I. Mu, K. Baird, and S.I. Hay. 2012. A Long Neglected World Malaria Map : Plasmodium vivax Endemicity in 2010. 6. doi:10.1371/journal.pntd.0001814.

Gilberger, T., J.K. Thompson, T. Triglia, R.T. Good, M.T. Duraisingh, and A.F. Cowman. 2003. A Novel Erythrocyte Binding Antigen-175 Paralogue from

Plasmodium falciparum Defines a New Trypsin-resistant Receptor on Human Erythrocytes *. 278:14480–14486. doi:10.1074/jbc.M211446200.

Gilson, P.R., and B.S. Crabb. 2009. Morphology and kinetics of the three distinct phases of red blood cell invasion by Plasmodium falciparum merozoites. *Int. J. Parasitol.* 39:91–96. doi:10.1016/j.ijpara.2008.09.007.

Glenister, F.K., R.L. Coppel, A.F. Cowman, N. Mohandas, and B.M. Cooke. 2002. Contribution of parasite proteins to altered mechanical properties of malaria-infected red blood cells. *Blood.* 99:1060–1063. doi:10.1182/blood.V99.3.1060.

Glodek, A.M., R. Mirchev, D.E. Golan, J.A. Khoory, J.M. Burns, S.S. Shevkoplyas, A. Nicholson-Weller, and I.C. Ghiran. 2010. Ligation of complement receptor 1 increases red blood cell membrane deformability. *Blood.* 116:6063–6071. doi:10.1182/blood-2010-04- 273904.

Goel, S., M. Palmkvist, K. Moll, N. Joannin, P. Lara, R.R. Akhouri, N. Moradi, K. Öjemalm, M. Westman, D. Angeletti, H. Kjellin, J. Lehtiö, O. Blixt, L. Ideström, C.G. Gahmberg, J.R. Storry, A.K. Hult, and M.L. Olsson. 2015. b r i e f c o m m u n i c at i o n s RIFINs are adhesins implicated malaria. 21. doi:10.1038/nm.3812.

Goel, V.K., X. Li, H. Chen, S.-C. Liu, A.H. Chishti, and S.S. Oh. 2003. Band 3 is a host receptor binding merozoite surface protein 1 during the Plasmodium falciparum invasion of erythrocytes. *Proc. Natl. Acad. Sci. U. S. A.* 100:5164–9. doi:10.1073/pnas.0834959100.

Gold, D.A., A.D. Kaplan, A. Lis, G.C.L. Bett, E. Emily, K.M. Cirelli, A. Bougdour, S.M. Sidik, J.R. Beck, S. Lourido, P.F. Egea, P.J. Bradley, M. Hakimi, and L. Randall. 2016. HHS Public Access. 17:642–652. doi:10.1016/j.chom.2015.04.003.The.

Griffiths, R.E., S. Kupzig, N. Cogan, T.J. Mankelow, V.M.S. Betin, K. Trakarnsanga, E.J. Massey, S.F. Parsons, D.J. Anstee, and J.D. Lane. 2012. The ins and outs of human reticulocyte maturation: Autophagy and the endosome/exosome pathway. *Autophagy.* 8:1150–1151. doi:10.4161/auto.20648.

Grüber, A., K. Gunalan, J.K. Ramalingam, M.S.S. Manimekalai, G. Grüber, and P.R. Preiser. 2011. Structural characterization of the erythrocyte binding domain of the reticulocyte binding protein homologue family of Plasmodium yoelii. *Infect. Immun.* 79:2880–2888. doi:10.1128/IAI.01326-10.

Gruszczyk, J., N.T.Y. Lim, A. Arnott, W.-Q. He, W. Nguitragool, W. Roobsoong, Y.-F. Mok, J.M. Murphy, K.R. Smith, S. Lee, M. Bahlo, I. Mueller, A.E. Barry, and W.-H. Tham. 2016. Structurally conserved erythrocyte-binding domain in Plasmodium provides a versatile scaffold for alternate receptor engagement. *Proc. Natl. Acad. Sci. U. S. A.* 113:E191-200. doi:10.1111/j.1365-2567.2007.02752.x.

Guerreiro, A., E. Deligianni, J.M. Santos, P.A.G.C. Silva, C. Louis, A. Pain, C.J. Janse, B. Franke-Fayard, C.K. Carret, I. Siden-Kiamos, and G.R. Mair. 2014. Genome-wide RIP-Chip analysis of translational repressor-bound mRNAs in the Plasmodium gametocyte. *Genome Biol.* 15:493. doi:10.1186/s13059-014-0493-0.

Gulliver, G. 1875. Observations on the Sizes and Shapes of the Red Corpuscles of the Blood of Vertebrates, with Drawings of them to a uniform Scale, and exterided and revised Tables of Measurements. *Proc. Zool. Soc. Lond.* 474–495.

Gunalan, K., X. Gao, K.J.L. Liew, and P.R. Preiser. 2011. Differences in erythrocyte receptor specificity of different parts of the Plasmodium falciparum reticulocyte binding protein homologue. *Infect. Immun.* 79:3421–3430. doi:10.1128/IAI.00201-11.

Gunalan, K., E. Lo, J.B. Hostetler, D. Yewhalaw, J. Mu, D.E. Neafsey, G. Yan, and L.H. Miller. 2016. Role of Plasmodium vivax Duffy-binding protein 1 in invasion of Duffy-null Africans. *Proc. Natl. Acad. Sci. U. S. A.* 113:1606113113-. doi:10.1073/pnas.1606113113.

Gupta, S., R.W. Snow, C. Donnelly, K. Marsh, and C. Newbold. 1999. Immunity to non-cerebral severe malaria is acquired after one or two infections. 5:3–6.

Gurkan, U.A., and O. Akkus. 2008. The mechanical environment of bone marrow: A review. *Ann. Biomed. Eng.* 36:1978–1991. doi:10.1007/s10439-008-9577-x.

Guttery, D.S., D.J.P. Ferguson, B. Poulin, Z. Xu, U. Straschil, O. Klop, L. Solyakov, S.M. Sandrini, D. Brady, C.A. Nieduszynski, C.J. Janse, A.A. Holder, A.B. Tobin, and R. Tewari. 2012. A putative homologue of CDC20/CDH1 in the malaria parasite is essential for male gamete development. *PLoS Pathog.* 8. doi:10.1371/journal.ppat.1002554.

Guttery, D.S., M. Roques, A.A. Holder, and R. Tewari. 2015. Commit and Transmit: Molecular Players in Plasmodium Sexual Development and Zygote Differentiation. *Trends Parasitol.* 31:676–685. doi:10.1016/j.pt.2015.08.002.

Haggstrom, M. 2009. https://commons.wikimedia.org/wiki/File:Hematopoiesis_simple.svg.

Haldar, K., and N. Mohandas. 2009. Malaria, erythrocytic infection, and anemia. *hematology*.

Hall, N., M. Karras, J.D. Raine, J.M. Carlton, T.W.A. Kooij, M. Berriman, L. Florens, C.S. Janssen, A. Pain, G.K. Christophides, K. James, K. Rutherford, B. Harris, D. Harris, C. Churcher, M.A. Quail, D. Ormond, J. Doggett, H.E. Trueman, J. Mendoza, S.L. Bidwell, M. Rajandream, D.J. Carucci, J.R.Y. Iii, F.C. Kafatos, C.J. Janse, B. Barrell, C.M.R. Turner, A.P. Waters, and R.E. Sinden. 2005. R ESEARCH A RTICLE. 82–87.

Han, J.-H., S.-K. Lee, B. Wang, F. Muh, M.H. Nyunt, S. Na, K.-S. Ha, S.-H. Hong, W.S. Park, J. Sattabongkot, T. Tsuboi, and E.-T. Han. 2016. Identification of a reticulocyte-specific binding domain of Plasmodium vivax reticulocyte-binding protein 1 that is homologous to the PfRh4 erythrocyte-binding domain. *Sci. Rep.* 6:26993. doi:10.1038/srep26993.

Hanssen, E., C. Dekiwadia, D.T. Riglar, M. Rug, L. Lemgruber, A.F. Cowman, M. Cyrklaff, M. Kudryashev, F. Frischknecht, J. Baum, and S.A. Ralph. 2013. Electron tomography of Plasmodium falciparum merozoites reveals core cellular events that underpin erythrocyte invasion. *Cell. Microbiol.* 15:1457–1472. doi:10.1111/cmi.12132.

Hargreaves, D.C., P.L. Hyman, T.T. Lu, V.N. Ngo, A. Bidgol, G. Suzuki, Y.-R.R. Zou, D.R. Littman, and J.G. Cyster. 2001. A coordinated change in chemokine responsiveness guides plasma cell movements. *J. Exp. Med.* 194:45–56. doi:10.1084/jem.194.1.45.

Hastings, I. 2011. How artemisinin-containing combination therapies slow the spread of antimalarial drug resistance. *Trends Parasitol.* 27:67–72. doi:10.1016/j.pt.2010.09.005.

Hedley, B.D., and M. Keeney. 2013. Technical issues: Flow cytometry and rare event analysis. *Int. J. Lab. Hematol.* 35:344–350. doi:10.1111/ijlh.12068.

Hegner, R. 1938. Relative frequency of ring-stage plasmodia in reticulocytes and mature erythrocytes in man and monkey. *Am. J. Epidemiol.* 690–718.

Hietanen, J., A. Chim-Ong, T. Chiramanewong, J. Gruszczyk, W. Roobsoong, W.H. Tham, J. Sattabongkot, and W. Nguitragool. 2016. Gene models, expression repertoire, and immune response of Plasmodium vivax reticulocyte binding proteins. *Infect. Immun.* 84:677–685.

doi:10.1128/IAI.01117-15.

Hikosaka, K., Y. ichi Watanabe, F. Kobayashi, S. Waki, K. Kita, and K. Tanabe. 2011. Highly conserved gene arrangement of the mitochondrial genomes of 23 Plasmodium species. *Parasitol. Int.* 60:175–180. doi:10.1016/j.parint.2011.02.001.

Hliscs, M., C. Millet, M.W. Dixon, I. Siden-Kiamos, P. Mcmillan, and L. Tilley. 2015. Organization and function of an actin cytoskeleton in Plasmodium falciparum gametocytes. *Cell. Microbiol.* 17:207–225. doi:10.1111/cmi.12359.

Hoeijmakers, W.A.M., C. Flueck, K.J. Françoijs, A.H. Smits, J. Wetzel, J.C. Volz, A.F. Cowman, T. Voss, H.G. Stunnenberg, and R. Bártfai. 2012. Plasmodium falciparum centromeres display a unique epigenetic makeup and cluster prior to and during schizogony. *Cell. Microbiol.* 14:1391–1401. doi:10.1111/j.1462-5822.2012.01803.x.

Hoeijmakers, W.A.M., A.M. Salcedo-Amaya, A.H. Smits, K.J. Françoijs, M. Treeck, T.W. Gilberger, H.G. Stunnenberg, and R. Bártfai. 2013. H2A.Z/H2B.Z double-variant nucleosomes inhabit the AT-rich promoter regions of the Plasmodium falciparum genome. *Mol. Microbiol.* 87:1061–1073. doi:10.1111/mmi.12151.

Holder, A.A., M.J. Lockyer, K.G. Odink, J.S. Sandhu, V. Riveros-Moreno, S.C. Nicholls, Y. Hillman, L.S. Davey, M.L. V. Tizard, R.T. Schwarz, and R.R. Freeman. 1985. Primary structure of the precursor to the three major surface antigens of Plasmodium falciparum merozoites. *Nature*. 317:270–273. doi:10.1038/317270a0.

Holder, a a. 2009. The carboxy-terminus of merozoite surface protein 1: structure, specific antibodies and immunity to malaria. *Parasitology*. 136:1445–1456. doi:10.1017/S0031182009990515.

Hostetler, J.B., E. Lo, U. Kanjee, C. Amaratunga, S. Suon, S. Sreng, S. Mao, D. Yewhalaw, A. Mascarenhas, D.P. Kwiatkowski, M.U. Ferreira, P.K. Rathod, G. Yan, R.M. Fairhurst, M.T. Duraisingh, and J.C. Rayner. 2016. Independent Origin and Global Distribution of Distinct Plasmodium vivax Duffy Binding Protein Gene Duplications. *PLoS Negl. Trop. Dis.* 10:e0005091. doi:10.1371/journal.pntd.0005091.

Howell, D.P.G., R. Samudrala, and J.D. Smith. 2006. Disguising itself-insights into Plasmodium falciparum binding and immune evasion from the DBL

crystal structure. *Mol. Biochem. Parasitol.* 148:1–9. doi:10.1016/j.molbiopara.2006.03.004.

Howes, R.E., A.P. Patil, F.B. Piel, O.A. Nyangiri, C.W. Kabaria, P.W. Gething, P.A. Zimmerman, C. Barnadas, C.M. Beall, A. Gebremedhin, D. Ménard, T.N. Williams, D.J. Weatherall, and S.I. Hay. 2011. The global distribution of the Duffy blood group. *Nat. Commun.* 2:266. doi:10.1038/ncomms1265.

Huang, S., A. Amaladoss, M. Liu, H. Chen, R. Zhang, P.R. Preiser, M. Dao, and J. Han. 2014. In vivo splenic clearance correlates with in vitro deformability of red blood cells from Plasmodium yoelii-infected mice. *Infect. Immun.* 82:2532–2541. doi:10.1128/IAI.01525-13.

Hviid, L., and A.T.R. Jensen. 2015. PfEMP1 - a parasite protein family of key importance in plasmodium falciparum malaria immunity and pathogenesis. 88. Elsevier Ltd. 51-84 pp.

Iborra, F.J., a Pombo, D. a Jackson, and P.R. Cook. 1996. Active RNA polymerases are localized within discrete transcription "factories' in human nuclei. *J. Cell Sci.* 109 (Pt 6:1427–1436.

Imai, T., H. Ishida, K. Suzue, M. Hirai, T. Taniguchi, H. Okada, T. Suzuki, C. Shimokawa, and H. Hisaeda. 2013. CD8(+) T cell activation by murine erythroblasts infected with malaria parasites. *Sci. Rep.* 3:1572. doi:10.1038/srep01572.

Imai, T., H. Ishida, K. Suzue, T. Taniguchi, H. Okada, C. Shimokawa, and H. Hisaeda. 2015a. Cytotoxic activities of CD8+ T cells collaborate with macrophages to protect against blood-stage murine malaria. *Elife.* 2015:1–49. doi:10.7554/eLife.04232.

Imai, T., H. Ishida, K. Suzue, T. Taniguchi, H. Okada, C. Shimokawa, and H. Hisaeda. 2015b. Cytotoxic activities of $CD8^+$ T cells collaborate with macrophages to protect against blood-stage murine malaria. *Elife.* 4. doi:10.7554/eLife.04232.

Imirzalioglu, C., N. Soydan, M. Schaller, R.G. Bretzel, T. Chakraborty, and E. Domann. 2006. Diagnosis of Mixed Plasmodium malariae and P . vivax Infection in a Development Aid Volunteer by Examination of Bone-Marrow Specimens by Real-Time PCR. 44:2307–2310. doi:10.1128/JCM.02687-05.

Itkin, T., S. Gur-Cohen, J. a Spencer, A. Schajnovitz, S.K. Ramasamy, A.P. Kusumbe, G. Ledergor, Y. Jung, I. Milo, M.G. Poulos, A. Kalinkovich, A. Ludin, O. Kollet, G. Shakhar, J.M. Butler, S. Rafii, R.H. Adams, D.T.

Scadden, C.P. Lin, and T. Lapidot. 2016. Distinct bone marrow blood vessels differentially regulate haematopoiesis. *Nature*. 532:323–8. doi:10.1038/nature17624.

Ittarat, W., A.L. Pickard, P. Rattanasinganchan, P. Wilairatana, S. Looareesuwan, K. Emery, J. Low, R. Udomsangpetch, and S.R. Meshnick. 2003. Recrudescence in artesunate-treated patients with falciparum malaria is dependent on parasite burden not on parasite factors. *Am. J. Trop. Med. Hyg*. 68:147–152.

Jambou, R., V. Combes, M.J. Jambou, B.B. Weksler, P.O. Couraud, and G.E. Grau. 2010. Plasmodium falciparum adhesion on human brain microvascular endothelial cells involves transmigration-like cup formation and induces opening of intercellular junctions. *PLoS Pathog*. 6:1–13. doi:10.1371/journal.ppat.1001021.

Janes, J.H., C.P. Wang, E. Levin-Edens, I. Vigan-Womas, M. Guillotte, M. Melcher, O. Mercereau-Puijalon, and J.D. Smith. 2011. Investigating the host binding signature on the Plasmodium falciparum PfEMP1 protein family. *PLoS Pathog*. 7. doi:10.1371/journal.ppat.1002032.

Janse, C.J., B. Franke-Fayard, G.R. Mair, J. Ramesar, C. Thiel, S. Engelmann, K. Matuschewski, G.J. Van Gemert, R.W. Sauerwein, and A.P. Waters. 2006. High efficiency transfection of Plasmodium berghei facilitates novel selection procedures. *Mol. Biochem. Parasitol*. 145:60–70. doi:10.1016/j.molbiopara.2005.09.007.

Janse, C.J., H. Kroeze, A. van Wigcheren, S. Mededovic, J. Fonager, B. Franke-Fayard, A.P. Waters, and S.M. Khan. 2011. A genotype and phenotype database of genetically modified malaria-parasites. *Trends Parasitol*. 27:31–39. doi:10.1016/j.pt.2010.06.016.

Janse, C.J., A.P. Waters, J. Kos, and C.B. Lugt. 1994. Comparison of in vivo and in vitro antimalarial activity of artemisinin, dihydroartemisinin and sodium artesunate in the Plasmodium berghei-rodent model. *Int. J. Parasitol*. 24:589–594. doi:10.1016/0020-7519(94)90150-3.

Jaureguiberry, S., P. Ndour, C. Roussel, F. Ader, I. Safeukui, M. Nguyen, S. Biligui, L. Ciceron, O. Mouri, E. Kendjo, and M. Vray. 2014. Postartesunate delayed hemolysis is a predictable event related to the lifesaving effect of artemisinins. 124:167–176. doi:10.1182/blood-2014-02-555953.S.J.

Jennings, G.J., C.S. Toebe, A. Van Belkum, and M.F. Wiser. 1998. The complete

sequence of Plasmodium berghei merozoite surface protein-1 and its inter- and intra-species variability. *Mol. Biochem. Parasitol.* 93:43–55. doi:10.1016/S0166-6851(98)00016-4.

Jewett, T.J., and L.D. Sibley. 2003. Aldolase forms a bridge between cell surface adhesins and the actin cytoskeleton in apicomplexan parasites. *Mol. Cell.* 11:885–894. doi:10.1016/S1097-2765(03)00113-8.

Jiang, J., J.W. Barnwell, E.V.S. Meyer, and M.R. Galinski. 2013. Plasmodium vivax Merozoite Surface Protein-3 (PvMSP3): Expression of an 11 Member Multigene Family in Blood-Stage Parasites. *PLoS One.* 8. doi:10.1371/journal.pone.0063888.

Jiang, L., M.J. López-Barragán, H. Jiang, J. Mu, D. Gaur, K. Zhao, G. Felsenfeld, and L.H. Miller. 2010. Epigenetic control of the variable expression of a Plasmodium falciparum receptor protein for erythrocyte invasion. *Proc. Natl. Acad. Sci. U. S. A.* 107:2224–2229. doi:10.1073/pnas.0913396107.

Jin, B., Y. Li, and K.D. Robertson. 2011. DNA methylation: superior or subordinate in the epigenetic hierarchy? *Genes Cancer.* 2:607–17. doi:10.1177/1947601910393957.

Joergensen, L., D.C. Bengtsson, A. Bengtsson, E. Ronander, S.S. Berger, L. Turner, M.B. Dalgaard, G.K.K. Cham, M.E. Victor, T. Lavstsen, T.G. Theander, D.E. Arnot, and A.T.R. Jensen. 2010. Surface co-expression of two different PfEMP1 antigens on single plasmodium falciparum-infected erythrocytes facilitates binding to ICAM1 and PECAM1. *PLoS Pathog.* 6. doi:10.1371/journal.ppat.1001083.

Joice, R., S.K. Nilsson, J. Montgomery, S. Dankwa, E. Egan, B. Morahan, K.B. Seydel, L. Bertuccini, P. Alano, K.C. Williamson, M.T. Duraisingh, T.E. Taylor, D. a Milner, and M. Marti. 2014. Plasmodium falciparum transmission stages accumulate in the human bone marrow. *Sci. Transl. Med.* 6:244re5. doi:10.1126/scitranslmed.3008882.

Joneckis, C.C., R.L. Ackley, E.P. Orringer, E.A. Wayner, and L. V Parise. 1993. Integrin a 4 $\diamondsuit$ 1 and glycoprotein IV (CD36) are expressed on circulating reticulocytes in sickle cell anemia. *Blood.* 82:3548–3555.

Josling, G.A., and M. Llinás. 2015. Sexual development in Plasmodium parasites: knowing when it's time to commit. *Nat. Rev. Microbiol.* 13:573–587. doi:10.1038/nrmicro3519.

Kadekoppala, M., S.A. Ogun, S. Howell, R.S. Gunaratne, and A.A. Holder. 2010.

Systematic genetic analysis of the Plasmodium falciparum MSP7-like family reveals differences in protein expression, location, and importance in asexual growth of the blood-stage parasite. *Eukaryot. Cell*. 9:1064–1074. doi:10.1128/EC.00048-10.

Kafsack, B.F.C., N. Rovira-graells, T.G. Clark, and C. Bancells. 2014. A transcriptional switch underlies commitment to sexual development in human malaria parasites. 507:248–252. doi:10.1038/nature12920.A.

Kaneko, O., J. Mu, T. Tsuboi, X. Su, and M. Torii. 2002. Gene structure and expression of a Plasmodium falciparum 220-kDa protein homologous to the Plasmodium vivax reticulocyte binding proteins. *Mol. Biochem. Parasitol.* 121:275–278. doi:10.1016/S0166-6851(02)00042-7.

Kaplan, R.N., B. Psaila, and D. Lyden. 2007. Niche-to-niche migration of bone-marrow-derived cells. *Trends Mol. Med.* 13:72–81. doi:10.1016/j.molmed.2006.12.003.

Kato, K., D.C.G. Mayer, S. Singh, M. Reid, and L.H. Miller. 2005. Domain III of Plasmodium falciparum apical membrane antigen 1 binds to the erythrocyte membrane protein Kx. *Proc. Natl. Acad. Sci. U. S. A.* 102:5552–5557. doi:10.1073/pnas.0501594102.

Ke, H., P.A. Sigala, K. Miura, J.M. Morrisey, M.W. Mather, J.R. Crowley, J.P. Henderson, D.E. Goldberg, C.A. Long, and A.B. Vaidya. 2014. The heme biosynthesis pathway is essential for Plasmodium falciparum development in mosquito stage but not in blood stages. *J. Biol. Chem.* 289:34827–34837. doi:10.1074/jbc.M114.615831.

Kedzierski, L., C.G. Black, and R.L. Coppel. 2000. Characterisation of the merozoite surface protein 4/5 gene of Plasmodium berghei and Plasmodium yoelii. *Mol. Biochem. Parasitol.* 105:137–147. doi:10.1016/S0166-6851(99)00178-4.

Keel, S., L. Liu, E. Nemeth, S. Cherian, J.L. Abkowitz, H. Cancer, and L. Angeles. 2015. HHS Public Access. 43:1–25. doi:10.1016/j.exphem.2015.03.001.Evidence.

Kelley, L.L., W.F. Green, G.G. Hicks, M.C. Bondurant, M.J. Koury, and H.E. Ruley. 1994. Apoptosis in erythroid progenitors deprived of erythropoietin occurs during the G1 and S phases of the cell cycle without growth arrest or stabilization of wild-type p53. *Mol. Cell. Biol.* 14:4183–92. doi:10.1128/MCB.14.6.4183.Updated.

Khan, S.M., B. Franke-Fayard, G.R. Mair, E. Lasonder, C.J. Janse, M. Mann, and A.P. Waters. 2005. Proteome analysis of separated male and female gametocytes reveals novel sex-specific Plasmodium biology. *Cell*. 121:675–687. doi:10.1016/j.cell.2005.03.027.

Khurana, I. 2005. Text book of medical physiology. 148.

King, C.L., J.H. Adams, J. Xianli, B.T. Grimberg, a. M. McHenry, L.J. Greenberg, a. Siddiqui, R.E. Howes, M. da Silva-Nunes, M.U. Ferreira, and P. a. Zimmerman. 2011. Fya/Fyb antigen polymorphism in human erythrocyte Duffy antigen affects susceptibility to Plasmodium vivax malaria. *Proc. Natl. Acad. Sci.* 108:20113–20118. doi:10.1073/pnas.1109621108.

Klonis, N., D.J. Creek, and L. Tilley. 2013a. Iron and heme metabolism in Plasmodium falciparum and the mechanism of action of artemisinins. *Curr. Opin. Microbiol*. 16:722–727. doi:10.1016/j.mib.2013.07.005.

Klonis, N., S.C. Xie, J.M. McCaw, M.P. Crespo-Ortiz, S.G. Zaloumis, J.A. Simpson, and L. Tilley. 2013b. Altered temporal response of malaria parasites determines differential sensitivity to artemisinin. *Proc. Natl. Acad. Sci. U. S. A.* 110:5157–62. doi:10.1073/pnas.1217452110.

Koch, M., and J. Baum. 2015. The mechanics of malaria parasite invasion of the human erythrocyte - towards a reassessment of the host cell contribution. *Cell. Microbiol*. n/a-n/a. doi:10.1111/cmi.12557.

de Koning-Ward, T.F., M.W.A. Dixon, L. Tilley, and P.R. Gilson. 2016. Plasmodium species: master renovators of their host cells. *Nat. Rev. Microbiol*. 14:14. doi:10.1038/nrmicro.2016.79.

de Koning-Ward, T.F., D.R. Drew, J.M. Chesson, J.G. Beeson, and B.S. Crabb. 2008. Truncation of Plasmodium berghei merozoite surface protein 8 does not affect in vivo blood-stage development. *Mol. Biochem. Parasitol*. 159:69–72. doi:10.1016/j.molbiopara.2008.01.005.

Kopp, H.-G., S.T. Avecilla, A.T. Hooper, and S. Rafii. 2005. The bone marrow vascular niche: home of HSC differentiation and mobilization. *Physiology (Bethesda)*. 20:349–356. doi:10.1152/physiol.00025.2005.

Koulnis, M., Y. Liu, K. Hallstrom, and M. Socolovsky. 2011. Negative autoregulation by fas stabilizes adult erythropoiesis and accelerates its stress response. *PLoS One*. 6. doi:10.1371/journal.pone.0021192.

Koulnis, M., E. Porpiglia, P.A. Porpiglia, Y. Liu, K. Hallstrom, D. Hidalgo, and M.

Socolovsky. 2012. Contrasting dynamic responses in vivo of the Bcl-x L and Bim erythropoietic survival pathways. *Blood*. 119:1228–1239. doi:10.1182/blood-2011-07-365346.

Koury, M.J., S.T. Koury, P. Kopsombut, and M.C. Bondurant. 2005. In vitro maturation of nascent reticulocytes to erythrocytes. *Blood*. 105:2168–2174. doi:10.1182/blood-2004-02-0616.

Koury, M.J., S.T. Sawyer, and M.C. Bondurant. 1984. Splenic erythroblasts in anemia-inducing Friend disease: a source of cells for studies of erythropoietin-mediated differentiation. *J. Cell. Physiol*. 121:526–532.

Kriek, N., L. Tilley, P. Horrocks, R. Pinches, B.C. Elford, D.J.P. Ferguson, K. Lingelbach, and C.I. Newbold. 2003. Characterization of the pathway for transport of the cytoadhereince- mediating protein, PfEMP1, to the host cell surface in malaria parasite-infected erythrocytes. *Mol. Microbiol*. 50:1215–1227. doi:10.1046/j.1365-2958.2003.03784.x.

Krishna, S., L. Bustamante, R.K. Haynes, and H.M. Staines. 2008. Artemisinins: their growing importance in medicine. *Trends Pharmacol. Sci*. 29:520–527. doi:10.1016/j.tips.2008.07.004.

Kumpula, E.P., and I. Kursula. 2015. Towards a molecular understanding of the apicomplexan actin motor: On a road to novel targets for malaria remedies? *Acta Crystallogr. Sect. FStructural Biol. Commun*. 71:500–513. doi:10.1107/S2053230X1500391X.

LaCrue, A.N., M. Scheel, K. Kennedy, N. Kumar, and D.E. Kyle. 2011. Effects of artesunate on parasite recrudescence and dormancy in the rodent malaria model plasmodium vinckei. *PLoS One*. 6. doi:10.1371/journal.pone.0026689.

Ladda, R., M. Aikawa, and H. Sprinz. 1969. Penetration of Erythrocytes by Merozoites of Mammalian and Avian Malarial Parasites Author (s): Roger Ladda , Masamichi Aikawa and Helmuth Sprinz Published by : Allen Press on behalf of The American Society of Parasitologists Stable URL : http://www.jst. 55:633–644.

Lafuse, W.P., R. Story, J. Mahylis, G. Gupta, S. Varikuti, H. Steinkamp, S. Oghumu, and A.R. Satoskar. 2013. Leishmania donovani Infection Induces Anemia in Hamsters by Differentially Altering Erythropoiesis in Bone Marrow and Spleen. *PLoS One*. 8:1–12. doi:10.1371/journal.pone.0059509.

Lamikanra, A. a., A.T. Merryweather-Clarke, A.J. Tipping, and D.J. Roberts. 2015. Distinct Mechanisms of Inadequate Erythropoiesis Induced by Tumor

Necrosis Factor Alpha or Malarial Pigment. *PLoS One*. 10:e0119836. doi:10.1371/journal.pone.0119836.

Lamour, S.D., U. Straschil, J. Saric, and M.J. Delves. 2014. Changes in metabolic phenotypes of Plasmodium falciparum in vitro cultures during gametocyte development. *Malar. J.* 13:468. doi:10.1186/1475-2875-13-468.

Langreth, S.G., J.B. JENSEN, R.T. REESE, and W. TRAGER. 1978. Fine Structure of Human Malaria In Vitro *†. *J. Protozool*. 25:443–452. doi:10.1111/j.1550-7408.1978.tb04167.x.

Lanigan, A., and M.T. Fordham. 2017. International Journal of Pediatric Otorhinolaryngology Temporal bone extramedullary hematopoiesis as a cause of pediatric bilateral conductive hearing loss : Case report and review of the literature. *Int. J. Pediatr. Otorhinolaryngol*. 97:135–138. doi:10.1016/j.ijporl.2017.03.032.

Lanzer, M., H. Wickert, G. Krohne, L. Vincensini, and C. Braun Breton. 2006. Maurer's clefts: A novel multi-functional organelle in the cytoplasm of Plasmodium falciparum-infected erythrocytes. *Int. J. Parasitol*. 36:23–36. doi:10.1016/j.ijpara.2005.10.001.

Lapidot, T., and O. Kollet. 2002. The essential roles of the chemokine SDF-1 and its receptor CXCR4 in human stem cell homing and repopulation of transplanted immune-deficient NOD/SCID and NOD/SCID/B2m(null) mice. *Leukemia*. 16:1992–2003. doi:10.1038/sj.leu.2402684.

Lasonder, E., Y. Ishihama, J.S. Andersen, A.M.W. Vermunt, A. Pain, R.W. Sauerwein, W.M.C. Eling, N. Hall, A.P. Waters, H.G. Stunnenberg, and M. Mann. 2002. Analysis of the Plasmodium falciparum proteome by high-accuracy mass spectrometry. *Nature*. 419:537–42. doi:10.1038/nature01111.

Laurentino, E.C., S. Taylor, G.R. Mair, E. Lasonder, R. Bartfai, H.G. Stunnenberg, H. Kroeze, J. Ramesar, B. Franke-Fayard, S.M. Khan, C.J. Janse, and A.P. Waters. 2011. Experimentally controlled downregulation of the histone chaperone FACT in Plasmodium berghei reveals that it is critical to male gamete fertility. *Cell. Microbiol*. 13:1956–1974. doi:10.1111/j.1462-5822.2011.01683.x.

Lee, K., P. Orlandi, D. Haynes, F. Klotz, M. Carter, D. Camus, M. Zegan, and J. Chulay. 1990. Plasmodium falciparum. 25:1877–1884.

Lee, W., B. Russell, Y. Lau, M. Fong, C. Chu, K. Sriprawat, R. Suwanarusk, F. Nosten, and L. Renia. 2013. Giemsa-Stained Wet Mount Based Method for

Reticulocyte Quantification : A Viable Alternative in Resource Limited or Malaria Endemic Settings. 8:6–9. doi:10.1371/journal.pone.0060303.

Lelliott, P.M., S. Lampkin, B.J. McMorran, S.J. Foote, and G. Burgio. 2014. A flow cytometric assay to quantify invasion of red blood cells by rodent Plasmodium parasites in vivo. *Malar. J.* 13:100. doi:10.1186/1475-2875-13-100.

Lelliott, P.M., B.J. Mcmorran, and S.J. Foote. 2015. Erythrocytic Iron Deficiency Enhances Susceptibility to Plasmodium chabaudi Infection in Mice Carrying a Missense Mutation in Transferrin Receptor 1. 83:4322–4334. doi:10.1128/IAI.00926-15.Editor.

Lenox, L.E., J.M. Perry, and R.F. Paulson. 2017. BMP4 and Madh5 regulate the erythroid response to acute anemia. 105:2741–2749. doi:10.1182/blood-2004-02-0703.Supported.

Leoni, S., D. Buonfrate, A. Angheben, F. Gobbi, and Z. Bisoffi. 2015. The hyper-reactive malarial splenomegaly: a systematic review of the literature. *Malar. J.* 14:185. doi:10.1186/s12936-015-0694-3.

Li, B., R. Zhang, J. Li, L. Zhang, G. Ding, P. Luo, S. He, Y. Dong, W. Jiang, Y. Lu, H. Cao, J. Zheng, and H. Zhou. 2008. Antimalarial artesunate protects sepsis model mice against heat-killed Escherichia coli challenge by decreasing TLR4, TLR9 mRNA expressions and transcription factor NF-κB activation. *Int. Immunopharmacol.* 8:379–389. doi:10.1016/j.intimp.2007.10.024.

Li, J., and E.-T. Han. 2012. Dissection of the Plasmoidum vivax reticulocyte binding-like proteins (PvRBPs).

Li, Q., L.H. Xie, A. Haeberle, J. Zhang, and P. Weina. 2006. The evaluation of radiolabeled artesunate on tissue distribution in rats and protein binding in humans. *Am. J. Trop. Med. Hyg.* 75:817–826. doi:75/5/817 [pii].

Lim, C., L. Pereira, K.S. Saliba, A. Mascarenhas, J.N. Maki, L. Chery, E. Gomes, P.K. Rathod, and M.T. Duraisingh. 2016. Reticulocyte Preference and Stage Development of *Plasmodium vivax* Isolates. *J. Infect. Dis.* 214:1081–1084. doi:10.1093/infdis/jiw303.

Lin, J.T. 2011. Drug-Resistant Malaria : The Era of ACT. 12:165–173. doi:10.1007/s11908-010-0099-y.Drug-Resistant.

Lindern, B.M. Von, W. Zauner, G. Mellitzer, P. Steinlein, G. Fritsch, and K. Huber. 2017. The Glucocorticoid Receptor Cooperates With the Erythropoietin Receptor and c-Kit to Enhance and Sustain Proliferation of

Erythroid Progenitors In Vitro. 94:550–559.

Liu, J., X. Guo, N. Mohandas, J.A. Chasis, and X. An. 2010. Membrane remodeling during reticulocyte maturation. *Blood*. 115:2021–2027. doi:10.1182/blood-2009-08-241182.

Liu, J., J. Zhang, Y. Ginzburg, H. Li, F. Xue, L. De Franceschi, J.A. Chasis, N. Mohandas, and X. An. 2013. Quantitative analysis of murine terminal erythroid differentiation in vivo: novel method to study normal and disordered erythropoiesis. *Blood*. 121:e43-9. doi:10.1182/blood-2012-09-456079.

Liu, Y., R. Pop, C. Sadegh, C. Brugnara, V.H. Haase, and M. Socolovsky. 2006. Suppression of Fas-FasL coexpression by erythropoietin mediates erythroblast expansion during the erythropoietic stress response in vivo. *Blood*. 108:123–133. doi:10.1182/blood-2005-11-4458.

Liu, Y., R. Tewari, J. Ning, A.M. Blagborough, S. Garbom, J. Pei, N. V. Grishin, R.E. Steele, R.E. Sinden, W.J. Snell, and O. Billker. 2008. The conserved plant sterility gene. *Genes Dev*. 22:1051–1068. doi:10.1101/gad.1656508.plasma.

Lok, C.N., and P. Ponka. 2000. Identification of an erythroid active element in the transferrin receptor gene. *J. Biol. Chem*. 275:24185–24190. doi:10.1074/jbc.M000944200.

Lomberk, G., L. Wallrath, and R. Urrutia. 2006. The Heterochromatin Protein 1 family. *Genome Biol*. 7:228. doi:10.1186/gb-2006-7-7-228.

Looareesuwan, S., P. Wilairatana, C. Viravan, S. Vanijanonta, P. Pitisuttithum, and D.E. Kyle. 1997. Open randomized trial of oral artemether alone and a sequential combination with mefloquine for acute uncomplicated falciparum malaria. *Am. J. Trop. Med. Hyg*. 56:613–7.

Lopaticki, S., A.G. Maier, J. Thompson, D.W. Wilson, W.H. Tham, T. Triglia, A. Gout, T.P. Speed, J.G. Beeson, J. Healer, and A.F. Cowman. 2011. Reticulocyte and erythrocyte binding-like proteins function cooperatively in invasion of human erythrocytes by malaria parasites. *Infect. Immun*. 79:1107–1117. doi:10.1128/IAI.01021-10.

Lopez-rubio, J.J., A.M. Gontijo, M.C. Nunes, N. Issar, R.H. Rivas, and A. Scherf. 2007. 5 J flanking region of var genes nucleate histone modification patterns linked to phenotypic inheritance. 66:1296–1305. doi:10.1111/j.1365-2958.2007.06009.x.

Loy, D.E., W. Liu, Y. Li, G.H. Learn, L.J. Plenderleith, S.A. Sundararaman, P.M. Sharp, and B.H. Hahn. 2016. Out of Africa: origins and evolution of the human malaria parasites Plasmodium falciparum and Plasmodium vivax. *Int. J. Parasitol.* 47:87–97. doi:10.1016/j.ijpara.2016.05.008.

MacRae, J.I., M.W. Dixon, M.K. Dearnley, H.H. Chua, J.M. Chambers, S. Kenny, I. Bottova, L. Tilley, and M.J. McConville. 2013. Mitochondrial metabolism of sexual and asexual blood stages of the malaria parasite Plasmodium falciparum. *BMC Biol.* 11:67. doi:10.1186/1741-7007-11-67.

Maggio-Price, L., D. Brookoff, and L. Weiss. 1985. Changes in hematopoietic stem cells in the Bone Malaria of Mice with Plasmodium berghei malaria. 66:1080–1085.

Mair, G.R., J.A.M. Braks, L.S. Garver, G. Dimopoulos, N. Hall, J.C.A.G. Wiegant, R.W. Dirks, S.M. Khan, C.J. Janse, and A.P. Waters. 2006. Translational Repression is essential for Plasmodium sexual development and mediated by a DDX6-type RNA helicase. *Methods.* 46:3684–3692. doi:10.1038/nature09421.Oxidative.

Mair, G.R., E. Lasonder, L.S. Garver, B.M.D. Franke-Fayard, C.K. Carret, J.C.A.G. Wiegant, R.W. Dirks, G. Dimopoulos, C.J. Janse, and A.P. Waters. 2010. Universal features of post-transcriptional gene regulation are critical for Plasmodium zygote development. *PLoS Pathog.* 6. doi:10.1371/journal.ppat.1000767.

Makani, J., A.N. Komba, S.E. Cox, J. Oruo, K. Mwamtemi, J. Kitundu, P. Magesa, S. Rwezaula, E. Meda, J. Mgaya, K. Pallangyo, E. Okiro, D. Muturi, C.R. Newton, G. Fegan, K. Marsh, and T.N. Williams. 2017. Malaria in patients with sickle cell anemia : burden , risk factors , and outcome at the outpatient clinic and during hospitalization. 115:1–3. doi:10.1182/blood-2009-07-233528.The.

Małkiewicz, A., and M. Dziedzic. 2012. Bone marrow reconversion - imaging of physiological changes in bone marrow. *Pol. J. Radiol.* 77:45–50.

Malleret, B., A. Li, R. Zhang, K.S.W. Tan, R. Suwanarusk, C. Claser, J.S. Cho, E.G.L. Koh, C.S. Chu, S. Pukrittayakamee, M.L. Ng, F. Ginhoux, L.G. Ng, C.T. Lim, F. Nosten, G. Snounou, L. R??nia, and B. Russell. 2015. Plasmodium vivax: Restricted tropism and rapid remodeling of CD71-positive reticulocytes. *Blood.* 125:1314–1324. doi:10.1182/blood-2014-08-596015.

Malleret, B., F. Xu, N. Mohandas, R. Suwanarusk, C. Chu, J.A. Leite, K. Low, C.

Turner, K. Sriprawat, R. Zhang, O. Bertrand, Y. Colin, F.T.M. Costa, C.N. Ong, M.L. Ng, C.T. Lim, F. Nosten, L. Rénia, and B. Russell. 2013. Significant Biochemical, Biophysical and Metabolic Diversity in Circulating Human Cord Blood Reticulocytes. *PLoS One*. 8. doi:10.1371/journal.pone.0076062.

Malley, D.P.O. 2007. Benign extramedullary myeloid proliferations. 405–415. doi:10.1038/modpathol.3800768.

Mantel, C., S. Messina-Graham, and H.E. Broxmeyer. 2010. Upregulation of nascent mitochondrial biogenesis in mouse hematopoietic stem cells parallels upregulation of CD34 and loss of pluripotency: A potential strategy for reducing oxidative risk in stem cells. *Cell Cycle*. 9:2008–2017. doi:10.4161/cc.9.10.11733.

Mantel, P.Y., A.N. Hoang, I. Goldowitz, D. Potashnikova, B. Hamza, I. Vorobjev, I. Ghiran, M. Toner, D. Irimia, A.R. Ivanov, N. Barteneva, and M. Marti. 2013. Malaria-infected erythrocyte-derived microvesicles mediate cellular communication within the parasite population and with the host immune system. *Cell Host Microbe*. 13:521–534. doi:10.1016/j.chom.2013.04.009.

MAP, malaria atlas project. 2015. www.map.ox.ac.uk.

Marín-Menéndez, A., A. Bardají, F.E. Martínez-Espinosa, C. Bôtto-Menezes, M. V. Lacerda, J. Ortiz, P. Cisteró, M. Piqueras, I. Felger, I. Müeller, J. Ordi, H. del Portillo, C. Menéndez, M. Wahlgren, and A. Mayor. 2013. Rosetting in Plasmodium vivax: A Cytoadhesion Phenotype Associated with Anaemia. *PLoS Negl. Trop. Dis.* 7:1–8. doi:10.1371/journal.pntd.0002155.

Marshall, V.M., A. Silva, M. Foley, S. Cranmer, L. Wang, D.J. McColl, D.J. Kemp, and R.L. Coppel. 1997. A second merozoite surface protein (MSP-4) of Plasmodium falciparum that contains an epidermal growth factor-like domain. *Infect. Immun.* 65:4460–4467.

Marshall, V.M., W. Tieqiao, and R.L. Coppel. 1998. Close linkage of three merozoite surface protein genes on chromosome 2 of Plasmodium falciparum. *Mol. Biochem. Parasitol.* 94:13–25.

Martín-jaular, L., A. Elizalde-torrent, R. Thomson-luque, M. Ferrer, J.C. Segovia, E. Herreros-aviles, C. Fernández-becerra, and H. a Portillo. 2013. Reticulocyte-prone malaria parasites predominantly invade CD71 hi immature cells : implications for the development of an in vitro culture for Plasmodium vivax. *Malar. J.* 12:434. doi:10.1186/1475-2875-12-434.

Martín-Jaular, L., A. de Menezes-Neto, M. Monguió-Tortajada, A. Elizalde-Torrent, M. Díaz-Varela, C. Fernández-Becerra, F.E. Borras, M. Montoya, and H.A. del Portillo. 2016. Spleen-Dependent Immune Protection Elicited by CpG Adjuvanted Reticulocyte-Derived Exosomes from Malaria Infection Is Associated with Changes in T cell Subsets' Distribution. *Front. Cell Dev. Biol.* 4:1–11. doi:10.3389/fcell.2016.00131.

Martinelli, R., A.S. Zeiger, M. Whitfield, T.E. Sciuto, A. Dvorak, K.J. Van Vliet, J. Greenwood, and C. V Carman. 2014. Probing the biomechanical contribution of the endothelium to lymphocyte migration : diapedesis by the path of least resistance. 3720–3734. doi:10.1242/jcs.148619.

Marty, A.J., J.K. Thompson, M.F. Duffy, T.S. Voss, A.F. Cowman, and B.S. Crabb. 2006. Evidence that Plasmodium falciparum chromosome end clusters are cross-linked by protein and are the sites of both virulence gene silencing and activation. *Mol. Microbiol.* 62:72–83. doi:10.1111/j.1365-2958.2006.05364.x.

Matsuoka, Y., Y. Saski, R. Nakatsuka, M. Takhashi, R. Iwaki, Y. Uemura, and Y. Sonoda. 2011. Low Level of C-Kit Expression Marks Deeply Quiescent Murine. 1783–1791. doi:10.1002/stem.721.

Maxie, G. 2015. Jubb, Kennedy and Palmer's pathology of domestic animals; volume 3. 159–160.

Mayor, A., A. Bardají, I. Felger, C.L. King, P. Cisteró, C. Dobaño, D.I. Stanisic, P. Siba, M. Wahlgren, H. Del Portillo, I. Mueller, C. Menéndez, J. Ordi, and S. Rogerson. 2012. Placental infection with plasmodium vivax: A histopathological and molecular study. *J. Infect. Dis.* 206:1904–1910. doi:10.1093/infdis/jis614.

Mbengue, A., S. Bhattacharjee, T. Pandharkar, H. Liu, G. Estiu, M. Ghorbal, M. Pfrender, S. Emrich, N. Mohandas, and A.M. Dondorp. 2015. A molecular mechanism of artemisinin resistance in Plasmodium falciparum malaria. doi:10.1038/nature14412.

Mbengue, B., B. Niang, M.S. Niang, M.L. Varela, B. Fall, M.M. Fall, R.N. Diallo, B. Diatta, D.C. Gowda, A. Dieye, and R. Perraut. 2016. Inflammatory cytokine and humoral responses to Plasmodium falciparum glycosylphosphatidylinositols correlates with malaria immunity and pathogenesis. *Immunity, Inflamm. Dis.* 4:24–34. doi:10.1002/iid3.89.

McColl, D.J., A. Silva, M. Foley, J.F.J. Kun, J.M. Favaloro, J.K. Thompson, V.M.

Marshall, R.L. Coppel, D.J. Kemp, and R.F. Anders. 1994. Molecular variation in a novel polymorphic antigen associated with Plasmodium falciparum merozoites. *Mol. Biochem. Parasitol.* 68:53–67. doi:10.1016/0166-6851(94)00149-9.

Mcrobert, L., L. Mcrobert, P. Preiser, P. Preiser, S. Sharp, S. Sharp, W. Jarra, W. Jarra, M. Kaviratne, M. Kaviratne, M.C. Taylor, M.C. Taylor, L. Renia, L. Renia, C.J. Sutherland, and C.J. Sutherland. 2004. Distinct Traf cking and Localization of STEVOR Proteins in Three Stages of the. *Society*. 72:6597–6602. doi:10.1128/IAI.72.11.6597.

Mebius, R.E., and G. Kraal. 2005. STRUCTURE AND FUNCTION OF THE SPLEEN. 5:606–616. doi:10.1038/nri1669.

Meibalan, E., M.A. Comunale, A.M. Lopez, L.W. Bergman, A. Mehta, A.B. Vaidya, and J.M. Burns. 2015. Host erythrocyte environment influences the localization of exported protein 2, an essential component of the Plasmodium translocon. *Eukaryot. Cell.* 14:371–384. doi:10.1128/EC.00228-14.

Melo, G.C., W.M. Monteiro, A.M. Siqueira, S.R. Silva, B.M.L. Magalhães, A.C.C. Alencar, A. Kuehn, H.A. Del Portillo, C. Fernandez-Becerra, and M.V.G. Lacerda. 2014. Expression levels of pvcrt-o and pvmdr-1 are associated with chloroquine resistance and severe Plasmodium vivax malaria in patients of the Brazilian Amazon. *PLoS One*. 9:1–10. doi:10.1371/journal.pone.0105922.

Menard, D., E.R. Chan, C. Benedet, A. Ratsimbasoa, S. Kim, P. Chim, C. Do, B. Witkowski, R. Durand, M. Thellier, C. Severini, E. Legrand, L. Musset, B.Y.M. Nour, O. Mercereau-Puijalon, D. Serre, and P.A. Zimmerman. 2013. Whole Genome Sequencing of Field Isolates Reveals a Common Duplication of the Duffy Binding Protein Gene in Malagasy Plasmodium vivax Strains. *PLoS Negl. Trop. Dis.* 7. doi:10.1371/journal.pntd.0002489.

Ménard, R. 2001. Gliding motility and cell invasion by Apicomplexa: Insights from the Plasmodium sporozoite. *Cell. Microbiol.* 3:63–73. doi:10.1046/j.1462-5822.2001.00097.x.

Mendez-Ferrer, S., A. Chow, M. Merad, and P.S. Frenette. 2009. NIH Public Access. 16:235–242. doi:10.1097/MOH.0b013e32832bd0f5.Circadian.

Mesen-Ramirez, P., F. Reinsch, A. Blancke Soares, B. Bergmann, A.K. Ullrich, S. Tenzer, and T. Spielmann. 2016. Stable Translocation Intermediates Jam Global Protein Export in Plasmodium falciparum Parasites and Link the PTEX

Component EXP2 with Translocation Activity. *PLoS Pathog*. 12:1–28. doi:10.1371/journal.ppat.1005618.

Mideo, N., S.E. Reece, A.L. Smith, and C.J.E. Metcalf. 2013. The Cinderella syndrome : why do malaria-infected cells burst at midnight ? *Trends Parasitol*. 29:10–16. doi:10.1016/j.pt.2012.10.006.

Miller, B.Y.L.H., M. Aikawa, and J.G. Johnson. 1979. BETWEEN AND ERYTHROCYTES Attachment and Junction Formation. *J. Exp. Med.* 149:172–184.

Miller, L.H., H.C. Ackerman, X.Z. Su, and T.E. Wellems. 2013. Malaria biology and disease pathogenesis: insights for new treatments. *Nat Med*. 19:156–167. doi:10.1038/nm.3073.

Millholland, M.G., R. Chandramohanadas, A. Pizzarro, A. Wehr, H. Shi, C. Darling, C.T. Lim, and D.C. Greenbaum. 2011. The malaria parasite progressively dismantles the host erythrocyte cytoskeleton for efficient egress. *Mol Cell Proteomics*. 10:M111 010678. doi:10.1074/mcp.M111.010678.

Mills, K.E., J.A. Pearce, B.S. Crabb, and A.F. Cowman. 2002. Truncation of merozoite surface protein 3 disrupts its trafficking and that of acidic-basic repeat protein to the surface of Plasmodium falciparum merozoites. *Mol. Microbiol*. 43:1401–1411. doi:10.1046/j.1365-2958.2002.02834.x.

Mkumbaye, S.I., C.W. Wang, E. Lyimo, J.S. Jespersen, A. Manjurano, J. Mosha, R.A. Kavishe, S.B. Mwakalinga, D.T.R. Minja, J.P. Lusingu, T.G. Theander, and T. Lavstsen. 2017. The severity of *Plasmodium falciparum* infection is associated with transcript levels of *var* genes encoding EPCR-binding PfEMP1. *Infect. Immun.* IAI.00841-16. doi:10.1128/IAI.00841-16.

Mok, B.W., U. Ribacke, N. Rasti, F. Kironde, Q. Chen, P. Nilsson, and M. Wahlgren. 2008. Default pathway of var2csa switching and translational repression in plasmodium falciparum. *PLoS One*. 3. doi:10.1371/journal.pone.0001982.

Mongui, A., D.I. Angel, C. Guzman, M. Vanegas, and M.A. Patarroyo. 2008. Characterisation of the Plasmodium vivax Pv38 antigen. *Biochem. Biophys. Res. Commun.* 376:326–330. doi:10.1016/j.bbrc.2008.08.163.

Mons, B. 1990. Preferential invasion of malarial merozoites into young red blood cells.

Mons, B., C.J. Janse, E.G. Boorsma, and H.J. Van der Kaay. 1985. Synchronized

erythrocytic schizogony and gametocytogenesis of Plasmodium berghei in vivo and in vitro. *Parasitology*. 91:423–430. doi:10.1017/S0031182000062673.

Moreno, A., E. Ferrer, S. Arahuetes, C. Eguiluz, N. Van Rooijen, and A. Benito. 2006. The course of infections and pathology in immunomodulated NOD/LtSz-SCID mice inoculated with Plasmodium falciparum laboratory lines and clinical isolates. *Int. J. Parasitol.* 36:361–369. doi:10.1016/j.ijpara.2005.10.012.

Motoi Ishidate, J. 1990. The micronucleus assay with mouse peripheral blood reticulocytes using acridine orange-coated slides. 245:245–249.

Muley, A.P., J. Lakhani, and M. Parekh. 2011. Case report Sickle cell hemoglobinopathy protection against malaria : is it changing ? 2:818–819.

Muller, W.A. 2013. Getting leukocytes to the site of inflammation. *Vet. Pathol.* 50:7–22. doi:10.1177/0300985812469883.

Muta, K., and S.B. Krantz. 1993. Apoptosis of human erythroid colony-forming cells is decreased by stem cell factor and insulin-like growth factor I as well as erythropoietin. *J Cell Physiol*. 156:264–271. doi:10.1002/jcp.1041560207.

Muzykantov, V.R. 2011. NIH Public Access. 7. 403-427 pp.

Nacher, M., P. Singhasivanon, U. Silachamroon, S. Treeprasertsuk, T. Tosukhowong, S. Vannaphan, F. Gay, D. Mazier, and S. Looareesuwan. 2002. Decreased Hemoglobin Concentrations, Hyperparasitemia, and Severe Malaria Are Associated With Increased Plasmodium Falciparum Gametocyte Carriage. *J. Parasitol.* 88:97–101. doi:10.1645/0022-3395(2002)088[0097:DHCHAS]2.0.CO;2.

Nandakumar, S.K., J.C. Ulirsch, and V.G. Sankaran. 2016. Advances in understanding erythropoiesis: Evolving perspectives. *Br. J. Haematol.* 173:206–218. doi:10.1111/bjh.13938.

Nantakomol, D., A.M. Dondorp, S. Krudsood, R. Udomsangpetch, K. Pattanapanyasat, V. Combes, G.E. Grau, N.J. White, P. Viriyavejakul, and N.P.J. Day. 2011. Circulating Red Cell – derived Microparticles in Human Malaria. 203. doi:10.1093/infdis/jiq104.

Nayyar, G.M.L., J.G. Breman, P.N. Newton, and J. Herrington. 2012. Poor-quality antimalarial drugs in southeast Asia and sub-Saharan Africa. *Lancet Infect. Dis.* 12:488–496. doi:10.1016/S1473-3099(12)70064-6.

Nee, S., S.A. West, and A.F. Read. 2002. Inbreeding and parasite sex ratios.

Proc. R. Soc. London Ser. B-Biological Sci. 269:755–760. doi:10.1098/rspb.2001.1938.

Nery, S., A.M. Deans, M. Mosobo, K. Marsh, J.A. Rowe, and D.J. Conway. 2006. Expression of Plasmodium falciparum genes involved in erythrocyte invasion varies among isolates cultured directly from patients. *Mol. Biochem. Parasitol.* 149:208–215. doi:10.1016/j.molbiopara.2006.05.014.

Network, M.G.E. 2015. A novel locus of resistance to severe malaria in a region of ancient balancing selection. doi:10.1038/nature15390.

Nguyen Duy Sy, Dao Boi Hoan, Nguyen Phuong Dung, Nguyen Van Huong, Le Nguyen Binh, Mai Van Son, and S.R. Meshnick. 1993. Treatment of malaria in Vietnam with oral artemisinin. *Am. J. Trop. Med. Hyg.* 48:398–402.

Niang, M., A.K. Bei, K.G. Madnani, S. Pelly, S. Dankwa, U. Kanjee, K. Gunalan, A. Amaladoss, K.P. Yeo, N.S. Bob, B. Malleret, M.T. Duraisingh, and P.R. Preiser. 2014. STEVOR is a plasmodium falciparum erythrocyte binding protein that mediates merozoite invasion and rosetting. *Cell Host Microbe*. 16:81–93. doi:10.1016/j.chom.2014.06.004.

Nielsen, M.A., T. Staalsoe, J.A.L. Kurtzhals, B.Q. Goka, D. Dodoo, M. Alifrangis, G. Theander, B.D. Akanmori, L. Hviid, D. Dodoo, M. Alifrangis, T.G. Theander, B.D. Akanmori, and L. Hviid. 2002. Plasmodium falciparum Variant Surface Antigen Expression Varies Between Isolates Causing Severe and Nonsevere Malaria and Is Modified by Acquired Immunity. doi:10.4049/jimmunol.168.7.3444.

Nilsson, S.K., L.M. Childs, C. Buckee, and M. Marti. 2015. Targeting Human Transmission Biology for Malaria Elimination. *PLOS Pathog.* 11:e1004871. doi:10.1371/journal.ppat.1004871.

Nkhoma, S., D. Psr, and D. Psr. 2007. Is sulphadoxine-pyrimethamine (SP) still useful as the first-line antimalarial drug in Malawi or it must be quickly withdrawn from the antimalarial repertoire ? 19–20.

Noji, H., T. Shichishima, Y. Saitoh, T. Kai, T. Yamamoto, K. Ogawa, M. Okamoto, K. Ikeda, and Y. Maruyama. 2001. The distribution of PIG-A gene abnormalities in paroxysmal nocturnal hemoglobinuria granulocytes and cultured erythroblasts. *Exp. Hematol.* 29:391–400. doi:10.1016/S0301-472X(00)00684-6.

Nourshargh, S., and R. Alon. 2014. Leukocyte Migration into Inflamed Tissues. *Immunity*. 41:694–707. doi:10.1016/j.immuni.2014.10.008.

Nrpt.co.uk. 2017. http://www.nrpt.co.uk/training/body/skeletal/long.htm.

Ntumngia, F.B., R. Thomson-Luque, L. de M. Torres, K. Gunalan, L.H. Carvalho, and J.H. Adams. 2016. A Novel Erythrocyte Binding Protein of *Plasmodium vivax* Suggests an Alternate Invasion Pathway into Duffy-Positive Reticulocytes. *MBio*. 7:e01261-16. doi:10.1128/mBio.01261-16.

Nunes, M.C., J.P.D. Goldring, C. Doerig, and A. Scherf. 2007. A novel protein kinase family in Plasmodium falciparum is differentially transcribed and secreted to various cellular compartments of the host cell. *Mol. Microbiol.* 63:391–403. doi:10.1111/j.1365-2958.2006.05521.x.

Oburoglu, L., M. Romano, N. Taylor, and S. Kinet. 2016. Metabolic regulation of hematopoietic stem cell commitment and erythroid differentiation. *Curr. Opin. Hematol.* 23:198–205. doi:10.1097/MOH.0000000000000234.

Ockenhouse, C.F., E. Angov, K.E. Kester, C. Diggs, L. Soisson, J.F. Cummings, A. V. Stewart, D.R. Palmer, B. Mahajan, U. Krzych, N. Tornieporth, M. Delchambre, M. Vanhandenhove, O. Ofori-Anyinam, J. Cohen, J.A. Lyon, and D.G. Heppner. 2006. Phase I safety and immunogenicity trial of FMP1/AS02A, a Plasmodium falciparum MSP-1 asexual blood stage vaccine. *Vaccine*. 24:3009–3017. doi:10.1016/j.vaccine.2005.11.028.

Oeuvray, C., H. Bouharoun-Tayoun, H. Grass-Masse, J.P. Lepers, L. Ralamboranto, A. Tartar, and P. Druilhe. 1994. A novel merozoite surface antigen of Plasmodium falciparum (MSP-3) identified by cellular-antibody cooperative mechanism antigenicity and biological activity of antibodies. *Mem. Inst. Oswaldo Cruz*. 89 Suppl 2:77–80. doi:S0074-02761994000600018 [pii].

Ohr, I.C. 1967. Inefficacy of erythropoietic response of BALB / c mice to hypoxia ’. 213.

Orjih, A.U. 2005. Comparison of Plasmodium falciparum growth in sickle cells in low oxygen environment and candle-jar. *Acta Trop.* 94:25–34. doi:10.1016/j.actatropica.2005.02.001.

Orr, R.Y., N. Philip, and A.P. Waters. 2012. Improved negative selection protocol for Plasmodium berghei in the rodent malarial model. *Malar. J.* 11:103. doi:10.1186/1475-2875-11-103.

Packard, R. 2000. Malaria drug resistance. *Bull. World Health Organ.* 78:407. doi:10.1056/NEJMp1404358.

Palis, J. 2014. Primitive and definitive erythropoiesis in mammals. *Front.*

Physiol. 5 JAN:1–9. doi:10.3389/fphys.2014.00003.

Palitzsch, K.D., S. Falk, H. Miiller, and H.J. Stutte. 1987. Splenic haematopoiesis in patients with cirrhosis of the liver. 179–183.

Panichakul, T., J. Sattabongkot, K. Chotivanich, J. Sirichaisinthop, L. Cui, and R. Udomsangpetch. 2007. Production of erythropoietic cells in vitro for continuous culture of Plasmodium vivax. *Int. J. Parasitol*. 37:1551–1557. doi:10.1016/j.ijpara.2007.05.009.

Papayannopoulou, B.T., and M. Brice. 1992. Integrin Expression Profiles During Erythroid Differentiation. 79:1686–1694.

Parker, M.L., F. Peng, and M.J. Boulanger. 2015. The structure of plasmodium falciparum blood-stage 6-cys protein Pf41 reveals an unexpected intra-domain insertion required for Pf12 coordination. *PLoS One*. 10:1–16. doi:10.1371/journal.pone.0139407.

Pathak, V.A., and K. Ghosh. 2016. Erythropoiesis in Malaria Infections and Factors Modifying the Erythropoietic Response. 2016. doi:10.1155/2016/9310905.

Paul, A.S., E.S. Egan, M.T. Duraisingh, and I. Diseases. 2016. HHS Public Access. 22:220–226. doi:10.1097/MOH.0000000000000135.Host-parasite.

Paulson, R.F., L. Shi, and D.-C. Wu. 2011. Stress erythropoiesis: new signals and new stress progenitor cells. *Curr. Opin. Hematol*. 18:139–45. doi:10.1097/MOH.0b013e32834521c8.

Pearson, R., A. R, A. S, M. O, A.-G. J, and et al. Amaratunga. 2016. Genomic analysis of local variation and recent evolution in Plasmodium vivax. *Nat Genet*. in pess:959–964. doi:10.1038/ng.3599.Genomic.

Peatey, C.L., J. a. Watson, K.R. Trenholme, C.L. Brown, L. Nielson, M. Guenther, N. Timmins, G.S. Watson, and D.L. Gardiner. 2013. Enhanced gametocyte formation in erythrocyte progenitor cells: A site-specific adaptation by plasmodium falciparum. *J. Infect. Dis*. 208:1170–1174. doi:10.1093/infdis/jit309.

Pelle, K.G., K. Oh, K. Buchholz, V. Narasimhan, R. Joice, D. a Milner, N.M. Brancucci, S. Ma, T.S. Voss, K. Ketman, K.B. Seydel, T.E. Taylor, N.S. Barteneva, C. Huttenhower, and M. Marti. 2015. Transcriptional profiling defines dynamics of parasite tissue sequestration during malaria infection. *Genome Med*. 7:1–20. doi:10.1186/s13073-015-0133-7.

Pereira, J.P., J. An, Y. Xu, Y. Huang, and J.G. Cyster. 2009. Cannabinoid

receptor 2 mediates the retention of immature B cells in bone marrow sinusoids. *Nat. Immunol.* 10:403–411. doi:10.1038/ni.1710.

Pereira, M.A., T.M. Clausen, C. Pehrson, and Y. Mao. 2016. Placental Sequestration of Plasmodium falciparum Malaria Parasites Is Mediated by the Interaction Between VAR2CSA and Chondroitin Sulfate A on Syndecan-1. 1–26. doi:10.1371/journal.ppat.1005831.

Perkins, M.E., and L.J. Rocco. 1988. Sialic acid-dependent binding of Plasmodium falciparum merozoite surface antigen , Pf200 , to human erythrocytes . This information is current as M E Perkins and L J Rocco Email Alerts Information about subscribing to The Journal of Immunology is online a.

Perkins, S.L., I.N. Sarkar, and R. Carter. 2007. The phylogeny of rodent malaria parasites: Simultaneous analysis across three genomes. *Infect. Genet. Evol.* 7:74–83. doi:10.1016/j.meegid.2006.04.005.

Perrin, A.J., S.J. Bartholdson, and G.J. Wright. 2015. P-selectin is a host receptor for Plasmodium MSP7 ligands. *Malar. J.* 14:238. doi:10.1186/s12936-015-0750-z.

Perry, J.M., O.F. Harandi, P. Porayette, S. Hegde, A.K. Kannan, and R.F. Paulson. 2009. Maintenance of the BMP4-dependent stress erythropoiesis pathway in the murine spleen requires hedgehog signaling. *Blood.* 113:911–918. doi:10.1182/blood-2008-03-147892.

Peterson, D.S., and T.E. Wellems. 2000. EBL -1 , a putative erythrocyte binding protein of Plasmodium falciparum , maps within a favored linkage group in two genetic crosses. 105:105–113.

Philip, N., and A.P. Waters. 2015. Conditional degradation of plasmodium calcineurin reveals functions in parasite colonization of both host and vector. *Cell Host Microbe.* 18:122–131. doi:10.1016/j.chom.2015.05.018.

Pisciotta, J.M., P.F. Scholl, J.L. Shuman, V. Shualev, and D.J. Sullivan. 2017. Quantitative characterization of hemozoin in Plasmodium berghei and vivax. *Int. J. Parasitol. Drugs Drug Resist.* 7:110–119. doi:10.1016/j.ijpddr.2017.02.001.

Pivkin, I. V., Z. Peng, G.E. Karniadakis, P.A. Buffet, M. Dao, and S. Suresh. 2016. Biomechanics of red blood cells in human spleen and consequences for physiology and disease. *Proc. Natl. Acad. Sci.* 113:201606751. doi:10.1073/pnas.1606751113.

Ponts, N., L. Fu, E.Y. Harris, J. Zhang, D.-W.D. Chung, M.C. Cervantes, J. Prudhomme, V. Atanasova-Penichon, E. Zehraoui, E.M. Bunnik, E.M. Rodrigues, S. Lonardi, G.R. Hicks, Y. Wang, and K.G. Le Roch. 2013. Genome-wide mapping of DNA methylation in the human malaria parasite Plasmodium falciparum. *Cell Host Microbe*. 14:696–706. doi:10.1016/j.chom.2013.11.007.

Ponts, N., E. Harris, and J. Prudhomme. 2010. Nucleosome landscape and control of transcription in the human malaria parasite. *Genome Res.* 20:228–238. doi:10.1101/gr.101063.109.identified.

Porpiglia, E., D. Hidalgo, M. Koulnis, A.R. Tzafriri, and M. Socolovsky. 2012. Stat5 Signaling Specifies Basal versus Stress Erythropoietic Responses through Distinct Binary and Graded Dynamic Modalities. *PLoS Biol*. 10. doi:10.1371/journal.pbio.1001383.

del Portillo, H.A., S. Longacre, E. Khouri, and P.H. David. 1991. Primary structure of the merozoite surface antigen 1 of Plasmodium vivax reveals sequences conserved between different Plasmodium species. *Proc Natl Acad Sci U S A*. 88:4030–4034. doi:10.1073/pnas.88.9.4030.

del Portillo, H. a, C. Fernandez-Becerra, S. Bowman, K. Oliver, M. Preuss, C.P. Sanchez, N.K. Schneider, J.M. Villalobos, M. a Rajandream, D. Harris, L.H. Pereira da Silva, B. Barrell, and M. Lanzer. 2001. A superfamily of variant genes encoded in the subtelomeric region of Plasmodium vivax. *Nature*. 410:839–842. doi:10.1038/35071118.

Pothapregada, S., and B. Kamalakannan. 2014. Hemophagocytic syndrome in Plasmodium vivax malaria. *J. Vector Borne Dis.* 51:144–146.

Poulin, B., E.-M. Patzewitz, D. Brady, O. Silvie, M.H. Wright, D.J.P. Ferguson, R.J. Wall, S. Whipple, D.S. Guttery, E.W. Tate, B. Wickstead, A. a Holder, and R. Tewari. 2013. Unique apicomplexan IMC sub-compartment proteins are early markers for apical polarity in the malaria parasite. *Biol. Open*. 2:1160–70. doi:10.1242/bio.20136163.

Raess, B.U., D.M. Record, and G. Tunnicliff. 1985. Interaction of phenylglyoxal with the human erythrocyte (Ca2+ + Mg2+)-ATPase. Evidence for the presence of an essential arginyl residue. *Mol. Pharmacol*. 27:444–50. doi:10.1097/MOH.0b013e328345213e.Normal.

Ralph, S.A., C. Scheidig-Benatar, and A. Scherf. 2005. Antigenic variation in Plasmodium falciparum is associated with movement of var loci between

subnuclear locations. *Proc. Natl. Acad. Sci. U. S. A.* 102:5414–9. doi:10.1073/pnas.0408883102.

Ramiro, R.S., S.E. Reece, and D.J. Obbard. 2012. Molecular evolution and phylogenetics of rodent malaria parasites. *BMC Evol Biol*. 12:219. doi:10.1186/1471-2148-12-219.

Rayner, J.C., M.R. Galinski, P. Ingravallo, and J.W. Barnwell. 2000. Two Plasmodium falciparum genes express merozoite proteins that are related to Plasmodium vivax and Plasmodium yoelii adhesive proteins involved in host cell selection and invasion. *Proc. Natl. Acad. Sci. U. S. A.* 97:9648–9653. doi:10.1073/pnas.160469097.

Rayner, J.C., E. Vargas-Serrato, C.S. Huber, M.R. Galinski, and J.W. Barnwell. 2001. A Plasmodium falciparum homologue of Plasmodium vivax reticulocyte binding protein (PvRBP1) defines a trypsin-resistant erythrocyte invasion pathway. *J. Exp. Med.* 194:1571–81. doi:10.1084/jem.194.11.1571.

Regev-Rudzki, N., D.W. Wilson, T.G. Carvalho, X. Sisquella, B.M. Coleman, M. Rug, D. Bursac, F. Angrisano, M. Gee, A.F. Hill, J. Baum, and A.F. Cowman. 2013. Cell-cell communication between malaria-infected red blood cells via exosome-like vesicles. *Cell*. 153:1120–1133. doi:10.1016/j.cell.2013.04.029.

Reichardt, H.M., K.H. Kaestner, J. Tuckermann, O. Kretz, O. Wessely, R. Bock, P. Gass, W. Schmid, P. Herrlich, P. Angel, and G. Schütz. 1998. DNA binding of the glucocorticoid receptor is not essential for survival. *Cell*. 93:531–541. doi:10.1016/S0092-8674(00)81183-6.

Reiling, L., J.S. Richards, F.J.I. Fowkes, D.W. Wilson, W. Chokejindachai, A.E. Barry, W.H. Tham, J. Stubbs, C. Langer, J. Donelson, P. Michon, L. Tavul, B.S. Crabb, P.M. Siba, A.F. Cowman, I. Mueller, and J.G. Beeson. 2012. The Plasmodium falciparum Erythrocyte Invasion Ligand Pfrh4 as a Target of Functional and Protective Human Antibodies against Malaria. *PLoS One*. 7:1–12. doi:10.1371/journal.pone.0045253.

Ricchi, P. 2017. Extramedullary Haematopoiesis in Patients with Thalassaemia Major : Should We Search for It Regularly ? 173–174. doi:10.1159/000464399.

Rice, B., M. Acosta, A. Pacheco, J. Carlton, J.W. Barnwell, and A.A. Escalante. 2014. HHS Public Access. 8:583–592. doi:10.1002/aur.1474.Replication.

Riglar, D.T., D. Richard, D.W. Wilson, M.J. Boyle, C. Dekiwadia, L. Turnbull, F. Angrisano, D.S. Marapana, K.L. Rogers, C.B. Whitchurch, J.G. Beeson, A.F. Cowman, S.A. Ralph, and J. Baum. 2011. Super-resolution dissection of

coordinated events during malaria parasite invasion of the human erythrocyte. *Cell Host Microbe*. 9:9–20. doi:10.1016/j.chom.2010.12.003.

Riglar, D.T., L. Whitehead, A.F. Cowman, K.L. Rogers, and J. Baum. 2015. Localization-based imaging of malarial antigens during red cell entry reaffirms role for AMA1 but not MTRAP in invasion. *J Cell Sci*. 228–242. doi:10.1242/jcs.177741.

Rogers, N.J., B.S. Hall, J. Obiero, G.A.T. Targett, and C.J. Sutherland. 2000. A Model for Sequestration of the Transmission Stages of Plasmodium falciparum: Adhesion of Gametocyte-Infected Erythrocytes to Human Bone Marrow Cells. *Infect. Immun.* 68:3455–3462. doi:10.1128/IAI.68.6.3455-3462.2000.

Rosenthal, P.J. 2008. Artesunate for the Treatment of Severe Falciparum Malaria. *N. Engl. J. Med.* 17:1829–1836. doi:10.1056/NEJMct0709050.

Rossi, E. 2005. Hepcidin - the Iron Regulatory Hormone Hepcidin. 26:47–49.

Rovira-Graells, N.N., A.P. Gupta, E. Planet, V.M. Crowley, S. Mok, L. Ribas de Pouplana, P.R. Preiser, Z. Bozdech, A. Cortes, L.R. De Pouplana, and A. Cortés. 2012. The variantome of the malaria parasite Plasmodium falciparum. *Genome Res.* 22:925–938. doi:10.1101/gr.129692.111.22.

Rovira-Vallbona, E., C. Dobaño, A. Bardají, P. Cisteró, C. Romagosa, E. Serra-Casas, L. Quintó, Q. Bassat, B. Sigaúque, P.L. Alonso, J. Ordi, C. Menéndez, and A. Mayor. 2011. Transcription of var genes other than var2csa in Plasmodium falciparum parasites infecting mozambican pregnant women. *J. Infect. Dis.* 204:27–35. doi:10.1093/infdis/jir217.

Ru, Y.-X., B.-Y. Mao, F. Zhang, T. Pang, S. Zhao, J. Liu, and S.N. Wickramasinghe. 2009. Invasion of erythroblasts by Pasmodium vivax: A new mechanism contributing to malarial anemia. *Ultrastruct. Pathol.* 33:236–242. doi:10.3109/01913120903251643.

Rug, M., M. Cyrklaff, A. Mikkonen, L. Lemgruber, S. Kuelzer, C.P. Sanchez, J. Thompson, E. Hanssen, M. O'Neill, C. Langer, M. Lanzer, F. Frischknecht, A.G. Maler, and A.F. Cowman. 2014. Export of virulence proteins by malaria-infected erythrocytes involves remodeling of host actin cytoskeleton Melanie. *Blood*. 124:3459–3469. doi:10.1182/blood-2014-06-583054.The.

Russell, D.G., and R.E. Sinden. 1981. The role of the cytoskeleton in the motility of coccidian sporozoites. *J. Cell Sci.* 50:345–359.

Rutledge, G.G., U. Böhme, M. Sanders, A.J. Reid, J.A. Cotton, O. Maiga-

Ascofare, A.A. Djimdé, T.O. Apinjoh, M. Amenga-Etego, Lucas Manske, J.W. Barnwell, B. Renaud, François Ollomo, F. Prugnolle, N.M. Anstey, S. Auburn, R.N. Price, J.S. McCarthy, D.P. Kwiatkowski, M. Newbold, Chris I. Berriman, and M.B.& F.P. Thomas D. Otto, Aude Gilabert, Thomas Crellen, Ulrike Böhme, Céline Arnathau, Mandy Sanders, Samuel Oyola, Alain Prince Okouga, Larson Boundenga, Eric Wuillaume, Barthélémy Ngoubangoye, Nancy Diamella Moukodoum, Christophe Paupy, Patrick Durand, Virginie. 2017. Plasmodium malariae and P. ovale genomes provide insights into malaria parasite evolution. *Nature*. in press:101–104. doi:10.1038/nature21038.

Sabater, A.M., M. Moreno, F.J. Moreno, C. Eguiluz, N. Van Rooijen, and A. Benito. 2005. Experimental infection of immunomodulated NOD/LtSz-SCID mice as a new model for Plasmodium falciparum erythrocytic stages. *Parasitol. Res.* 95:97–105. doi:10.1007/s00436-004-1249-7.

Sadahira, Y., M. Mori, and T. Kimoto. 1990. Isolation and short-term culture of mouse splenic erythroblastic islands. *Cell Struct. Funct.* 15:59–65. doi:10.1247/csf.15.59.

Saeed, M., W. Roeffen, N. Alexander, C.J. Drakeley, G.A.T. Targett, and C.J. Sutherland. 2008. Plasmodium falciparum Antigens on the Surface of the Gametocyte-Infected Erythrocyte. *PLoS One*. 3:e2280. doi:10.1371/journal.pone.0002280.

Safeukui, I., N.D. Gomez, A.A. Adelani, F. Burte, N.K. Afolabi, R. Akondy, O. Sodeinde, J. Kazura, R. Ahmed, N. Mohandas, and D. Fernandez-reyes. 2015. Malaria Induces Anemia through CD8 ¤ T Cell-Dependent Parasite. 6:1–13. doi:10.1128/mBio.02493-14.Editor.

Sage, P., and C. Carman. 2012. Settings and mechanisms for trans-cellular diapedesis Peter. 100:130–134. doi:10.1016/j.pestbp.2011.02.012.Investigations.

Saito, H., Y. Yokoi, S. Watanabe, J. Tajima, H. Kuroda, and T. Namihisa. 1988. Reticular meshwork of the spleen in rats studied by electron microscopy. *Am. J. Anat.* 181:235–52. doi:10.1002/aja.1001810303.

Salcedo-Sora, J.E., E. Caamano-Gutierrez, S.A. Ward, and G.A. Biagini. 2014. The proliferating cell hypothesis: A metabolic framework for Plasmodium growth and development. *Trends Parasitol.* 30:170–175. doi:10.1016/j.pt.2014.02.001.

Sanders, P.R., G.T. Cantin, D.C. Greenbaum, P.R. Gilson, T. Nebl, R.L. Moritz, J.R. Yates, A.N. Hodder, and B.S. Crabb. 2007. Identification of protein complexes in detergent-resistant membranes of Plasmodium falciparum schizonts. *Mol. Biochem. Parasitol.* 154:148–157. doi:10.1016/j.molbiopara.2007.04.013.

Sanders, P.R., P.R. Gilson, G.T. Cantin, D.C. Greenbaum, T. Nebl, D.J. Carucci, M.J. McConville, L. Schofield, A.N. Hodder, J.R. Yates, and B.S. Crabb. 2005. Distinct protein classes including novel merozoite surface antigens in raft-like membranes of Plasmodium falciparum. *J. Biol. Chem.* 280:40169–40176. doi:10.1074/jbc.M509631200.

Sanders, P.R., L.M. Kats, D.R. Drew, R.A. O'Donnell, M. O'Neill, A.G. Maier, R.L. Coppel, and B.S. Crabb. 2006. A set of glycosylphosphatidyl inositol-anchored membrane proteins of Plasmodium falciparum is refractory to genetic deletion. *Infect. Immun.* 74:4330–4338. doi:10.1128/IAI.00054-06.

Saraf, A., S. Cervantes, E.M. Bunnik, N. Ponts, M.E. Sardiu, D.W.D. Chung, J. Prudhomme, J.M. Varberg, Z. Wen, M.P. Washburn, L. Florens, and K.G. Le Roch. 2016. Dynamic and combinatorial landscape of histone modifications during the intraerythrocytic developmental cycle of the malaria parasite. *J. Proteome Res.* 15:2787–2801. doi:10.1021/acs.jproteome.6b00366.

Sarin, H. 2010. Physiologic upper limits of pore size of different blood capillary types and another perspective on the dual pore theory of microvascular permeability. *J. Angiogenes. Res.* 2:1–19. doi:10.1186/2040-2384-2-14.

Satchwell, T.J. 2016. Erythrocyte invasion receptors for Plasmodium falciparum: New and old. *Transfus. Med.* 26:77–88. doi:10.1111/tme.12280.

Schaefer, A., J. Riet, K. Ritz, M. Hoogenboezem, E.C. Anthony, F.P.J. Mul, C.J. De Vries, M.J. Daemen, C.G. Figdor, J.D. Van Buul, P.L. Hordijk, A. Schaefer, J. Riet, K. Ritz, M. Hoogenboezem, E.C. Anthony, F.P.J. Mul, C.J. De Vries, M.J. Daemen, C.G. Figdor, J.D. Van Buul, and P.L. Hordijk. 2014. Actin-binding proteins differentially regulate endothelial cell stiffness , ICAM-1 function and neutrophil transmigration Actin-binding proteins differentially regulate endothelial cell stiffness , ICAM-1 function and neutrophil transmigration. 4470–4482. doi:10.1242/jcs.164814.

Schmidt, E.P., W.L. Lee, R.L. Zemans, C. Yamashita, and G.P. Downey. 2011. On, around, and through: neutrophil-endothelial interactions in innate immunity. *Physiol.* 26:334–347. doi:10.1152/physiol.00011.2011.

Scholl, P.F., a K. Tripathi, and D.J. Sullivan. 2005. Bioavailable iron and heme metabolism in Plasmodium falciparum. *Curr. Top. Microbiol. Immunol.* 295:293–324. doi:10.1007/3-540-29088-5_12.

Seed, J.R., and M.A. Wenck. 2003. Role of the long slender to short stumpy transition in the life cycle of the african trypanosomes. *Kinetoplastid Biol. Dis.* 2:3. doi:10.1186/1475-9292-2-3.

Seong-kyun, L., W. Bo, J.-H. Han, M.H. Nyunt, F. Muh, P. Chootong, K. Ha, W.S. Park, S.-H. Hong, J.H. Park, and E.-T. Han. 2016. Characterization of a novel merozoite surface protein of Plasmodium vivax, Pv41. *Acta Trop.* 126:222–228. doi:10.1016/j.actatropica.2013.03.002.

Sharp, S., T. Lavstsen, Q.L. Fivelman, M. Saeed, L. McRobert, T.J. Templeton, A.T.R. Jensen, D.A. Baker, T.G. Theander, and C.J. Sutherland. 2006. Programmed Transcription of the var Gene Family, but Not of stevor, in Plasmodium falciparum Gametocytes. *Eukaryot. Cell.* 5:1206–1214. doi:10.1128/EC.00029-06.

Shen, B., and L.D. Sibley. 2014. Toxoplasma aldolase is required for metabolism but dispensable for host-cell invasion. *Proc. Natl. Acad. Sci.* 111:3567–3572. doi:10.1073/pnas.1315156111.

Sherling, E.S., and C. van Ooij. 2016. Host cell remodeling by pathogens: The exomembrane system in Plasmodium-infected erythrocytesa. *FEMS Microbiol. Rev.* 40:701–721. doi:10.1093/femsre/fuw016.

Shi, H., Z. Liu, A. Li, J. Yin, A.G.L. Chong, K.S.W. Tan, Y. Zhang, and C.T. Lim. 2013. Life Cycle-Dependent Cytoskeletal Modifications in Plasmodium falciparum Infected Erythrocytes. *PLoS One.* 8:1–10. doi:10.1371/journal.pone.0061170.

Sigala, P.A., J.R. Crowley, J.P. Henderson, and D.E. Goldberg. 2015. Deconvoluting heme biosynthesis to target blood-stage malaria parasites. *Elife.* 4:e09143. doi:10.7554/eLife.09143.

Sigala, P.A., J.R. Crowley, S. Hsieh, J.P. Henderson, and D.E. Goldberg. 2012. Direct tests of enzymatic heme degradation by the malaria parasite Plasmodium falciparum. *J. Biol. Chem.* 287:37793–37807. doi:10.1074/jbc.M112.414078.

Da Silva, E., M. Foley, A.R. Dluzewski, L.J. Murray, R.F. Anders, and L. Tilley. 1994. The Plasmodium falciparum protein RESA interacts with the erythrocyte cytoskeleton and modifies erythrocyte thermal stability. *Mol.*

Biochem. Parasitol. 66:59–69. doi:10.1016/0166-6851(94)90036-1.

Silvestrini, F., E. Lasonder, A. Olivieri, G. Camarda, B. van Schaijk, M. Sanchez, S. Younis Younis, R. Sauerwein, and P. Alano. 2010. Protein Export Marks the Early Phase of Gametocytogenesis of the Human Malaria Parasite Plasmodium falciparum. *Mol. Cell. Proteomics*. 9:1437–1448. doi:10.1074/mcp.M900479-MCP200.

Silvestrini, F., M. Tibúrcio, L. Bertuccini, and P. Alano. 2012. Differential adhesive properties of sequestered asexual and sexual stages of Plasmodium falciparum on human endothelial cells are tissue independent. *PLoS One*. 7:1–8. doi:10.1371/journal.pone.0031567.

Sinden, R.E. 1982. Gametocytogenesis of Plasmodium falciparum in vitro: ultrastructural observations on the lethal action of chloroquine. *Ann. Trop. Med. Parasitol.* 76:15–23.

Sinden, R.E. 2015. The cell biology of malaria infection of mosquito: advances and opportunities. *Cell. Microbiol.* 17:451–466. doi:10.1111/cmi.12413.

Singh, A.P., H. Ozwara, C.H.M. Kocken, S.K. Puri, A.W. Thomas, and C.E. Chitnis. 2005. Targeted deletion of Plasmodium knowlesi Duffy binding protein confirms its role in junction formation during invasion. *Mol. Microbiol.* 55:1925–1934. doi:10.1111/j.1365-2958.2005.04523.x.

Singh, S., M.M. Alam, I. Pal-Bhowmick, J.A. Brzostowski, and C.E. Chitnis. 2010. Distinct external signals trigger sequential release of apical organelles during erythrocyte invasion by malaria parasites. *PLoS Pathog.* 6. doi:10.1371/journal.ppat.1000746.

Singh, S., S. Soe, S. Weisman, J.W. Barnwell, J.L. Pérignon, and P. Druilhe. 2009. A conserved multi-gene family induces cross-reactive antibodies effective in defense against Plasmodium falciparum. *PLoS One*. 4. doi:10.1371/journal.pone.0005410.

Sinha, A., K.R. Hughes, K.K. Modrzynska, T.D. Otto, C. Pfander, N.J. Dickens, A. a Religa, E. Bushell, A.L. Graham, R. Cameron, B.F.C. Kafsack, A.E. Williams, M. Llinás, M. Berriman, O. Billker, and A.P. Waters. 2014. A cascade of DNA-binding proteins for sexual commitment and development in Plasmodium. *Nature*. 507:253–7. doi:10.1038/nature12970.

Smalley, M.E., Abdalla S, and Brown j. 1981a. The distribution of Plasmodium falciparum in the peripheral blood and bone marrow of Gambian children. *Trans R Soc Trop Med Hyg*. 75:103–5.

Smalley, M.E., J. Brown, and N.M. Bassett. 1981b. The rate of production of plasmodium falciparum gametocytes during natural infections. *Trans. R. Soc. Trop. Med. Hyg.* 75:318–319. doi:10.1016/0035-9203(81)90349-7.

Smith, J.D., C.E. Chitnis, A.G. Craig, D.J. Roberts, E. Diana, D.S. Peterson, R. Pinches, C.I. Newbold, and H. Louis. 1995. Europe PMC Funders Group Switches in Expression of Plasmodium falciparum var Genes Correlate with Changes in Antigenic and Cytoadherent Phenotypes of Infected Erythrocytes. 82:101–110.

Smith, J.D., G. Subramanian, B. Gamain, D.I. Baruch, and L.H. Miller. 2000. Classification of adhesive domains in the Plasmodium falciparum Erythrocyte Membrane Protein 1 family. 110:293–310.

Socolovsky, M., H.S. Nam, M.D. Fleming, V.H. Haase, C. Brugnara, and H.F. Lodish. 2001. Ineffective erythropoiesis in Stat5a-/-5b-/- mice due to decreased survival of early erythroblasts. *Blood*. 98:3261–3273. doi:10.1182/blood.V98.12.3261.

Solaini, G., A. Baracca, G. Lenaz, and G. Sgarbi. 2010. Hypoxia and mitochondrial oxidative metabolism. *Biochim. Biophys. Acta*. 1797:1171–7. doi:10.1016/j.bbabio.2010.02.011.

de Sousa, T.N., F.S. Kano, C.F.A. de Brito, and L.H. Carvalho. 2014. The duffy binding protein as a key target for a Plasmodium vivax vaccine: Lessons from the Brazilian Amazon. *Mem. Inst. Oswaldo Cruz*. 109:608–617. doi:10.1590/0074-0276130592.

Spencer, J.A., F. Ferraro, E. Roussakis, A. Klein, J. Wu, J.M. Runnels, W. Zaher, L.J. Mortensen, C. Alt, R. Turcotte, R. Yusuf, D. Côté, S.A. Vinogradov, D.T. Scadden, and C.P. Lin. 2014. Direct measurement of local oxygen concentration in the bone marrow of live animals. *Nature*. 508:269–73. doi:10.1038/nature13034.

Srivastava, A., D.J. Creek, K.J. Evans, D. De Souza, L. Schofield, S. Müller, M.P. Barrett, M.J. McConville, and A.P. Waters. 2015. Host Reticulocytes Provide Metabolic Reservoirs That Can Be Exploited by Malaria Parasites. *PLoS Pathog.* 11:1–22. doi:10.1371/journal.ppat.1004882.

Srivastava, A., N. Philip, K.R. Hughes, K. Georgiou, I. Macrae, M.P. Barrett, D.J. Creek, M.J. Mcconville, and P. Waters. 2016. Stage-Specific Changes in Plasmodium Metabolism Required for Differentiation and Adaptation to Different Host and Vector Environments. 1–30.

doi:10.1371/journal.ppat.1006094.

Stafford, W., R. Stockley, S. Ludbrook, and A. Holder. 1996. Isolation, Expression and Characterization of the Gene for an ADP-Ribosylation Factor from the Human Malaria Parasite, Plasmodium Falciparum. *Eur. J.* …. 242:104–13. doi:10.1111/j.1432-1033.1996.0104r.x.

Starnes, G.L., M. Coincon, J. Sygusch, and L.D. Sibley. 2009. Aldolase Is Essential for Energy Production and Bridging Adhesin-Actin Cytoskeletal Interactions during Parasite Invasion of Host Cells. *Cell Host Microbe*. 5:353–364. doi:10.1016/j.chom.2009.03.005.

Steiniger, B., P. Barth, and A. Hellinger. 2001. The perifollicular and marginal zones of the human splenic white pulp : do fibroblasts guide lymphocyte immigration? *Am. J. Pathol.* 159:501–12. doi:10.1016/S0002-9440(10)61722-1.

Steiniger, B., P. Barth, B. Herbst, A. Hartnell, and P.R. Crocker. 1997. The species-specific structure of microanatomical compartments in the human spleen: strongly sialoadhesin-positive macrophages occur in the perifollicular zone, but not in the marginal zone. *Immunology*. 92:307–16. doi:10.1046/j.1365-2567.1997.00328.x.

Steiniger, B., M. Bette, and H. Schwarzbach. 2011. The Open Microcirculation in Human Spleens : A Three-Dimensional Approach. doi:10.1369/0022155411408315.

Steiniger, B.S. 2015. Human spleen microanatomy: Why mice do not suffice. *Immunology*. 145:334–346. doi:10.1111/imm.12469.

Stitzel, M., and G. Seydoux. 2008. Regulation of the Oocyte-to-Zygote Transition. *Science (80-.).*

Stubbs, J., K.M. Simpson, T. Triglia, D. Plouffe, C.J. Tonkin, M.T. Duraisingh, A.G. Maier, E. a Winzeler, and A.F. Cowman. 2005. Molecular mechanism for switching of P. falciparum invasion pathways into human erythrocytes. *Science*. 309:1384–1387. doi:10.1126/science.1115257.

Stutte, H.J., T. Sakuma, S. Falk, and M. Schneider. 1986. AM + / v A Splenic erythropoiesis in rats under hypoxic and post-hypoxic conditions. 251–261.

Su, X., M.T. Ferdig, Y. Huang, C.Q. Huynh, a Liu, J. You, J.C. Wootton, and T.E. Wellems. 1999. A genetic map and recombination parameters of the human malaria parasite Plasmodium falciparum. *Science*. 286:1351–1353. doi:10.1126/science.286.5443.1351.

Swanson, P.A., G.T. Hart, M. V Russo, D. Nayak, T. Yazew, M. Pe, S.M. Khan, C.J. Janse, S.K. Pierce, and B. Mcgavern. 2016. CD8 + T Cells Induce Fatal Brainstem Pathology during Cerebral Malaria via Luminal Antigen- Specific Engagement of Brain Vasculature. 1–34. doi:10.1371/journal.ppat.1006022.

Takala-harrison, S., T.G. Clark, C.G. Jacob, M.P. Cummings, and O. Miotto. 2013. Genetic loci associated with delayed clearance of Plasmodium falciparum following artemisinin treatment in Southeast Asia. 110. doi:10.1073/pnas.1211205110.

Takala-harrison, S., C.G. Jacob, C. Arze, M.P. Cummings, J.C. Silva, M. Khanthavong, B. Hongvanthong, P. Starzengruber, H. Fuehrer, P. Swoboda, W.A. Khan, A.P. Phyo, M.M. Nyunt, M.H. Nyunt, T.S. Brown, M. Adams, C.S. Pepin, J. Bailey, J.C. Tan, M.T. Ferdig, T.G. Clark, O. Miotto, B. Macinnis, D.P. Kwiatkowski, N.J. White, P. Ringwald, and C. V Plowe. 2015. Independent Emergence of Artemisinin Resistance Mutations Among Plasmodium falciparum in Southeast Asia. 211. doi:10.1093/infdis/jiu491.

Takala, S.L., and C. V. Plowe. 2009. Genetic diversity and malaria vaccine design, testing and efficacy: Preventing and overcoming “vaccine resistant malaria.” *Parasite Immunol*. 31:560–573. doi:10.1111/j.1365-3024.2009.01138.x.

Talman, A.M., R.E.L. Paul, C.S. Sokhna, O. Domarle, F. Ariey, J.F. Trape, and V. Robert. 2004. Influence of chemotherapy on the Plasmodium gametocyte sex ratio of mice and humans. *Am. J. Trop. Med. Hyg.* 71:739–744. doi:71/6/739 [pii].

Tamez, P. a., H. Liu, S. Fernandez-Pol, K. Haldar, and A. Wickrema. 2009. Stage-specific susceptibility of human erythroblasts to Plasmodium falciparum malaria infection. *Blood*. 114:3652–3655. doi:10.1182/blood-2009-07-231894.The.

Tamez, P. a., H. Liu, A. Wickrema, and K. Haldar. 2011. P. falciparum Modulates Erythroblast Cell Gene Expression in Signaling and Erythrocyte Production Pathways. *PLoS One*. 6:e19307. doi:10.1371/journal.pone.0019307.

Taylor, H.M., M. Grainger, and A.A. Holder. 2002. Variation in the expression of a *Plasmodium falciparum* protein family implicated in erythrocyte invasion. *Infect. Immun.* 70:5779–89. doi:10.1128/IAI.70.10.5779.

Taylor, H.M., L. McRobert, M. Grainger, A. Sicard, A.R. Dluzewski, C.S. Hopp, A.A. Holder, and D.A. Baker. 2010. The malaria parasite cyclic GMP-

dependent protein kinase plays a central role in blood-stage schizogony. *Eukaryot. Cell*. 9:37–45. doi:10.1128/EC.00186-09.

Teuscher, F., M.L. Gatton, N. Chen, J. Peters, D.E. Kyle, and Q. Cheng. 2010. Artemisinin-induced dormancy in *Plasmodium falciparum*: duration, recovery rates, and implications in treatment failure. *J. Infect. Dis.* 202:1362–8. doi:10.1086/656476.

Tewari, R., S.A. Ogun, R.S. Gunaratne, A. Crisanti, and A.A. Holder. 2005. Disruption of Plasmodium berghei merozoite surface protein 7 gene modulates parasite growth in vivo. *Blood*. 105:394–396. doi:10.1182/blood-2004-06-2106.

Tham, W.H., J. Healer, and A.F. Cowman. 2012. Erythrocyte and reticulocyte binding-like proteins of Plasmodium falciparum. *Trends Parasitol*. 28:23–30. doi:10.1016/j.pt.2011.10.002.

The WHO. 2017. http://www.who.int/mediacentre/factsheets/fs094/en/.

Thompson, J., C.J. Janse, and A.P. Waters. 2001a. Comparative genomics in Plasmodium: a tool for the identification of genes and functional analysis. *Mol. Biochem. Parasitol*. 118:147–154. doi:10.1016/S0166-6851(01)00377-2.

Thompson, J.K., T. Triglia, M.B. Reed, and A.F. Cowman. 2001b. A novel ligand from Plasmodium falciparum that binds to a sialic acid-containing receptor on the surface of human erythrocytes. 41:47–58.

Tiab, M., F. Mechinaud, and J.L. Harousseau. 2000. Haemophagocytic syndrome associated with infections. *Baillieres. Best Pract. Res. Clin. Haematol.* 13:163–78. doi:10.1053/beha.2000.0066.

Tibúrcio, M., M.W. a. Dixon, O. Looker, S.Y. Younis, L. Tilley, and P. Alano. 2015a. Specific expression and export of the Plasmodium falciparum Gametocyte EXported Protein-5 marks the gametocyte ring stage. *Malar. J.* 14:334. doi:10.1186/s12936-015-0853-6.

Tibúrcio, M., M. Niang, G. Deplaine, S. Perrot, E. Bischoff, P.A. Ndour, F. Silvestrini, A. Khattab, G. Milon, P.H. David, M. Hardeman, K.D. Vernick, R.W. Sauerwein, P.R. Preiser, O. Mercereau-Puijalon, P. Buffet, P. Alano, and C. Lavazec. 2012. A switch in infected erythrocyte deformability at the maturation and blood circulation of Plasmodium falciparum transmission stages. *Blood*. 119:172–180. doi:10.1182/blood-2012-03-414557.

Tibúrcio, M., R. Sauerwein, C. Lavazec, and P. Alano. 2015b. Erythrocyte remodeling by Plasmodium falciparum gametocytes in the human host

interplay. *Trends Parasitol*. 31. doi:10.1016/j.pt.2015.02.006.

Tibúrcio, M., F. Silvestrini, L. Bertuccini, A.F. Sander, L. Turner, T. Lavstsen, and P. Alano. 2013. Early gametocytes of the malaria parasite Plasmodium falciparum specifically remodel the adhesive properties of infected erythrocyte surface. *Cell. Microbiol*. 15:647–659. doi:10.1111/cmi.12062.

Toobiak, S., M. Shaklai, and N. Shaklai. 2012. Carbon monoxide induced erythroid differentiation of K562 cells mimics the central macrophage milieu in erythroblastic islands. *PLoS One*. 7:1–8. doi:10.1371/journal.pone.0033940.

Trager, W., and J. Jensen. 1976. Human Malaria. 673–675.

Traore, K., A. Lavoignat, G. Bonnot, F. Sow, G.C. Bess, M. Chavant, F. Gay, O. Doumbo, and S. Picot. 2015. Drying anti-malarial drugs in vitro tests to outsource SYBR green assays. 4–9. doi:10.1186/s12936-015-0600-z.

Travlos, G. 2006. Normal Structure, Function, and Histology of the Bone Marrow. *Toxicol. Pathol*. 34:548–565. doi:10.1080/01926230600939856.

Treeck, M., S. Zacherl, S. Herrmann, A. Cabrera, M. Kono, N.S. Struck, K. Engelberg, S. Haase, F. Frischknecht, K. Miura, T. Spielmann, and T.W. Gilberger. 2009. Functional analysis of the leading malaria vaccine candidate AMA-1 reveals an essential role for the cytoplasmic domain in the invasion process. *PLoS Pathog*. 5. doi:10.1371/journal.ppat.1000322.

Tremp, A.Z., F.S. Al-Khattaf, and J.T. Dessens. 2014. Distinct temporal recruitment of Plasmodium alveolins to the subpellicular network. *Parasitol. Res*. 113:4177–4188. doi:10.1007/s00436-014-4093-4.

Udeinya, I.J., L.H. Miller, I.A. McGregor, and J.B. Jensen. 1983. Plasmodium falciparum strain-specific antibody blocks binding of infected erythrocytes to amelanotic melanoma cells. *Nature*. 303:429–431. doi:10.1038/303429a0.

Varricchio, L., V. Tirelli, E. Masselli, B. Ghinassi, N. Saha, P. Besmer, and A.R. Migliaccio. 2012. The Expression of the Glucocorticoid Receptor in Human Erythroblasts is Uniquely Regulated by KIT Ligand: Implications for Stress Erythropoiesis. *Stem Cells Dev*. 21:2852–2865. doi:10.1089/scd.2011.0676.

Varshney, A., V. Barwa, L. Saini, P. Lamba, and R.K. Yadav. 2017. Case Report. 3:81–84.

Vega-Rodríguez, J., R. Pastrana-Mena, K.N. Crespo-Lladó, J.G. Ortiz, I. Ferrer-Rodríguez, and A.E. Serrano. 2015. Implications of Glutathione Levels in the Plasmodium berghei Response to Chloroquine and Artemisinin. *PLoS One*.

10:e0128212. doi:10.1371/journal.pone.0128212.

Vestweber, D. 2015. How leukocytes cross the vascular endothelium. *Nat. Rev. Immunol.* 15:692–704. doi:10.1038/nri3908.

Villeval, J.-L., A. Lew, and D. Metcalf. 1990. Changes in hemopoietic and regulator levels in mice during fatal or nonfatal malarial infections: I. Erythropoietic populations. *Exp. Parasitol.* 71:364–374. doi:10.1016/0014-4894(90)90062-H.

Volz, J., T.G. Carvalho, S.A. Ralph, P. Gilson, J. Thompson, C.J. Tonkin, C. Langer, B.S. Crabb, and A.F. Cowman. 2010. Potential epigenetic regulatory proteins localise to distinct nuclear sub-compartments in Plasmodium falciparum. *Int. J. Parasitol.* 40:109–121. doi:10.1016/j.ijpara.2009.09.002.

Wang, C.W., and L. Hviid. 2015. Rifins, rosetting, and red blood cells. *Trends Parasitol.* 31:285–286. doi:10.1016/j.pt.2015.04.009.

Warburg, O. 1959. On the origin of cancer metastasis. *Am. Assoc. Adv. Sci.* 18:43–73. doi:10.1016/S0306-9877(96)90136-X.

Watermeyer, J.M., V.L. Hale, F. Hackett, D.K. Clare, E.E. Cutts, I. Vakonakis, R.A. Fleck, M.J. Blackman, and H.R. Saibil. 2016. A spiral scaffold underlies cytoadherent knobs in Plasmodium falciparum-infected erythrocytes. *Blood.* 127:343–351. doi:10.1182/blood-2015-10-674002.

Weber, C.M., and S. Henikoff. 2014. Histone variants: dynamic punctuation in transcription. *Genes Dev.* 28:672–682. doi:10.1101/gad.238873.114.

Weiss, G.E., B.S. Crabb, and P.R. Gilson. 2016. Overlaying Molecular and Temporal Aspects of Malaria Parasite Invasion. *Trends Parasitol.* 32:284–295. doi:10.1016/j.pt.2015.12.007.

Weiss, G.E., P.R. Gilson, T. Taechalertpaisarn, W.H. Tham, N.W.M. de Jong, K.L. Harvey, F.J.I. Fowkes, P.N. Barlow, J.C. Rayner, G.J. Wright, A.F. Cowman, and B.S. Crabb. 2015. Revealing the Sequence and Resulting Cellular Morphology of Receptor-Ligand Interactions during Plasmodium falciparum Invasion of Erythrocytes. *PLoS Pathog.* 11:1–25. doi:10.1371/journal.ppat.1004670.

White, N.J. 2013. Pharmacokinetic and pharmacodynamic considerations in antimalarial dose optimization. *Antimicrob. Agents Chemother.* 57:5792–5807. doi:10.1128/AAC.00287-13.

WHO. 2010. Global report on antimalarial drug efficacy and drug resistance: 2000-2010.

WHO. 2011. Haemoglobin concentrations for the diagnosis of anaemia and assessment of severity. *Geneva, Switz. World Heal. Organ.* 1–6. doi:2011.

WHO. 2015. Eliminating Malaria.

Wickramasinghe, S.N., and S.H. Abdalla. 2000. Blood and bone marrow changes in malaria. *Bailliere's Best Pract. Res. Clin. Haematol.* 13:277–299. doi:10.1053/beha.1999.0072.

Wilson, A., and A. Trumpp. 2006. Bone-marrow haematopoietic-stem-cell niches. *Nat. Rev. Immunol.* 6:93–106. doi:10.1038/nri1779.

World Health Organization. 2015. Treatment of Severe Malaria. *Guidel. Treat. Malar.* 71–88. doi:10.1016/0035-9203(91)90261-V.

Wu, X.L., W.G. Zhang, X.M. Shi, P. An, W. Sen Sun, C.L. Qiao, and Z. Wang. 2011. Effect of artemisinin combined with glucocorticoid on the expressions of glucocorticoid receptor ?? mRNA, glucocorticoid receptor ?? mRNA and P300/CBP protein in lupus nephritis mice. *Chin. J. Integr. Med.* 17:277–282. doi:10.1007/s11655-011-0693-3.

Wykes, M.N., and M.F. Good. 2009. What have we learnt from mouse models for the study of malaria? *Eur. J. Immunol.* 39:2004–2007. doi:10.1002/eji.200939552.

Wykes, M.N., and J. Horne-Debets. 2012. Dendritic cells: The Trojan horse of malaria? *Int. J. Parasitol.* 42:583–587. doi:10.1016/j.ijpara.2012.03.002.

Xie, L.H., Q. Li, J. Zhang, and P.J. Weina. 2009. Pharmacokinetics, tissue distribution and mass balance of radiolabeled dihydroartemisinin in male rats. *Malar. J.* 8:112. doi:10.1186/1475-2875-8-112.

Xu, H., Y. He, X. Yang, L. Liang, Z. Zhan, Y. Ye, X. Yang, F. Lian, and L. Sun. 2007. Anti-malarial agent artesunate inhibits TNF-??-induced production of proinflammatory cytokines via inhibition of NF-??B and PI3 kinase/Akt signal pathway in human rheumatoid arthritis fibroblast-like synoviocytes. *Rheumatology.* 46:920–926. doi:10.1093/rheumatology/kem014.

Yahata, K., M. Treeck, R. Culleton, T.-W. Gilberger, and O. Kaneko. 2012. Time-lapse imaging of red blood cell invasion by the rodent malaria parasite Plasmodium yoelii. *PLoS One.* 7:e50780. doi:10.1371/journal.pone.0050780.

Yap, G.S., and M.M. Stevenson. 1992. Plasmodium chabaudi AS: Erythropoietic responses during infection in resistant and susceptible mice. *Exp. Parasitol.* 75:340–352. doi:10.1016/0014-4894(92)90219-Z.

Yeoman, J.A., E. Hanssen, A.G. Maier, N. Klonis, B. Maco, J. Baum, L. Turnbull,

C.B. Whitchurch, M.W.A. Dixon, and L. Tilley. 2011. Tracking glideosome-associated protein 50 reveals the development and organization of the inner membrane complex of Plasmodium falciparum. *Eukaryot. Cell*. 10:556–564. doi:10.1128/EC.00244-10.

Yoeli, M., I. July, and T.R. Cross. 1948. N O N - P I G M E N T E D MALARIA PARASITES IN THE BONE MARROW FROM A MIXED I N F E C T I O N OF L E I S H M A N I A AND P L A S M O D I U M V I V A X . 42:99–101.

Yokoyama, T., T. Etoh, H. Kitagawa, S. Tsukahara, and Y. Kannan. 2003. Migration of erythroblastic islands toward the sinusoid as erythroid maturation proceeds in rat bone marrow. *J. Vet. Med. Sci*. 65:449–452.

Young, J.A., Q.L. Fivelman, P.L. Blair, P. De La Vega, K.G. Le Roch, Y. Zhou, D.J. Carucci, D.A. Baker, and E.A. Winzeler. 2005. The Plasmodium falciparum sexual development transcriptome: A microarray analysis using ontology-based pattern identification. *Mol. Biochem. Parasitol*. 143:67–79. doi:10.1016/j.molbiopara.2005.05.007.

Zennadi, R., E.J. Whalen, E.J. Soderblom, S.C. Alexander, J.W. Thompson, L.G. Dubois, M.A. Moseley, and M.J. Telen. 2012. Erythrocyte plasma membrane – bound ERK1 / 2 activation promotes ICAM-4 – mediated sickle red cell adhesion to endothelium. *Blood*. 119:1217–1227. doi:10.1182/blood-2011-03-344440.The.

Zhang, Y., C. Huang, S. Kim, M. Golkaram, M.W.A. Dixon, L. Tilley, J. Li, S. Zhang, and S. Suresh. 2015. Multiple stiffening effects of nanoscale knobs on human red blood cells infected with Plasmodium falciparum malaria parasite. *Proc. Natl. Acad. Sci. U. S. A.* 112:6068–73. doi:10.1073/pnas.1505584112.

Zuccala, E.S., T.J. Satchwell, F. Angrisano, Y.H. Tan, M.C. Wilson, K.J. Heesom, and J. Baum. 2016. Quantitative phospho-proteomics reveals the Plasmodium merozoite triggers pre-invasion host kinase modification of the red cell cytoskeleton. *Sci. Rep.* 6:19766. doi:10.1038/srep19766.